

Review

A critical review of *in vitro* and *in vivo* biomedical applications of gold nanoparticles: From toxicology to cancer therapyIlyas Ozcicek ^{a,b,*} ^a Department of Medical Biology, School of Medicine, Istanbul Medipol University, Istanbul, Turkey^b Research Institute for Health Sciences and Technologies (SABITA), Istanbul Medipol University, Istanbul, Turkey

ARTICLE INFO

Keywords:

Gold nanoparticle
Nanotoxicity
Biodistribution
Cancer therapy
Drug delivery
Gene silencing
Imaging
Detection
Tissue engineering
Antibacterial

ABSTRACT

Due to their unique and fascinating physicochemical properties, gold nanoparticles (AuNPs) are frequently used in the biomedical field including drug delivery, cancer therapy, biosensor, bioimaging, gene therapy, tissue engineering and antibacterial applications. Their superior properties such as high biocompatibility with living organisms, stability, SPR properties, small size, large surface area, adjustable stability, easy synthesizability and surface modification have increased the success of AuNPs in nanomedicine applications. AuNPs, which can be synthesized by many methods, can be easily adjusted in size and shape. Various mechanisms are being proposed to increase the affinity of functional group-bearing AuNPs to biomolecules and turn them into effective drug delivery systems with improved specificity. Among other metallic nanoparticles, AuNPs have great potential to be used in bio-imaging field. Considering the superior properties of AuNPs and controllable interactions with different biomolecules, AuNPs can be used as biosensor platforms in various diagnostic processes. This review article will be focused on the recent advances in various biomedical applications of AuNPs including toxicity, cancer therapy, drug delivery, gene silencing, bio-imaging, tissue engineering, diagnostic applications, and antibacterial studies. It is concluded that clinical studies on AuNPs with expanded strategies will be witnessed in the coming years.

1. Introduction

Innovative research in the nanomedicine area has enabled the new nano-theragnostic biomaterial developments for areas such as diagnosis, treatment, and biological imaging [1]. The interactions of nanoparticles with the bio-systems have decisive effects on their bioactivity, and theragnostic biomaterial designs appropriate to the nature of these interactions are very important. Nanomaterials can interact with bio-systems in very different ways according to their shape, size, and surface functionalization. The interactions of nanoparticles with receptors of cells, cytoplasmic organelles, nucleic acids, and proteins at nanoscale occur depending on various parameters such as colloidal forces, dynamic bio-physicochemical interactions, electrostatic attractions, and thermodynamic changes at the bio-nano interface [2–4].

Gold nanoparticles (AuNPs) are innovative metallic nanomaterials that can be easily synthesized via chloroauric acid reduction method and have diameters ranging from 5 to 100 nm. Since AuNPs are nanosized, they can easily interact with different biomolecules. Based on the shape, size, and surface properties, AuNPs can be specifically designed for

various nanomedicine applications [2]. AuNPs attract great interest in the nanomedicine area due to their unique chemical/physical properties, biocompatibility, stability, low cytotoxicity, optical superiority, antioxidant structure and easy functionalization of their surfaces. As shown in Fig. 1, thanks to these superior characteristics, AuNPs have a wide range of different nanomedicine applications such as drug carrier system, DNA transfer, gene silencing, bio-imaging, detection, biosensor, nanotoxicology, cancer therapy, targeting, photodynamic/photothermal therapy, tissue engineering and antibacterial studies [5–8].

While gold is an inert, solid, and yellow substance in nature, its physicochemical properties and color vary depending on shape and size in the form of nanoparticles (AuNPs) [9]. It is possible to produce various sizes and shapes of AuNPs via fine-tuning synthesis protocols (Fig. 2) [10]. AuNPs can be synthesized using chemical, physical, and biological techniques [11,12]. The citrate reduction synthesis method is the most widely preferred synthesis type. The AuNPs in the diameter range of 10–20 nm can be synthesized using this technique developed by Turkevich in 1951 [13]. In this method, citrate molecules (as both a

* Corresponding author at: Department of Medical Biology, School of Medicine, Istanbul Medipol University, Istanbul, Turkey.

E-mail addresses: ilyasozcicek@gmail.com, iozcicek@medipol.edu.tr.

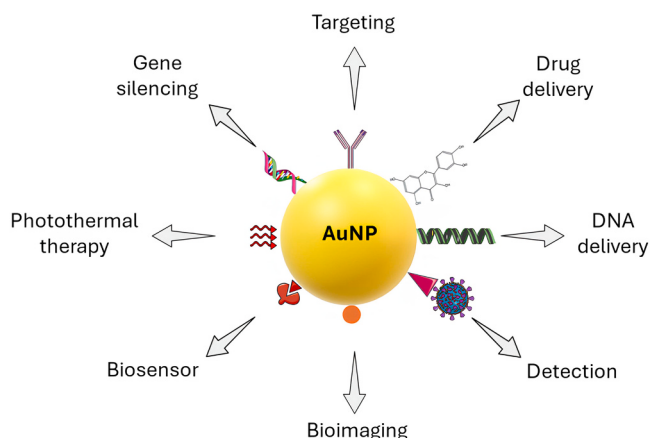


Fig. 1. Various biomedical applications of AuNPs in nanomedicine. This figure was produced using elements from the Server Medical Art PowerPoint image bank.

reducing and stabilizing chemical) allow the formation of negatively surface charged nanoparticles, preventing aggregation and obtaining a colloidal gold suspension. The AuNPs of various sizes and shapes can be obtained via seed-mediated growth methods [7,14,15]. In addition to chemical methods, there are also physical AuNPs synthesis techniques such as UV radiation, photochemical processes, microwave irradiation and sono-chemical approaches [16–18]. Biological synthesis methods have also attracted great interest in recent years, and microorganisms, enzymes and various plants are used as stabilizing/reducing agents. Thus, it is possible to produce biocompatible AuNPs with more environmentally friendly approaches and at lower costs [12,19].

Surface modification of AuNPs is very significant in terms of their functionality, stability, biocompatibility and use for various biomedical purposes. Superficial functionalization of AuNPs can be achieved by synthesis methods involving covalent interactions or by electrostatic physical interactions [20]. Bare nanoparticles which have not any surface modification tend to cluster and be quickly eliminated from the biological systems for *in vivo* applications. AuNPs have strong interaction tendencies into functional groups such as amino (-NH₂), thiol (-SH), phosphine (-PH₂), and hydroxyl (-OH) groups. Among these, sulfur-bearing groups (-SH) are the most effective functional group for AuNPs. Therefore, if one of these functional groups is present in the biomolecules desired to be conjugated to the particle structure, the conjugation of the ligand molecules with the nanoparticles is very easy.

[21,22]. Especially since DNA and RNA molecules are negatively charged biomolecules, they can easily interact electrostatically with positively charged nanoparticles with appropriate surface functionalization, without the need for additional covalent chemical bonds [23, 24]. The polymeric surface modification of AuNPs is one of the most widely used coating methods, and polyethylene glycol (PEG) modification is frequently applied (Fig. 3) [25]. PEG surface coating increases the colloidal stability of AuNPs as it creates steric hindrance and causes the particles to repel each other. It also increases the cellular uptake and systemic biodistribution rate of AuNPs [5–7,26,27].

AuNPs applications and research are now enormously common in the areas of biomedicine and bioengineering. AuNPs are becoming progressively prevalent in nanomedicine, biomedical engineering, targeted drug delivery, cancer therapy, biosensor, gene delivery, tissue/organ engineering, cancer diagnostics, nanotherapeutics, CRISPR/Cas9 research, bioimaging, implants and prosthetics. The primary goal of this article is to review the latest progress, options, barriers, toxicity, recent clinical applications, and views of AuNPs in practice, biomedical applications. In recent years, applications of surface modified AuNPs in nanomedicine and biomedical engineering have been reviewed that indicate critical development in this area. However, since numerous research results are published every year in various biomedical fields, there is a great need to collect rapid and breathtaking new developments in detail. This review gives a detailed and systematic summary of exclusive physical, chemical and optical properties of AuNPs, their various methods of modification, and their different applications in biomedical engineering.

This comprehensive review article will focus on the recent advances in various biomedical applications of AuNPs including toxicity, drug delivery, cancer therapy, gene silencing, bio-imaging, tissue engineering, diagnostic applications, and antibacterial studies. Thus, more understandable, and systematic literature information regarding the effectiveness of the changing physicochemical properties (such as synthesis method, shape, size, concentration, and surface functionalization) of AuNPs in the various cellular and *in vivo* applications will be presented.

2. Toxicology and biodistribution of gold nanoparticles

With the rapid developments in nanotechnology science, investigating the toxic effects of used nanomaterials attracts more attention. As shown in Fig. 4, in addition to various physical/chemical features of the nanoparticles (shape, size, and surface functionalization), the other issues such as concentration, exposure time, application method, cell type

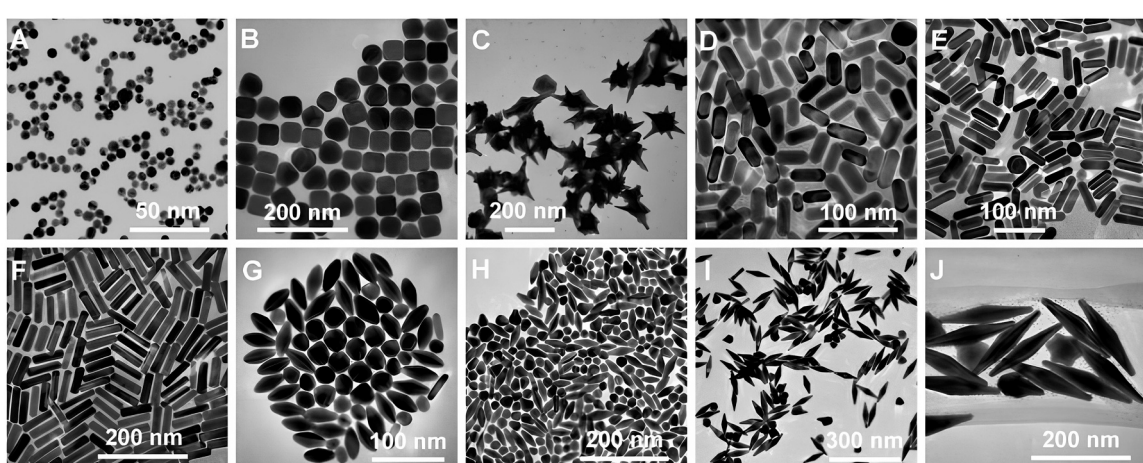


Fig. 2. Representative TEM images of AuNPs of different shapes and sizes. (A) Nanospheres. (B) Nanocubes. (C) Nanostars. (D) Nanorods (E) Nanorods. (F) Nanorods. (G) Nanobipyramids. (H) Nanobipyramids. (I) Nanobipyramids. (J) Nanobipyramids. Adapted with permission from reference [10]. Copyright (2008), American Chemical Society.

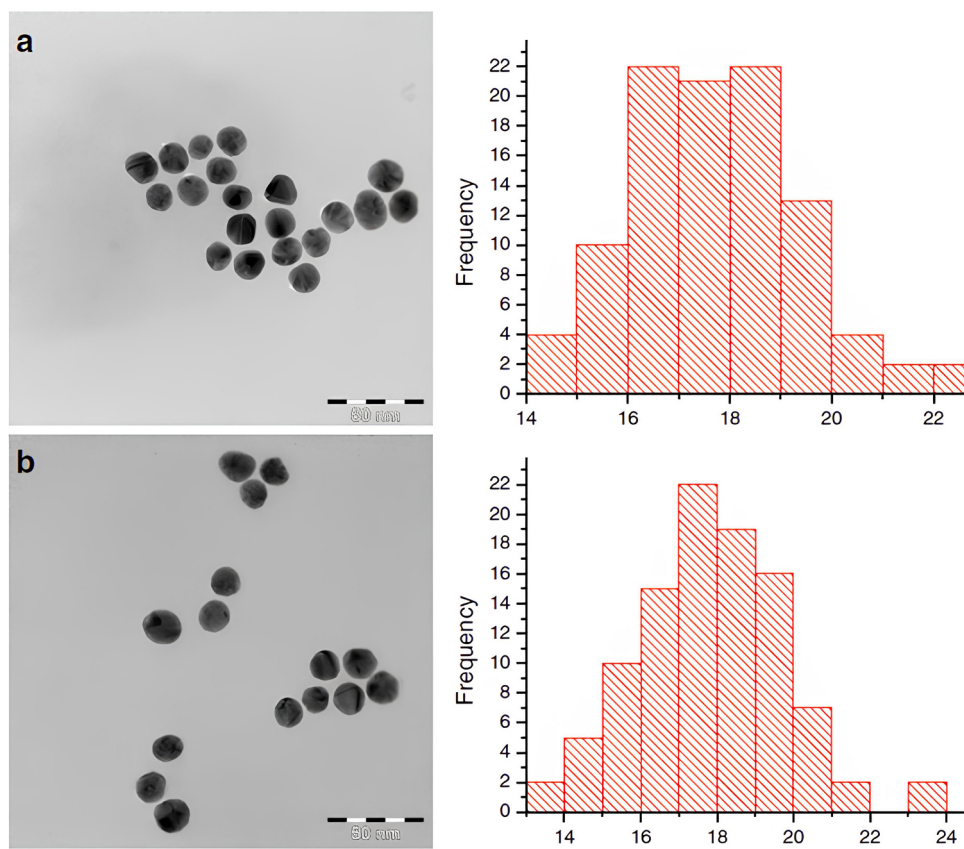


Fig. 3. TEM images and accompanying histograms of AuNPs. (a) Citrate capped AuNPs. (b) 16.8 µg/mL PEG coated AuNPs. Adapted with permission from reference [25]. Copyright (2011), Springer Nature.

are also decisive on the nanotoxicological effects that occur as a result of the interplay of nanoparticles with biological systems [28]. To date, in addition to issues such as *in vitro/in vivo* biodistribution, cellular uptake and localization of AuNPs; the effects of various physicochemical characteristics of nanomaterials on parameters such as oxidative stress, viability, DNA damage and apoptosis have been evaluated on a wide scale. All these characteristic features of AuNPs have decisive effects on interaction with biological systems and effectiveness. Although studies on the toxicology of AuNPs are predominantly *in vitro* evaluations, the *in vivo* animal studies on systemic distribution are fundamental and decisive for the definitive assessment of nanotoxicity [28–30].

2.1. *In vitro* toxicity and cellular uptake of gold nanoparticles

The majority of nanotoxicological and biodistribution assessments of AuNPs are performed *in vitro* because they are easy to conduct. Some important cellular studies selected from the literature to understand the *in vitro* effects of AuNPs are systematically summarized in Table 1 [5, 31–72]. The size, shape, surface modification, concentration of the AuNPs used in these studies, as well as the selected cell type and exposure time, led to different effects on the toxic situations and cellular uptake of Au-based nanoparticles. In some studies, using small sized (in the size range of 1.5–10 nm) spherical gold nanoparticles, it has been shown that significant toxic effects on cells (such as cell death, ROS production, DNA damage, apoptosis, necrosis, and DNA methylation) were observed, depending on the concentration of AuNPs [31,33,35,39, 40,47,54,61,63]. On the other hand, there are also some cellular studies reporting that the toxic effects on the cells were minimized as a result of appropriate surface functionalization (such as PEG, transferrin, PMA, PCD, RGD-peptide, DNA, PAA, glutathione-CR₈ and gadolinium-AS1411) applied to small-sized (in the size range of

2.4–18 nm) AuNPs [34,36–38,44,48,49,57,64,65,69,70]. Apart from these, it has been evaluated that medium and larger sized AuNPs, which do not have any surface modification, generally did not cause an important toxic effect on the cells, depending on the dose and exposure time [5,31,41,53,61,66]. In this respect, it can be concluded that the toxic effects of AuNPs increase as their size decreases. Especially, the high level of toxic effects of ultrasmall AuNPs is an important problem in terms of their biomedical use. However, it seems possible that these toxic effects can be minimized by choosing an appropriate surface modification.

Appropriate and effective surface functionalization of AuNPs not only makes them biocompatible and stable but also leads to decisive effects on their cellular uptake and localization. In some studies, using AuNPs modified with PEG, it has been shown that nanoparticles can escape from endosomal vesicles and localize in different cell compartments (such as cytosol and nucleus), and at the same time, the amount of cellular Au uptake increased [5,34,37,49,50,65,70]. In a study, RGD-peptide coating increased AuNPs (diameter: 15 nm) entry into the HeLa cells by 5-fold and nuclear localization was observed [44]. Falagan-Lotsch et al. showed that PAA-coated AuNPs (diameter: 20 nm) were more uptake by HDF cells than citrate-stabilized or PEG-modified nanoparticles [46]. In a study investigating the effects of AuNPs (diameter: 50 nm) with dPGS or PEI surface modification on A 549 cells, decrease in the number of lipid droplets/multivesicular intracellular bodies and increase in the number of mitochondria and small cellular vesicles were shown [67]. Appropriate surface functionalization of AuNPs is one of the most critical parameters in terms of their toxic effects, cellular uptake and bioavailability. The ability to offer effective nanoparticle delivery to different cellular compartments provides the potential for effective theragnostic use in targeted therapies. In this regard, an effective increase in cellular uptake and biocompatibility with

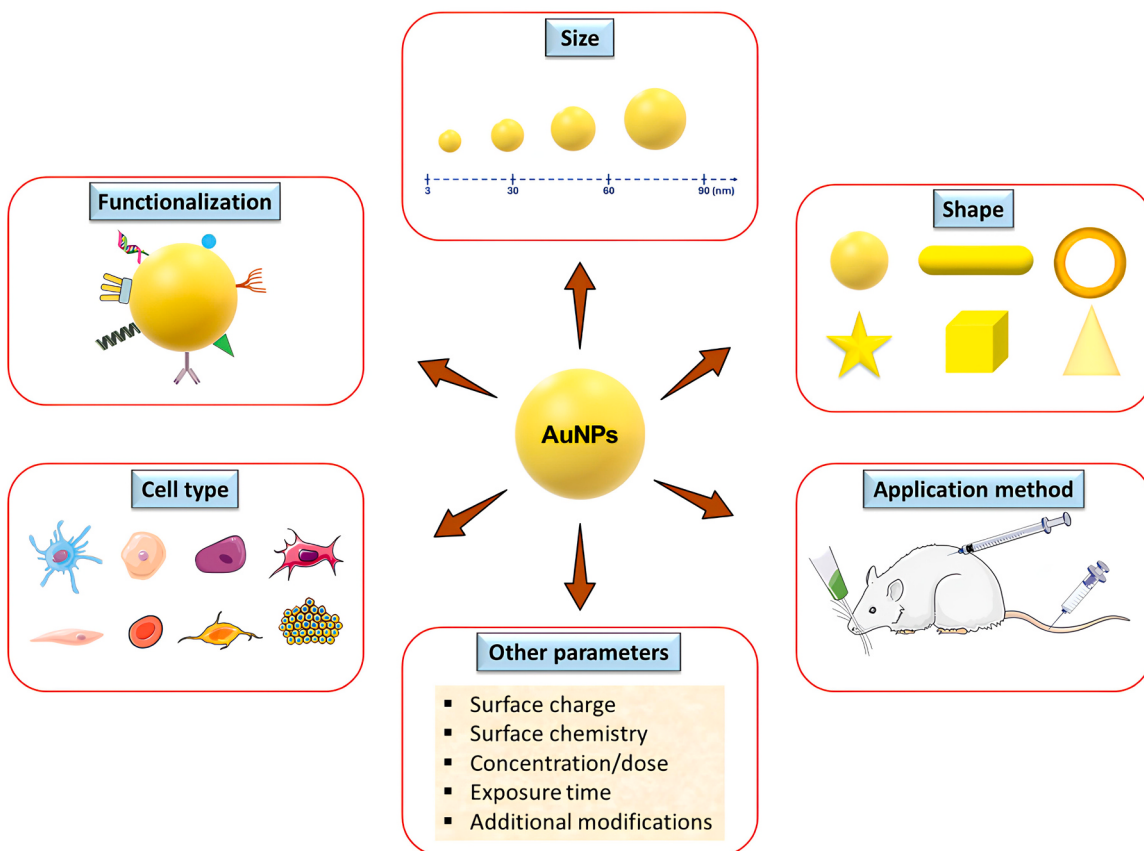


Fig. 4. Different parameters influencing the gold nanoparticles' toxicity: Size, Functionalization, Shape, Cell type, Application method and Other parameters. This figure was produced using elements from the Server Medical Art PowerPoint image bank.

widely used polymers is promising.

The surface charge of AuNPs also determines their cellular effects. Stojiljkovic et al. reported that AuNPs of different sizes (diameters: 15, 40 and 80 nm) were more taken up by the cells (N9 microglial and SH-SY5Y cells) as a result of the cationic surface charge (+) provided via coating them with poly-L-lysine [51]. Our study showed that PEI surface modification (+) increased biocompatibility and cellular (DRG sensory neurons) AuNPs (diameters: 20 and 50 nm) uptake [5]. Biomolecules such as cell membranes, DNA and RNA are negatively charged structures due to the phosphate groups they carry, and the use of positively charged nanoparticles leads to an increase in electrostatic interaction. As a result of an effective surface interaction, the entry of AuNPs into the cell increases and thus their theragnostic use efficiency is strengthened. The cell type chosen in the *in vitro* studies can also be a determinant on the toxic effects of AuNPs, their cellular uptake amount and intracellular localization [36,40,43,51,53]. In an AuNPs-based (diameters: 30, 50 and 90 nm) toxicity study performed using two different cell types (HepG2 and HL-60 cells), the HL-60 cells were evaluated to be more sensitive to the increase in concentration (concentration range: 1–25 µg/mL) [41]. It is important to optimize the concentrations of AuNPs so that they can be used effectively and safely for various biomedical purposes. In this regard, in literature, AuNPs have been frequently studied with varying concentrations in cellular studies. In these studies, sometimes increasing AuNPs concentrations may have toxic effects on the cells and their metabolic activities [36,40,43,51,53]. Nanomaterial size and composition plays an apparent role in the cellular toxic response. In addition, this response is variable between cell types and it is probably correlated to the physiological function of the cell types. Since differences in metabolic processes may occur depending on the cell type, it can be considered normal for AuNPs to give different results in different cells.

In a study investigating the toxic effects of PMA-modified AuNPs (diameter: 4 nm, concentration range: 0–200 nM) using three cell types (C17.2, PC12 and HUVEC cells), no toxic effects were observed up to 50 nM, after which an increase in ROS levels and disruptions in the cell cytoskeleton were observed [38]. Ozcicek et al. reported that an increase in the concentration (range: 1–100 µg/mL) of AuNPs (diameters: 20 and 50 nm) with different surface chemistry (citrate stabilized, PEG or PEI coated) led to a decrease in the viability of DRG primary sensory neurons [5]. In another study, biogenically synthesized AuNPs (diameter: 20 nm) showed toxic effects on the cells (A 549 and Vero cells) at a concentration (range: 20–100 µg/mL) of 60 µg/mL [72]. Most gold nanomaterials may exhibit a biocompatible profile at low doses, but they may cause toxic effects when added to cell culture media at high concentrations. It was concluded that the toxic effect depending on the nanomaterial concentration could be eliminated by using AuNP at a minimal concentration sufficient to provide therapeutic effect.

A variation in the shape of Au nanomaterials during their synthesis will change their physicochemical properties and cellular effects. Gold nanorods (AuNRs) are frequently preferred in different biomedical applications thanks to their fascinating physicochemical features. The surface functionalization process is essential for the stability of AuNRs and to reduce their possible toxic effects. CTAB (cetyltrimethylammonium bromide), which has a highly toxic chemical, is mostly preferred for the synthesis and stabilization of AuNRs via the seeding-growth method. Thus, it is very important to coat the surfaces of AuNRs by bio-compatible molecules using ligand exchange chemistry. Parameter changes (concentration, size, surface coating, selected cell type and exposure time) that are valid for spherical AuNPs are also valid for rod-shaped nanoparticles [6]. In a study using PAA or PEG-coated AuNRs, it was shown that PAA-modified AuNRs (16 nm × 50 nm) were specifically uptake by the cells (HDF and human cell lines) in

Table 1
Some *in vitro* toxicity and cellular uptake studies of gold nanoparticles.

Cell types	Particle Dimensions	Particle Surface Group	Concentrations	Time of Exposure	Effects	References
L5178Y cells	(4, 15, 100 and 200 nm)	AuNPs	(0–200 µg/mL)	(6, 24 and 48 h)	The AuNPs of 4 nm size induced cellular toxicity.	[31]
MRC-5 cells	(20 nm)	AuNPs	(1 nM)	(72 h)	Lipid peroxidation, autophagosome formation and upregulation of genes/proteins associated with oxidative stress.	[32]
HeLa cells	(2 nm)	Pentanethiol-capped AuNPs	(0–10 µM)	(24 h)	The AuNPs with hydrophobic surfaces caused more toxic effects.	[33]
A 549 cells	(15 nm)	AuNPs and AuNPs-PEG	(20 nM)	(1, 4 and 24 h)	PEG-coated AuNPs entered the cells as smaller and more numerous vesicles, and also showed accumulation in the cytosol.	[34]
HaCaT cells	(1.5 nm)	TMAT (+), MES (-) or MEEE (neutral) modified AuNPs	(0–100 µg/mL)	(24 h)	The cell death occurred through apoptosis and necrosis.	[35]
HeLa, A 549 and MDA-MB-435 cells	(15–45 nm; aggregated: 26–98 nm)	Transferrin coated AuNPs	(0.2–1 nM)	(2–8 h)	Although the aggregation of the AuNPs did not cause toxic effects, it reduced cellular AuNPs uptake depending on the cell type.	[36]
COS-1 cells	(2.4, 5.5, 8.2, 16, 38 and 89 nm)	PEG modified AuNPs	(3–200 nM)	(2 h)	Minimal toxicity in all groups, although the fluorescent properties of small-sized AuNPs were weak, they have been shown to enter the cell and nucleus effectively.	[37]
C17.2, PC12 and HUVEC cells	(4 nm)	PMA coated AuNPs	(0–200 nM)	(24 h)	No toxic effects were observed up to 50 nM, after which an increase in ROS levels and disruptions in the cell cytoskeleton were observed.	[38]
Cell types	Particle Dimensions	Particle Surface Group	Concentrations	Time of Exposure	Effects	References
Balb/3T3 cells	(5 and 15 nm)	AuNPs	(10–300 µM)	(72 h)	While AuNPs–5 nm sized showed toxic effects above 50 µM, those with a size of 15 nm were not toxic.	[39]
Vero, NIH3T3 and MRC5 cells	(10–40 nm)	AuNRs	(0–720 ng/mL)	(72 h)	Dose-dependent decrease in cell growth. Apoptosis, autophagy, and DNA damage depending on cell type.	[40]
HL-60 and HepG2 cells	(30, 50 and 90 nm)	AuNPs	(1–25 µg/mL)	(24, 48 and 72 h)	AuNPs-induced cytotoxicity was time and dose-dependent. HL-60 cells were more sensitive.	[41]
A 549 and Vero cells	(10 nm)	PCD-AuNPs	(0–40 µg/mL)	(48 h)	No indication of cytotoxicity for both cell types.	[42]
U-87, PC-3, MDA-MB-231, HepG2, HT-29 and RAW 264.7 cells	(82 nm length–22 nm width)	CTAB, PSS, PEG, mSiO ₂ , dSiO ₂ or TiO ₂ coated AuNRs	(5–150 µg/mL)	(24 h)	While CTAB, PSS or mSiO ₂ coated AuNRs showed toxic effects, PEG, dSiO ₂ or TiO ₂ coated ones did not induce cellular damage. The level of cellular uptake of AuNRs varied with surface coating and cell type.	[43]
HeLa cells	(15 nm)	Pent-RGD-NLS-AuNPs	(10 nM)	(6–8 h)	RGD-peptide coating increased AuNPs entry into the cells by 5-fold and nuclear localization was observed.	[44]
HSC and HepG2 cells	(7 nm × 30 nm and 14 nm × 56 nm)	CTAB, oleate or BSA modified AuNRs	(5 µg/200 µL)	(6, 12, 24 and 48 h)	Small sized AuNRs were less cytotoxic and showed greater cellular uptake than commonly used larger ones, despite the same surface functionalization.	[45]
HDF cells	(AuNPs: 20 nm; AuNRs: 16 nm × 45–50 nm)	Citrate or PAA modified AuNPs; CTAB, PAA or PEG modified AuNRs	(0.1 nM)	(chronic: 20 weeks and non-chronic: acute period)	No toxicological effects. The PAA-coated AuNPs were more uptake than the AuNPs-citrate. PAA-coated AuNRs were more taken up than PEG-coated ones. PEG-coated AuNRs were observed in the cytosol and they caused many gene expression changes associated with cellular stress/toxicity in the long term.	[46]
Cell types	Particle Dimensions	Particle Surface Group	Concentrations	Time of Exposure	Effects	References
hESC cells	(1.5, 4 and 14 nm)	AuNPs or MSA coated AuNPs	(0.6 µg/mL–1.5 nm; 10 µg/mL-the others)	(24 h)	The AuNPs-MSA of 1.5 nm size were toxic, while those of other sizes were not. The AuNPs of 4 nm size reduced DNA methylation.	[47]
CaSki cells	(10–50 nm)	DNA-AuNPs	(1 × 10 ⁻⁹ M)	(2–24 h)	No indication of cytotoxicity. DNA modification and small size increased cellular AuNPs uptake.	[48]
(HCT116, Huh7, PC3, HeLa, BEL7402, HEK293T, L02 and HFF cells)	(GNRs with different aspect ratios)	CTAB, PSS, PAH coated AuNRs	(0.25–4 nM)	(72 h)	The results indicated that the surface chemistry but not the aspect ratio of GNRs mediates their biological toxicity. PSS/PAH coatings were decreased the toxicity.	[49]
hMSC cells	(50 nm)	FITC-PEG-AuNPs	(0.1, 0.5 and 1 nM)	(24 h)	No toxicological effects. The PEG-coated AuNPs were further uptake into the cells.	[50]

(continued on next page)

Table 1 (continued)

Cell types	Particle Dimensions	Particle Surface Group	Concentrations	Time of Exposure	Effects	References
N9 microglial and SH-SY5Y cells	(15, 40 and 80 nm)	AuNPs; BSA (-) or poly-L-lysine (+) coated AuNPs	(1×10^9 AuNPs per mL)	(1 and 6 h)	The cationic AuNPs were more uptake by the cells. Cell type, AuNPs size and surface coating were major determinants of cellular uptake of the nanomaterials.	[51]
HT29 cells	(32 nm)	AuNPs	(2–10 $\mu\text{g}/\text{mL}$)	(24 h)	Significant reduction in viability, no genotoxic effects.	[52]
OVCAR5, OVCAR8 and SKOV3 cells	(18, 40, 60 and 80 nm)	AuNPs-citrate	(6.4, 12.8, 25.6 and 38.6 $\mu\text{g}/\text{mL}$)	(1, 6, 12 and 24 h)	Metabolic activity and proliferation rate decreased dose-dependently, but the AuNPs were not toxic. Diameter, dose, and cell type affected AuNPs uptake.	[53]
HepG2 and HeLa cells	(6.2, 24.3, 42.5 and 61.2 nm)	PEG coated AuNPs	(0.25, 0.5 and 1 mM)	(48 h)	When the dose of gold nanoparticles reached a certain amount (1 mM), toxicity and ROS production increased significantly with size reduction of AuNPs.	[54]
DU145 and HeLa cells	(26 nm \times 54 nm)	^M TAB AuNRs	(50 μM)	(24 h)	Induction of autophagy, no genotoxicity, alterations of actin cytoskeleton, destabilization of lysosomes, or in the migration of cells.	[55]
Cell types	Particle Dimensions	Particle Surface Group	Concentrations	Time of Exposure	Effects	References
VSMC cells	(22 nm \times 66 nm)	CTAB, PSS or PDDAC coated AuNRs	(15–300 μM)	(3 h)	The absence/presence of serum in the cell media, surface modification and dose of the AuNPs had important impacts on the cell viability and AuNRs uptake.	[56]
A 549 cells	(3–4 nm)	Modified AuNPs	(0.78–100 $\mu\text{g}/\text{mL}$)	(24 h)	No cellular viability effects. Decrease in glutathione level and increase in DNA damage/genotoxicity.	[57]
HaCaT and L929 cells	(60 nm)	KGF conjugated AuNPs	(1.61×10^{-11} M)	(24 h)	No toxicological effects. The KGF conjugated AuNPs promoted keratinocyte proliferation.	[58]
HepG2 cells	(40, 60 and 90 nm)	TN conjugated AuNPs	(0–160 μM)	(24 h)	TN conjugated AuNPs triggered dose-dependent cell death by ROS production, DNA damage and apoptosis.	[59]
7721, GES-1 and 4T1 cells	(AuNPs: 15, 45 and 80 nm; AuNR: 10 nm \times 33 nm; NS: 15 nm)	AuNPs, AuNRs and AuNSs	(AuNPs: 100–800 mg/L, AuNRs: 0.5–8 mg/L and NS: 1–50 mg/L)	(12–24 h)	A decrease in the viability of the cells was observed depending on the dose. Changes in endocytosis mechanism and exocytosis rate depending on size and shape.	[60]
HT-29 and HepG2 cells	(10, 30 and 60 nm)	AuNPs-citrate	(10 ppb–10 ppm)	(16 and 32 h)	DNA damage induced by smaller size AuNPs, time-dependent decrease in cell viability, ROS production.	[61]
NIH3T3 cells	(50–70 nm)	AuNPs	(increasing concentrations)	(24 h)	Cytotoxic effect due to dose increase.	[62]
HepG2 and L02 cells	(5, 20 and 50 nm)	AuNPs	(0–12.5 $\mu\text{g}/\text{mL}$)	(72 h)	Small-sized AuNPs (5 nm) showed high level dose-dependent toxic effect, especially for L02 cells.	[63]
HeLa cells	($d < 3$ nm)	Glutathione and CR ₈ coated AuNPs	(500 nM)	(10 min, 1, 3 and 6 h)	The increase in surface coverage rate of AuNPs increased the level of nanoparticle uptake while slowing down cellular interactions and connections.	[64]
Cell types	Particle Dimensions	Particle Surface Group	Concentrations	Time of Exposure	Effects	References
E17.5 cells	(18 nm)	PEG coated AuNPs	(0.001, 0.01, 0.1 and 1 mg/mL)	(24 h)	No toxicity, efficient nanoparticle uptake and concentration in intracellular compartments	[65]
NRK cells	(10, 25, 50, 70 and 100 nm)	AuNPs-citrate	(1 nM)	(24 h)	No cellular viability effects. Increased intracellular Ca ⁺⁺ ions concentration and Golgi organelle fragmentations depending on size.	[66]
A 549 cells	50 nm	dPGS or PEI	(0.23 nM)	(1, 3, 6, 12 and 24 h)	No toxicity, changes in the number of organelles depending on nanoparticle entry, decrease in the number of lipid droplets/multivesicular bodies and increased number of small vesicles/mitochondria.	[67]
SW620, HEK293, HCT116 and LS174T cells	(13 nm \times 57 nm)	CTAB-Oleate, DOPC-DSPE lipids-mPEG or PSS modified AuNRs	(0–200 $\mu\text{g}/\text{mL}$)	(24 h)	Removing CTAB from the surface of the AuNRs and coating them with phospholipids provided stability and biocompatibility. SW620, HCT116 and LS174T cells showed 100 % viability even at high dose, while some toxicity was observed in HEK293 cells.	[68]
DRG cells	(20 and 50 nm)	AuNPs-citrate, AuNPs-PEG, or AuNPs-PEI	(1, 10 and 100 $\mu\text{g}/\text{mL}$)	(0–72 h)	The increase in concentration and decrease in AuNPs size slightly reduced cellular viability. PEI or PEG coating increased biocompatibility and cellular AuNPs uptake.	[5]
RAW 264.7 and MDA-MB-231 cells	(4 and 10 nm)	Gadolinium chelate-AS1411 conjugated AuNPs (with or without PEG)	(30 nM)	(90 min–4 h)	PEG coating failed to reduce protein adsorption. AuNPs uptake by macrophages varied depending on configurations such as aptamer configurations and PEG chain length. PEG modification and nanoparticle size reduction increased AuNPs uptake.	[69]

(continued on next page)

Table 1 (continued)

Cell types	Particle Dimensions	Particle Surface Group	Concentrations	Time of Exposure	Effects	References
Neonatal rat cardiomyocyte cells	(5, 18 and 25 nm)	PEG modified AuNPs	(100 μM–1 pM)	(5 and 10 days)	PEG-coated AuNPs were non-toxic under all the conditions (size, concentration, and time).	[70]
Cell types	Particle Dimensions	Particle Surface Group	Concentrations	Time of Exposure	Effects	References
HEK 293 T cells	(10 nm)	AuNPs	(12–800 μg/mL)	(24 h)	No significant cellular viability effects.	[71]
A 549 and Vero cells	(20 nm)	AuNPs	(20–100 μg/mL)	(48 h)	Biogenically synthesized AuNPs showed toxic effects on the cells at a concentration of 60 μg/mL.	[72]

Abbreviations: AuNP: spherical gold nanoparticle, AuNR: gold nanorod, AuNS: gold nano star, L5178Y: mouse lymphoma cell line, MRC-5: human fetal lung fibroblast cells, Hela: human cervix adenocarcinoma cells, A 549: human alveolar epithelial cells, PEG: polyethylene glycol, HaCaT: human keratinocyte cells, TMAT: trimethylammonium ethanethiol, MES: mercaptoethanesulfonate, MEEE: mercaptoethoxyethoxyethanol, COS-1: fibroblast-like cell lines derived from monkey kidney tissue, C17.2: cellosaurus cell line, PC12: pheochromocytoma cell line from the adrenal medulla, HUVECs: Human Umbilical Vein Endothelial Cells, Balb/3T3: mouse fibroblast cell line, Vero: African green monkey kidney cells, NIH3T3: mouse embryonic fibroblast cells, MRC5: human normal lung fibroblast cells, HL-60: human leukemia cells, HepG2: hepatoma cells, PCD: positively charged and stable AuNP-dendron conjugates, U-87: human glioblastoma cells, PC-3: human prostate cancer cells, MDA-MB-231: human breast cancer cells, HT-29: human colon cancer cells, RAW 264.7: mouse macrophage cells, CTAB: cetyltrimethylammonium bromide, PSS: poly(sodium 4-styrenesulfonate), mSiO₂: inorganic mesoporous silica, dSiO₂: dense silica, TiO₂: titanium dioxide, PAH: poly allylamine hydrochloride, HSC: hepatic stellate cells, BSA: bovine serum albumin, HDF: human dermal fibroblast cells, PAA: poly(acrylic acid), hESC: human embryonic stem cells, MSA: mercaptosuccinic acid, CaSki: human cervical cancer cells, DNA: deoxyribonucleic acid, hMSC: human mesenchymal stem cells, SH-SY5Y: human neuroblastoma cell line, HT29: human colorectal adenocarcinoma cells, OVCAR/SKOV: ovarian cancer cells, DU145: human prostate cancer cells, MTAB: (16-mercaptohexadecyl) trimethylammonium bromide, VSMC: rat vascular smooth muscle cells, PDDAC: poly-diallyl dimethyl ammonium chloride, HaCaT: human keratinocytes cells, L929: human fibroblast cells, KGF: keratinocyte growth factor, TN: therapeutic thionine dye, 7721/GES-1: cellosaurus cell line, 4T1: mouse mammary tumor cells, L02: normal human hepatocyte cells, d: diameter, E17.5: embryonic mouse hippocampus neurons, NRK: normal rat kidney epithelial cells, dPGS: dendritic polyglycerol sulfate, PEI: poly-ethyleneimine, SW620: human colorectal adenocarcinoma cells, HEK293: human embryonic kidney cells, HCT116: human colorectal adenocarcinoma cells, LS174T: colorectal adenocarcinoma cells, DRG: primary mouse dorsal root ganglion sensory neurons. Huh7: human hepatocellular carcinoma, PC3: human prostate cancer cell line, BEL7402: cellosaurus cell line, HFF: fibroblast cells.

higher amounts and also the toxic effects were eliminated [46]. When evaluated the cytotoxicity of the AuNRs (22 nm × 82 nm) with different surface modifications (PSS, PEG, CTAB, dSiO₂, mSiO₂, or TiO₂) on the various cell types, (PC-3, U-87, RAW 264.7, MDA-MB-231, HT-29 and HepG₂ cells) systematically; CTAB, PSS or mSiO₂ coated AuNRs showed toxic effects but other ones did not induce the cellular damage [43].

In addition to the surface modification, the absence/presence of serum in the biological media and the concentration of AuNRs used also have a determining effect on the cellular toxicity [56,60]. Possible toxic effects of AuNRs may also vary based on the cell type. In a study where phospholipid coating was used instead of CTAB on AuNRs (13 nm × 57 nm); SW620, HCT116 and LS174T cells showed 100 % viability even at high dose (200 μg/mL), while some toxicity was observed in HEK293 cells [68].

2.2. In vivo toxicity and systemic biodistribution of gold nanoparticles

Since a whole animal is more complicated than a single cell, there is a greater need for *in vivo* toxicological and biodistribution studies of gold nanoparticles. Some important current *in vivo* studies selected from the literature to understand the toxicological and organ/tissue distribution effects of AuNPs are systematically summarized in Table 2 [5,45,54,55,58,61–63,65,66,68,73–90]. In addition to the size, shape and dose of Au nanomaterials selected in the studies; the organism used, the routes of administration, and the duration of exposure determine the possible effects of AuNPs. The route of administration is mostly intravenous (IV) injection, but there are also intraperitoneal (IP), subcutaneous, abdominal, topical and intragastric administration routes.

Foreign materials in the bloodstream are initially defined by reticuloendothelial system (RES) elements via the process of opsonization. Then these foreign substances are mainly delivered to spleen and liver via being coated with antibodies to be eliminated by macrophage cells in these RES organs. In this respect, the liver and spleen are the most permeable organs in terms of nanomaterial accumulation [91]. Significant toxic effects have been reported in some systemic toxicity and distribution studies using small-sized bare spherical-shaped AuNPs. Balasubramanian et al. reported that accumulation of the AuNPs mostly

in the spleen/liver and important expression changes in most genes related to toxicity/metabolism in these organs as a result of IV injection of the Au-nanomaterials (diameter: 20 nm) into the Wistar rats [78]. Differently, Lasagna-Reeves et al. showed that they did not encounter any toxic findings despite high accumulation in the spleen and liver as a result of IP injection of AuNPs (diameter: 12.5 nm) into C57/BL6 mice [76]. In some *in vivo* studies conducted to compare the toxic effects of bare gold nanoparticles of various sizes (diameters: 5, 10, 20, 30 and 50 nm), it has been reported that smaller sized AuNPs generally lead to greater toxic effects. The size of the AuNPs also determined the differences in *in vivo* biodistribution and excretion pathway [61,63,81]. According to *in vivo* toxic effect and biodistribution studies of bare AuNPs, although different results have been obtained, it is evaluated that small sized AuNPs cause more toxic effects, parallel to the data obtained in cell studies.

Based on the fact that small sized bare AuNPs were more toxic, the toxicity and distribution of various small sized AuNPs (diameters: 1.2, 6, 13 and 16 nm) whose surfaces have been modified with various molecules (PEG, glutathione, p-CALNN, CS or PEI) have been investigated on a large scale in some *in vivo* studies. In these studies, thanks to the additional surface functionalization of AuNPs, a higher amount of stable AuNPs distribution was reported in various tissues/organs such as spleen and liver in the long term. Also, the surface coatings of the AuNPs resulted in generally negligible levels of low toxic effects and immunogenicity [74,81,83,86]. There are also some *in vivo* studies where both the surface modification and size effects of AuNPs were evaluated together. Zhang et al. reported that 10 and 60 nm sized particles were more toxic than 5 and 30 nm sized AuNPs, as a result of IP injection of four different sized PEG-coated AuNPs into the mice [79]. Similarly, in a study using AuNPs of four different sizes whose surfaces were coated with PEG, it was reported that smaller sized AuNPs showed effective biodistribution in the other organs in addition to the liver and spleen [54]. Ozcicek et al. reported that smaller sizes led to greater distribution in the mice tissues and additional PEG or PEI surface coating promoted AuNPs biodistribution, as a result of IV injection of AuNPs with two different sizes (20 and 50 nm) and surface functionalization (PEG or PEI) into the BALB/c mice [5]. The surface properties of AuNPs are one

Table 2
Some *in vivo* toxicity and biodistribution studies of gold nanoparticles.

Organism used	Particle Dimensions	Particle Surface Group	Doses/Routes of Administration	Time of Exposures	Effects	References
C57BL/6 mice	(IV: 2 and 40 nm; IP: 40 nm)	AuNPs-citrate	(IV/IP–2 nm: 1 mL of solution–12 µg/mL; IP–40 nm: 1 mL of solution–58 µg/mL)	(1, 4 and 24 h)	IV: Rapid aggregation of the endocytosed AuNPs in liver macrophages; IP: Accumulation of AuNPs in the spleen/liver, regardless of size. No penetration by the placental barrier.	[73]
BALB/c mice	(13 nm)	PEG coated AuNPs	(0.17, 0.85, 4.26 mg/kg; IV)	(5 and 30 min.; 4 and 24 h; 7 days)	High accumulation in spleen and liver; long circulation in blood. Apoptosis and acute inflammation in the liver. Vesicles and lysosomes containing PEG-modified AuNPs in Kupffer cells of liver and spleen-macrophages.	[74]
CD1 mice	(15 nm)	PAH or PSS coated AuNPs; HSA additional coating	(150–200 µL; IV)	(7 days)	The highest AuNP concentration in the heads of mice was detected between 19 and 24 h. The main accumulation of AuNPs occurred in the hippocampus, thalamus, hypothalamus, and cerebral cortex.	[75]
C57/BL6 mice	(12.5 nm)	AuNPs-citrate	(40, 200 and 400 µg/kg; IP–every day)	(8 days)	AuNPs accumulation was highest in the liver and spleen, and least in the brain. No evidence of toxic effects was observed.	[76]
ICR mice	(13.5 nm)	AuNPs	(137.5–2200 µg/kg; oral, IP and IV)	(14–28 days)	While low doses of AuNPs did not cause toxic effects, high doses affected the organ index. IV NPs administration was toxicologically safest.	[77]
Wistar rats	(20 nm)	AuNPs-citrate	(0.2-mL AuNPs: 15.1 mg/mL; IV)	(1 day; 1 weeks; 1 and 2 months)	AuNPs accumulated predominantly in the spleen and liver, and most gene expression changes (related to, lipid metabolism, detoxification, cell cycle, circadian rhythm, and defense response) occurred in the organs.	[78]
Organism used	Particle Dimensions	Particle Surface Group	Doses/Routes of Administration	Time of Exposures	Effects	References
Mice	(5, 10, 30 and 60 nm)	PEG coated AuNPs	(4000 µg/kg; IP)	(28 days)	Spleen and liver are the major organs with the highest accumulation. The toxicity of the 10 nm and 60 nm sized AuNPs was clearly higher than that of the 5 nm and 30 nm sized AuNPs.	[79]
Wistar rats	(20 nm)	AuNPs	(20 µg/kg–every day for 3 days; IP)	(24 h after last dose)	Significant oxidative stress, increased lipid peroxidation, DNA damage and inflammatory response in the brain.	[80]
Wistar-Kyoto rats	(Spherical ones: 10 and 20 nm; hexagonal: 50 nm)	AuNPs	(50 and 100 µL; IP infusion)	(3 and 7 days)	Hepatocyte damage, atrophy, necrosis, and phagocytic activity, especially caused by smaller sized and administered in high doses AuNPs.	[81]
Balbc/cAnNHsd mice	(1.2 nm)	Glutathione coated AuNPs	(0–60 µM in 200 µL PBS; subcutaneous)	(24 h; 2–4 weeks)	No illness or stress, low immunogenic effect and greater AuNPs distribution in the kidney, liver, and spleen in the long term.	[82]
Wistar rats	(16 nm)	AuNPs-citrate or p-CALNN coated AuNPs	(0.7 mg/kg; IV)	(30 min. and 28 days)	Enhanced distribution of pentapeptide-coated AuNPs to organs other than liver/spleen, intact liver histology and no <i>in vivo</i> toxicity.	[83]
SD rats	(2.5 nm)	AuNPs	(12–24 µg/per injection, abdominal)	(2, 6, 16, 24, 36 and 48 h)	Similar AuNPs biodistribution in the organs, biological half-life: 12.9 ± 4.9 h. Most of the gold in the brain were in venous blood rather than tissue.	[84]
Balb/c mice	(7 nm × 30 nm and 14 nm × 56 nm)	CTAB, oleate or BSA modified AuNRs	(5 mg/kg; IV)	(1, 5, 10, 15 and 30 days)	Smaller sized AuNRs preserved their physicochemical properties and accumulated mostly in the spleen and liver.	[45]
Organism used	Particle Dimensions	Particle Surface Group	Doses/Routes of Administration	Time of Exposures	Effects	References
Balb/c mice	(2 nm)	TEG stabilized AuNPs (+/-)	(2 µM in 50 µL; IV)	(24 h)	Surface charge of nanoparticles determined suborgan biodistribution of the AuNPs.	[85]
Mice	(6.2, 24.3, 42.5 and 61.2 nm)	PEG coated AuNPs	(3 mg/kg; IV)	(4, 24 and 48 h; 6, 10, 20, 30 and 90 days)	While larger sized AuNPs accumulated mostly in the spleen and liver, smaller sized ones were distributed in other tissues in addition to these organs. Most of the AuNPs were cleared from the organs within 30 days.	[54]
C57/BL6 mice	(26 nm × 54 nm)	MTABAuNRs	(0.37 and 1.8 mg/kg; IV)	(24 h and 10 days)	AuNRs accumulate mostly in the liver, spleen and lungs. No toxicity and normal spleen pathology. High stability and biocompatibility.	[55]
SD rats	(60 nm)	KGF conjugated AuNPs	(5.75×10^{-11} M in hydrogel; topical)	(10 days)	KGF-conjugated AuNPs promoted wound healing by promoting re-epithelialization rather than granulation in the wound model.	[58]

(continued on next page)

Table 2 (continued)

Organism used	Particle Dimensions	Particle Surface Group	Doses/Routes of Administration	Time of Exposures	Effects	References
Wistar rats	(10, 30 and 60 nm)	AuNPs-citrate	(0.4 mL/day from stock solution; IP)	(9 days)	Size of the AuNPs determined the differences in <i>in vivo</i> biodistribution and excretion pathway.	[61]
Wistar rats	(50–70 nm)	AuNPs	(toxic and non-toxic doses; IP)	(3 days)	Slight changes in the liver and kidney as a result of low dose AuNPs administration. High dose AuNP caused mild toxic effects in all the organs.	[62]
BALB/c mice	(5, 20 and 50 nm)	AuNPs	(0.5 mg/kg; IV)	(7 and 14 days)	The most detected NPs group in the liver, spleen and blood circulation was 50 nm sized AuNPs. Increase in neutrophil count and mild hepatotoxicity as a result of exposure to 5 nm diameter AuNPs.	[63]
Organism used	Particle Dimensions	Particle Surface Group	Doses/Routes of Administration	Time of Exposures	Effects	References
CD1 mice	(18 nm)	PEG coated Cy5.5-AuNPs	(IV: 200 μL of solution—0.11 μg/mL; IP*: 1 μL of solution—1.1 μg/mL)	(2, 5, 15, 30 days)	Penetration of the AuNPs into the brain parenchyma, biodistribution preferentially in neurons rather than microglia and high stability resulting from resistance to cellular metabolism.	[65]
Balb/c mice	(50 nm)	AuNPs-citrate	(30, 60 and 90 nM—200 μL per mouse every day; intragastric)	(18 days)	Gold nanoparticle exposure caused some early pathological changes in the kidneys, which increased dose-dependently.	[66]
CD-1 mice	(6 nm)	PEG, CS or PEI coated AuNPs	(5, 5, 0.8 μg/g respectively; IV)	(0.5–24 h; 7–28 days)	The surface chemistry of AuNPs determined the <i>in vivo</i> biodistribution, uptake, excretion, and stability of the modified nanoparticles.	[86]
SD rats and <i>Macaca fascicularis</i>	(12 nm × 47 nm)	PEG coated AuNRs	(5, 10 and 20 mg/kg; 1 mg/kg respectively; IV)	(2 and 12 weeks)	No significant toxicity and histological abnormality, AuNPs biodistribution mostly in the RES organs.	[87]
Wistar mice	(AuNPs: 21–24 nm; AuNRs: 12 nm × 40 nm; 23 nm × 79 nm)	Citrate stabilized or AuNPs-PEG; CTAB, PEG, Cys, Mph, Chol or DSPE coated AuNRs	(0.250 mL—60 μg Au; IP)	(6 h)	Mph-functionalized AuNRs showed high penetration into the brain with the ability to cross the BBB. The increase in the size of AuNRs slowed the NRs accumulation in the brain while maximizing the other organs. PEG-coated AuNPs showed maximum toxicity despite high biodistribution in the organs.	[88]
Organism used	Particle Dimensions	Particle Surface Group	Doses/Routes of Administration	Time of Exposures	Effects	References
BALB/c nude mice	(13 nm × 57 nm)	CTAB-Oleate, DOPC-DSPE lipids-mPEG or PSS modified AuNRs	(100 μL of solution—2000 μg/mL; IV)	(1–9 days)	High accumulation of AuNRs in the spleen and liver decreased in course of time. Small amount of nanorod distribution in the other organs. No toxic effects were found. A small fraction of the injected AuNRs dose reached the subcutaneous tumor tissue.	[68]
C57BL/6 mice	(20 nm)	AuNPs-citrate	(150 μL of solution—2.9 × 10 ¹¹ AuNPs; IV)	(6 h)	Reduced inflammation in cerebral micro vessels in the sepsis model, increased BBB penetration, decrease in TNF concentration in the brain and reduction in ICAM-1 expression in cerebral blood vessels/PMN leukocytes.	[89]
BALB/C mice	(20 and 50 nm)	AuNPs-citrate, AuNPs-PEG, or AuNPs-PEI	(5 mg/kg; IV)	(1, 5, 15 and 30 days)	The spleen and liver had the highest accumulation of AuNPs, while the brain was the most selective organ. Smaller AuNPs accumulated more in the tissues. The PEG coating promoted the biodistribution of AuNPs more than PEI.	[5]
Zebrafish (<i>Danio rerio</i>) embryo-larvae	(10, 20, 40, 80 and 100 nm)	(TNFα, NHS/PAMAM and PEG coated AuNPs)	(0.25–2 mg/L; adding to the media)	(24 and 72 h)	Size and time dependent accumulation of AuNPs in the intestine and pronephric tubules. No kidney damage or cellular oxidative stress was observed. PEG or TNFα surface coating increased the accumulation of AuNPs in the pronephric tubules.	[90]

Abbreviations: AuNP: spherical gold nanoparticle, AuNR: gold nanorod, IV: intravenous injection, IP: intraperitoneal injection, min.: minutes, PEG: polyethylene glycol, PAH: polyallylamine hydrochloride, PSS: polystyrene-4-sulfonate, HAS: human serum albumin, p-CALNN: pentapeptide consisting of the amino acids Cys-Ala-Leu-Asn-Asn, SD: Sprague Dawley, MTAB: (16-mercaptophexadecyl) trimethylammonium bromide, KGF: keratinocyte growth factor, IP*: intraparenchymal injection, PEI: polyethyleneimine, CS: chitosan, CTAB: cetyltrimethylammonium bromide, Cys: cysteamine, Mph: 4-mercaptoethanol, Chol: cholesterol, TNFα: tumor necrosis factor, NHS/PAMAM: N-Hydroxysuccinimide/Poly(amidoamine), PMN: polymorphonuclear leukocytes.

of the most important features as they can seriously influence the interactions between gold nanomaterials and biological targets affecting their cellular uptake, stability, toxicity, biodistribution, and capability to avoid immune clearance. Appropriate functionalization of the AuNPs surface has been reported to be a successful approach to moderate biological properties of gold nanomaterials, achieving needed therapeutic efficacy *in vivo* without causing any toxic effects.

The application route, surface charge and concentration of nanoparticles used *in vivo* studies to organisms are other important

parameters that affect the biodistribution and possible toxic effects of nanoparticles. Elci et al. reported that the surface charge of AuNPs determined sub-organ biodistribution of the TEG stabilized AuNPs (diameter: 2 nm) [85]. In a study comparing IV or IP administration of AuNPs-citrate (diameter: 13.5 nm) to ICR mice, the IV route of administration was shown to be toxicologically safer [77]. In two different studies using varying doses of AuNPs, it was reported that increasing nanoparticle concentration caused evident cytopathological changes in the various organs [62,66]. Similar to cellular studies, in systemic

studies, a variation in the shape of Au-nanomaterials may affect their possible toxic effects. Some *in vivo* studies based on AuNRs have revealed findings on these issues. In a mice *in vivo* study using AuNRs with different sizes (7 nm × 30 nm and 14 nm × 56 nm) and surface modifications (CTAB, oleate or BSA), it was reported that smaller sized nanorods mostly accumulated in the liver and spleen by preserving their physicochemical properties [45]. Appropriate surface functionalization (such as MTAB, PEG, DOPC-DSPE lipids and PSS) applied to the AuNRs generally increased their stability and *in vivo* biocompatibility [55,68, 87].

The blood-brain-barrier (BBB) is a highly selective layer that prevents the entry of harmful materials into the brain and central-nervous system (CNS) and regulates the passage of different molecules, including nanoparticles. These very selective characteristics of the BBB make it difficult to deliver diagnostic and therapeutic materials to the brain. In a study conducted within the scope of brain research on AuNPs (15 nm

sized; PAH or PSS modified particles and HAS additionally coating) in CD1 mice, it was shown that AuNPs accumulated mostly in the thalamus, hypothalamus, cerebral cortex parts and hippocampus of the brain [75]. In a study conducted by IP injection of bare AuNPs without any surface coating into the Wistar rats, Siddiqi et al. reported significantly increased oxidative stress, lipid peroxidation, DNA damage and inflammatory response in the brain of the rats [80]. This result reveals that it is not enough for nanoparticles to reach the brain and also suitable surface functionalization is necessary so that the AuNPs can be used as theragnostic safely in terms of nanotoxicology. A frequently preferred surface modification such as PEG not only increases the biocompatibility of AuNPs in the mice brain but also increases their stability and uptake in neurons rather than glial cells [65]. In an *in vivo* Wistar mice study in which the varying sizes and surface modifications of gold nanorods were investigated together, it was reported that Mph-modified AuNRs had the highest level of BBB penetration. In the same study, it was shown that

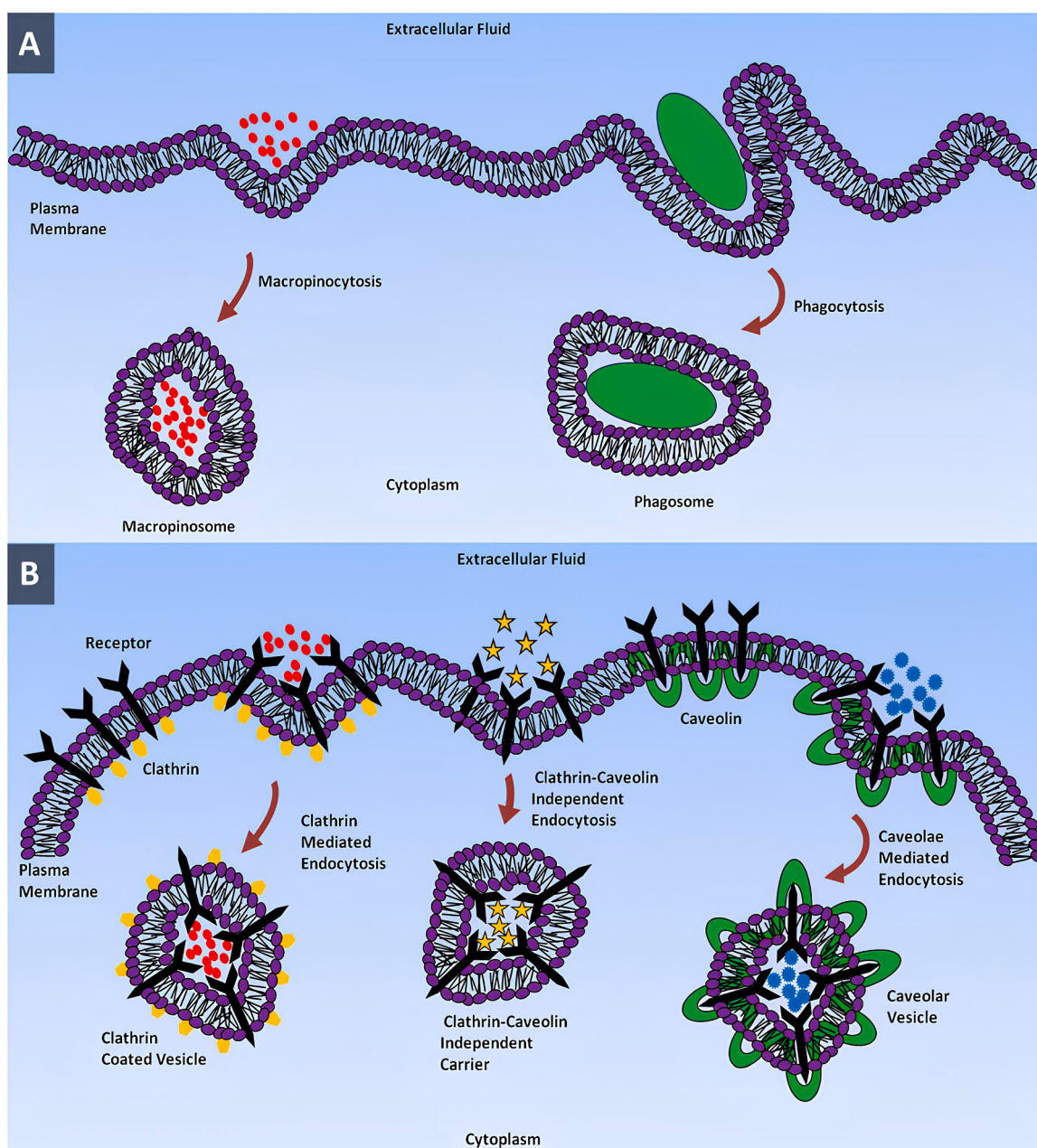


Fig. 5. Entry of nanoparticles into cells using different endocytic pathways. (A) Macropinocytosis and phagocytosis. (B) Clathrin-mediated endocytosis, clathrin-caveolin independent endocytosis and caveolae-mediated endocytosis. Adapted with permission from reference [97]. Copyright (2018), Springer Nature.

increasing the size of AuNRs slowed down nanoparticle accumulation in the brain while maximizing it in other organs [88].

Further animal model studies are needed to define the clearance, biodistribution and toxicological effects of gold nanoparticles. Furthermore, these valuable *in vivo* studies of gold nanoparticles are very valuable in terms of shedding light on the theragnostic applications of metallic nanoparticles. A systematic nanotoxicity investigation must be applied for each specific case under precise controlled conditions before biomedical applications of gold nanoparticles can be carried out in humans. Again, it should be considered that *in vitro* cellular conditions are different and enough to not fully reflect the real *in vivo* environment. The low cellular/*in vivo* toxicity and non-immunogenicity of most AuNPs-based studies in the literature make us relatively hopeful concerning their future potential nanomedicine applications.

Most AuNP-based preclinical studies conducted to date have demonstrated good safety profiles with minimal toxicity. However, the limited number of comprehensive nanotoxicological studies leaves a poor understanding of the adverse effects of long-term gold accumulation in the body. Since AuNPs exhibit different nanotoxicological profiles depending on the synthesis method, size, shape, surface functionalization and route of administration, each formulation needs to be examined separately to understand the biodistribution, pharmacokinetics and possible toxicological profile of AuNP-based systems. These situations remain significant limitations in the translation of AuNPs into clinical settings. Unlike most multifunctional nanoparticles reported in the literature, AuNPs that are being investigated clinically need to have predictable *in vivo* behavioral profiles. In this respect, AuNPs with simpler compositions seem to be essential. This situation is a significant barrier to the clinical transition of complex hybrid nanostructures with many components. As a result of excessive surface functionalization, AuNPs remain in the body for longer periods of time, and their potential for toxic effects due to the components increases. In order to alleviate concerns about long-term gold accumulation in the body, the benefits of AuNP-based treatments must outweigh the potential risks of toxic effects.

3. Gold nanoparticles in cancer therapy

According to American Cancer Society statistics published in 2024, more than 2 million new cancer cases occur every year in the United States alone (the equivalent of about 5480 diagnoses each day). These newly diagnosed cancer cases lead to over 600,000 deaths annually [92]. Radiotherapy, chemotherapy, and surgery are used in traditional cancer therapy. Treatment plans are created for each cancer patient according to the type and stage of the disease, and radiotherapy using high ionizing radiation is the most common therapy option. On the other hand, despite the widespread use of radiotherapy, normal tissue toxicity is a major problem [93,94]. Similarly, side effects and bioavailability problems of the anti-cancer drugs used in chemotherapy are limiting aspects of traditional chemotherapeutic approaches [95].

Among the gold-based nanotherapeutic materials produced in different shapes (such as rod, spherical, star, shell, cluster), spherical AuNPs are the most widely used nanotherapeutic material. The advantageous aspects of spherical AuNPs are that they can be synthesized easily and that the physicochemical structure of their surfaces is suitable for additional modifications [30,96]. As shown in Fig. 5, there are different pathways for nanoparticles to enter the cells, including clathrin-caveolin-independent, clathrin-mediated, and caveolae-mediated endocytosis except pinocytosis/phagocytosis pathways [97].

AuNPs enter cells mostly by receptor-associated endocytosis (RME). Interactions between ligand molecules on nanoparticle surfaces and cell membrane receptors play a significant role in the effectiveness of this process. In the next step, the nanoparticles invaginate from the membrane and they are internalized into the cells by endosomal vesicles. The AuNPs with appropriate surface functionalization, size and physicochemical properties can escape from these endosomal/lysosomal

pathways and remain in the cytoplasm and nucleus in sufficient quantity and time for therapeutic effectiveness. In this context, AuNPs provide promising results in the cancer therapy area, considering their fascinating physicochemical/optical properties, stability, size, and easy modification [7,93,96,98].

Especially for *in vivo* applications, nanoparticle application through the animal's tail vein is one of the most advantageous methods in terms of bioavailability and toxicity. In terms of avoiding reticulo-endothelial system (RES) elements and the opsonization process, the shape, size and especially appropriate surface modification of the AuNPs are the determining parameters [99].

3.1. Gold nanoparticle based cancer therapy using chemotherapeutic drugs and other agents

In chemotherapeutic approaches where chemical drugs are used in cancer therapy, unfortunately the therapeutic agents cannot reach the cells in the cancerous tissue at sufficient levels and cause serious toxic side effects. Moreover, drug resistance emerges over time due to some metabolic and structural changes in cancer cells. Thus, there is a need for innovative drug transport systems that will increase the accumulation and bioavailability of the cancer drugs at the target site and at the same time reduce their undesirable toxic side effects [100,101].

In a study, Malik et al. synthesized AuNPs (sizes: 20–50 nm) using *Gymnema sylvestre* leaf extract, honey and *Aloe vera*, and performed conjugation with some FDA-approved anticancer drugs (HIF1- α inhibitor, 4-hydroxy Tamoxifen, and ODQ) after PEG coating. When the activities of the designed nanoconjugates were investigated on invasive ductal carcinoma breast cells, it was reported that 4OHT conjugated AuNPs showed significant anticancer activity in three different drugs [102]. In another study using the glioma tumor model (rat C6), the BBB permeability of AuNPs-PEG of different sizes (diameters: 5–90 nm) was tested. The study also used retro-inverso bradykinin (RI-BK), which selectively increases BBB permeability without damaging normal brain tissue. The AuNPs of 70 nm size have been reported to have maximum glioma permeability [103]. Doxorubicin (DOX) is a common chemotherapy drug that provides effective results in the treatment of multiple malignancies. Due to the hydrophobic structure of the DOX molecule, its stability and specificity must be increased. For this purpose, mPEG molecules with DOX at one end and a thiol group at the other end are generally used [104]. Cui et al. reported that when they modified the amino and carbonyl groups of DOX with mPEG and lipoic acid (LA), respectively, the stability, dispersion, and solubility of the resulting ultrasmall sized gold nanoconjugate increased (Fig. 6) [105].

It has been shown that following endocytosis of nanoconjugates by the cells, DOX is released in two basic stages: response to the acidic microenvironment in the lysosomes and production of free DOX by esterases in the cytoplasm. Thus, as a result of this innovative drug release design, the cytoplasm served as a reservoir for sustained drug release into the nucleus. As a result, highly increased antitumor activity of designed gold nanoconjugates compared to the free DOX molecule was demonstrated [105]. In another study, it has been shown that as a result of the conjugation of synthesized DOX analogues and PEG stabilizing ligands to AuNPs (diameter: 49 nm), the drug release can be succeeded by the effect of reducing agents such as glutathione or under acidic conditions. In the *in vivo* evaluation of the designed nanoconjugates on the mice, it was reported that the conjugates were quite stable under physiological conditions and did not cause any histopathological observable differences [106]. In a study conducted within the scope of cancer stem cell (CSCs) therapy, it was shown that AuNPs (diameter: 30 nm) bound to DOX through an acid-labile hydrazone and a PEG spacer bond significantly reduced the mammosphere formation capacity and cancer-initiating activity PEG spacer on the cells. It was also revealed that the application of nanoconjugate caused an important increase in the tumor growth inhibition in the mice tumor model. Drug delivery mediated by AuNPs also highly reduced tumor growth in the

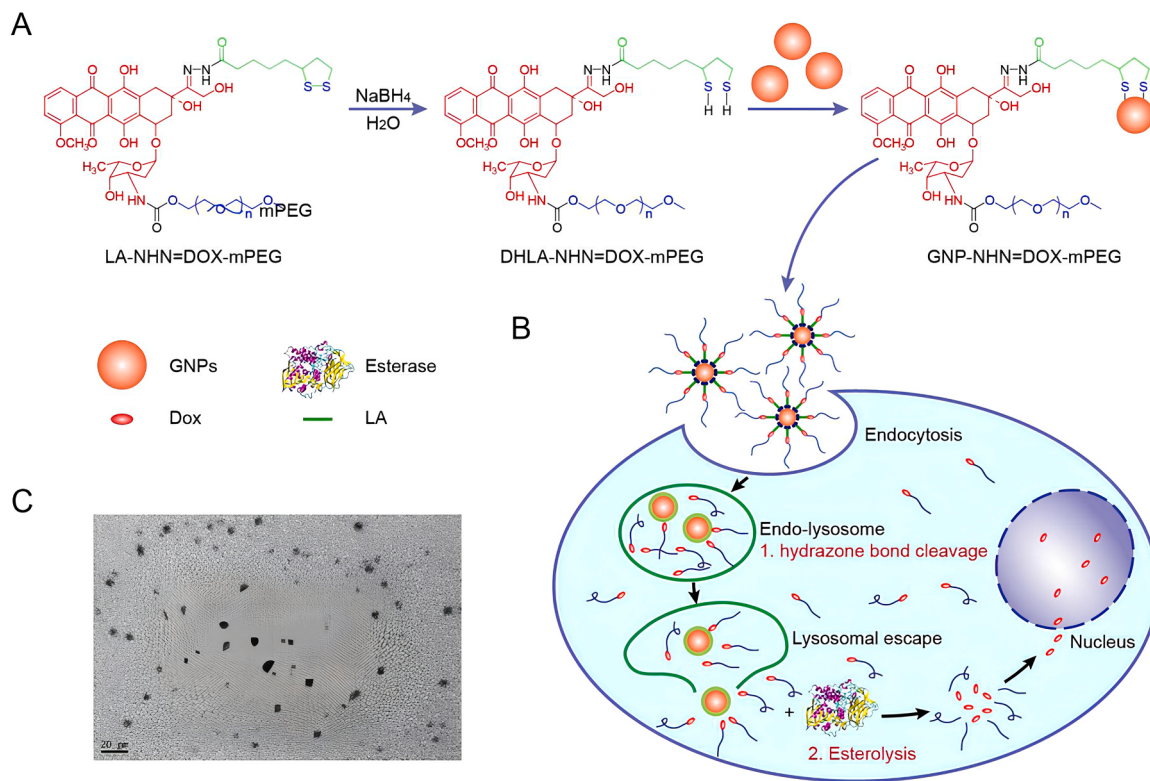


Fig. 6. (A) The structure of GNP-NHN=DOX-mPEG. (B) An illustration of its intracellular drug release mechanism. (C) TEM image of GNP-NHN=DOX-mPEG. The scale bar is 20 nm. Adapted with permission from reference [105]. Copyright (2017), American Chemical Society.

off-treatment phase by reducing breast CSCs in tumors [107].

Physicochemical properties that vary depending on the size of gold cores can affect many parameters, including cell penetration rate, efficacy, cytotoxicity, biodistribution and antitumor performance. In a study comparing gold cores of different sizes (10, 20 or 60 nm), it was reported that although the 60 nm Au-core conjugate had the highest drug releasing/loading efficiency, the 10 nm sized Au-core conjugate exhibited the best antitumor activity against the liver cancer models [108]. In addition to molecules such as DOX and PEG, there are also anticancer therapies using different specific ligands (such as peptides, proteins, dendrimers, and oligonucleotides) conjugated with AuNPs. In a study using a multifunctional AuNPs-based (Au-PEG-PAMAM dendrimer-DOX) drug delivery system platform (diameter: 20–25 nm) for pH-triggered intracellular delivery, it was proven that DOX released from nanoconjugates at pH of physiological level was negligible, but the release increased significantly in the weakly acidic environments. Thus, the authors reported that the biocompatible and stable nanoplatform they obtained showed significant anticancer activity on the A549 cancer cells, with effective release from lysosomes in a short time [109]. Ruan et al. aimed to increase BBB penetration and target glioma cells by using the PEG-DOX-AuNPs acid-responsive carrier platform (diameter: 39.9 nm) they developed, functionalized with angiopep2, a ligand specific to LRP1 (low density lipoprotein receptor-related protein-1). The intracellular density, stability, and glioma distribution of the delivery system were found to be higher in glioma-bearing mice [110]. In another study in which DOX-loaded oligonucleotides (ONTs) were conjugated to AuNPs (diameter: 13 nm, 80 % binding efficiency), high levels of anticancer cellular activity were achieved on the SW480 colon cancer cell line. Significant inhibition of tumor growth occurred after regular administration in the tumor-bearing xenograft mouse model [111]. Kalimuthu et al. used their selected peptide-drug conjugates with the AuNPs (diameter: 25–40 nm) to increase bioavailability and stability of the therapeutic agents. It has been shown that only the peptides had short half-lives, whereas in the conjugate form the duration was

significantly increased [112].

Paclitaxel (PTX) is an anticancer drug extensively used in first-line treatment for many types of solid cancer, including ovarian cancer and breast cancer. On the other hand, considering the low solubility of PTX, its adverse effects and drug resistance, some difficulties are encountered in the widespread use of this important drug [113]. Due to the developments in nanotechnology science, the targeted PTX nanoconjugates have been developed using various nano biomaterials, which promote stability, bioavailability, and controlled release of the drug, including Abraxane [114]. By using PAX conjugated with AuNPs, the bioavailability and loading capacity of the drug increases, normal healthy cells are less affected by toxic effects, the circulation time of the drug increases with improved stability, and also effective targeting can be achieved on the tumor cells [113,115–117]. Heo et al. demonstrated the AuNPs-5' (diameter: 20–40 nm) surface functionalized with PEG, biotin (a targeting ligand for cancer), PTX and rhodamine B-linked beta-cyclodextrin (β -CD, a drug pocket), therapeutic efficacy on the A549, MG63 and HeLa cells [118]. In a study, a series of thiol-terminated-(PEG)-(PTX) derivatives were conjugated with AuNPs. The synergistic release properties of the designed nanoconjugate significantly improved its long-term circulation, targeted PTX release in the cells of tumor, and enhanced tumor cell killing activity thanks to its increased stability in the biological environment [119]. In another study using folic acid-PTX modified AuNPs-PEG (diameter: 28 nm), which stimulated apoptosis by targeting the folate receptor overexpressed in cancer cells, higher levels of anticancer activity than free PTX have been demonstrated on the Hela, HL-7702, HCT-116 and SMMC-7721 cells [120]. The position of the drug also appears as an important parameter in AuNPs-PAX nanoconjugates. Wang et al. reported that nanoconjugates (diameter: 353 nm) containing PTX between AuNPs and PEG exhibited higher water solubility, biocompatibility, stability and increased anticancer therapeutic efficacy [121].

Apart from these drugs, the delivery and anti-cancer ability of AuNP-based hybrid materials has also been tested using flavonoids. Flavonoids

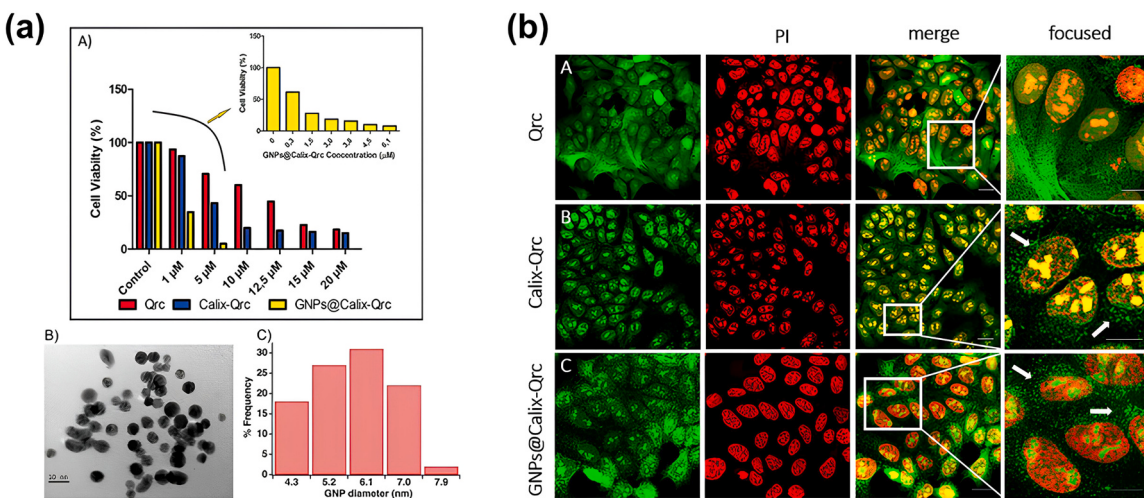


Fig. 7. (a) Cell viability and characterization results of the materials. (a-A) Viability of SW-620 cells after treatment with various concentrations of Qrc, Calix-Qrc, and the GNPs@Calix-Qrc complex measured by the Alamar Blue assay. Three sets of independent experiments were performed to calculate the mean values and standard deviations (SD) and analyzed by two-way ANOVA. $p < 0.0001$. (a-B) TEM image of the finely dispersed GNPs@Calix-Qrc complex and (a-C) Size distribution of GNPs as determined by TEM image analysis. (b) Cellular uptake of (b-A) Qrc, (b-B) Calix-Qrc, and (b-C) GNPs@Calix-Qrc in the DLD1 colon cancer cell line. Cells were incubated at 37°C with $10 \mu\text{M}$ of each compound for 45 min, then fixed and stained with propidium iodide, and analyzed by LSCM. In merged images, the scale bar = $20 \mu\text{M}$, and in focused images, the scale bar = $10 \mu\text{M}$. Vesicular-like structures indicated with white arrows. Adapted with permission from reference [133]. Copyright (2019), American Chemical Society.

are a class of easily purified secondary plant polyphenolic metabolites that have important anti-cancer, antioxidant and anti-inflammatory features. On the other hand, their poor water solubility and stability problems are the major obstacles to clinical bioavailability. In this direction, the rapid developments in nanotechnology science have enabled the synthesis of nanoconjugates that are stable, biocompatible and provide target-specific drug delivery [122]. There are some anti-cancer efficacy studies using AuNPs functionalized with the catechin epigallocatechin-3-gallate (EGCG), the primary flavonoid of green tea. In these studies, significant anticancer activity was demonstrated compared to the free agent in various cancer types (prostate, melanoma, and Elrich Ascites carcinoma), as a result of the successful functionalization of AuNPs of different sizes (1.6–610 nm diameter range) with EGCG [123–125]. Some studies have reported that quercetin (Qrc) has significant pharmacological properties, including anticancer, antioxidant, antibacterial and anti-inflammatory effects. Qrc is a polyphenolic bio-flavonoid substance and it has a very robust antioxidant effect by providing oxidative stability [126–128]. In some literature studies, it has been concluded that Qrc provides significant anticancer activity by promoting apoptosis, autophagy or inhibiting angiogenesis and metastasis in the selected cancer models (breast, adenocarcinoma, hepatocarcinoma, cervical, and liver cancers), as a result of its conjugated use with AuNPs of varying diameters (5.2–106 nm diameter range) [129–132]. Yilmaz et al. encapsulated Qrc in a supramolecular calix-arene scaffold to achieve the active compound releasing via pH-triggered way and achieve improved cytotoxicity against SW-620 cells. When they used the complex decorated with AuNPs (diameter: 6.1 nm), they achieved very strong cytotoxic *in vitro* results (51.9-fold enhanced cytotoxic activity) and considerable tumor growth-inhibition in the animal tumor model (Fig. 7) [133].

Curcumin is a polyphenolic natural material with encouraging therapeutic profits. But its poor water solubility and low bioavailability seriously limit its therapeutic use. These negative and disadvantageous properties of curcumin can be improved by using it simply and easily conjugated with AuNPs. Studies in the literature prove that various AuNPs-curcumin conjugations show increased cytotoxic and apoptotic activity on various types of the cancer cells (such as human prostate cancer cells, human colorectal adenocarcinoma cell line breast (MCF-7) human-cancer cells, colon (HCT-116) cell lines, SHSY5Y cells, PC-3 cells,

melanoma cells, A 549 cells, MDAMB-231 cells, DU 145 cells and SKBR-3 cells). In addition, these nanoconjugates enhanced antioxidant and anticancer activity by increasing the amount of cellular therapeutic agent uptake [134–142].

In recent years, significant efforts have been made to continue the synthesis of nanoparticles with green methods in order to reduce the toxic effects of nanomaterials in living systems [143]. Green synthesis methods of nanoparticles have a number of advantages such as simplicity, biocompatibility, cost-effectiveness and environmental friendliness [144,145]. Plant-mediated synthesis generally contributes to the synthesis of AuNPs with unique properties such as superior chemical stability, optical properties, streamlined shapes and sizes, as well as acceptable biocompatibility [146]. Biosynthesis of metallic nanoparticles using bacteria, fungi, truffles/tubers and plant extracts has become acceptable for pharmaceutical and medical applications such as nano drug delivery systems [147]. The findings of Al-Mafarjy et al. demonstrated that *Coleus scutellarioides* (L.) Benth leaf extract has the potential to be an effective bio reducer in synthesizing stable AuNPs with anticancer activity and antioxidant properties [148]. In a study where stable, environmentally friendly and rapid biosynthesis of AuNPs was achieved using a sonochemical technique, the mushroom extract was used as both a reducing and stabilizing agent. The researchers demonstrated the use of biosynthesized AuNPs as effective anticancer agents against MDA-MB-231 cells with 1.8 % cell viability at the highest concentration ($80 \mu\text{g/mL}$) [149]. In another study, the researchers designed a one-pot green protocol in which anticancer drugs (curcumin and doxorubicin) could be loaded directly onto the surface of AuNPs during their formation. They also demonstrated that low-intensity pulsed ultrasound (LIPUS) could be used to effectively induce the release of active agents from the surface of AuNPs in an ex vivo tissue model [150]. Donga et al. reported that the AuNPs synthesized using mango (*Mangifera indica*) seed extract, which is generally discarded into the environment, exhibited moderate anticancer activity and dose-dependent antioxidant activity in *in vitro* studies [151]. Natural anticancer agents are promising due to their biocompatibility. However, one of the major problems of using natural anticancer agents, such as curcumin, is their low bioavailability and solubility under physiological conditions. In one study, the researchers investigated the effect of green-synthesized AuNPs in enhancing the efficacy of curcumin as an

anticancer agent. They showed that the prepared AuNP-Cur nano-complex had higher apoptotic and antiproliferative effects against HCT-116 and MCF-7 cells compared to free curcumin [152]. Zhao et al. successfully synthesized a novel gold nanoparticle (Do-AuNP) from water extracts of *Dendrobium officinale* (DO) without using any chemical agents. Their results showed that Do-AuNP had better anti-tumor efficiency on liver cancer compared with DO extraction alone without increasing toxicity in vivo and in vitro [153]. In another study, Clarence et al. investigated the anticancer potentials of the AuNPs gained by green synthesis method using an endophytic strain *Fusarium solani* ATLOY – 8 has been isolated from the plant *Chonemorpha fragrans*. The AuNPs synthesized by researchers showed cytotoxicity against MCF-7 and HeLa cancer cells. Such successful results offer a versatile and significant biomedical application potential for a safer chemotherapeutic agent with low systemic toxicity [154]. In a study where aqueous *Anacardium occidentale* leaf extract was used in the preparation of AuNPs via green synthesis, the researchers showed that the nanoparticles they obtained showed good antibacterial activity against *Bacillus subtilis* and *Escherichia coli* and exhibited 74.47 % viability on PBMC cells and 23.56 % on MCF-7 cell lines at a maximum concentration of 100 µg/mL [155]. When all these literature results are evaluated together, it is clear that the production of AuNPs via green synthesis represents a more environmentally friendly, cost-effective and biocompatible alternative to traditional chemical synthesis methods. Bioactive constituents in plant biowastes act as stabilizing and reducing agents when AuNPs form. The synergistic role of such bioactive components on anticancer activity should not be ignored.

3.2. Gold nanoparticle based cancer therapy using PTT and combined approaches

Nanoparticle-mediated photothermal therapy (PTT) is a widely studied field with the advantage of providing targeted cancer therapy through hyperthermia in tumor tissue, alone or in combined approaches without damaging healthy tissues. In this approach, nanoparticles targeted at the tumor part are irradiated with a light source that produces heat, and as a result, apoptotic and necrotic pathways in the tumor cells are stimulated [156,157]. AuNPs with spherical, rod, star and cage-like shapes are frequently studied nanoparticles in cancer PTT area [156, 158].

The efficiency of PTT agent AuNPs synthesized in rod shape by optimizing in point of shape and size can be increased providing strong absorption in the near infrared region (NIR, 700–900 nm) as a result of the alteration in surface plasma resonance (SPR) [159]. As a result of

synthesis optimization in the spherical AuNPs, the LSPR absorption band is in the range of 500–600 nm [160]. The LSPR absorption band of Au-nanocages gold nanoshells and nanostars is in the NIR region [161–163]. Therefore, the progress of innovative synthesis methods for AuNPs optimized in point of shape, size and structure will increase the anti-tumor effectiveness of nanomaterials by maximizing the photothermal effect. At the same time, the duration, irradiation number, power density and wavelength of the laser light source used are the basic and determining parameters for obtaining successful hyperthermic results (Fig. 8). In addition, AuNPs can be used in a hybrid form with different types of nanomaterials (such as silica, iron oxide, graphene), therefore their optical properties can be improved and they can simultaneously play a hyperthermic role as an additional photothermal agent [164–166].

As a result of correct combinations and suitable surface functionalizations, AuNP-mediated PTT applications enable many biological changes that maximize the cytotoxic effect on cancer cells, reduce the required treatment dose in drug therapies, provide targeting and also enhance the effectiveness of cancer therapy [167,168]. The clinical application of PTT is limited by undesirable thermal damage to normal tissues, limited tissue penetration, and thermotolerance induced by HSPs. To overcome these limitations, the researchers designed a novel gene-photothermal synergistic therapeutic nanoplatform consisting of a highly branched Au nanoctopus (AuNO) core and a mesoporous polydopamine (mPDA) shell. They modified the CRISPR-Cas9 RNP-loaded nanocomplex with PEG-FA. They demonstrated that the developed system exhibited high photothermal conversion efficiency (PCE, 47.68 %) and excellent tissue penetration. Sequential coating of the system with RNPs and PEG-FA could reduce HSP90α expression in tumor sites, increase apoptosis, and reduce the heat resistance of cancer cells. These results are highly promising for overcoming the obstacles to the clinical use of AuNPs [169].

The eco-friendly and green synthesis of AuNPs from renewable sources such as bacteria, plants, fungi and algae has recently attracted great attention due to the use of sustainable raw materials. Despite all these promising developments, green synthesis of gold nanoparticles faces several challenges such as scalability, variability in particle size and limitations in morphology control, which need to be considered to fully utilize their potential [170]. In a study, Dheyab et al. produced the biocompatible AuNPs by an effective and green method using mango-peel extracts as both reducing and stabilizing agents through a sonochemical process. In particular, they reported that the synthesized AuNPs showed a remarkable photothermal effect at the concentration of 40 µgAu/mL, destroying about 66 % of MDA-MB-231 cells within

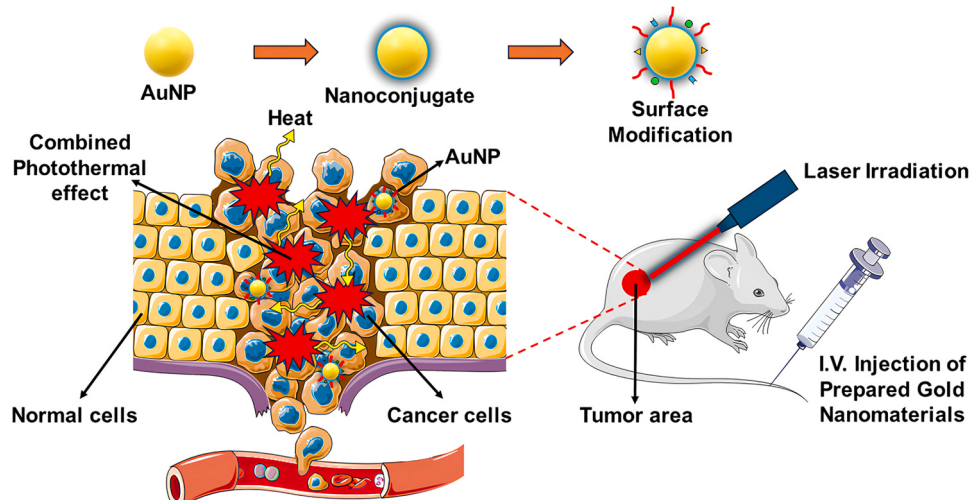


Fig. 8. Schematic illustration of combined PTT on cancer cells. This figure was produced using elements from the Server Medical Art PowerPoint image bank.

15 min of near-infrared laser irradiation [171]. In another study using a plant compound called apigenin (API), which has therapeutic potential, in AuNP synthesis, the researchers showed that the PTT they applied led to the indiscriminate destruction of almost half of both mouse fibroblastic (L929) and colorectal cancer (CT26) cells [172]. In their study, Shabani et al. green synthesized the AuNPs using Rutin extract as a reducing and stabilizing agent. They then investigated the therapeutic effects of these nanoparticles on breast cancer cells *in vitro* using a 500 mW laser with a wavelength of 532 nm. Their findings demonstrated the significant efficacy of Ru-AuNPs combined with laser radiation (150 J/cm² laser energy for 300 s) in the treatment of MCF-7 cells [173]. Wang and colleagues reported that stable Scu-AuNPs synthesized using Scutellaria barbata extract exhibited 70 % and 85 % cytotoxicity against A549 and 4T1 cells, respectively, under NIR irradiation. Unlike traditional chemotherapy, the Scu-AuNPs used by the researchers are part of a combination of chemotherapy and photothermal therapy [174]. The thermal effects of PTT at the tumor site can enhance the cellular penetration and absorption of therapeutic agents, thereby increasing the dose and bioavailability of drugs within the tumor.

3.2.1. Black phosphorus-gold hybrid nanomaterials for PTT

Several PTT studies have proposed an effective hybrid material complex based on AuNPs and black phosphorus (BP). BP, a new class of 2-dimensional nanomaterial, has attracted great interest in the PTT cancer therapy area in recent years thanks to its great physical and chemical advantages [175]. Yang et al. obtained BP nanosheets (BP-AuNSs) loaded with Au nanoparticles by an easy one-step synthetic method. They demonstrated that Au-nanomaterials not only increased the PTT activity of nanostructures but also endowed BP-AuNSs with the potential to act as powerful surface-enhanced Raman scattering (SERS) materials for Raman bio detection. The study showed that under irradiation with an 808 nm laser, BP-AuNSs were capable of generating

enough hyperthermia to exterminate the cancer cells, and the transplanted tumors disappeared in the majority of the tumor-bearing mice [176]. In another study, BP nanosheets integrated with AuNPs and polypyrrole (PPy) have been used synergistically for sonodynamic and PTT cancer therapy. The nanocomposites used in the study showed high-level *in vitro* sonodynamic and photothermal conversion effects on the tumor cells. Moreover, a high level of therapeutic efficacy was demonstrated in the 4T1 mouse tumor model, with negligible side effects reported [177]. Cancer immunotherapies have been developing rapidly in recent years and these are some of the most innovative and powerful methods of fighting malignancies. Jia et al. developed BP-Au-thiosugar nanosheets (BATNS) and showed in detail their high anticancer effects, photothermal conversion efficiency, enhanced stability and immunotherapy mechanism. Their demonstrated efficacy was achieved by promoting the infiltration of natural killer (NK) cells in a mouse hepatocellular carcinoma (HCC) model (Fig. 9) [178].

3.2.2. Iron oxide-gold hybrid nanomaterials for PTT

Iron-oxide nanoparticles (Fe_3O_4 -NPs) have excellent physical and chemical features which make them ideal for various nanomedicine applications. In addition, AuNPs have been preferred as a promising strategy for forming shells on the surface of Fe_3O_4 NPs thanks to their stability, fascinating optical features, and biocompatibility in recent years. Therefore, the arrival of effective PTT nanomaterials integrating Au shell NPs and magnetic Fe_3O_4 core will be of excellent importance for cancer therapy area [179].

When Dheyab et al. investigated the PTT efficiency of the Au-coated Fe_3O_4 nanoparticles (diameter: 20.8 nm) on the breast cancer-MCF-7 cell-line, they observed a significant cell reduction (73.8 %) after 10 min of NIR laser (808 nm, 200 mW) irradiation [179]. In another study, Au-coated superparamagnetic Fe_2O_3 (SPIONs) nanoparticles (16 nm in diameter) with MUC-1 aptamer surface modification as a

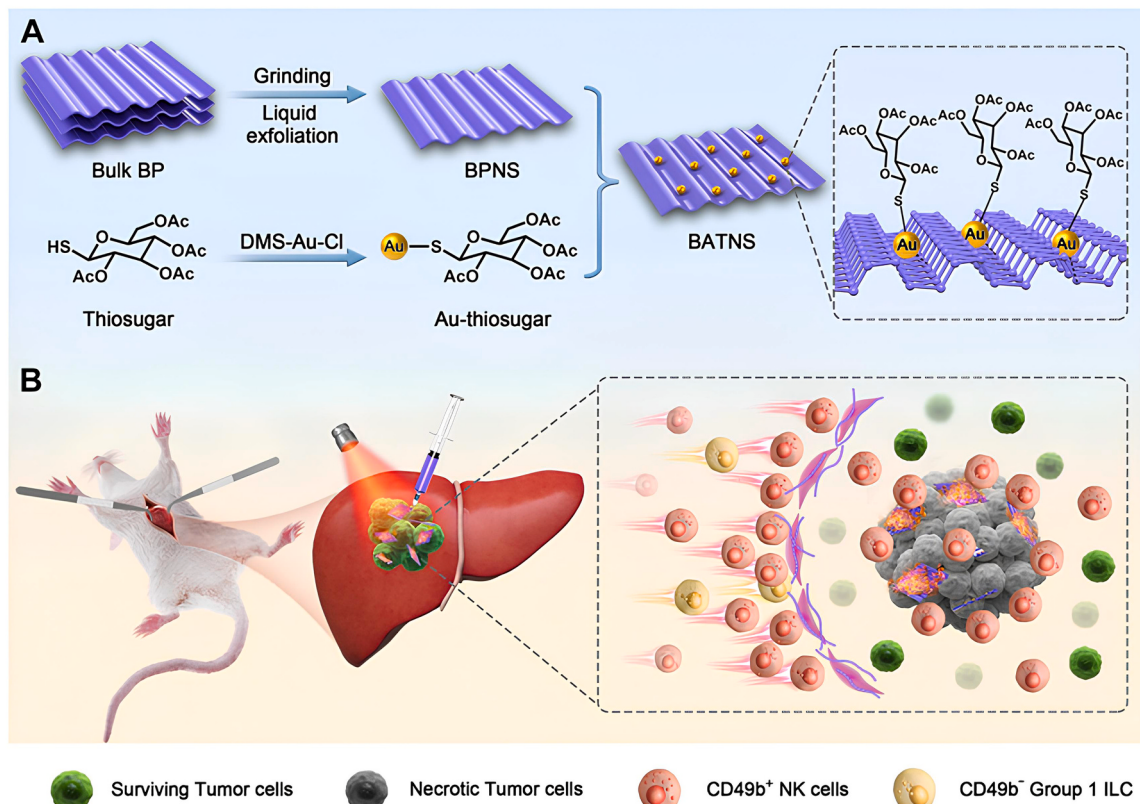


Fig. 9. The schematic illustration of BP-Au-thiosugar nanosheets (BATNS) as photothermal-induced tumor killing agent for HCC. (A) The synthesis of BATNS. (B) The schematic illustration of BP-Au-thiosugar nanosheets (BATNS) as photothermal-induced tumor killing agent induce the increase of local NK cell infiltration caused by the thermal effect of BATNS photothermal treatment for HCC. Adapted with permission from reference [178]. Copyright (2022), Springer Nature.

targeting agent were developed for PTT of breast cancer cells (CHO and MCF-7 cells). When NIR laser exposure (640–710 nm, 0.7 W/cm², 1–5 min. irradiation time) was applied following incubation of the cells with nanoparticles for 12 h, it was observed that MCF-7 cell death occurred at a higher rate than CHO cells. Additionally, the aptamer

surface functionalization has been reported to increase the amount of cellular nanoparticles intake [180].

Stimulation and imaging guided PTT approaches have produced more effective and targeted therapeutic results than early PTT studies. In this case, the nanohybrid structure also acts as a magnetic resonance

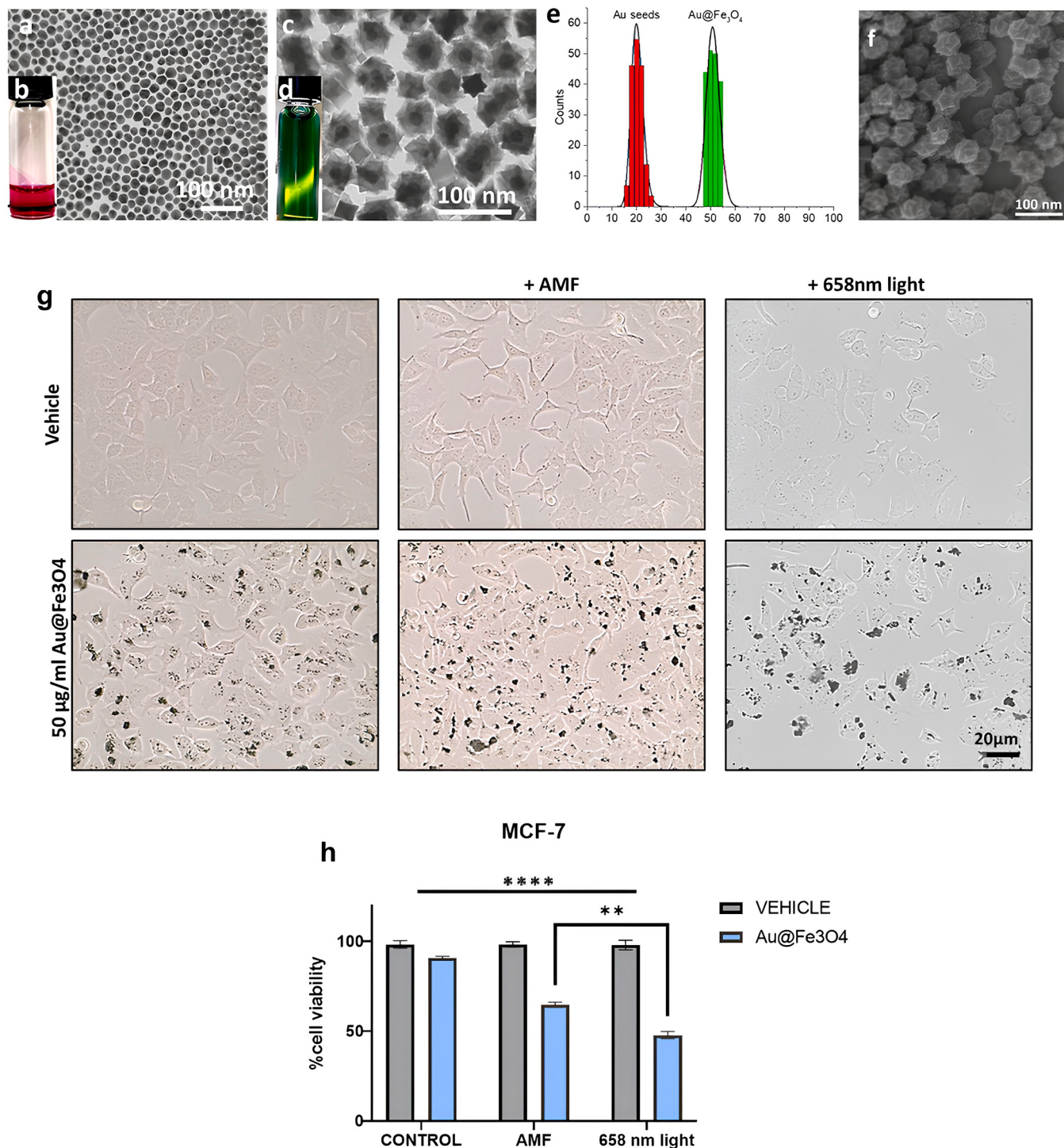


Fig. 10. The characteristic features of the designed Au@Fe₃O₄ nanostars and evaluation of the magneto-mechanical stress/the photothermal effects on the cancer cells. (a,b) TEM images of Au seeds (ca. 20 nm) and picture of a suspension of the same NPs in toluene. (c,d) TEM micrograph of Au@Fe₃O₄ nanostars with the corresponding image of the same MP-NPs dispersed in water. (e) size distribution of the Au seed and Au@Fe₃O₄ nanostars. (f) SEM image of the Au@Fe₃O₄ nanostars. (g) Representative bright field optical images of unloaded (upper images) and loaded (50 mg/mL) MCF7 tumor cells before and after exposition to the AMF or to 658 nm light. (h) Cell viability by trypan blue staining. **p < 0.01 indicates significant difference between Au@Fe₃O₄ nanostar-loaded MCF7 exposed to AMF or 658 nm light; ***p < 0.0001 indicates significant difference between Au@Fe₃O₄ nanostar-loaded MCF7 before and after AMF or light treatment. Adapted with permission from reference [184]. Copyright (2022), American Chemical Society.

imaging (MRI) contrast agent in addition to PTT thanks to its Fe_2O_3 core structure. In a study using hybrid nanostructures ($\text{IO}@\text{Au}$, diameter: 33 nm) that enable PTT under MRI guidance, geometric model definition of the tumor and the nanoparticle distribution map were obtained in the mice bearing CT26 colon tumors under the MR imaging guidance. In this way, the model was validated by testing in the experiment by measuring the temperature changes of the tumor under (808 nm NIR laser, 1.4 W/cm², 15 min.) laser irradiation and thermal mapping was provided [181]. Abed et al. a theranostic multifunctional nanocomplex consisting of gold ($\text{Fe}_2\text{O}_3@\text{Au}$ -iron (III) oxide shell–core NPs (37 nm diameter) and the Balb/c mice including colorectal-CT26-tumor model were i.v. injected with the hybrid nanoparticles. When a magnet was inserted the tumor location and NIR-laser irradiation (NIR laser-808 nm, 1.4 W/cm² for 15 min.) was applied to concentrate the nanoparticles in the relevant region, a significantly higher temperature rate was obtained in the targeted tumor area. This effective combined PTT application provided complete remission of the tumor growth [182]. Au- Fe_3O_4 shell-core polyvinylpyrrolidone capped nanostructures (164 nm in diameter), developed by Caro et al. as a multi-modal nanoplatform for *in vivo* imaging and focused PTT, were first shown to be highly biocompatible in the cellular studies (HFF-1 and C6 cells). The localized two-photon (TP) glioblastoma killing performance of the nanoplatform was demonstrated in an *in vitro* 3D glioblastoma multiforme. Then, effective results were shown when imaging-guided combined PTT (720 nm, 1.75 W) was applied to the nude mice tumor model [183]. Unlike previous studies, Muzzi et al. designed magnetic-plasmonic star-shaped $\text{Au}@\text{Fe}_3\text{O}_4$ nano-heterocomplex (diameter: 60 nm) with Au core and ferrite shell structure for the purpose of combined PTT. Nano-heterostructures, which have been shown to be highly biocompatible on the endothelial progenitor cells (ECFCs), provided a combined PTT effect with 658 nm light stimulation (300 mW/cm²) and external AMF magneto-mechanical stress nano-shell induction on the breast cancer (MCF-7) cell line (Fig. 10) [184].

The efficient synthesis of $\text{Fe}_3\text{O}_4@\text{AuNPs}$ has attracted research interest with the aim of extending their use over a wide range of applications, including bioseparation, targeted delivery and bioimaging [185]. $\text{Fe}_3\text{O}_4@\text{AuNPs}$ offer numerous potentials for a powerful platform for medical applications due to their superior magnetic and optical properties [186]. $\text{Fe}_3\text{O}_4@\text{Au}$ core@shell nanoparticles have gained broad attention due to their unique innovations in MRI and PTT. Dheyab et al. used the ability of sonochemical approach to synthesize high yield theragnostic agent $\text{Fe}_3\text{O}_4@\text{AuNPs}$ with a size of approximately 22 nm in 5 min. They reported that the synthesized $\text{Fe}_3\text{O}_4@\text{AuNPs}$ have great potential as an ideal candidate for MR imaging and PTT [187].

3.2.3. Graphene-gold hybrid nanomaterials for PTT

Graphene and its derivative nanomaterials constitute a new class of theragnostic agent in the biomedical area. Graphene oxide coated AuNPs (GO/Au-GA nanocomplex) have attracted great attention thanks to their excellent optical properties, low toxicity, and high stability in recent years. Considering its high-level photo-thermal conversion efficiency and special surface properties, it acts as a nanoplatform to facilitate tumor treatments and diagnostic processes by conjugating drugs and other imaging agents to the structure with covalent/non-covalent methods. The graphene-based NPs are strong light absorbent in the NIR region. Therefore, graphene oxide coated AuNPs are excellent candidates for various cancer PTT applications [188]. Zedan et al. proposed ultrasmall sized gold-graphene nanocomposites as new photo-thermal energy converters. They stably bonded ultrasmall AuNPs (diameter range 2–4 nm) to graphene and also, they showed that the laser irradiation of Au nanostructures subjected to controlled shape changing (transitioning from spherical to short and long AuNRs) in the GO solutions increased their PTT efficiency to produce more heat [189]. Additional surface modification of the gold-graphene nanohybrid structures with PEG molecule designed for PTT applications significantly reduced the cytotoxicity of the material and increased

biocompatibility. In a study, after PEGylation of carboxylated nano-graphene oxide (c-NGO/AuNPs, 128 nm sized) platforms decorated with citrate-coated AuNPs, its biocompatibility was demonstrated in 72-hours incubation with both the normal and cancerous cells [190]. In another study, AuNRs attached PEG modified GO-nanocomposites (39.3 nm × 10 nm in sizes) were designed as PTT platform. Thus, the toxicity caused by CTAB molecules has been shown to be reduced. For PTT, it has been shown that epidermoid carcinoma (A431) cells incubated with the nanocomposites for 24 h had a remarkable decrease (40 %) in cellular viability after 5 min of irradiation with Xe-lamp light (NIR region, 60 W cm⁻²). *In vivo* studies revealing the anti-tumor efficiency of the designed nanocomposites have shown that nude mice tumor volumes were effectively reduced by the PTT process [191]. Modification of GO/Au nanomaterial-based PTT platforms with targeting ligands is an important approach to promote anticancer activity. Yang et al. reported that biocompatible MUC1 aptamer-AuNPs-GO nanocomposites facilitated the targeted treatment of human breast (MCF-7) tumor cells by triggering apoptosis via NIR light-activatable PTT (808 nm, 3 W, 5 min. irradiation time) [192]. As an innovative combined approach, the design of imaging-guided PTT nanoplatforms has enabled to monitor anticancer activity in a localized manner at specific tumor regions. After the nano-theranostic platform (CPGA, 15 nm diameter) was injected IV into the tumor-bearing mice (SCC7), PA-signals and enzyme-triggered high fluorescence were observed in the tumor location in time, which peaked at the time point of 6 h. In the same study, it was reported that great inhibition of tumor was achieved without recurrence after the (808 nm, 0.75 W cm⁻²) laser irradiation [193]. In another study, Sun et al. showed that *in situ* synthesis of GO/AuNRs (31 nm × 8 nm sizes) theragnostic nanocomplex for PTT and effective imaging of tumor computed tomography. After the (iohexol) preclinical-CT agent in combination with GO/AuNRs hybrids was injected into the nude mice xenograft tumor, it has been shown that excellent CT imaging and PTT effects were obtained with the implementation of the laser irradiation (808 nm laser at 0.3–0.4 W/cm² power density for 10 min) [194].

3.2.4. Silica-gold hybrid nanomaterials for PTT

Mesoporous silica nanoparticles (MSNPs) have various advantages including easy modification, high surface areas, tailorabile mesoporous structure, large pore volumes, high biocompatibility, mechanical and chemical stability [195,196]. Silica modified core-shell nanomaterials have got great value for PTT purposes recently. While the silica shell portion of the hybrid nanostructure provides stability, biocompatibility, and suitable surface chemistry for additional modifications, the core part helps as a functional portion and it can be accessed via SPR or magnetic properties. Mostly, Au is preferred as the core-metal for its great SPR and other superior physicochemical properties [197]. Significant PTT activity in the NIR region (0.57 W/cm², 808 nm, 5 min. irradiation time) of the silica-gold-silica nanocomposites (240 nm in diameter) has been reported in the mouse alveolar macrophage cells [198]. The use of targeting ligands in cancer PTT applications increases the effectiveness of the therapy as it provides effective nanoparticle endocytosis in cancer cells. Liu et al. designed mesoporous silica-coated AuNRs (13 × 47 nm) nanoconjugates functionalized PEG molecule, tLyp-1 peptide (targeting agent) and indocyanine green (ICG, NIR imaging agent) for effective PTT applications. While fluorescence imaging was achieved with ICG in the designed theranostic nanocomposite structure, it has been shown that the tLyp-1 peptide structure provided more effective endocytosis in the (MDA-MB-231) cell line. Additionally, high levels of targeted PTT activity have been reported as a result of laser irradiation in the NIR region (785 nm, 3–5 min.) [199]. The design of gold-silica nanostructures for both drug carriers and PTT purposes provides the opportunity for synergistic combined cancer therapy. In a study, the design of a redox triggered DOX/MSN-gold drug delivery system was reported for the purpose of chemo-photothermal synergistic cancer therapy. The combined chemotherapy-PTT (808 nm, 0.5, 1, 2, 3

and 4 W for 3 min by the NIR laser) synergistic activity of the designed nanohybrid structure was reported on the A549 cancer cells with simultaneous redox triggered DOX release [200]. Activation of tumor-infiltrated defense cells through induction of specific adaptive immune response is a promising immunotherapeutic approach for treatment of cancer. Ong et al. reported the effective transfer of high amounts of CpG-ODNs to the tumor part using extra-large pore MSNPs (Au@XL-MSNs/PEG, 130 nm diameter) decorated with AuNPs for the activation of dendritic cells. Using combined immunotherapy and PTT (808 nm, NIR laser irradiation, 0.15 W/cm² for 5 min.), they demonstrated significant tumor inhibition after intratumorally injection in an animal *in vivo* model (tumor-bearing C57/BL6 mouse model) in addition to success in cellular studies [201]. Since rapid developments in nanoparticle synthesis techniques enable the production of more stable and biocompatible nanomaterials, this situation has a direct impact on their PTT effectiveness. In a study, improved gold-silica-core-shell NPs (13 nm diameter) through pulsed laser ablation in liquid (PLAL) have been reported to be less toxic, stable, reproducible and scalable. The improved physicochemical properties of the nanoparticles also directly affected their biological activity in cancer PTT (520 nm laser irradiation, 100 and 400 cm⁻² for 30 min.), and the results of high biocompatibility and therapeutic effect were reported after incubation with the MCF-7 cells [202]. The tumor-targeting use of the silica-gold-silica hybrid nanoparticles (SGS, 480–510 nm) diameter combined with human mesenchymal stem cells (hMSCs) is a very innovative approach for cancer PTT applications. The stable and biocompatible SGSs loaded hMSCs were applied intravenously to the tumor-bearing BALB/c mice, significantly higher heat generation and PTT efficiency were reported with the (660 nm, 2 W/cm², for 2 min.) laser irradiation 3 days after injection [203]. Deinavizadeh et al. designed DOX-loaded hybrid nanocomposites (164 nm in diameter) supported by AuNRs on the thiol-modified mesoporous silica for synergistic PTT-chemotherapy. It was reported that the designed hybrid nanostructure showed high biocompatibility, cellular internalization and combined chemo photothermal activity (808 nm, NIR laser irradiation, 3.6 W/cm² for 5 min) on the A549 lung cancer cells in addition to pH/NIR dual-responsive drug release behavior (Fig. 11) [204].

Cancer is currently among the deadliest diseases of the world, and there is a great need for modern approaches that include innovative technologies for cancer therapy. AuNPs have a major place in innovative approaches and they are ideal nanomaterials for PTT applications in addition to the targeted delivery of various natural/synthetic therapeutic agents. Apart from its use as targeted AuNPs with appropriate surface modifications, its therapeutic effects have also been extensively studied in hybrid complexes with various materials. Synthesis methods and physicochemical properties of AuNPs have decisive effects on their effectiveness and safety in cancer therapy. Especially with the combined use of therapeutic molecules, targeting ligands and various additional nanomaterials with AuNPs, very promising synergistic chemo photothermal therapy results have been achieved recently. In addition, the use of image guiding strategies together with the designed hybrid nanocomplexes has enabled more effective therapeutic results in tumor-bearing animal models. Despite the utilities of AuNPs in the field of cancer nanomedicine are quite obvious, there is a great need for more detailed cellular and *in vivo* studies and analysis before their large-scale use. Additionally, personalized approaches are required to develop optimal AuNPs that can provide high levels of therapeutic efficacy and bioavailability for each tumor disease type. It is concluded that in the coming years we will witness clinical studies on AuNPs with the expanded strategies. Thus, available data on the applications of AuNPs in treatment of cancer were analyzed in this part of the review article.

AuNP-based nanotherapeutics have a long way to go before they are approved to treat patients in a clinical setting. To date, there are not clinically approved AuNP-based therapeutics. In general, AuNPs tested in clinical trials do not appear to pose significant safety concerns. In order to accelerate the clinical transition of AuNPs, larger sample groups

can be used in clinical trials. In addition, trials can be conducted with higher quality, more comprehensive and more frequent. In the studies conducted, AuNPs were eliminated hepatically in the long term and showed good tumor targeting. However, more comprehensive studies are needed on the potential side effects of long-term Au accumulation in the body. Each preparation should be tested individually. Additionally, different drugs used simultaneously in clinical applications may affect the toxicity and pharmacokinetics of AuNPs. Clinical grade AuNPs will mostly be prepared by biotechnology companies rather than pharmaceutical companies. This leads to higher costs for AuNP-based preparations. Increased collaboration between academia, clinics, and industry is needed to overcome financial barriers. Global and collaborative policies and approaches are also required for increased success of AuNPs in the clinic.

4. Drug and nucleic acid delivery using gold nanoparticles

4.1. Other drug delivery strategies using gold nanoparticles

AuNPs show different physicochemical properties depending on size and shape, and they have a wide variety of colors (such as red, brown, blue, purple and orange) in the solutions. AuNPs are great nominee nanomaterials for the effective transport of different therapeutic molecules to the target sites. The cargo to be transported may be small molecules of drug or some biomolecules such as RNA, DNA, protein, and peptide. While molecules of drug can be directly conjugated to the surface of AuNPs as a single layer through chemical and physical interactions, drug-nanomaterial conjugation can also be achieved after additional surface functionalization. Various mechanisms are being developed to increase the affinity of functional group-bearing AuNPs to biomolecules and turn them into effective drug delivery systems with improved specificity. In this context, PEG, peptide molecules, folate, bovine serum albumin (BSA), antibodies, polypeptides and oligonucleotides are molecules frequently used in the surface modification of Au-nanomaterials. Suitable surface functionalization increases the bio-distribution, cellular uptake, stability and ultimately bioavailability of nanoparticles [205–208]. If AuNPs do not contain an active targeting agent, they pass through biological barriers and passively accumulate in the target area, depending on their physicochemical properties [209]. The use of nano drug-carrier complexes improves the solubility, stability, biodistribution and pharmacokinetic properties of free drug molecules. Due to the increased total surface area of nano carrier systems, drug loading capacity becomes more efficient. Also, due to its controlled and extended release properties, the drug bioavailability in the body increases and adverse effects decrease [206,207].

AuNPs can be conjugated directly with drug molecules by physical/electrostatic interactions or covalent/ionic bonding. In a study, as a result of the direct stable AuNPs conjugation (13.54 nm in diameter) with some antibiotics (ampicillin, streptomycin and kanamycin), a higher level of bactericidal activity was observed in the standard agar well diffusion assay [210]. Alternatively, drug conjugation with suitable surface functionalization, instead of using bare AuNPs, reduces the cytotoxicity of the Au-conjugate and increases its stability/circulation lifetime [205]. PEG molecules are the most widely used surface modification polymer, and in various animal biodistribution studies, the PEG-functionalized gold nanomaterials have been reported to exhibit importantly extended blood-circulation and tissue distribution than the bare ones. PEG molecules also increase the stability of nanoparticles by inhibiting their agglomeration [205,211,212]. The release of conjugated therapeutic drug molecules from AuNPs reaching target tissues and cells can be achieved by different release forms such as pH-triggered, light-mediated, enzyme-related and glutathione-mediated. pH-mediated release method is one of the optimal and widely used drug release approaches, especially triggered by acidic conditions in the microenvironment of cancer cells or some intracellular structures (such as lysosomes, endosomes and vesicles) [213]. However, conditions such as

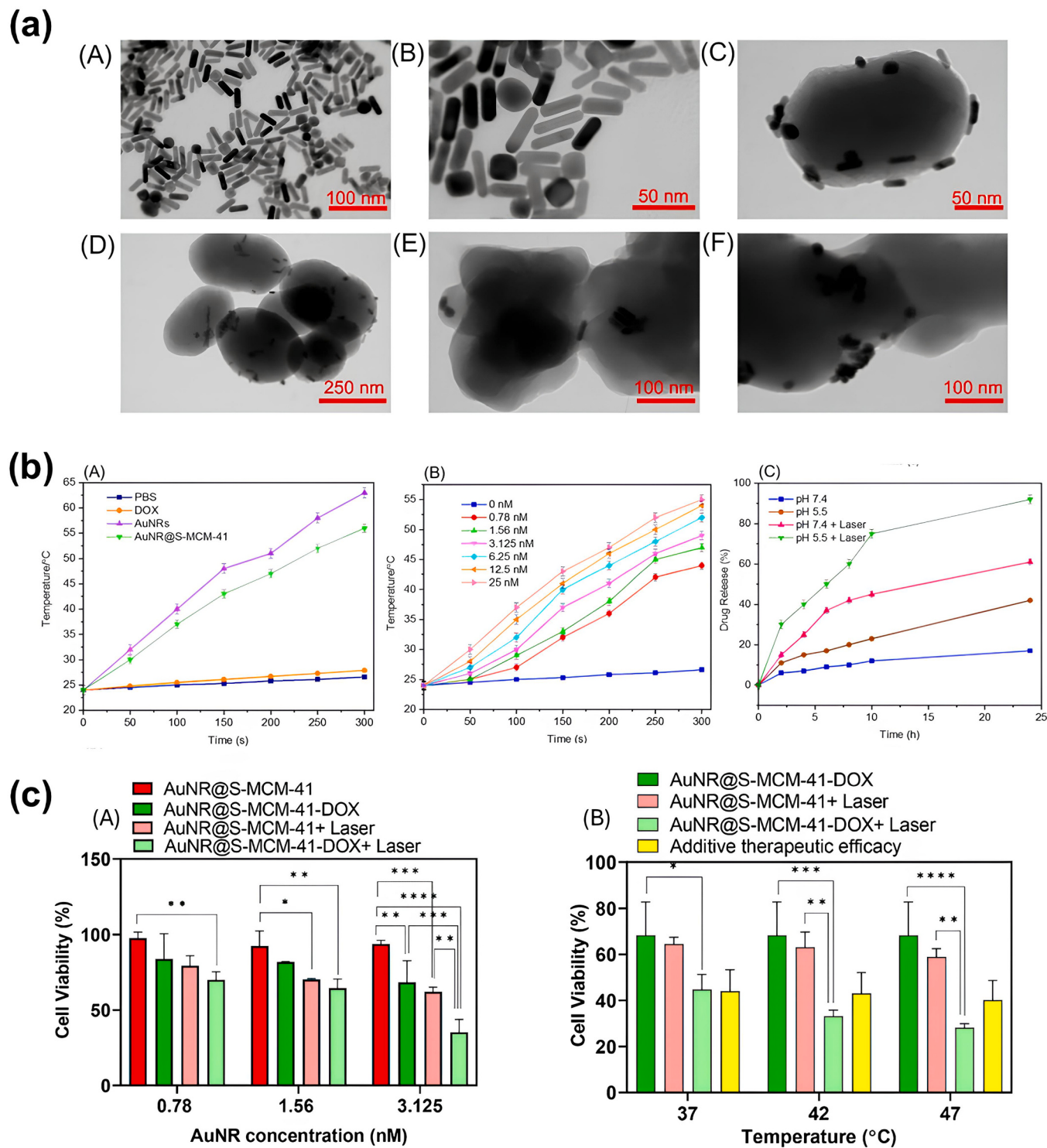


Fig. 11. TEM images/temperature elevation impact assessments of the designed nanomaterials and comparative cell viabilities of A549 incubated with the nanomaterials. (a) TEM images of (a-A), (a-B) AuNRs; (a-C), (a-D) AuNR@S-MCM-41; (a-E), (a-F) AuNR@S-MCM-41-DOX. (b) (b-A) Temperature elevation of PBS, DOX, AuNRs, and AuNR@S-MCM-41 (25 nM AuNR) after irradiating with 808 nm laser intensity (3.6 W cm^{-2}); (b-B) Temperature evolution curves of the solutions containing various concentrations of AuNR@S-MCM-41 (0, 0.78, 1.56, 3.125, 6.25, 12.5 and 25 nM) under NIR laser irradiation with power density of 3.6 W cm^{-2} . (b-C) Cumulative DOX release from AuNR@S-MCM-41-DOX in PBS at pH 7.4 and 5.5 without and with NIR irradiation. (c) (c-A) Comparative cell viabilities of A549 incubated with AuNR@S-MCM-41 or AuNR@S-MCM-41-DOX at different concentrations under exposure to 808 nm laser, (c-B) A comparison of the viability of the A549 cells treated by AuNR@S-MCM-41 +Laser, AuNR@S-MCM-41-DOX and AuNR@S-MCM-41-DOX+Laser. Adapted with permission from reference [204]. Copyright (2024), Springer Nature.

alkalization of extracellular/intracellular fluids and irregular acidification in some solid tumors are a limitation for pH-mediated drug release [214]. The enzyme degradation approach can be used for the specific release of drug molecules from AuNP complexes by EPR effect [215]. However, the fact that such releasing nano systems require quite complex formulations and also the enzymatic nature of lysosomes are challenging aspects of enzyme-mediated methods. Light-mediated drug release is an alternative and innovative strategy, and very successful results have been demonstrated in a short time. However, such drug release mechanisms, which use relatively short wavelength light, have some undesirable side effects such as scattering, toxicity and tissue penetration [205].

AuNPs can be used as nanocarriers for the transfer of molecules on a larger scale, such as drugs, proteins and peptide molecules. In particular, peptide-based drug delivery structures have attracted significant interest in recent years thanks to their superior features, facilitating cellular interactions and enabling specific targeting of the cells. Ruff et al. investigated the effects of the properties such as surface charge, morphology, size and concentration of the AuNPs modified with specific peptides- β -amyloid (CLPFFD) on the integrity and permeability of the designed *in vitro* model of BBB membrane. They showed that small-sized AuNPs strongly affected BBB integrity and the negative nanoparticle

surface charge prevented BBB penetration. Additionally, it has been reported that the inhibitory charge effect caused by the peptide molecule can be compensated by covalent binding to a PEG ligand, which stabilizes the AuNPs in a diluted form [216]. In another study, the anticancer drug molecule functionalized with Neuropilin-1 receptor targeting peptide (CRGDK) was transferred to the cancer cells *in vitro* using AuNPs stabilized with the antioxidant molecule glutathione (GSH) in order to enhance the therapeutic effect of platinum (IV) molecule on the prostate cancer cells. Thus, ensuring high levels of the targeted cellular drug uptake and cellular toxicity has been reported [217]. The peptides for cell penetrating (CPPs) and gold nano-based nanocarriers have emerged as a powerful way for the development of robust drug transport systems. In a study comparing the therapeutic efficiencies of DOX-loaded BP100 CPP modified AuNPs and DOX-loaded RGD peptide Au-nanoconjugates, it was shown that the DOX-BP100@AuNPs conjugate complex gave better results in terms of stability, cellular internalization and drug loading [218]. In a study investigating the effects of amino acids on the stabilization of AuNPs by rationally designed peptide scaffolds, Hou et al. reported that phosphotyrosine (pY) significantly increased stabilization and biocompatibility of the Au-nanoconjugates. High levels of cellular death were demonstrated in the SGC-7901 cancer cells incubated with DOX-loaded pY-coated AuNPs. They

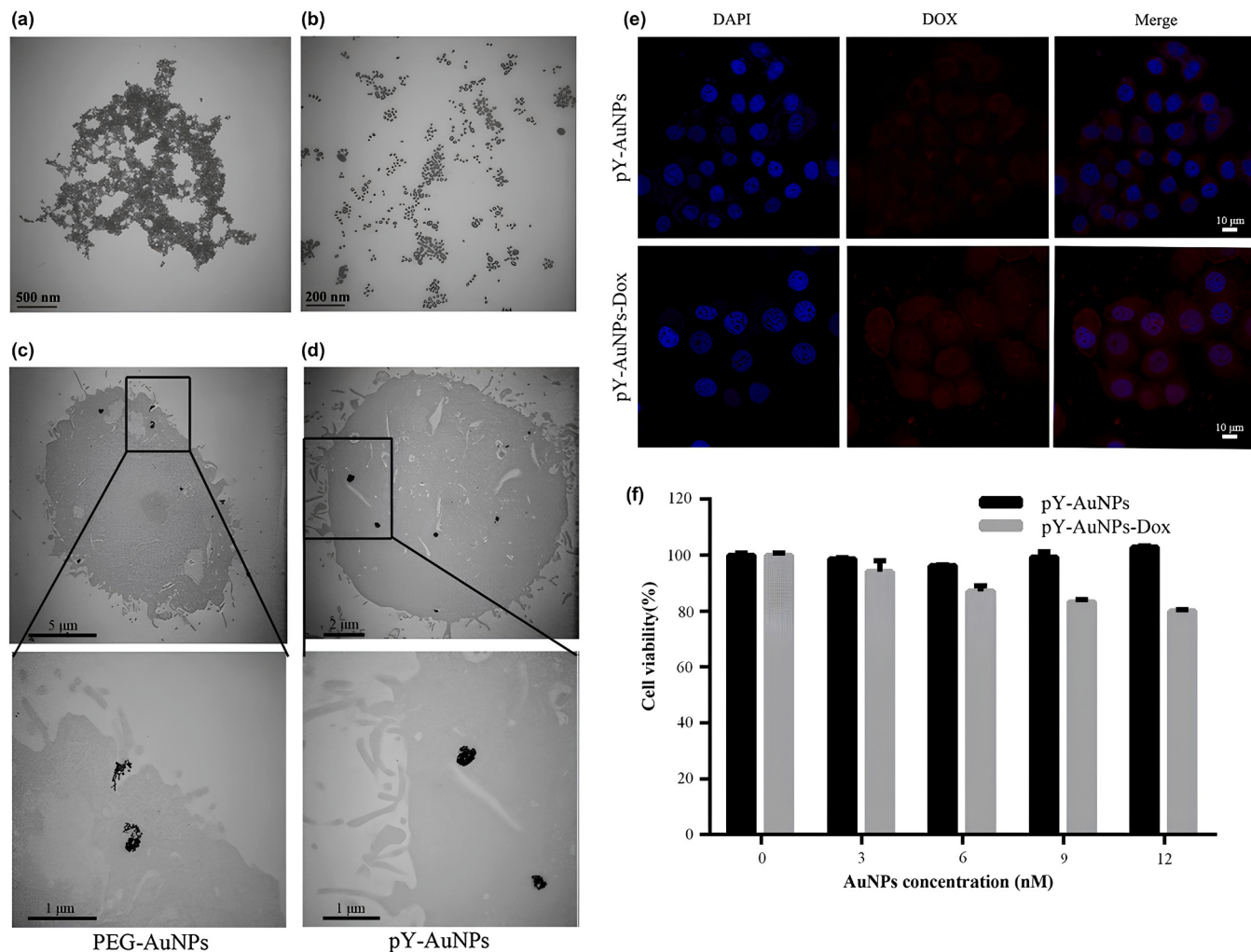


Fig. 12. The stability of pY peptide modified AuNPs. (a) Typical TEM image of AuNPs modified with non-phosphorylated peptide in aqueous solutions (scale bars: 500 nm). (b) Typical TEM image of AuNPs modified with phosphorylated peptide in aqueous solutions (scale bars: 200 nm). Typical TEM images of SGC-7901 cells incubated with PEG-AuNPs or pY-AuNPs for 12 h. (c) PEG-AuNPs. (d) pY-AuNPs. The pY-AuNPs-Dox successfully delivered Dox into cells and caused cytotoxicity. (e) Confocal study of Dox distribution in cells (scale bars: 10 μ m). (f) Cell viability assay after pY-AuNPs or pY-AuNPs-Dox treatment for 24 h. Adapted with permission from reference [219]. Copyright (2019), Springer Nature.

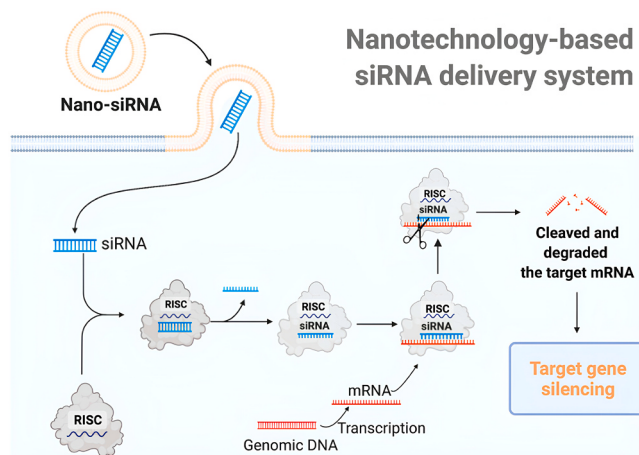


Fig. 13. The mechanism of nanotechnology-based siRNA delivery systems. Utilizing delivery materials, siRNA can be delivered directly into the cell. The siRNA is integrated into the RNA induced silencing complex (RISC) and the sense (passenger) strand is degraded by the RISC protein Argonaute-2. The remaining antisense strand acts as a guide for recognizing the complementary messenger RNA. The activated RISC-siRNA complex binds to and degrades the target mRNA, leading to the silence of the target gene. Adapted with permission from reference [222]. Copyright (2022), MDPI.

hypothesized that the pY-peptides could be a new phosphatase sensitive reagent to stabilize gold nanomaterials (Fig. 12) [219].

4.2. Gene therapy using gold nanoparticles

Gene therapy is an innovative technique that offers a suitable way for the therapy of acquired and genetic diseases. Although the viruses commonly used in this field provide high levels of effectiveness, synthetic nucleic acid transport systems have been designed due to safety issues of viruses such as toxicity and immune response. On the other hand, non-viral synthetic vectors have some limitations regarding effectiveness, application and intranuclear localization. Thus, there is a big need for powerful nanotechnological approaches that will protect nucleic acid molecules from degradation by nucleases, increase their cellular uptake, and ensure their release into the nucleus without disrupting their functions [208,220,221].

4.2.1. RNA interference approaches

RNA interference (RNAi) technology is of great interest for the therapy of a wide range of syndromes. In this context, promising results have been obtained with the use of synthetic small interfering RNA (siRNA) molecules. Synthetic siRNA molecules are generally produced as double chains (with 2-nucleotide overhangs at the 3' ends) with a length of 21–23 nucleotides. In order for the gene silencing mechanism to begin, siRNA must reach the cell cytoplasm and interact with a protein named RNA-induced silencing complex (RISC) and its chains must be separated (Fig. 13) [222]. While the passenger chain is being degraded, the RISC complex attached to the guide chain recognizes the target mRNA as a complement and breaks it down. Finally, the expression of the relevant protein in the cell is suppressed at the end of the target mRNA degradation process [223,224].

In the systemic studies, there are some difficulties such as serum nucleases, immune system cells in the blood and various tissue barriers to ensure that siRNA reaches the target cells while preserving its function after application. As a result of systemic administration, naked siRNA is eliminated in a short time through renal clearance, and siRNA is also excreted through the intestine. Other obstacles are the cell membrane and the hydrophobic/large structure of siRNA for the siRNA molecules to reach the target tissues. The entry of siRNA into the cells usually occurs through endocytosis pathways, and in order for siRNAs to

be functionally effective, they must escape from endosomes and remain stable in the cytoplasm [225–227]. Considering the difficulties in siRNA applications, the nanotechnological approaches to improve the effectiveness and pharmacokinetic properties of RNAi technology in various treatments have gained great interest. In this context, AuNPs designed with appropriate physicochemical properties are very suitable nanomaterials for siRNA-based gene silencing studies [228].

The size of AuNPs is very decisive on cellular internalization, nanoparticle uptake efficiency and toxicity issues, and it can be easily controlled by changing synthesis parameters. Although it is generally accepted that smaller sized AuNPs passively undergo greater cellular internalization, their toxic effects increase as the size decreases. After i.v. administration of AuNPs, they must stay in the circulation of blood for enough duration in order to functionally reach the target tissues, escaping from immune system cells and renal clearance. Considering that the pore diameter is approximately 8 nm in diameter in the kidney glomerular tissue, which has a filtration function, the diameter of the nanomaterials carrying therapeutic agents must be 20 nm and above to avoid renal clearance process. Surface functionalization of AuNPs is another significant factor to be considered in the various cellular and systemic applications and is preferred to ensure stability and bioavailability [5,12,223,229,230]. The surface charge/chemistry of nanoparticles affects not only their cellular uptake rates but also their cellular places and removal status. Colloidal nanoparticles interact with biological fluids such as human plasma to form a protein coating (corona) on the surface of NPs (NP-protein complex) [231]. Thus, appropriate surface modification of AuNPs is very important for their biomedical applications [232]. AuNPs can be functionalized with oligonucleotides by non-covalent interactions or covalent bonds. Nucleic acid strands can be modified with thiol (-SH) groups for covalently attaching them to Au-nanomaterials. Takeuchi et al. conjugated thiolated siRNA (SH-hexaethyleneglycol-siRNA) to the surface of AuNPs via a bond of coordinate and they demonstrated the antiangiogenic activity of this siRNA nanocarrier complex [233]. As a different strategy, Reich et al. used various ratios of thiolated siRNAs and biotin-modified thiolated siRNAs as modifying on the AuNPs surface. They then incubated the designed nanostructures with streptavidin, a molecule that specifically binds to biotin, and used it as a nanoplateform for the binding of biotin-TAT (transactivating transcriptional activator: positive-charged cell penetrating peptide) peptide [234].

Nucleic acids can also interact with Au-nanomaterials by electrostatic interactions. Nucleic acids which are strongly anionic can interact by positively charged AuNPs [205]. Cationic polymers are routinely coated onto AuNPs to increase the binding affinity to anionic genetic materials. It is common to use AuNPs with polyethyleneimine (PEI) surface modification to ensure effective oligonucleotide binding with only electrostatic interaction without the need for any covalent bonding. In addition to PEI, the use of cationic lipids such as DOBAb; positively charged molecules/polymers including PLL, chitosan, protamine, polyamine and hydrophilic polymers such as PEG increases stability, bi-distribution, cellular uptake and functional activity of nucleotide-bearing AuNPs [235–242]. In a study, it has been reported that facile electrostatic interaction of the siRNA molecule with PEI-coated AuNPs (diameter: 15 nm) leads to a remarkable reduction in the target protein expression (an oncogene polo-like kinase 1) in the MDA-MB-435s cells. It has been argued that these results are related to the increased stability and cellular internalization of the nanoconjugate [243]. Kim et al. were designed size-adjustable and reversibly stabilized nanoarchitectures (38 nm diameter) using siRNA-attached unimer-polyion-complex (positively charged PEG-PLL copolymer/siRNA complex-uPIC) and 20 nm diameter AuNPs for the systemic transport of siRNA to solid type tumors. They showed that siRNA release was triggered by increasing glutathione concentration after the entry of the complex into the cell, and gene silencing (sequence-specific) occurred robustly and without causing cytotoxicity. Furthermore, they reported that systemically administered nanocomplexes exhibited extended

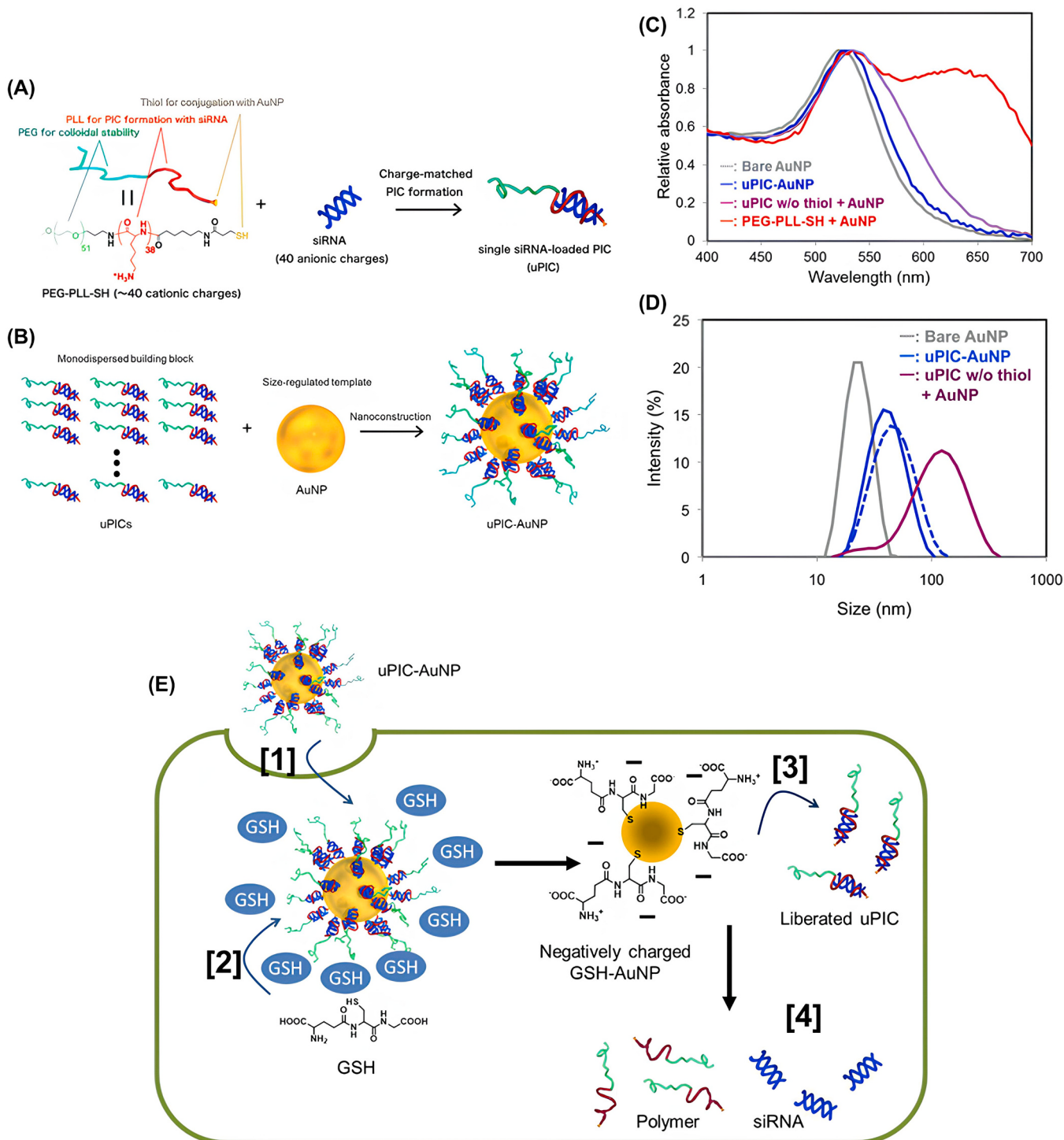


Fig. 14. Schematic illustration showing the nanoconstruction of uPIC-AuNPs from monodispersed building blocks. (A) Formation of uPICs comprising a single pair of PEG-PLL and siRNA. (B) Thiol-gold coordination complex between uPICs and AuNP. (C) UV-vis absorbance spectra of various sample solutions. Bare AuNP: AuNPs without PICs in 10 mM Hepes buffer (pH 7.2), uPIC-AuNP: uPIC-loaded AuNPs in 10 mM Hepes (pH 7.2) containing 150 mM NaCl, uPIC w/o thiol + AuNP: the mixture of AuNPs and uPICs prepared with nonthiolated PEG-PLL in 10 mM Hepes (pH 7.2) containing 150 mM NaCl, and PEG-PLL-SH + AuNP: the mixture of AuNPs and thiolated PEG-PLL without siRNA. (D) Intensity-based DLS histograms of various sample solutions. Bare AuNP: AuNPs without PICs in 10 mM Hepes buffer (pH 7.2), uPIC-AuNP: uPIC-loaded AuNPs in 10 mM Hepes (pH 7.2) containing 150 mM NaCl (solid line) or 10 % FBS (dashed line), and uPIC w/o thiol + AuNP: the mixture of AuNPs and uPICs prepared with nonthiolated PEG-PLL in 10 mM Hepes (pH 7.2) containing 150 mM NaCl. All samples were incubated overnight at ambient temperature (AuNP concentration: 12 nM). (E) Schematic illustration of the proposed mechanism for intracellular siRNA release from uPIC-AuNPs in the presence of GSH. Adapted with permission from reference [244]. Copyright (2014), American Chemical Society.

circulation in the blood, and subcutaneously infused nanocomplexes accumulated efficiently in a cervical cancer model which is luciferase-expressing, achieving remarkable gene silencing in the tumor bearing tissue (Fig. 14) [244].

In a different study, AuNRs/PSS/PAH-siRNA nanocomplex was designed to silence gene mutations of interleukin-8 (IL-8), which are overexpressed in most pancreatic cancers, and effective gene silencing was reported in the Panc-1 and MiaPaCa-2 cancer cells [245]. Kong et al. reported the use of PEI-entrapped Au-nanomaterials modified with a targeting RGD peptide via PEG spacer as a multifunctional vector nanoplatform for effective transport of the Bcl-2 (B-cell lymphoma-2) siRNA molecules into the GBM cells [246].

Another commonly used approach is to form thin multiple modifications on the surface of AuNPs using a layer-by-layer technique by polyelectrolytes which are oppositely charged and molecules. With this technique, genetic material is released over an extended time period, and increased resistance to nucleases is provided due to the increased stability of the nanocomplex [223,247]. In a study, three different polyelectrolyte-PEs (PEI, poly-L-arginine-PLL and poly (allylamine) hydrochloride modified with citraconic anhydride) was used to design the AuNPs-PE nano formulations using the (LBL)-layer-by-layer technique for effective *in vitro* BACE1 siRNA (β -site APP cleaving enzyme-1) transfer to the NB4 1A3 (murine neuronal) and N2a cells [248]. In another study, Shaabani et al. proposed the design of chitosan (CS)-coated AuNPs by the LBL self-assembly method in order to achieve a more stable and efficient siRNA transport system. Enhanced down-regulation of Green Fluorescent Protein (eGFP) in the eGFP-H1299 lung cells-epithelial demonstrated that AuNPs-CS-LBL protected siRNA from enzymatic demolition, its cellular intake and endosomal escape by making it easier (Fig. 15) [249]. In another study reported by Shaabani et al., it was aimed to down-regulate PHD-2 (prolyl-hydroxylase domain 2) by siRNA in order to up-regulate the expression of angiogenesis factors in the diabetic wound model under hypoxic conditions. In this context, they designed LBL self-assembled siRNA loaded AuNPs as stable nanocarriers with two various outer layers (Poly-L-arginine and Chitosan) to ensure effective gene silencing, low toxicity and increased cellular uptake [250].

They reported that the outer PLA-layer improved the endosomal escape and transfection efficiency of siRNA compared to CS. Additionally, they also showed that the use of PLA@AuNPs in a complex by desloratadine further improved endosomal escape [250].

Therefore, combined therapy strategies are coming to the fore thanks to the development of innovative nanocarriers that enable the loading and directing of different drugs/biomolecules onto the same carriers [251]. Jaskula-Sztul et al. used the octreotide (OCT)-modified rod-shaped Au-nanomaterials (AuNRs) for the co-transport of siRNA and doxorubicin (DOX) against achaete-scute complex-like 1 (ASCL1) in order for targeted combined neuroendocrine (NE) cancer therapy. As a result, they reported that the AuNRs-based nanocarriers carrying all three components (ASCL1 siRNA, DOX and OCT) showed much higher efficacy therapeutically on the NE-cancer cells [252]. In another study, a GNR-siRNA nanoplatform was designed targeting the selected BAG3 gene to efficiently block the heat shock response, after surface modification of the AuNRs with PSS and PDDAC. Cellular and animal *in vivo* study data of the nanoplatform providing improved cellular uptake and transfection efficiency in the cancer cells revealed the capability of the siRNA-GNRs nanocomplex to sensitize the cancerous cells to photothermal therapy under moderate irradiation of the laser via down-regulating improved expression of BAG3 gene and apoptosis enhancement [253]. In a recent study, co-transport of DOX and Bcl-2 which is an anti-apoptotic gene-siRNA as a multifunctional delivery system based on the AuNPs (13 nm diameter) was demonstrated as an effective combined breast cancer cell (TNBC) therapy approach [254].

4.2.2. CRISPR-Cas9 based systems

It will be possible to treat some genetic diseases that are difficult to

treat, thanks to the advantages offered by the innovative "CRISPR-Cas9" system, such as being specific to the region, high sensitivity, ease of application and potential for use in a wide range of areas. The discovery of short palindromic sequences which are regularly interspaced and the nuclease system (CRISPR/Cas9) has led to important developments in the genetic engineering area [255,256]. In an advanced designed CRISPR-Cas9 system, there are two essential basic components, namely Cas9-endonuclease enzyme and single-guiding RNA (sgRNA), as well as ribonucleoprotein (RNP) complexes [257]. Innovative carrier systems are needed to ensure effective delivery specific to the target disease, adequate cellular uptake and stability of the system [258]. Delivery methods of the CRISPR-Cas9 based complexes are generally divided into three groups: viral ones, non-viral (extracellular vesicles, nanoparticles and plasmids) methods, and physical (microinjection and electroporation) methods (Fig. 16) [257].

The advantages such as the unique physicochemical properties of AuNPs, their biomolecule loading capacity, the ability to precisely control their synthesis, and the ease of modification of their surfaces enable efficient DNA, RNA and protein transfer [259]. Mout et al. reported that direct nuclear/cytoplasmic transport of the Cas9 enzyme/sgrNA complex with the carrier arginine-modified AuNPs into the various cell types with high efficiency (~90%). Additionally, they showed that the gene editing efficiency increased up to 30% after the nanocomplex transfer [260]. CRISPR-AuNPs offer a new nano-therapeutic approach for treating Duchenne Muscular Dystrophy (DMD) caused via small deletions and point mutations. In a study, a nanodevice consisting of AuNPs conjugated to DNA and complexed with the positively charged endosomal disrupting polymer [poly (N-(N-(2-aminoethyl)- 2-aminoethyl) aspartamide)] has been reported to repair DNA damage causing DMD in the mice by stimulating the homology-directed DNA repair mechanism through efficient delivery of the donor Cas9 RNP and DNA [261]. Fragile X syndrome (FXS) is a genetic disease based on a single gene mutation related to autism, caused by a repeat expansion mutation in the FMR1 gene, which encodes FMRP, a fragile X mental retardation protein (an mRNA-binding protein in brain tissue) [262]. Lee et al. reported that the CRISPR-Cas9 RNP can edit genes of major brain cell types (neurons, astrocytes and microglia) by intracranial injection into the adult mice brain using AuNP-based nanoconjugates. They showed that the positive effect achieved by efficiently knocking down the target gene mGluR5 could also relieve the animals from the repetitive exaggerated behaviors caused by FXS [263]. The use of gold nanomaterials enables effective transport of the CRISPR-Cas9 complex to target cells through different mechanisms. In one study, researchers aimed to develop a multi-purposed nanocomplex for cancer treatment with sgPLK-1-Cas9plasmids (CPs). They concentrated the CPs on TAT-peptide-functionalized AuNPs by electrostatic interaction and then coated the surface of gold nanoconjugates with the lipids (DOTAP, DOPE, cholesterol, PEG2000-DSPE). The authors demonstrated that upon entry of the designed system into the tumor cells, nucleus-targeted and effective tumor inhibition occurred following laser thermo-triggered release of CPs into the cell cytosol facilitating powerful knockouts of related melanoma gene (Plk-1) [264]. In another study, Ju et al. reported that the self-assembly of clustered Au-nanomaterials (AuNCs) with SpCas9 protein (AuNCs-SpCas9) under physiological conditions and the sufficient transport of SpCas9 into nucleus of the cells highly dependent on pH conditions. The assembled SpCas9-AuNC nanoparticles were shown to be effective in knocking out the E6 oncogene, inducing apoptosis, and restoring the p53 gene functions in the cervical cancerous cells [265]. Tao et al. reported the design of protamine-modified AuNCs as an alternative nanocarrier for efficient genome editing via the delivery and delivery of a Cas9-sgRNA plasmid. They demonstrated efficient cellular delivery and effective delivery to the cell nucleus. Their designed nanocomplexes have the potential for functional use in bioimaging in addition to cancer therapy [266].

Thanks to their fascinating physical and chemical features, Au-based

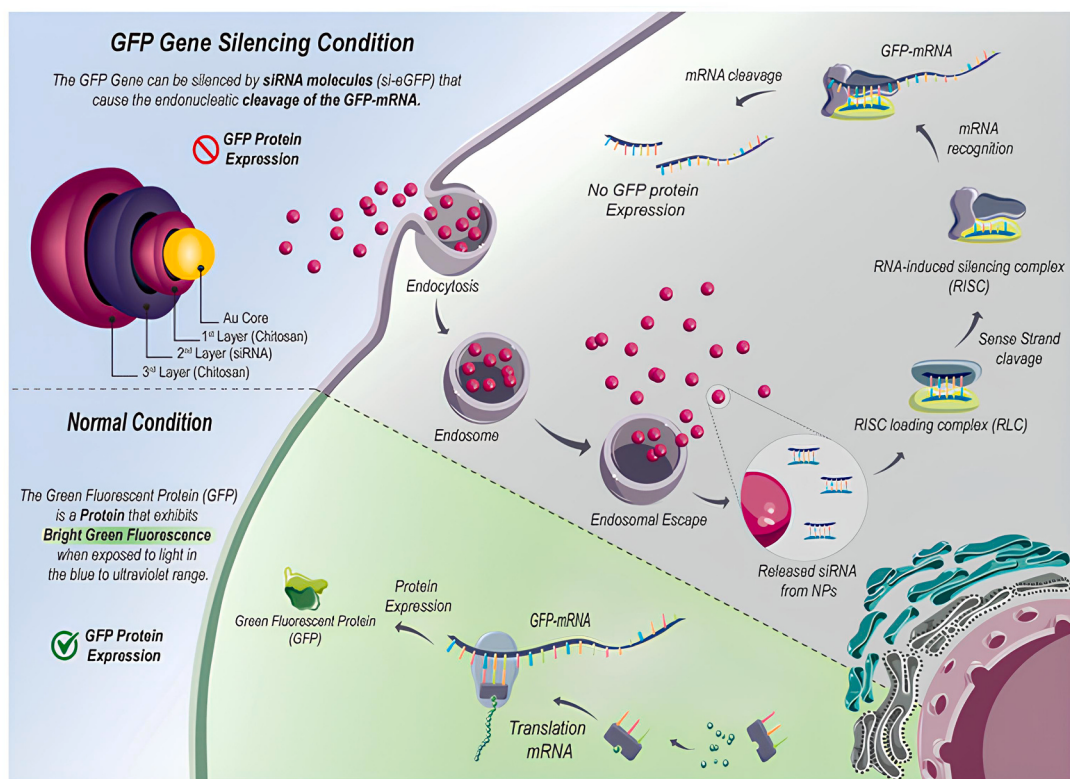
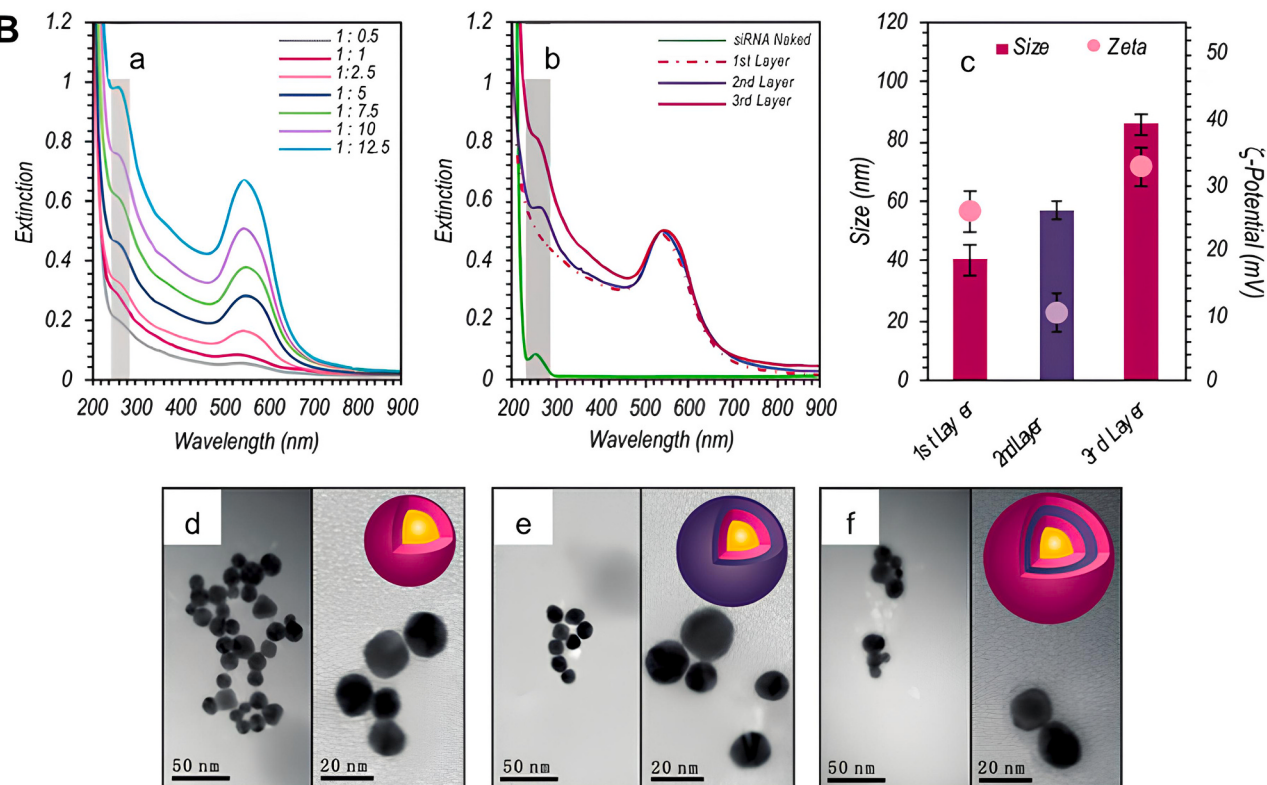
A**B**

Fig. 15. (A) Schematic representation of LBL-CS-AuNPs for siRNA delivery. Under normal conditions, H1299-eGFP cells continuously express enhanced Green Fluorescent Protein (eGFP). When LBL-CS-AuNPs are taken up by cells via endocytosis, chitosan can induce endosomal escape. Then, the released siRNA (si-eGFP) is processed by the RNA-induced silencing complex (RISC), which targets and cleaves GFP-mRNA. The cleavage of GFP-mRNA leads to decreased GFP expression and a diminished green fluorescence intensity of H1299-eGFP cells. (B) Synthesis of Layer by Layer (LBL) CS-AuNPs. (B-a) UV-Vis spectra of CS-AuNPs-siRNA complexes for various mass ratios. (B-b) UV-Vis spectra upon sequential adsorption of siRNA and chitosan onto CS-AuNPs at weight ratio 1:10. (B-c) Representative particle size and zeta-potential after sequential adsorption of siRNA and chitosan on CS-AuNPs at weight ratio 1:10. (B-d, e, f) TEM images during the three steps of the LBL synthesis process. Adapted with permission from reference [249]. Copyright (2021), MDPI.

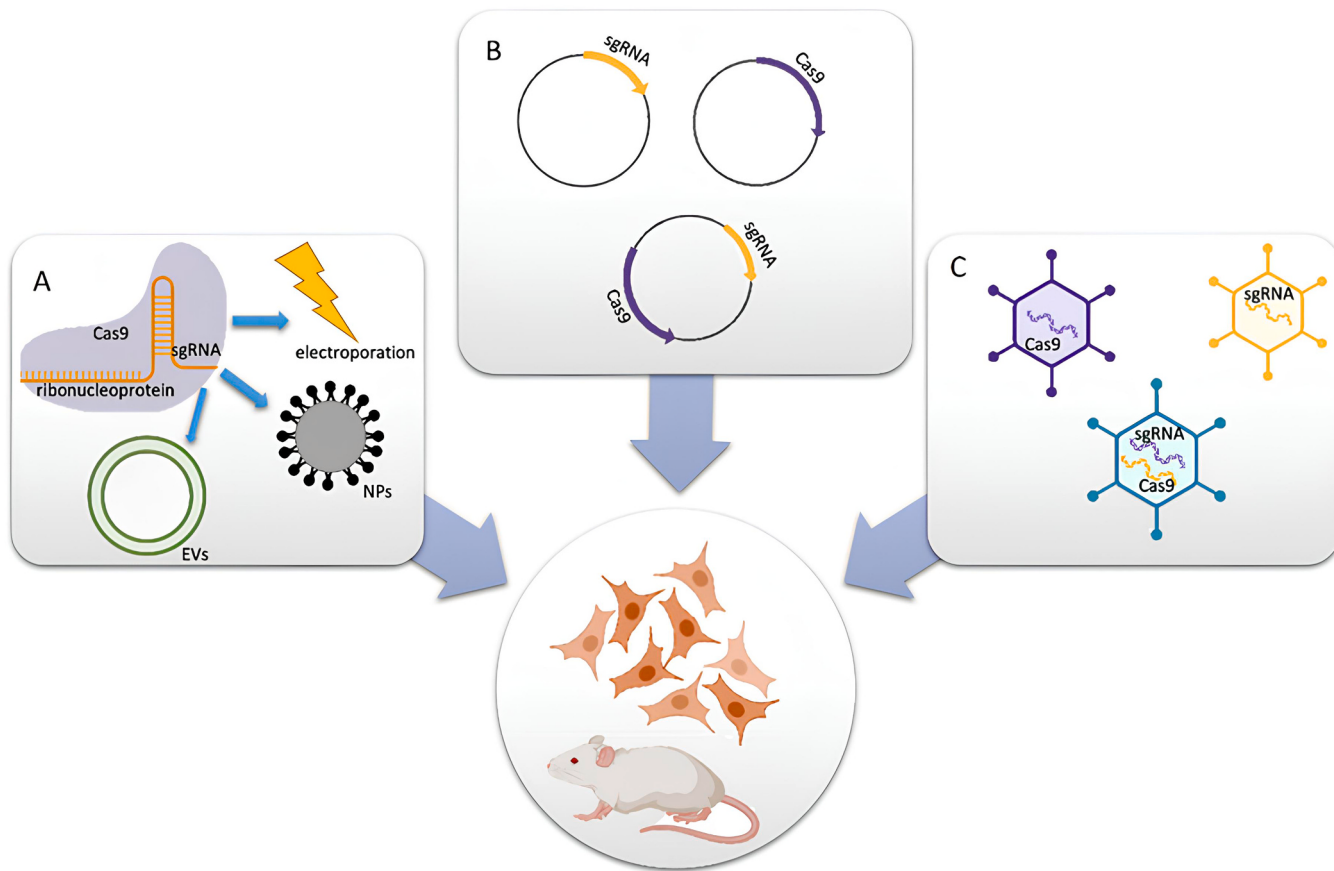


Fig. 16. Methods for the delivery of CRISPR/Cas9 components. (A) Cas9 protein and sgRNA form a ribonucleoprotein (RNP) complex, which is packaged into extracellular vesicles (EVs), nanoparticles, or electroporated directly into cells or model organisms. (B) Plasmids expressing Cas9 and/or sgRNA are transfected into cells. (C) Viral vectors encoding Cas9 and/or sgRNA deliver these components *in vitro* or *in vivo*. Adapted with permission from reference [257]. Copyright (2021), MDPI.

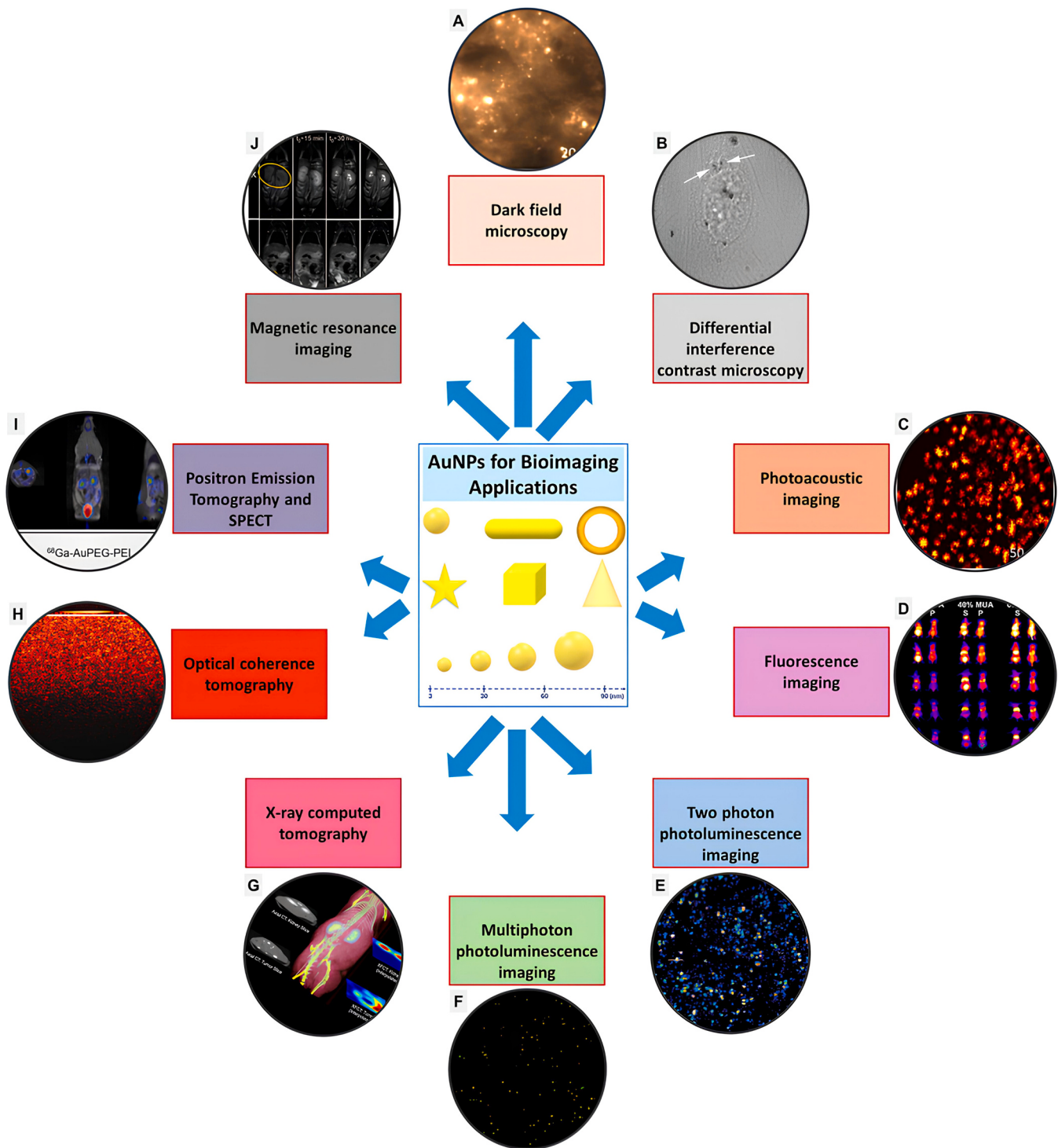
nanoparticles are considered highly suitable nanomaterials for effective gene and drug transport. In addition to features such as their low toxicity, stability, and easy size tunability, the efficient surface functionalization of AuNPs with the different therapeutic chemicals and biomolecules has made it possible to obtain encouraging results in cellular and animal studies. Various mechanisms are being proposed to increase the affinity of functional group-bearing AuNPs to biomolecules and turn them into effective drug delivery systems with improved specificity. Suitable surface modification increases the stability, biocompatibility, cellular uptake, biodistribution and finally bioavailability of AuNPs. AuNPs can be conjugated with biomolecules and drugs by covalent/ionic bonding or physical interactions. Gold nano-based gene therapy has exhibited excellent potential for correcting and silencing monogenic syndrome mutations. AuNPs can be used as nano-carrier platform for the delivery of molecules on a larger scale, such as drugs, proteins, peptide molecules, siRNA oligonucleotides, DNA molecules and CRISPR-Cas9 complexes. In particular, peptide-based drug transport systems have aroused big attention in recent years, because these systems facilitate cellular interactions and enable the specific cell targeting. While the delivery of larger molecules using AuNPs is an interesting field, innovative research is needed to increase their effective cellular uptake, tissue specific targeting and biocompatibility. Although gene and delivery systems exploiting AuNPs are very promising, more innovative optimization approaches that will increase *in vivo* efficiency and studies that will enable clinical transition are needed.

5. Gold nanoparticles for biological imaging

The unique optical and physical features of Au-based nanomaterials are related to surface plasma resonances (SPR). When light of certain wavelengths is applied to the nanoparticles, the free electrons of the AuNPs interact with the electromagnetic field of the light and begin to oscillate in resonance with the frequency of the light. SPR wavelengths of AuNPs change depending on the shape, surface chemistry, and size of the nanomaterials [267,268]. AuNPs have been used in numerous studies in the optical biological imaging area thanks to their excellent plasmonic features (Fig. 17) [269–278]. The interactions of AuNPs in the biological systems have been visualized thanks to developments in the optical imaging/microscopy technologies and *in vivo* contrast agent studies including differential interference contrast (DIC), microscopy dark field microscopy (DFM), photoacoustic imaging (PAM), fluorescence imaging, two photon/multiphoton photoluminescence imaging, optical coherence tomography (OCT), X-ray computed tomography (CT), magnetic resonance imaging (MRI), single photon emission computed tomography (SPECT), and positron emission tomography (PET) [279–292]. Thus, the localization, diffusion, cellular dynamics, membrane transitions and interactions of single or aggregated nanoparticles with biomolecules have become more understandable [293–297].

5.1. Dark field microscopy

In the dark-field microscopy imaging (iDFM) method, since only scattered beams hit the sample, it is suitable for imaging samples that are



(caption on next page)

Fig. 17. Bioimaging applications of gold nanoparticles. (A) Optical images in dark field transmission mode under white light, of MG-63 cells, incubated with fucoidan-AuNPs. Copyright (2020), MDPI. (B) Differential interference contrast (DIC) image of the hCMEC/D3 cells that treated with $100 \mu\text{g mL}^{-1}$ poly(2-hydroxypropylmethacrylamide)-coated AuNPs (Hydroxy@AuNP35). Copyright (2013), The Royal Society of Chemistry. (C) *In vitro* PAM images of the cells acquired at 650 nm wavelength. HeLa cells with internalized CGNP (chain-like AuNPs) clusters-RGD were imaged with a custom-built PAM system. Copyright (2021), Springer Nature. (D) Time- and MUA (11-mercaptopoundecanoic acid) feed percentage-dependent NIR-II fluorescence images showing the *in vivo* distribution of GNCs (gold nanoclusters) in mice after the intravenous injection. Copyright (2022), American Chemical Society. (E) Two-photon luminescence image of the peptide-functionalized GNRs on *Bacillus subtilis* spores excited by NIR laser pulses. Copyright (2008), Springer Nature. (F) Label-free characterization of multiphoton-induced luminescence from gold-silica nanoparticles on a glass slide. Individual particles are highlighted in a golden hue due to the composite image taken from acquisition channels 446, 525, and 575 nm. Copyright (2020), MDPI. (G) 3D volume rendering of the mouse from postmortem CT data along with smoothed XFCT images (bicubic interpolation) and corresponding axial CT images of the kidney and tumor slices. This figure illustrates the possibility of quantitative multimodal imaging of GNP distributions in an animal using XFCT and conventional CT together. Copyright (2016), Springer Nature. (H) OCT B-scan images of B-GNPs (branched gold nanoparticles) in water. Copyright (2012), Hindawi Publishing Corporation. (I) Tissue uptake of ^{68}Ga radiolabeled gold nanoparticles highlighted by fused PET-MRI images. Copyright (2024), The Royal Society of Chemistry. (J) T_1 -weighted images of a mouse 5 min before (t_0 -5 min) and 15, 30, and 45 min after intravenous injection of Au@TDTPA-Gd₅₀ (K for kidneys and B for bladder). Copyright (2008), American Chemical Society.
 (a) Adapted with permission from reference [269]. (b) Adapted with permission from reference [270]. (c) Adapted with permission from reference [271]. (d) Adapted with permission from reference [272]. (e) Adapted with permission from reference [273]. (f) Adapted with permission from reference [274]. (g) Adapted with permission from reference [275]. (h) Adapted with permission from reference [276]. (i) Adapted with permission from reference [277]. (j) Adapted with permission from reference [278].

especially difficult to image via bright-field microscopy. AuNPs show very strong scattering at the LSPR frequency, greatly improving the image of samples as dots [279,298]. DMF has important advantages such as high sensitivity, low imaging background, high resolution, high signal-to-noise ratio, and single particle analysis accuracy [299]. Therefore, DMF is a powerful technique for studying the interplays between cells and nanomaterials [300]. In the literature, AuNPs are used as probes in the iDMF area to investigate various cellular dynamics including endocytosis, viral infection, DNA damage, cell division and also different metabolic processes [301]. While next-generation sequencing techniques are a good alternative, their high cost and long analysis times make them insufficiently applicable in routine clinical diagnosis. To address this limitation, researchers reported a CRISPR/Cas13a-based miRNA biosensor using point-of-care (DF) imaging. They used magnetic-gold nanoparticle complexes (MGNPs) as signal probes. Through the designed combination of CRISPR/Cas13a, MGNPs, and DF imaging, they demonstrated single-base specificity, a detection limit of 25 pM, and detection of miR-21-5p within 30 min without requiring amplification [302].

5.2. Differential interference contrast (DIC) microscopy

The DIC microscopy technique, which produces a pseudo-3-D image with sufficiently high contrast and uses dual-beam interferometry, allows direct observation of multiple intracellular compartments such as motor protein-microtubule dynamics, organelle trafficking in the axons and cell division without the need for staining. Thanks to important optical features and photostability, Au-based nanomaterials have been preferred as a contrast agent in the DIC microscopy research area for the observation of nano-bio interactions in the cells [267,303]. In a study, Tkachenko et al. used video-enhanced color DIC microscopy and TEM to observe the subcellular distribution of AuNPs modified with nuclear localization peptides in three different cell types (3T3/NIH cells, HepG2 cells and HeLa cells). They reported that DIC microscopy is an effective technique for understanding the cellular intake mechanisms and nuclear localization of the AuNPs, relying on their surface modification and the using cell type [304]. The combined use of different colloidal particles in DIC microscopy enables selective imaging of nanoparticle probes in the living cells. Silver nanoparticles and AuNPs exhibit large apparent refractive indices near their SPR wavelengths. Although these nanoparticles display robust contrast in a narrow spectral band, their resolution at other wavelengths in DIC imaging remains weak. To address this challenge, Sun et al. modified the DIC microscope to allow synchronous imaging at two wavelengths. For this purpose, they hybridized two different nanoparticles (silver and gold NPs) on the same glass surface and selectively imaged them separately. In their study, they reported that the picture contrast of the silver and gold NPs changes

largely as a function of nanoparticle size and illumination wavelength in the DIC microscopy. They recorded high-contrast rapid images of the live cells with and without illuminating AuNPs probes and thus achieved precise probe determination. As a result, the simultaneous use of multiple probes with the dual-wavelength DIC technique enabled live cell imaging at high speed and contrast [305]. AuNRs are perfect orientation probes thanks to their anisotropic optical features. AuNRs combined with DIC microscopy technique have been used to resolve the rotational motions of nano cargos carried by the motor proteins. The researchers reported that in proportion to single-molecule polarization fluorescence imaging, this technique was more efficient in point of resistance to background noise and photobleaching [306]. Plasmon resonance energy transfer (PRET) is based on the principle that a plasmonic nanoparticle gives energy to a nearby acceptor molecule and plasmonic quenching of the donor nanoparticle. DIC microscopy enables synchronous imaging of complicated environments and noble metallic NPs in real time [307].

5.3. Photoacoustic imaging

Photoacoustic imaging (PAI) approach, based on the principle of energy conversion from light to ultrasound waves, allows obtaining real-time images that improve the quality of tissues at the molecular level. Photoacoustic energy signals produced by the pressure distribution and absorbed light hitting the tissues with laser beams can reach a depth of up to 7 cm in the tissues. Considering the advantages of AuNPs such as photostability and anti-photobleaching properties, their combined use with PAI enables high-contrast real-time imaging of tissues [308–310]. Au-based nanomaterials have the potential to be used as contrast agents in the field of cancer diagnosis, allowing quantitative and noninvasive imaging of tumor tissues. Zhang et al. showed that the PEG-modified Au-nanomaterials with high photoacoustic contrast administered systemically to the mice can be used as contrast agents for cancerous tissue monitoring *in vivo* with photoacoustic tomography (PAT) [311]. In another study, the researchers reported novel photolabile gold-PEG-diazirine nanocomplexes for *in vivo* PTT and photoacoustic imaging of tumors. Since AuNPs can be effectively shifted into the NIR region, small-sized AuNPs are unique nanomaterials for both advanced PAI applications and PTT applications of malignant tumors [312]. The design of the metallic nanoparticles using split fluorescent protein scaffolds as both molecular adhesives and Raman reporters has filled an important gap in terms of the creation of nanocomplexes with well-defined Raman hotspots and site-specific surface-enhanced Raman-scattering (SERS) activation of the complex biological nanoprobes. The nano system developed by the researchers provides an innovative approach for remote assembly of nanocluster probes for multimodal SERS and PAI on the biological targets with high selectivity and sensitivity in the cells and also potentially *in vivo* [313].

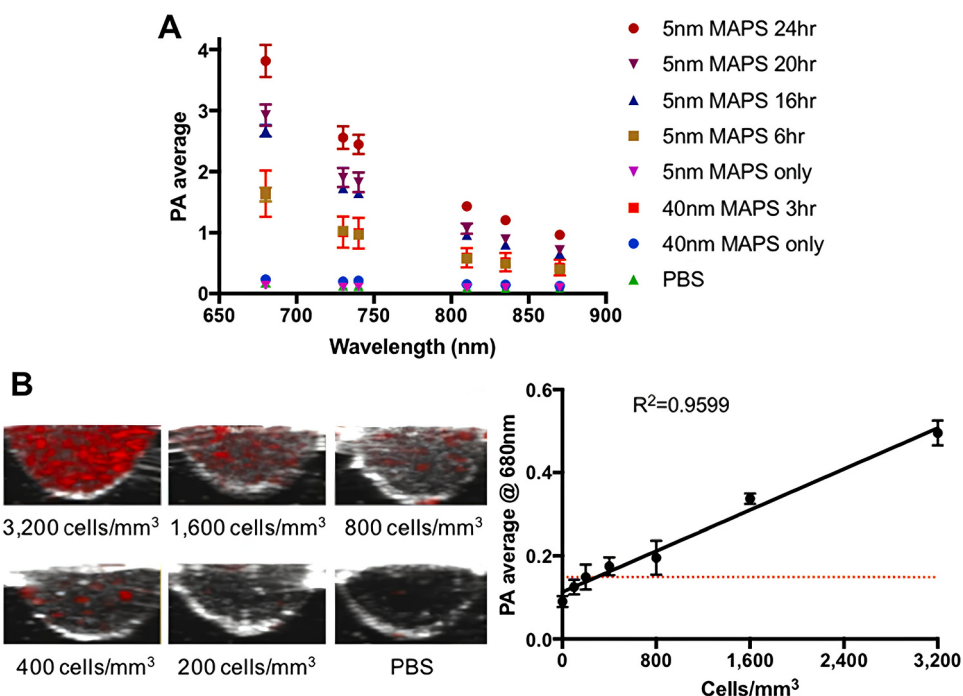


Fig. 18. (A) PA spectra of A431 cells labeled with either 5 nm or 40 nm MAPS over different time periods in comparison with the nanoparticles alone. The spectra were acquired from triplicate wells per sample ($n = 3$). For each well, PA signal was calculated as the average value from 5 different cross-sectional images at 680, 730, 740, 810, 830, and 870 nm. (B) Representative cross-sectional images of A431 cells labeled with 5 nm MAPS for 10 h at different concentrations. A linear regression fit of PA signal intensity as a function of a number of labeled A431 cells shows a detection limit of ~ 200 cells/ mm^3 , corresponding to $\sim 11,400$ cells inside a single 57 μL well. Adapted with permission from reference [314]. Copyright (2019), Optica Publishing Group.

“Ultra-small” AuNPs with sizes below 10 nm are extremely difficult to use as contrast agents for PAI due to the direct, non-linear relationship between their absorbance (their absorptions below the NIR range) and size. In order to demonstrate the applicability of responsive PAI with the ultrasmall Au-nanomaterials, Han et al. demonstrated the design of 5-nm plasmonic-nano sensors which are molecularly activated (MAPS) that generated a robust PA signal in the marked cancerous cells in the NIR region (Fig. 18) [314]. A new class of nanoparticles, gold-gold sulfide (GGS), is known to have strong NIR absorption but lack colloidal stability. To address this issue, the researchers synthesized highly stable GGS nanoparticles using a one-step synthesis method and applied different coatings (anionic: 3MPA, cationic: bPEI, and protein: BSA) to their surfaces. *In vitro* PA microscopy images recorded with near-infrared and visible lasers revealed that GGS nanoparticles were effectively internalized by MDA-MB-231 cells. A coating-dependent intracellular PA signal was observed in favor of GGS-3MPA, while the weakest signal was obtained with GGS-BSA, indicating low cellular uptake [315]. Anisotropic AuNPs are highly valuable as contrast agents because they do not photobleach and produce strong PA signals. A limiting factor in their use is the frequent use of cytotoxic reagents during synthesis. In one study, Zhang et al. designed novel PA probes based on nanostar cores and polymeric shells (PEG, chitosan, or melanin). The AuNP shell not only improved the biocompatibility of the nanostructures but also significantly influenced their performance [316].

5.4. Fluorescence imaging

Fluorescence imaging techniques rely on the basis of postponed photon emission from the fluorescent probe following irradiation of the biological sample to be imaged at a specific wavelength, has many advantages including low cost, improved resolution, rapid data acquisition and wide application field, etc. In fluorescence imaging area, AuNPs are used by conjugating with organic markers thanks to their superior

optical/plasmonic characteristics, photostability and capability to enhance the fluorescent signal [317]. It has been shown that the fluorescence excitation of the probe rises remarkably when the characteristic SPR parameters of the Au-nanomaterials overlap with the emission/absorption spectra of the fluorophore [318]. The unique plasmonic features of Au-nanomaterials allow the characterization of the samples with weak fluorescence emission and AuNPs facilitate the acquisition of higher resolution images since the diffraction limit can be exceeded. Especially in the natural biological microenvironment, it is very difficult to detect single biomolecules, and gold nano-antennas with various structural features have been shown to efficiently advance the fluorescence signal of the single molecules [319,320]. In a study investigating the role of SPR properties of the isolated gold nanorods on fluorescence enhancement, it has shown that the fluorescence of a weak emitter (crystal violet) can be increased more than 1000-fold with a single rod shaped Au-nanomaterial with a 629 nm SPR and at 633 nm excitation. They also reported that the fluorescence enhancement that developed upon increase in both excitation and emission rate decreased sharply when the SPR had only a partial overlap with the emission spectrum of the fluorophore or when the SPR wavelength moved away from the excitation laser wavelength [321]. Wientjes et al. reported that by binding to a gold nanoantenna, the light-harvesting complex 2 (LH2) showed more than a 500-fold increase in fluorescence at the single-molecule level. Their proposed bright antenna-enhanced LH2 emission is a very encouraging system for studying energy transfer and the role of quantum coherence at the level of single complexes [322]. Cillari et al. designed a poly(amidoamine)-based nanocomposite hydrogel containing AuNPs and carbon dots (CDS) and formed a 3D fluorescent network responsive to pH changes in the tumor microenvironment (TME; pH 5.5–7.4). Their findings may support the application of l-ARGO7@CDS/AuNPs nanogels for fluorescence-guided tumor detection and pH-sensitive monitoring of therapeutic outcomes, providing opportunities for personalized oncological treatments [323].

Fluorescence imaging techniques were used to investigate the

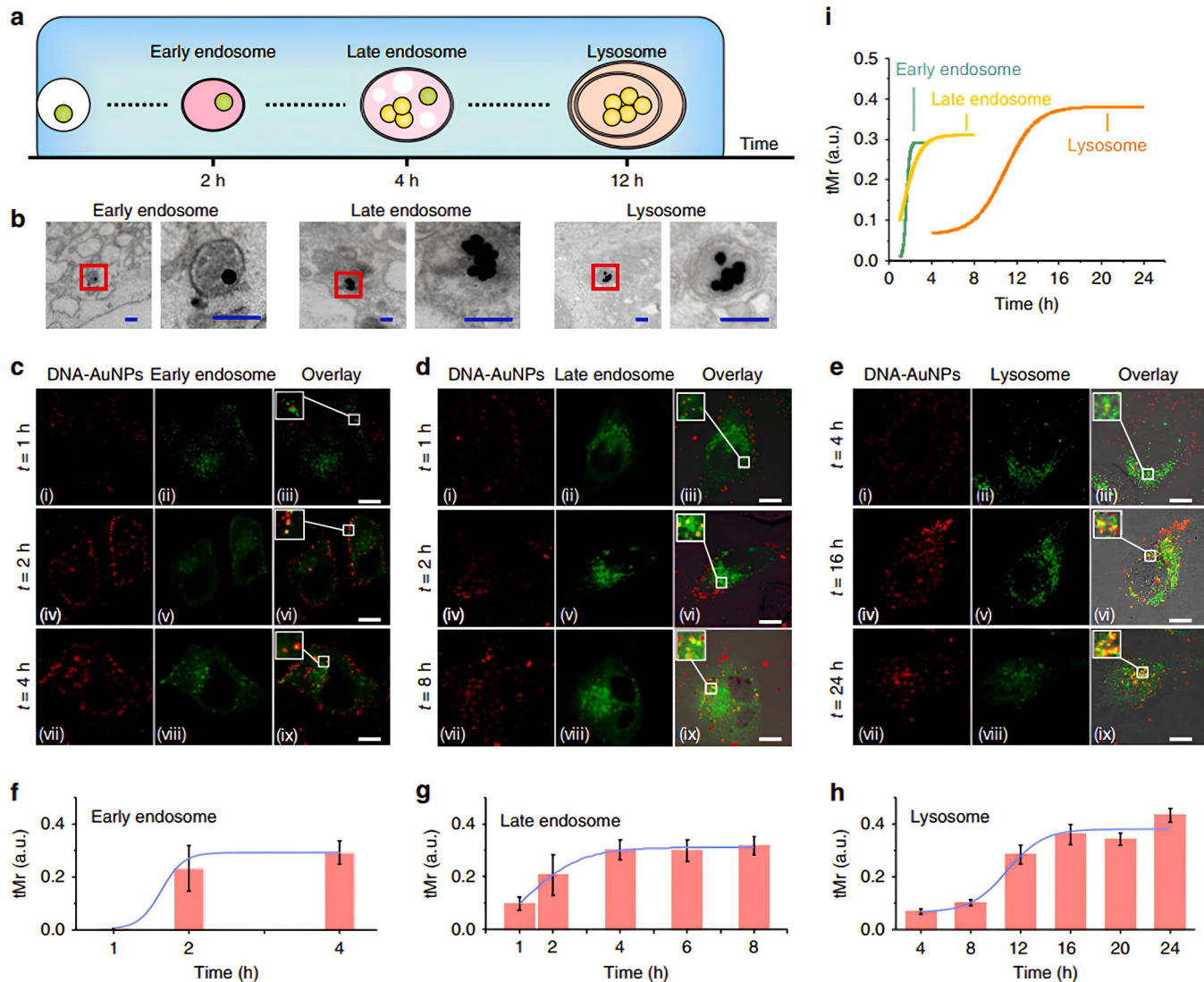


Fig. 19. Intracellular trafficking of fPlas-gold. (a) Schematic showing intracellular trafficking of fPlas-gold. (b) Representative TEM images of fPlas-gold trapped in early, late endosomes and lysosomes. Scale bar, 200 nm. (c–e) Fluorescence microscopy (FM) images showing co-localization of fPlas-gold (red) with early endosomes (green), late endosomes (green) and lysosomes (green). Scale bar, 10 μm. (f–i) Plots of thresholded Mander's co-localization coefficient (tMr) values over time for early, late endosomes and lysosomes, respectively. Adapted with permission from reference [327]. Copyright (2017), Springer Nature.

endocytic intake processes of Au-nanomaterials into the cells [324–326]. In a study, Liu et al. used DNA-modified Au (fPlas-gold) NPs as a dual-emitting plasmonic and fluorescent probe to investigate the intracellular delivery and aggregation situations of the nanoparticles. According to their obtained fluorescence and plasmonic images, fPlas-gold nanoparticles were single particles in the early stages of endocytosis, while they were clustered in the vesicular transport and maturation stage. They reported that the transport rates of encapsulated AuNPs-fPlas were related to the size of the aggregates, independently of endosomes and lysosomes (Fig. 19) [327]. Although gold nanoclusters show weak SPR properties because of their very small dimension, they have visible fluorescence features in the NIR region [328,329]. Thus, the intrinsic fluorescence properties of gold nanoclusters enabled the imaging of their cellular interactions and internalization [330,331]. The approach of combining efficient fluorescence detection with intracellular drug delivery is a significant foot in the theranostic agent development area. In a study, cross-linking between the gold nanoclusters led to an approximately 4-fold rise in fluorescence in proportion to the free ones and was accompanied by an increment in lifetime of fluorescence. Their results presented an innovative approach to synthesize

self-assemble nanoparticles from metallic nanoclusters with various kinds of polymers as crosslinking agents, exhibiting properties responsive to environmental stimuli, in a facile method [332]. In another study, Wang et al. demonstrated the Au-based nanoclusters (AuNCs-K) that can selectively spot nucleoli and enable fluorescence imaging. Because of their small dimensions and cationic surface (Lys-Cys-Lys surface ligands), the synthesized AuNCs-K were able to collect adequately at the nucleolar locations and provided certain morphological data [333].

Additionally, gold nanoclusters with various chemical properties have been used for effective and strong fluorescence imaging studies in the animal tumor models [334,335]. Hayashi et al. used the AuNPs with a diameter of 7 nm clustered with silica fluorescent core-shell nanoparticles for robust fluorescence-CT dual-mode monitoring of the cancerous tissues [336]. In another study, the use of folic acid-modified and photostable BSA-gold nanoclusters has been reported for targeted fluorescence monitoring of the human ovarian cancerous cells [337].

5.5. Two-photon/multiphoton photoluminescence imaging

The use of two NIR photon-exciting light in two-photon imaging technique (TPI) enables deeper (from several hundred micrometers to millimeters) and enhanced fluorescence imaging as it reduces tissue background scattering [338]. In particular, the SPR feature of gold nanorods (AuNRs) provides tens-hundreds of times increased photon absorption for TPI compared to conventionally used organic fluorophores [339]. Our recent study showed that very strong fluorescent radiation was obtained from the various cellular regions (especially from nucleoli) of the DRG sensory neurons under a TPI microscope without using any organic dye as a result of short-term incubation of the cells with AuNR-PEI nanostructures [6]. The two-photon photoluminescence (TPPL) features of gold nanomaterials are mainly dependent on the nanoparticle form. When Gao et al. researched the TPPL characteristics and scattering spectra of the Au nanomaterials of five various shapes (nanocubes, nanospheres, nanorods, nanobranches, and nanotriangles) at the single particle level, they reported that the TPPL spectra of these AuNPs were strongly modulated by plasma resonance. They showed that the TPPL density increased in the order of spherical AuNPs, cubic AuNPs, triangulated AuNPs, rod-shaped AuNPs, and Au nano-branches [340]. In another study, the researchers proposed a new type of contrast agents based on the Au-nanocages (AuNCs) with porous walls and hollow interiors to mark the hMSCs and monitor them *in vivo/in vitro* using photoacoustic microscopy and two-photon technique. The authors reported that they were able to monitor the cells marked using the designed AuNCs for at least 28 days *in vitro* and also monitor the cells that host the tumor site in nude mice *in vivo* [341]. TPL properties in Au enable high signal specificity for monitoring AuNPs in a biological system. Morales-Dalmau et al. reported that TPL imaging provided a powerful submicron resolution technique that can measure accumulated AuNRs in both the cells and tissues [342]. Since plant consumption is one of the causes of cyanide (CN-) exposure to mammals, sensitive and selective cyanide detection in plant tissues has become important. As an innovative approach address to this issue, the researchers have developed a novel dual-photo excitation (TPE) nano sensor that used a conjugate of graphene quantum dots and AuNPs to detect and image endogenous biological cyanide. The researchers' design proposed an innovative system for the design of a fluorescent two-photon nanocomplex that has potential for use in safety testing and food processing [343]. The performance of AuNRs in bioimaging is mainly concerned with the suitability of their surface coatings. Egorova et al. demonstrated that increased stability of the AuNRs coated with biocompatible self-assembling peptide amphiphiles and facilitated *in vivo* TPI [344]. In another study, a high-performance combined cancer therapy involving both PTT and chemotherapy has been reported to increase therapeutic efficiency using the AuNR@mSiO₂ loading molecular Dox assemblies. In this study, the researchers incorporated two-photon fluorescence excitation monitoring into LSCM multi-channelled imaging to monitor the drug delivery process in the killing HeLa cells and also perform imaging-guided cancer therapy [345]. Fluorescence imaging has advantages of high selectivity, non-invasiveness, high sensitivity, and *in situ* imaging. However, single-photon (OP) fluorescence imaging has the disadvantages of low spatiotemporal resolution and low tissue penetration depth. These disadvantages can be overcome by TP fluorescence imaging. Fluorescence lifetime imaging (FLIM) can effectively prevent autofluorescence interference and fluorescence intensity-driven fluorescence imaging fluctuations. Li et al. developed a dual-mode nanoprobe platform based on the incorporation of silica-coated gold nanoclusters (AuNCs@SiO₂) and nucleic acid probes for TP and FLIM imaging of intracellular endogenous miRNA-21 for the first time. These dual-mode platforms have promising clinical application potential in miRNA-based early diagnosis and therapy [346].

5.6. X-ray computed tomography

The disadvantage of computed tomography, which provides high-resolution anatomical imaging, is the requirement for X-ray contrast agent to separate organs/tissues with analogue or weak X-ray attenuation [347]. These contrast materials which are iodine-based have little circulation duration in the blood and these compounds are quickly taken out from the blood, resulting in the requirement for multiple injections and short imaging windows [348]. AuNPs have aroused great notice as an alternative contrast nanomaterial in recent years thanks to their advantageous physical/chemical features such as biocompatibility, easy synthesis, high X-ray absorption capacity, and stability [298]. Astolfo et al. investigated *in vivo* imaging of the AuNPs-loaded F98 cells in a mice model using X-ray CT [349]. In another study, AuNPs were grown on the PEG modified dendrimer to fabricate a contrast material for CT. It was reported that when a large number of Au ions were added, both the dimensions and surface plasmon absorption of the grown AuNPs raised. After injection into the mice, the engineered nanomaterial was shown to provide blood pool imaging that was larger than that of commercial iodine reagent [350]. The suitable surface functionalization of Au-nanomaterials is a significant factor in terms of increasing blood uptake and cancer specificity. Nakagawa et al. modified the AuNPs with PEG sequences on their surface to raise blood holding and conjugated them with a cancer-targeting ligand by the PEG-terminal chains. Their results demonstrated that the specific localization of the designed AuNPs in the cancerous tissue was significantly enhanced by conjugation with the antibody [351]. Size, shape, surface modification and concentration of AuNPs can impact on X-ray attenuation. In a study, AuNRs at higher concentrations and with larger aspect ratios displayed better impact on X-ray attenuation. Furthermore, PEG layer on the AuNRs declined X-ray attenuation through reducing the clustering of gold nanorods. They also reported that lesser sized sphere-shaped AuNPs (13 nm) could enhance X-ray attenuation more than bigger ones (60 nm) [352]. Dong et al. comprehensively researched the connection among AuNP dimension and X-ray-CT contrast. They synthesized AuNPs with dimensions extending from 4 nm to 152 nm and modified their surfaces by PEG molecules. Their X-ray attenuation is associated linearly by the AuNPs intensity. Although they did not find a statistically important alteration in CT contrast formation between different AuNP sizes, their results showed that the AuNPs-PEG of 15 nm or lesser had extended blood movement durations from both *ex vivo* analysis with ICP-OES and *in vivo* imaging studies (Fig. 20) [353].

In a study by Takiguchi et al., they performed X-ray imaging of a mouse using a colloidal solution of polyvinylpyrrolidone (PVP)-coated Au/Bi₂O₃/PVP nanoparticles. They demonstrated that the X-ray imaging capability of the synthesized Au/Bi₂O₃/PVP nanoparticles was superior to that of a commercial X-ray contrast agent [354]. In another study, researchers applied environmentally friendly chemical methods using the FDA-approved Pluronic F127 (PLU) block copolymer to simultaneously create and stabilize biocompatible AuNPs. Subsequent *in vivo* maternal and fetal toxicity tests in rats to assess the efficacy of the AuNP-PLU-UV formulation during pregnancy demonstrated that the treatment was safe for both mother and fetus. As a demonstration and proof of concept, they demonstrated that the nanocomposite performed similarly to commercially available contrast agents when used as a contrast agent in X-ray computed tomography scans [355].

5.7. Optical coherence tomography

Optical tomographic techniques that provide 3D images enable the diagnosis of diseases without harmful irradiation. Optical coherence tomography (OCT) is a powerful imaging method in which a beam is divided into two, one beam traveling along the sample and the other one using a reference beam. Plasmonic AuNPs have been designed as contrast materials thanks to their strong SPR. New types of Au-based nanomaterials have been designed to improve the contrast in OCT

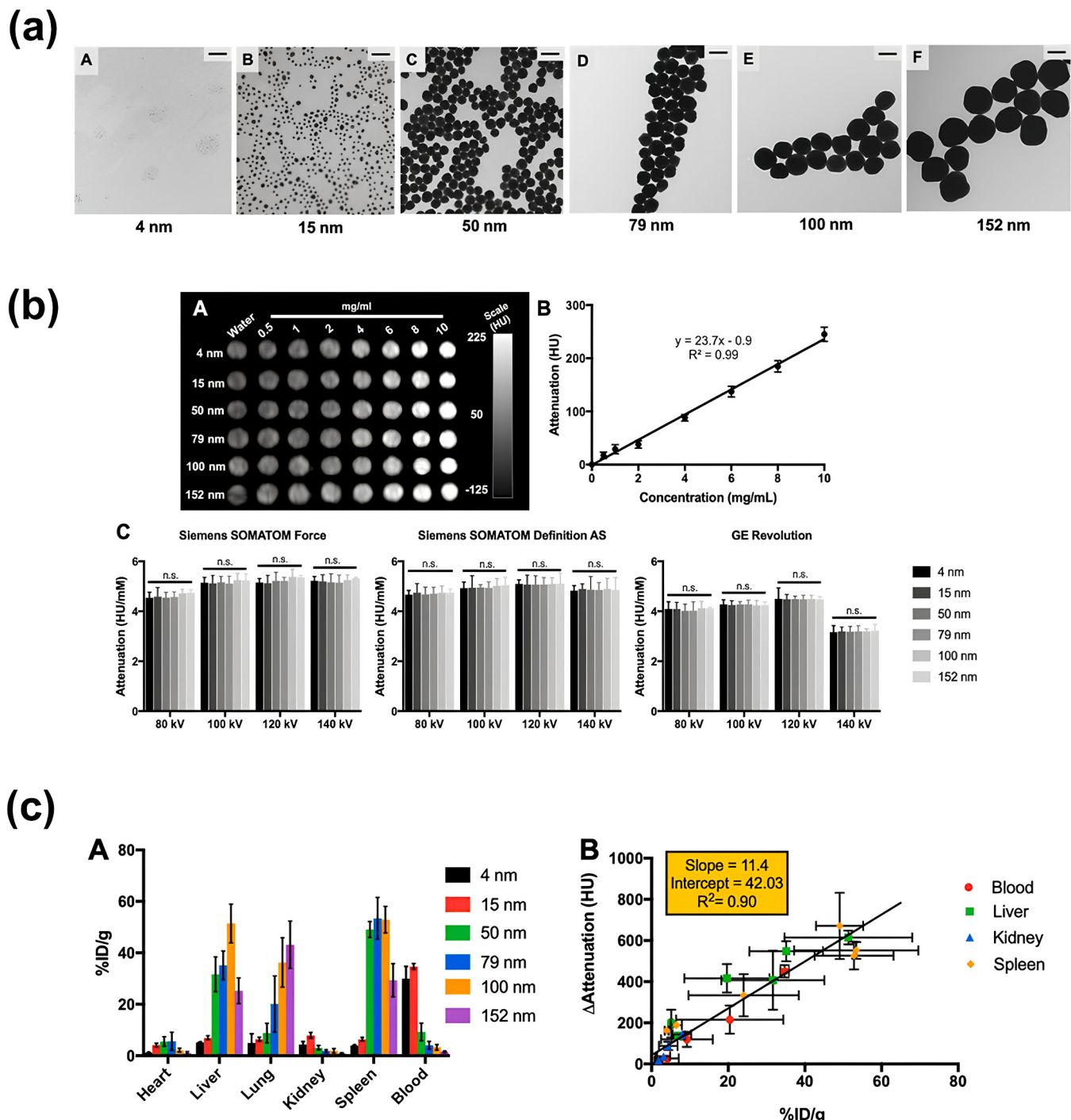


Fig. 20. (a) TEM images of the AuNPs. (a-A) 4 nm, (a-B) 15 nm, (a-C) 50 nm, (a-D) 79 nm, (a-E) 100 nm, (a-F) 152 nm AuNP. The scale bars represent 100 nm in all panels. (b) Representative sample phantom images and attenuation rate values for AuNP formulations. (b-A) Representative sample phantom images from Siemens SOMATOM Force CT scanner. (b-B) X-ray attenuation changes versus concentration for 50 nm AuNP scanned by a Siemens SOMATOM Definition AS CT at 80 kV. (b-C) Attenuation rate values for the AuNP formulation for the scanners noted at 80, 100, 120 and 140 kV. (c) Biodistribution and the attenuation changes of AuNPs in different organs. (c-A) Biodistribution of AuNP in different organs at 2 h post-injection. A Tukey's multiple comparisons test was done to compare the interactions between each AuNP size. (c-B) Comparison between the attenuation change in different organs derived from CT scans performed at 2 h post-injection and biodistribution of AuNP in different organs at 2 h post-injection determined with ICP-OES. Adapted with permission from reference [353]. Copyright (2019), Springer Nature.

monitoring. Genina et al. reported imaging of *ex vivo* and *in vitro* distribution of the AuNPs (Au nanocages) in the liver tissues using the OCT method. They showed that the application of the AuNPs significantly increased the imagination contrast in the blood vessels of the liver thanks to the localization of the nanomaterials there [356]. In another study, the researchers reported on a multimodal imaging platform

consisting of OCT methods for high-resolution, wide-field-of-view *in vivo* imaging of the gold nanomaterials. The platform they used included superimposed pictures of tissue morphology and microvascular, as well as the initial *in vivo* pictures of nanomaterial (Au-nanorods) pharmacokinetics obtained by photothermal-OCT [357]. In a study aiming to use stimuli-responsive gold nanoclusters (AuNCs) as an OCT contrast

material in the diagnosis of early-stage cancer, the designed AuNCs were implemented in a hamster cheek pouch model bearing carcinoma squamous tissue in early-stage. The study imaging the cancerous tissue with OCT approach has demonstrated the potential of diagnosis early-stage cancer using inorganic nanomaterial-based, molecularly programmable contrast materials that can produce stimulus-triggered and multiple diagnostic signals in early-stage cancer [358]. OCT-angiography (OCTA), which is a significant technique for examining microcirculation and vascular networks in alive tissues, has difficult aspects such as unusually slow flow of blood in angiogenic tumor vessels, weakening of light by cancerous tissue, and incomplete mapping of vascular networks. As a solution to this issue, the investigators have established that the usage of gold nano-prisms (GNPRs) as an OCT contrast agents meaningfully improved dynamic scattering signals in the micro vessels and also increased the sensitivity of OCTA in the melanoma tumors and skin tissue *in vivo* [359]. OCT is a promising imaging technique for skin cancer diagnosis. However, it is disadvantaged due to the low contrast between neoplastic and normal tissue. To defeat this restriction, Xu et al. used the AuNPs as OCT contrast agent and they applied the nanoparticles topically to reduce the risk of *i.v.* injection-related side effects. Additionally, the authors reported that the mixture of sonophoresis and DMSO was an efficient process to increase the skin penetration and diffusion rate of AuNPs [360]. In another study, the design of RGD peptide conjugated ultrapure chain-like Au-nanomaterial (RGD-CGNP) clusters was demonstrated for OCT enhanced molecular imaging and multi-modal PAM. Intravenous injection of the designed CGNP clusters-RGD bound to blood vessels which were newly developed in the sub-retinal pigment epithelium (RPE) space of the retina, named choroidal neovascularization (CNV) and caused in up to a 17-fold rise in PAM signal and 176 % rise in OCT signal [271]. Calvert et al. developed gold superclusters (AuSCs) tailored to clinical instrumentation and integrated into clinically relevant workflows. The polymeric coating they applied promoted the homogeneity of the AuSCs, providing a functional handle for targeting intravascular P-selectin, an early vascular endothelial marker of inflammation. In a rat model of intravascular inflammation, they demonstrated that the targeted AuSCs facilitated IV-OCT molecular imaging. The signal strength they obtained varied proportionally with the severity of vascular inflammation [361]. In another study, researchers designed gold nanocages with small edge lengths (~65 nm) and a surface plasmon resonance peak at approximately 1060 nm, representing a potential class of contrast agents for OCT. *In vivo* OCT imaging findings on mouse tissues demonstrated a significant increase in imaging contrast due to the presence of gold nanocages [362].

5.8. PET/SPECT techniques

Single photon emission computed tomography (SPECT) and positron emission tomography (PET) are frequently preferred in the field of biomedical tomography thanks to their high sensitivity and competence to classify unusual cells from healthful cells. But the limitations of traditional contrast materials are their poor tumor selectivity, short half-life and lack of spatial resolution [279,363]. AuNPs have been labeled using different radionuclides and extensively investigated for SPECT/PET applications. In a study, the design of a SPECT imaging probe targeting apoptotic macrophages was carried out to achieve precise assessment of the accurate localization and sensitivity of atherosclerotic plaques through dual-mode imaging using AuNPs-PEG-AnnexinV-Tc-⁹⁹ radionuclide nanoconjugates [364]. In another study, the design of the stable AuNPs fixed by ¹⁹⁹Au atoms for targeted high quality SPECT cancerous tissue imaging in a triple-negative breast cancer mouse model was described. It has been shown that conjugating ¹⁹⁹Au-AuNPs with DAPTA for CCR5 targeting leads to significant increase in the SPECT/CT tumor imaging specificity and sensibility as well as improvement in biodistribution profile [365]. Zhao et al. described the use of the ⁹⁹m-Tc-labeled PEI-entrapped multifunctional AuNPs (PENPs-Au-⁹⁹m-Tc)

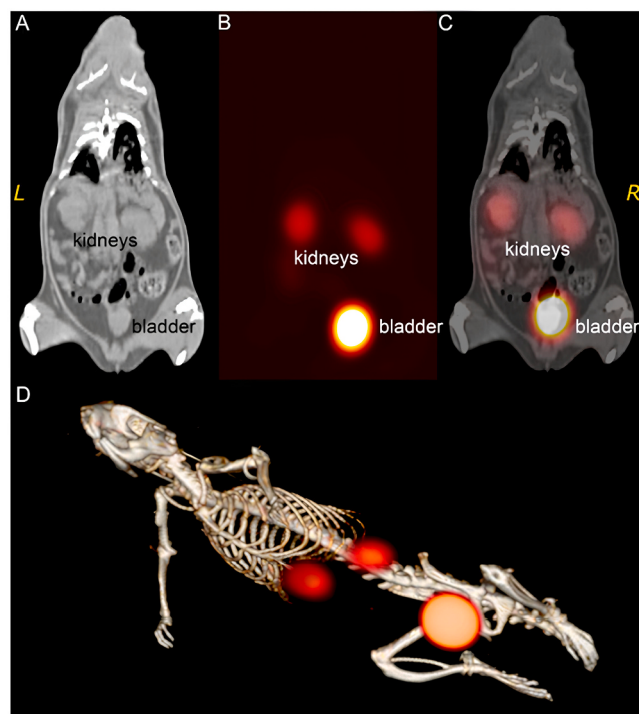


Fig. 21. CT, SPECT and fused SPECT/CT coronal image of ⁹⁹m-Tc-BSA-AuNCs distribution in the animal model at 90 min p.i. (A) CT image with clear anatomical visualization of kidneys. (B) SPECT coronal slice with the visible kidneys and bladder regions. (C) Fused images giving a more precise localization of the tracer uptake in the organ areas seen on planar images. (D) 3D volume rendered image using the data from (A–C). Adapted with permission from reference [368]. Copyright (2022), MDPI.

for double-mode SPECT/CT single-photon emission imaging applications. It has been shown that the nanoconjugate material with high radiochemical purity and stability synthesized by the researchers exhibited good SPECT/CT tomography implementation in various organs [366]. Imaging chemotherapy-induced apoptosis with a non-invasive method is very important in determining the therapeutic effectiveness of the drug. The design and use of dendrimer-entrapped-⁹⁹m-Tc-labeled Au-nanomaterials (Au-DENPs) for targeted CT/SPECT monitoring of chemotherapy-induced tumor apoptosis was demonstrated. Their designed duramycin-functionalized Au-DENPs can be used as a nanocomplex for the recognition of apoptosis and early stage tumor reaction to chemotherapy [367]. Merging optical imaging by other methods can provide significant advantages in diagnosing diseases. Jarockyte et al. investigated the bio-distribution of the technetium-⁹⁹m labeled biocompatible BSA-Au nanoclusters (AuNCs-BSA-⁹⁹mTc) as a photo-luminescence-CT/SPECT material in experimental Wistar rats. Based on their experiments, the researchers concluded that AuNCs-BSA-⁹⁹mTc could be used as prospective contrast materials for *in vivo* bloodstream imagination of excretory organs (Fig. 21) [368].

In a recent study, researchers developed two multi-modal radiotracers appropriate to PET/SPECT methods, consisting of an AuNPs core, a shell (glucosamine units) complicated in radioisotope entrapment, polymeric biocompatible sequences, and peripherally located targeting molecules. Of the AuPEG-PEI-GA-⁹⁹mTc or ⁶⁸Ga nanoconjugates they designed, ⁹⁹mTc nano-complexes stayed stable for above 22 h, whereas the ⁶⁸Ga including ones showed a small decline in stability after 1 h [277]. While radiation therapy is a powerful lung cancer treatment, challenges remain due to the low resolution, limited, or invasive applicability of real-time dosimetry methods. A study by Hosseiniabadi et al. aimed to use AuNP-induced pair production to obtain PET images during lung tumor radiotherapy and to evaluate their applicability for

real-time dose monitoring. Quantitative evaluation of MVIPET images demonstrated that lung tumors can be detected with this method as AuNP concentration and photon beam energy increase. MVIPET images obtained during radiotherapy can be used for real-time dose monitoring. This method can also verify a patient's radiation dose [369].

5.9. Magnetic resonance imaging (MRI)

Magnetic resonance imaging (MRI) is a method that relies on the nuclear spin principle, provides high-resolution images for *in vivo* monitoring of tissues and organs, and is frequently preferred in clinical diagnostic processes. Gold nanoparticles have been used mostly in hybrid forms with other metals for MRI purposes. Holbrook et al. designed a Gd(III)-dithiolane -AuNPs contrast materials that collect in the pancreas and offer considerable contrast improvement with MR imaging. The researchers reported that the nanoconjugates they prepared exhibited very high r1 relaxivity values per particle at both high and low magnetic field strengths thanks to the high Gd(III) charge [370]. In a study where the DNA-gadolinium-AuNPs nanoconjugates were used for T1-MR imaging *in vivo* of the transferred human NSCs, the DNA-Gd@AuNPs were shown to demonstrate an enhanced T1 relaxivity and tremendous cellular intake [371]. Although the prevalent therapeutic use of Au-nanomaterials outer the central nervous system, their biodistribution within the CNS following intravenous injection of the nanoparticles is quite limited owing to the discriminating structure of the BBB. MRI-guided focused ultrasound (MRgFUS) is an innovative approach that can enhance BBB penetrability, enabling transport of nanotherapeutics to the CNS. Using the MRgFUS technique in a rat model, Etame et al. showed for the first time the improved and safe transfer of their designed AuNPs by focusing on the CNS [372]. In another study, sugar/gadolinium loaded gold nanoparticles were used to label and image cells with MRI. Carbohydrate-coated paramagnetic AuNPs exploit the affinity of cells for simple sugars and they are permeable, highly efficient, and biocompatible reporter nanoprobe for MRI. Furthermore, the presence of sugars on the superficial of AuNPs increased the concentration of Gd cations on the cell surface. The researchers' results highlight the benefits of using sugars as an alternate to peptides, oligonucleotides or PEG molecules to yield nanoparticles for cellular labeling [373].

This section offers a review of the current developments concerning the usage of gold nanomaterials for bio-imaging applications. Among other metallic nanoparticles, Au-nanomaterials have excellent capability to be used in bio-imaging field. The AuNPs have a broad scope of SPR based on the nanoparticle's dimensions, shape and surface modification. AuNPs with various properties have been considerably researched experimentally for their optical superior characteristics and biological, cellular and *in vivo* applications. As a result of the use of AuNPs alone and as hybrid nanoconjugates in combination with the imaging techniques outlined above, it has been possible to understand their cellular interactions, localization, dynamics and the advantages they can provide to diagnostic processes. Although very promising results have been obtained as a result of the use of AuNPs in the biological imaging area, there are still some challenges. There is a big need to design 3D-nanoparticle tracking systems to recognize cellular bio-nano interactions. More sensitive and effective plasmonic AuNP-based nanoconjugates can be designed through alternative and innovative synthesis and surface modifications. *In vivo* tissue/organ imaging applications are nonetheless challenging owing to the little entrance depth of light. New hybrid nanoparticles that scatter NIR light should be developed to reduce the scattering background and improve detection depth. Additionally, bioimaging studies are required to reveal the interaction mechanisms of AuNPs with biomolecules in cells in more detail. In addition, stability, toxicology, risk and safety evaluations of AuNPs should be considered individually in a broad framework for their use in each bio-imaging technique.

Considering the unique SPR effects of AuNPs in photoimaging, their

clinical use as an alternative contrast agent in imaging systems is favorable. With appropriate surface modifications and design of hybrid structures, the use of AuNPs targeted and directed to the tumor site supports better contrast images. Although an abundance of preclinical data has shown the potential use of GNPs as radiosensitizers, this application has not been translated into the clinical setting. In order to increase the clinical use of AuNPs as imaging agents, a better understanding of their safety is necessary. In this regard, extensive testing is needed.

6. Gold nanoparticles for biological sensing

AuNPs which are inorganic metallic nanomaterials, are at the forefront in diagnostic and biosensor studies thanks to their unique physical/chemical and electronic features, stability, and controllable interplays with biomolecules as a result of suitable surface functionalization. Surface functionalization strategies of Au-nanomaterials are implemented via covalent or non-covalent based methods. Thiol (S-Au) binding handling the ligands which are sulfur containing (such as disulphides, cysteine groups, and organothiols) is the most commonly preferred covalent approach type. In the non-covalent approach, effective release of ionized ligands by natural forces is achieved through electrostatic and physical interactions [279,374–376]. For specific diagnostic use of AuNPs, their surfaces must be functionalized. Thus, specific identification components for the target analytes are provided on the surface. Since Au-nanomaterials can be easily conjugated by a wide range of recognition fragments (such as small biomolecules, oligonucleotides, peptides, antibodies, saccharides, toxins), biosensor applications come to the fore in their use for diagnostic purposes. In this context, AuNPs-based biosensor approaches working via various detection mechanisms have been designed in the literature, including colorimetric, fluorometric, electrochemical, surface-enhanced Raman scattering (SERS) based, bio-barcode assays and Quartz crystal microbalance sensors [279,375,377,378].

6.1. Colorimetric based sensing

This optical behavior of AuNPs, which exhibit SPR properties depending on size and shape, involves irradiation via certain wavelength light, which induces the electron oscillations in the transmission band of the nanoparticles. The colorimetric based biosensors have been improved by designing nanostructures of different shapes (spherical, rod, shell, star, pyramid etc.) for the detection of biomolecules, by taking benefits of this excellent optical property of AuNPs. Au-based colorimetric biosensors are one of the most advantageous material groups compared to other colorimetric sensors and provide very sensitive, simple and fast results for determining target analytes.

In the literature, the studies in which AuNPs were used for biosensing purposes have broadly targeted pathogens and their various biological structures. Highly uniform gold nano bipyramid structures (Au-NBPs) have been used in colorimetric ultraprecision detection of influenza virus. The researchers altered the refractive index of Au with a metallic silver shell modified on Au-NBPs, causing the longitudinal LSPR to be blue shifted, yielding a vivid color change. They used their proposed method to detect the H₅N₁ virus and achieved detection with a high level of sensitivity [379]. In another study, Tsai et al. used colorimetric AuNPs for tuberculosis (TB) diagnostics on an analytical device which is paper based. They were thus able to track alterations in the color of the Au-nanomaterials based on the effects of single-stranded DNA probe molecules hybridizing with the targeted double-stranded TB DNA with detection limit of 1.95×10^{-2} ng/mL for TB DNA [380]. The design of aptamer/AuNPs nanoconjugates has been used for the detection of various viral/bacterial proteins and toxins. A selective and sensitive colorimetric based biosensor was developed for the *staphylococcal* enterotoxin B (SEB) detection using AuNPs/SEB-binding aptamer (SEB2) nanostructures. The assay the researchers designed was highly

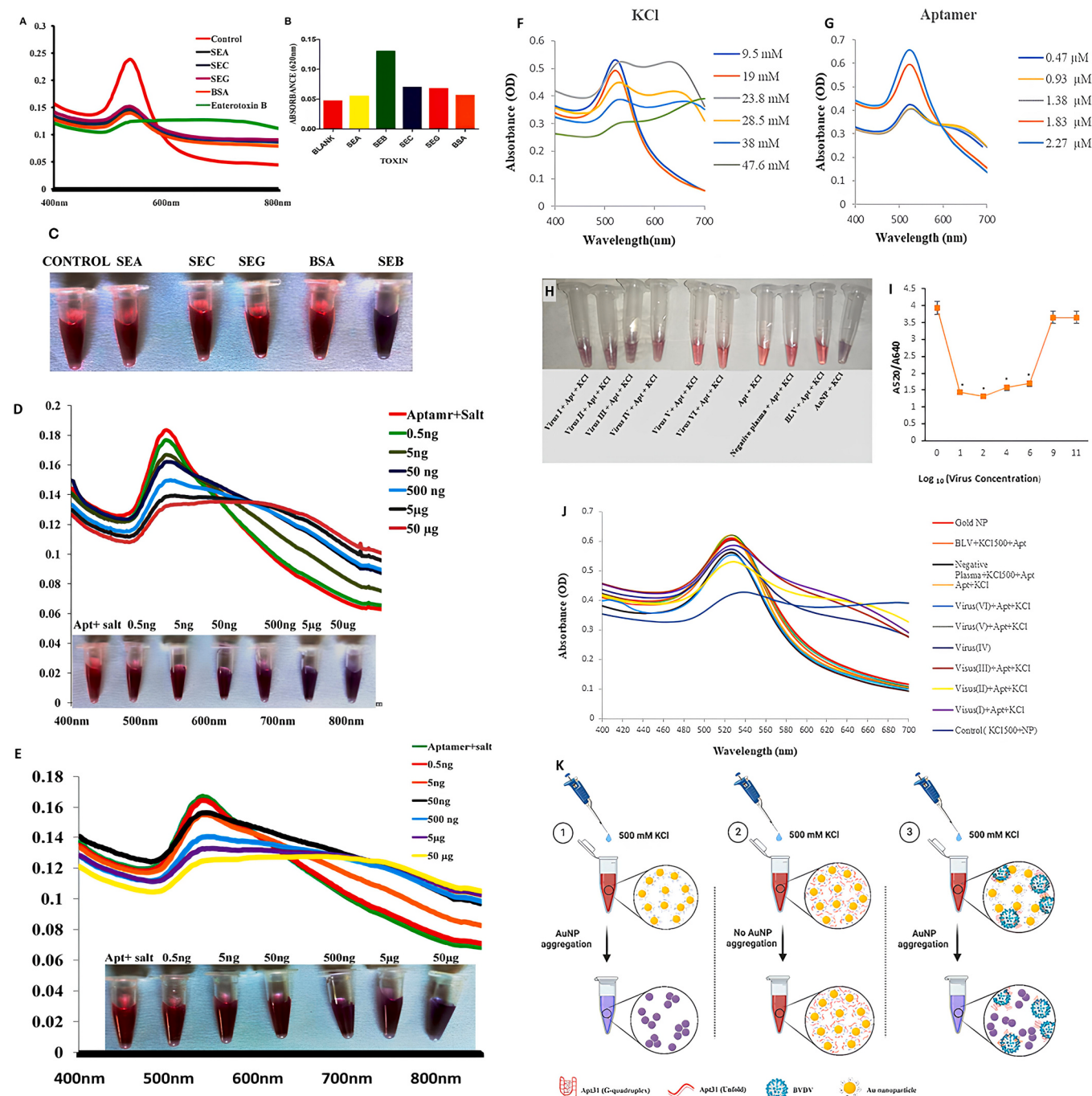


Fig. 22. Selectivity, sensitivity and robustness of Gold nano particle based colorimetric detection assay for the detection of staphylococcal enterotoxin B (SEB). (A) Absorption spectra of AuNPs/aptamer mixed solutions in the presence of other related toxin. (B) Absorption value at 620 nm of AuNPs/aptamer mixed solutions in the presence of other related toxin. (C) Visual observation of AuNPs/aptamer mixed solutions in presence of other related toxin. (D) Sensitivity of Gold nano particle based colorimetric detection assay. Absorption spectra of AuNPs/aptamer mixed solutions in the presence of various concentration of SEB. (E) Robustness of Gold nano particle based colorimetric SEB detection assay. Absorption spectra of AuNPs/aptamer mixed solutions in spiked milk sample with various concentration of SEB. Copyright © 2018 Mondal, Ramlal, Lavu, N and Kingston. (F-K) A label-free G-quadruplex aptamer/AuNPs-based colorimetric biosensor for rapid detection of bovine viral diarrhea virus genotype 1. (F) The UV-Vis absorbance spectra for AuNPs in 400–700 nm wavelength in the presence of final KCl concentrations of 9.5 mM to 47.6 mM. (G) Different concentrations of aptamer and 23.8 mM KCl. (H) Visual color change of AuNPs from red to purple in the presence of aptamer, KCl, and different concentrations of the BVDV from 0.27 to 2.7×10^{10} copies/mL. (I) The corresponding plot of A_{520}/A_{640} against \log_{10} virus concentration (copies/mL) from I to VI. (I): 0.27, (II): 2.7×10^1 , (III): 2.7×10^3 , (IV): 2.7×10^5 , (V): 2.7×10^8 , (VI): 2.7×10^{10} copies/mL. Apt: Apt31, BLV: Bovine leukemia virus. Values with $p < 0.05$ (*) were considered statistically important. (J) The absorbance spectra of the samples at 400–700 nm wavelength. (K) The mechanism of the action of the developed Apt31-biosensor. In stage 1, adding 10 μ L of 500 mM KCl leads to aggregation of AuNPs. In stage 2, the optimum concentration of Apt31 electrostatically binds to AuNPs and inhibits aggregation of AuNPs after the addition of the KCl solution. In stage 3, if the added plasma sample is infected with BVDV, Apt31 binds to the virus and separates from the surface of AuNPs. Subsequently, the addition of the KCl can result in aggregation of AuNPs and purple-blue color. Copyright: © 2024 Rabiei et al.

(a) Adapted with permission from reference [381]. (b) Adapted with permission from reference [382].

specific and sensitive for SEB compared to other toxins, with a detection limit of 0.5–50 ng/mL (Fig. 22 A-D) [381]. Another aptamer-AuNPs based colorimetric biosensor study was demonstrated by Rabiei et al. for the rapid detection of bovine viral diarrhea virus (BVDV) genotype 1. They used *in silico* methods to develop a G-quadruplex aptamer for the specific detection of BVDV-1. The aptamer they developed was experimentally confirmed and used for designing a colorimetric biosensor based on a AuNPs-aptamer complex. Their biosensor platform could identify the virus at as low as 0.27 copies/mL, which was an admissible amount in comparison to method of the qPCR (Fig. 22 F-K) [382].

E. coli is the most widespread food related bacteria, leading to diseases if left undiagnosed and untreated, which makes its detection more important. AuNPs have also been studied with various surface modifications and hybridizations for colorimetric *E. coli* detection. In a study, the AuNP aggregation state was successfully used for rapid detection and smart phone imaging of *E. coli* O157:H7 with a microfluidic colorimetric biosensor platform. The detection limit of their designed sensor device was 50 CFU/mL for *E. coli* O157:H7 [383]. In another study, the typing and colorimetric identification of the lipopolysaccharides of *E. coli* (LPS) was performed based on aptamer-modified a dual AuNPs probe. This caused a sandwich-mediated clustering of the Au-nanomaterials and a color alteration from red to blue. It could sense LPS in concentrations between 2.5 and 20 $\mu\text{g}\cdot\text{mL}^{-1}$ and with a 1 $\mu\text{g}\cdot\text{mL}^{-1}$ detection limit [384]. Gupta et al. used aptamer-conjugated graphene oxide (GO)-covered AuNPs for colorimetric naked eye identification of *E. coli*. GO covering enhanced the aptamer loading ability on nanoprobe making it more precision. The detection limit was 10^2 cells/mL [385].

Apart from pathogenic microorganisms and their products, Au-nanomaterials have also been used for colorimetric determination of different biomolecules (such as thrombin, human chorionic gonadotropin, myoglobin, proteins, and cholesterol). In these studies, the interactions of AuNPs with conjugations such as cationic polymer, peptide aptamer, G-quadruplex DNAzyme, aptamer and enzyme modification were successfully studied [386–390]. Colorimetric detection of cancer biomarkers using AuNPs has gained importance in recent years. Xiao et al. developed a powerful colorimetric biosensor based on extremely catalytic active AuNPs-modified Bi₂Se₃ (Au/Bi₂Se₃) nano-sheets for detection of cancer biomarker. Their designed biosensor platform showed high selectivity and sensitivity for the biomarker of cancer, even for a concentration as low as 160 pg/mL for CEA [391]. Prostate cancer is one of the most common male cancers worldwide, and determination of prostate specific antigen level (PSA) has become important. Detection of PSA levels in affected patients is known to be the current gold standard biological marker for pre-operative screening, diagnosis, treatment and follow-up of prostate cancer [392]. Xia et al. designed a colorimetric gold nano-based biosensor for the determination of PSA level. The platform they designed was based on the AuNPs formation inhibition and their method was basically different from the present peptide-based sensing approaches for PSA identification [393].

Diagnosing cancer at the earliest possible phase considerably increases the possibility of treatment and, therefore, survival. In a study aimed at designing a non-invasive and rapid bio-nano sensing method for early-stage screening of common lethal cancers, two circulating microRNA biomarkers up-regulated in plasma were targeted by a rapid and colorimetric bio-nano sensor based on non-crosslinking Au-nanoprobos without the necessity for amplification. The detection limit of the system developed by the researchers was determined to be less than one ng/ μL of total isolated miRNA using the instrument-free visual method [394]. The colorimetric biosensor platform designed for the detection of another miRNA (miRNA-21) was based on the peroxidase-like activity of graphene/AuNPs hybrids and it was visible and label-free. The sensor was reported to respond linearly to miRNA-21 from 10 nM to 0.98 μM with a detection limit of 3.2 nM ($S/N = 3$) under optimal conditions, emitting a low background signal [395]. Another colorimetric biosensor using the AuNPs/graphene oxide nanoconjugates as a dual nanoplatform was used for the identification of DNA hybridization. The DNA

detection limit of the platform developed by the researchers was reported as 8 nM and the optimum detection was 63 nM [396]. Colorimetric detection of exosomes and exosomal proteins is another application area of AuNPs-based biosensors. Since exosomes carry proteins that reflect the origin of the parent cells, the evaluation of these proteins serves as biomarkers for cancer diagnosis. Jiang et al. demonstrated a colorimetric sensor platform based on aptamer/AuNPs that describes exosome surface proteins within minutes to the naked eye [397]. In another study, the researchers proposed a sensitive colorimetric biosensor based on exosome-activated competitive response and etching of Au-nanobipyramidal@MnO₂ nanosheet structures (MnO₂-NSs@AuNPs) as the sensing method for exosome quantification. The method they developed showed high sensitivity to exosomes in the range of 8.5×10^2 – 8.5×10^4 particles μL^{-1} , along with a detection limit of 1.35×10^2 particles μL^{-1} , which is more sensitive than earlier described colorimetric systems [398].

To address the limitations of CRISPR/Cas12a-based nucleic acid and non-nucleic acid target detection, the researchers designed a programmable DNA nanoswitch (NS)-regulated plasmonic CRISPR/Cas12a-gold nanostars (Au NSTs) reporter platform for the spatial confinement-mediated detection of nucleic acid and non-nucleic acid biomarkers. By programming the target recognition sequence in the NS, a single crRNA was sufficient for biomarker detection. They reported a 122-fold decrease in the detection limit for PSA antigen and a 196-fold decrease for miRNA-375 [399]. In another study, Dighe et al. developed a colorimetric CRISPR-Cas12a assay that utilizes CRISPR gene editing technology, DNA hybridization principles, and AuNPs to target a range of emerging and antibiotic-resistant pathogens. The researchers' assay employed specially designed CRISPR-RNA and single-stranded oligonucleotides corresponding to a complementary single-stranded DNA sequence. The assay, which does not require DNA amplification, demonstrated the ability to rapidly detect pathogens with a clinical sensitivity limit of 7–8 copies/ μL [400]. In one study, Fu et al. developed a label-free, point-of-care approach for isothermal DNA detection via the trans-cutting activity of CRISPR-Cas12 and the growth of gold nanomaterials (AuNPs and AuNRs) in agarose gel. They applied the sensing strategy to detect BRCA-1, a breast cancer-associated biomarker, and reported detection limits of 1.72 pM (AuNP-based) and 2.07 pM (AuNR-based) [401]. Waitkus et al. developed a novel LSPR system based on the combination of gold nano mushrooms (AuNMs) and AuNPs to achieve a significant plasmonic resonance shift. They achieved a redshift of 31 nm by saturating the AuNMs with AuNPs. The LSPR substrate was packaged in a microfluidic cell and integrated with a CRISPR-Cas13a RNA detection assay for the detection of SARS-CoV-2 RNA targets. The new LSPR chip, which uses AuNPs as indicators, may offer a new opportunity to achieve next generation multiplexing and sensitive molecular diagnostic systems [402]. CRISPR/Cas-enhanced SARS-CoV-2 assays are considered an alternative to qRT-PCR due to their ease of use and ease of use. Some visual detection methods, which do not require a naked-eye device, have significant limitations regarding probe universality. In one study, researchers reported a sensitive, rapid, and specific SARS-CoV-2 POC assay that combines the superior DNase activity of Cas12a with a universal AuNP strand displacement probe. The modular design they developed can be used in many nucleic acid detection applications, such as bacteria and viruses, by modifying crRNA, and this has great potential for use in POC diagnostics [403].

6.2. Fluorometric based sensing

Fluorescence-based biosensors utilize the quenching property of Au-nanomaterials on fluorophores put near their surfaces, the effect occurring through a mechanism mediated by Förster Resonance Energy Transfer (FRET) between Au and the fluorophores. FRET happens when an excited donor molecule transfers energy to an acceptor molecule in its ground state, resulting in fluorescence emission from the acceptor.

Considering the high molar extinction coefficients and broad absorption bands of AuNPs, they can act as perfect fluorescence quenchers in FRET investigations [404]. Lysozyme (LYZ) performs an important function in the immune system of body, and observing its level can give insight into the evaluation of the diagnostic process of various diseases. Liu et al. used a sandwich FRET bio-nano sensor platform based on peptide-modified AuNPs and FAM-labeled aptamer for LYZ detection. They reported the design of an ultrafast sandwich FRET biosensor with a detection limit of 85 nM and a linear detection range of 0–1.75 μM for LYZ detection [405]. In another study, the researchers reported a FRET bio-nano sensor based on AuNPs and graphene quantum dots (GQDs) for the identification of the *mecA* gene sequence of *Staphylococcus aureus*. In the study, they showed that fluorescence quenching effectiveness could reach approximately 87 % with 100 nM target oligos by measuring the fluorescence signals before and after the addition of the targets. The limit of identification (LOD) of the designed FRET bio-nano sensor was approximately 1 nM for *S. aureus* gene detection [406]. MicroRNAs (miRNAs) which perform a significant role in regulating gene expression, may be related to abnormalities associated with tumor progression. A FRET based novel miRNA-195 targeting bio-nano sensor design placed on silica nanofibers integrated with rare earth-doped calcium fluoride particles ($\text{SiO}_2@\text{CaF}_2\text{:Yb},\text{Ho}$) and AuNPs was reported by Fu et al. [407]. In a study based on an effective fluorescence “turn-on” approach for the identification of glutathione (GSH) based on FRET between nitrogen and sulfur doped carbon dots (N,S-CDs) and AuNPs, the researchers reported satisfactory results when they used their designed biosensor to screen GSH in the serum samples [408]. In another study, the researchers used the fluorescence “turn-on” strategy based on AuNPs and C-dots for sensitive and selective trypsin detection. They succeeded quantitative assessment of trypsin with the detection limit of 0.84 ng mL⁻¹ in a range of 2.5–80 ng mL⁻¹ [409]. Mahani et al. designed a specific and label-free FRET-based IL-6 apta-sensor using a DNA aptamer functionalized with AuNPs and nitrogen-doped carbon quantum dots (NCDs) as donor-quencher pair. In another study, Yang et al. proposed an AuNPs-assisted CRISPR/dCas9-mediated fluorescence resonance energy transfer (FRET) platform for the specific, sensitive, and rapid detection of nucleic acids. Under optimal conditions, the designed Au-CFRET system was able to detect the CaMV35S promoter of genetically modified rice at as low as 21 copies μL⁻¹ [410].

6.3. Electrochemical based sensing

Electrochemical and AuNPs-based biosensors are other biosensing applications of AuNPs. The AuNPs-based electrochemical sensors benefit the high surface area/conductivity and unique catalytic characteristics of AuNPs. Pan et al. reported the design of an electrochemical tyrosinase biosensor using graphene-AuNPs composites to achieve rapid and direct detection of bisphenol A. Additionally, they calculated that the detection limit of their suggested biosensor was as small as 1 nM [411]. Electrochemical glucose detection using AuNPs-based nano biosensors is another use field. In a study, a nano-Au/graphene composite was produced by electrochemical co-reduction approach in one step and the developed bio-nano sensor was used for electrochemical detection of glucose. The designed glucose bio-nano sensor showed a great sensitivity of 56.93 μA mM⁻¹ cm⁻² for glucose [412]. In another study where Cu-nanoflower modified with graphene oxide-AuNPs nanofibers was used for electrochemical detection of glucose, it was reported that the designed Au-chip showed a low detection limit of 0.018 μM towards glucose [413].

The receptor of human epidermal growth factor protein (HER-3) is present in normal human fetal/adult tissues and it has also been stated to be expressed at both the protein and mRNA levels in a number of primary tumor constituents and cancer cell lines. Canbaz et al. designed a novel immunological bio-nano sensor for ultra-sensitive quantification of HER-3 by layering the electrode surface with hexanethiol, AuNPs, and cysteamine-Anti-HER-3 antibody, respectively. The suggested bio-nano

sensor demonstrated a satisfactory analytical working for the determination of HER-3 varying from 0.2 to 1.4 pg mL⁻¹ [414]. MicroRNA-21 is an oncogenic miRNA whose overexpression shows a considerable role in the development of carcinogenesis and it can be used as a biomarker for breast cancer identification [415]. Tian et al. designed a novel electrochemical biosensor platform for the recognition of circulating microRNA-21. They used an AuNP superlattice to amplify electrochemical signals. According to the strategy they use, microRNA can be found in a variation from 100 aM to 1 nM with a relatively low detection limit of 78 aM [416]. Another electrochemical biosensor design providing microRNA determination was proposed by Pothipor et al. They developed a sensor platform based on graphene quantum dots/AuNPs/GO films for the simultaneous determination of microRNAs (miRNA-210, miRNA-155 and miRNA-21 biomarkers) clinically relevant to breast cancer. Their designed platform offered a widespread linear dynamic scope from 0.001 to 1000 pM along with ultrasensitive small detection limits of 0.04, 0.33, and 0.28 fM for the determination of miRNA-21, miRNA-155, and miRNA-210, respectively [417]. Carcinoembryonic Antigen (CEA), an acidic glycoprotein with human embryonic antigen properties, is observed on the surface of cancerous cells that have developed from endodermal cells. In a recent study, the use of an electrochemical label-free bio-nano sensor was reported for the identification of CEA based on PPy-polydopamine (PPy-PDA/Au) and polymerized polycaprolactone (Ng-PCL) loaded AuNPs prepared by ring-opening polymerization (ROP). It was shown that the method has the benefits of wide linear range (1 pg mL⁻¹–100 ng mL⁻¹) and great sensitivity, and also the minimal detection limit is 0.234 pg mL⁻¹ under optimal experimental conditions [418].

The large amount of noble metal-based electrodes commonly used in electrochemical sensor-based E-CRISPR, a point-of-care (POC) testing platform, has limitations such as high cost and limited analytical performance. To address these limitations, the researchers reported a carbon-based E-CRISPR design modified with AuNPs and MXene Ti_3C_2 . They demonstrated that the developed E-CRISPR quantified human papillomavirus 18 DNA over a wide concentration range from 10 pM to 500 nM, with a detection limit of 1.95 pM [419]. In their study, Qin et al. developed a CRISPR/Cas12a assay using site-specific double-stranded DNA cleavage. They used a self-powered photoelectrochemical detection system, redox-cycling Ru(bpy)₃Cl₂ and p-aminophenol on a glassy carbon electrode modified with AuNPs/Mo₂C/MoO₃, for signal readout. The assay they designed could accurately detect target HIV nucleic acid as low as 0.4 fM [420]. Wang et al. reported the design of a novel self-assembled porous hydrogel material (Au@PEI-ABEI@Pt) for ultrasensitive detection of *Burkholderia pseudomallei* via electro-chemiluminescence (ECL) strategy. They reported that the highly biocompatible hydrogel complex could enable the widespread application of CRISPR/Cas12a on solid-phase carriers without affecting the specificity, sensitivity, and cutting activity of CRISPR/Cas12a [421].

6.4. Surface-enhanced Raman scattering (SERS) based sensing

Surface Enhanced Raman Scattering (SERS) based biosensors are based on the principle of inelastic scattering of photons by gold nanomaterials due to quantized vibration level that enhances the spectral signal in the sample. It has the benefit of being fast, highly specific and sensitive, and free of fluorescent markers. Due to its ultra-high selectivity and sensitivity, SERS has a considerable array of purposes in biology, biomedicine, nanotechnology, chemistry and other areas [298, 422]. Baniukevic et al. chose SERS technique as a robust, simple and indirect and to apply technique for the recognition of bovine leukemia virus antigen gp51. They used magnetic Au-nanomaterials (MNP-Au) coated with antibodies in a random manner or oriented for binding of gp51. The LOQ and LOD of the proposed immunoassay for antigen gp51 detection were found to be 3.14 μg mL⁻¹ and 0.95 μg mL⁻¹, respectively [423]. In another study, AuNPs improved SERS apta-sensors were used for the synchronized identification of *Staphylococcus aureus* and

Salmonella typhimurium. In their study, the signal of Raman was enriched with the closer space of the AuNPs and the application of aptamer achieved high specificity for target bacteria [424]. A study in which the design of a SERS-based lateral flow assay biosensor using AuNPs as Raman reporters enabled the identification of HIV-1 DNA with high sensitivity. It was viable to quantitatively explore HIV-1 DNA by great sensitivity via observing the specific Raman peak strength of the DNA-modified Au-nanomaterials. The identification limit of their SERS-based lateral flow assay was 0.24 pg/mL under optimized conditions [425]. In a study reporting a clean and fast freezing-based approach to accurately engineer DNA concentration on the surface of Au-nanomaterials, the researchers successfully demonstrated background-independent SERS microRNA detection with a short detection time [426]. Cai et al. demonstrated the design of plasmonic SERS bio-nano sensor based on multibranched AuNPs inserted in poly-dimethyl siloxane for the determination of hematin amount in human erythrocyte cells lacking the necessity of separating it from hemoglobin (Hb).

In the designed assay, the hematin (or hematin-comprising hemolysate of erythrocyte) was placed on the Au-film surface and it covered with AuNP-M fixed PDMS. They provided a high level of sensitivity to the hematin concentration by the generation of great SERS signals under excitement at 785 nm. In their study, the researchers achieved different cytosolic hematin concentrations for healthy and sickle erythrocytes ($\sim 18.5 \pm 4.5$ and 51.5 ± 6.2 μM for healthy and sickle erythrocytes, respectively), which may make the SERS biosensor platform they designed a potential application in clinical detection [427].

Developing accurate, specific, and rapid detection methods for foodborne viruses is crucial. To increase the accuracy and specificity of SERS-based target nucleic acid detection, researchers developed a technique that leverages the target recognition capabilities of CRISPR-Cas12a and ultrasensitive SERS tags. The designed nanosystem comprised a gold/nickel foam substrate (Au-NFs) and a reporter (ssDNA-ROX). The researchers' results showed that the nanosensor detected DNA within 30 min and had a detection limit of 8.23 fM [428]. In another study, researchers developed a novel gene detection platform based on AuNPs aggregation, coupled with SERS and the CRISP-R/Cas12a system, and used it for viral gene detection. The developed detection method enabled the efficient detection of *human papilloma-virus* (HPV) genes in serum and pseudovirus with high pM sensitivity within 40 min [429].

AuNPs are promising popular nanomaterials for different biosensor applications thanks to their exclusive optical and physical features. Considering the high sensitivity, suitable SPR properties, biocompatibility, rapid results, high surface area, catalytic properties, stability and controllable interactions with different biomolecules, AuNPs can be used as biosensor platforms alone and in hybrid/modified forms in various diagnostic processes. Although numerous studies have been published in the literature on the use of AuNPs as potential biosensor platforms, further research is required to facilitate the transition of designed systems to clinical diagnostic processes and to increase the efficiency of the devices. In addition, the surface modification of AuNPs and their use as hybrid nanoconjugates are important and necessary issues in order to improve systemic stability and target specificity. The integration of the AuNPs-based biosensor platforms with portable devices such as smartphones is an important and promising approach. In the near future, significant scientific developments are expected in the design of AuNP-based biosensor platforms for the fast, practical, highly sensitive, simple and reliable recognition of various clinically important biomolecules.

7. Gold nanoparticles for tissue engineering applications

Tissue engineering, which includes various multidisciplinary sciences (engineering, science, biology, medicine, materials science), aims to develop innovative and functional biomaterials that can support the

regeneration of tissues that have lost their function due to various diseases or traumas [430,431]. The utilization of scaffold biomaterials for the restoration of different systems and organs (such as bone, cardiovascular, nerve, muscle, and cartilage) is one of the common applications in tissue engineering. An ideal scaffold biomaterial must display features close to those found in native organs: 3D spongy micro-/nanostructure, suitable mechanical strength, biocompatibility, controlled degradation, sufficient cell attachment surface, etc. [432]. AuNPs have been used in the literature for different purposes such as improving the mechanical properties of tissue scaffolds, providing electrical conductivity, and also promoting cellular adhesion, proliferation, differentiation, and maturation [433].

7.1. Gold nanoparticles for cardiac tissue engineering

The effects and performances of the AuNPs have been extensively investigated in some scaffold-based cardiac tissue engineering (CTE) studies using various synthetic and natural biomaterials. Fleischer et al. reported that a nanocomposite scaffold consisting of coiled electrospun fibers integrating AuNPs promoted the cultivation of cardiac cells. The researchers also reported that their designed hybrid scaffold produced a robust contractile force, important contraction velocity, and small excitation limit, supporting cell organization into aligned and long tissues [434]. In another study, the effect of the use of AuNPs on cardiomyocyte growth in three-dimensional sodium alginate/chitosan scaffolds prepared within the scope of CTE was evaluated. They reported that the incorporation of AuNPs into the scaffold increased cardiac protein expression and cell proliferation [435]. In a study where electroconductive 3D-printed PCL/AuNPs nanocomposite scaffolds were developed for myocardial tissue engineering, it was shown that the usage of Au-nanomaterials together with PCL enhanced the mechanical, electrical, and wettability properties of the biomaterials [436]. In another study, Ghaziof et al. examined the influence of loading the cardiac drug spironolactone onto 3D printed PCL/AuNPs nanocomposite scaffolds that they designed in their previous studies for myocardial tissue engineering. In their cell culture studies, they showed that H9C2 cell proliferation increased with the addition of AuNPs to the structure, and cell adhesion/viability were significantly improved with the GEL/SPL coating [437].

The development of injectable hydrogels that mimic the mechanical and electrical characteristics of the myocardium is highly promising for CTE applications. When Baei et al. cultured MSCs on the AuNPs-chitosan-based thermosensitive conductive hydrogels that they developed within the scope of CTE, the researchers showed that the gold nano-conductive structure they designed supported cellular viability, metabolism, proliferation and cardiac differentiation [438]. In another study, the fabrication of gelatin methacrylate (GelMA) based conductive hybrid hydrogels containing AuNRs for CTE applications was reported. The researchers demonstrated that the cardiomyocyte cells cultured on the designed conductive hydrogels displayed brilliant adherence, metabolic activity, and cellular viability profiles [439]. Pena et al. demonstrated the design of a non-toxic, AuNPs-conductive, and reverse thermal injectable hydrogel (RTG)-based cardiac cell scaffold. They showed that the RTG-AuNPs hydrogel supported targeted survival and managed to a considerable improvement in the Cx43 level in the neonatal rat ventricular myocytes (NRVMs) cocultured with the cardiac fibroblasts (Fig. 23) [440]. In another study, the design of injectable, self-healing, and conductive hyaluronic acid (HA)-collagen hydrogels loaded with AuNPs and bacterial cellulose for heart tissue engineering applications was reported [441].

Decellularized matrix bio-scaffolds are valuable biomaterials for CTE applications. On the other hand, the lack of an effective electrical connection between cells may reduce the achievement of existing therapies. Shevach et al. investigated the functionality of the fibrous decellularized omental matrices for CTE applications by modifying them with the conductive AuNPs. They demonstrated the presence of massive

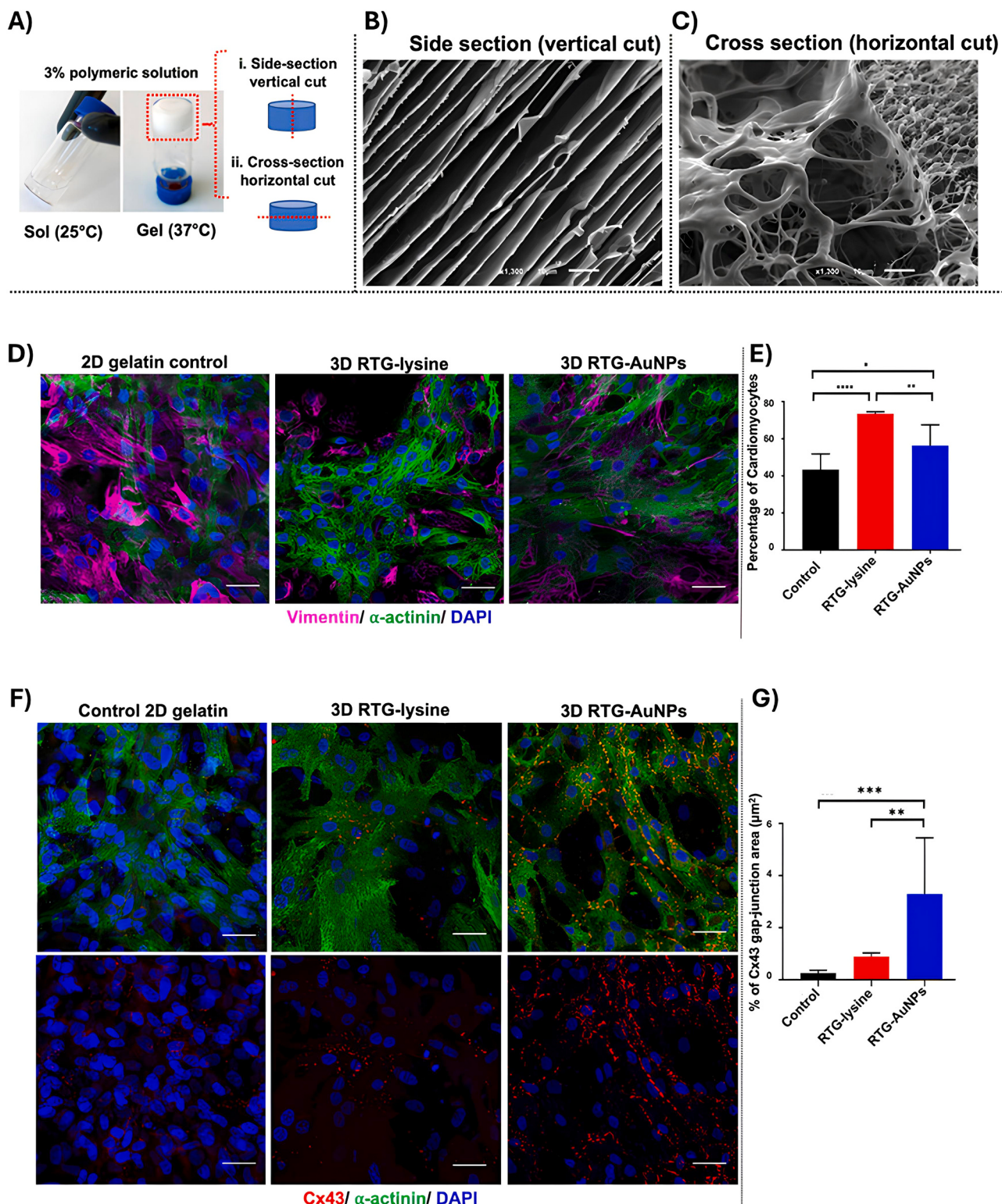


Fig. 23. Morphological characterization of the RTG–AuNPs material. (A) Morphological characterization of the RTG–AuNPs was analyzed in vertical and horizontal cuts. (B) Vertical cuts of the hydrogel demonstrate a laminar sheet-like configuration. (C) Horizontal cuts of the hydrogel showed a highly interconnected porosity. Immunocytochemistry labeling of NRVMs and CFs cultured in 2D and 3D systems for 21 days. (D) Antibody staining against α -actinin (green) and vimentin (pink) label NRVMs and CFs, respectively, with nuclei labeled using DAPI (blue). (E) Quantification of immunocytochemistry staining against α -actinin indicates the percentage of cells likely to be NRVMs, showing both 3D systems to contain a greater percentage of NRVMs than the 2D gelatin control. Scale bar 40 μm . p values: * < 0.023 , ** < 0.0017 , and *** < 0.0001 . Data are presented as mean \pm S.D. Immunocytochemistry labeling of gap junctions in NRVMs cultured in 2D and 3D systems for 21 days. (F) Antibody staining against connexin 43 (Cx43) (red) and α -actinin (green), with nuclei labeled using DAPI (blue). (G) Quantification of immunocytochemistry staining against Cx43 to indicate the surface area of NRVMs positive for this gap junction protein, showing the RTG–AuNP system to contain the largest Cx43-positive area. Scale bar: 40 μm . p values: ** < 0.0021 and *** < 0.0002 . Data are presented as mean \pm S.D. Adapted with permission from reference [440]. Copyright (2019), American Chemical Society.

striations and organized connexin 43 electrical coupling proteins, in addition to the elongated and aligned behavior of cardiac cells within the scaffolds. The superior functional properties of hybrid patches revealed the positive contribution of AuNPs [442]. In a study in which AuNPs-coated porcine cholecyst-derived bio-scaffolds were developed for CTE applications, the designed biocompatible material (C-ECM) was reported to be an appropriate material for the proliferation and growth of the cardiomyoblast cells [443].

7.2. Gold nanoparticles for neural tissue engineering

Neural damage affects millions of people globally and requires extreme medication costs. While there is a restricted restoration capability for peripheral nerves, functional gain is quite difficult for damage in the central nervous system (CNS). This status directs researchers to innovative and alternative technologies. In the neural tissue engineering (NTE) area, intensive efforts are being made to design bio-scaffolds with appropriate features that can assist the growth and renewal of the various neuronal cells. In biomaterial designs for NTE applications, it is important to first consider the ideal scaffold properties (biocompatibility, biodegradability, optimal mechanical properties, porosity and multiple cues) and to carry out the designs accordingly. Considering the molecular aspect of nerve regeneration, various growth factors that will support the differentiation, development, and adhesion of the neuronal cells should be used together with the biomaterials. Additionally, it is important to design micro/nano topography on biomaterial surfaces using suitable lithographic techniques that will promote the guidance of neurites and axons along linear lines [444,445]. Electrical stimulus has been proven to initiate molecular cascades that promote functional renovation of damaged nerves. Biomaterial design with conductive properties enhances the transmission of outer stimulus, which improves the restoration capability of damaged nerves. Conductive scaffolds are popular for NTE applications recently due to their positive effects on the neurons and glial cells [446]. In addition to conductive polymers that have been used for many years, modification of biomaterial surfaces with Au-nanomaterials has awakened notable concern recently. Unique physicochemical properties of Au-nanomaterials make them a suitable factor for improving the conductivity of biomaterials to enhance the electrical signal transport between neuronal cells.

Saderi et al. described the design of Au-nanomaterial-doped electrospun chitosan/PCL nanofibrous biomaterials for peripheral NTE applications. They exhibited that the proliferation, adhesion, and growth of the Schwann cells cultivated on the materials were enhanced in the presence of AuNPs [447]. In another study, the bio-transfer of the AuNPs and NGF encapsulated in the chitosan NPs (CSNPs) was demonstrated to promote the differentiation of human adipose-derived stem cells (h-ADSCs) into Schwann-like cells. Controlled sustained NGF release from the biocompatible nanoconjugates was demonstrated for 7 days, and the NGF/AuNPs delivery enhanced Schwann cell differentiation and myelination capacity [448]. In a similar study examining the bio-transfer of BDNF and Au-nanomaterials from laminin-functionalized and aligned electrospun PLGA scaffolds for NTE applications, high proliferation and differentiation of the h-ADSCs on the scaffolds into Schwann cells were reported [449]. Pooshidiani et al. reported the fabrication of a conductive biomaterial with regulated porosity via chitosan/PCL hybrid material for NTE applications. After *in situ* production of Au-nanomaterials on the scaffolds, the researchers showed that the developed biomaterial was highly biocompatible and significantly promoted the Schwann cell growth [450]. We investigated the behavior of the neuronal stem cells on the AuNPs/IKVAV pentapeptide modified nano/micro-channeled conductive PLGA/PCL film biomaterials. Au-nanomaterials surface modification enhanced the surface wettability of the scaffolds. We demonstrated significant neural cell differentiation and neurite extension after controlled electrical stimulation applied in the bioreactor system [451].

Injectable hydrogel biomaterials with greatly interconnected and

hydrated structures have exhibited important benefits for application in tissue engineering purposes. Mokhtari et al. demonstrated the design of an injectable and biocompatible hydrogel scaffold based on aldehyde modified-nanocrystalline cellulose, chitosan loaded with AuNPs, and collagen, (ADH-CNCs/CS-Au/Collagen) for TE purposes [452]. Most peripheral neural damage is difficult to treat because of extreme ROS production in inflamed organ locations, which can further worsen nerve damage. Designing scaffolds that scavenge endogenous ROS and stimulate the growth factors secretion is a popular strategy and it may overcome these challenges. Zhou et al. reported the design of mixed hydrogels having gradients in AuNPs for localized transport of mesenchymal stem cells (MSCs) and enhancement of neural tissue remodeling *in vivo*. They exhibited that composite hydrogel promoted the survival of MSCs and reduced the level of intracellular ROS production. Additionally, they implanted degradable biomaterials together with MSCs into sciatic neural defects in an animal injury model to demonstrate their satisfactory application value *in vivo* [453].

There are two alternatives for therapy after spinal cord injury (SCI): regeneration and neuroprotection. The aim of neuroprotective approaches is to prevent the spread of secondary damage. The purpose of regeneration is to repair neuronal communication and functional gain. The studies conducted with tissue scaffolds produced using various natural/synthetic biomaterials and techniques are alternative options for direct nerve regeneration and functional gain. Nanomaterials with various physicochemical properties have unique properties that enable them to overcome the difficulties encountered, especially in neuroprotective therapies. Nanocarrier systems can provide targeted therapies and elongated circulation times in the blood, increasing the bioavailability of neuroprotective drugs. In addition, due to their small dimensions, they can more simply route across biological cellular membranes and barriers and provide effective therapies. Moreover, since their total surface area is quite large, more drug loading can be done after appropriate surface functionalization [454,455]. In a study, Au-nanomaterials were coupled by ursodeoxycholic acid (UDCA) and embedded in a hydrogel composed of oxidized hyaluronate (OHA) and glycol chitosan (gC). As a result of direct injection of the obtained CHA-GNP-UDCA hydrogel into the spinal cord injury in the rats, NIR irradiation was applied to the lesion as a local therapy method. The optimized hybrid hydrogel was reported to inhibit the cystic cavity and inflammatory cytokines at the lesion site under NIR treatment [456]. In another research, Ko et al. reported the transfer of neuron-inducing grafts including (+) charged AuNPs for the therapy of rat SCI with inducing cellular differentiation of the transplanted NSCs into neurons. The researchers used an injectable gel cross-linked with oxidized hyaluronate and glycol chitosan as an instrument for NSCs transplantation. The NSC-pGPN group showed a high level of neuronal differentiation and the lowest rate of astrocyte differentiation. Additionally, they reported two-fold higher damaged axon regeneration in the NSC-pGPN group compared with the NSC gel group (Fig. 24) [457]. We reported the design of IKVAV-pentapeptide/NGF/BDNF coated and AuNPs conductive PLGA/PCL nerve guidance conduit (NGC) for the restoration of the rat SC damage. It was pointed out that micro-grooved group modified with Au-nanomaterials exceedingly promoted axonal alignment under bioreactor system circumstances and it also the developed ideal NGC (PLGA/PCL G₁-IKVAV-pentapeptide/NGF/BDNF-AuNPs) highly regenerated the rat SC injury. The findings suggest that the developed biomaterial could be a suitable candidate for SC restoration [458].

7.3. Gold nanoparticles for bone tissue engineering

Bone tissue engineering (BTE) is an area that aims to repair bone damage with innovative and applicable approaches, and electrically conductive bone scaffolds that can be physiologically stimulated via electrical stimulation are very promising biomaterials. Au-nanoparticles are innovative nanomaterials for BTE implementations, thanks to their

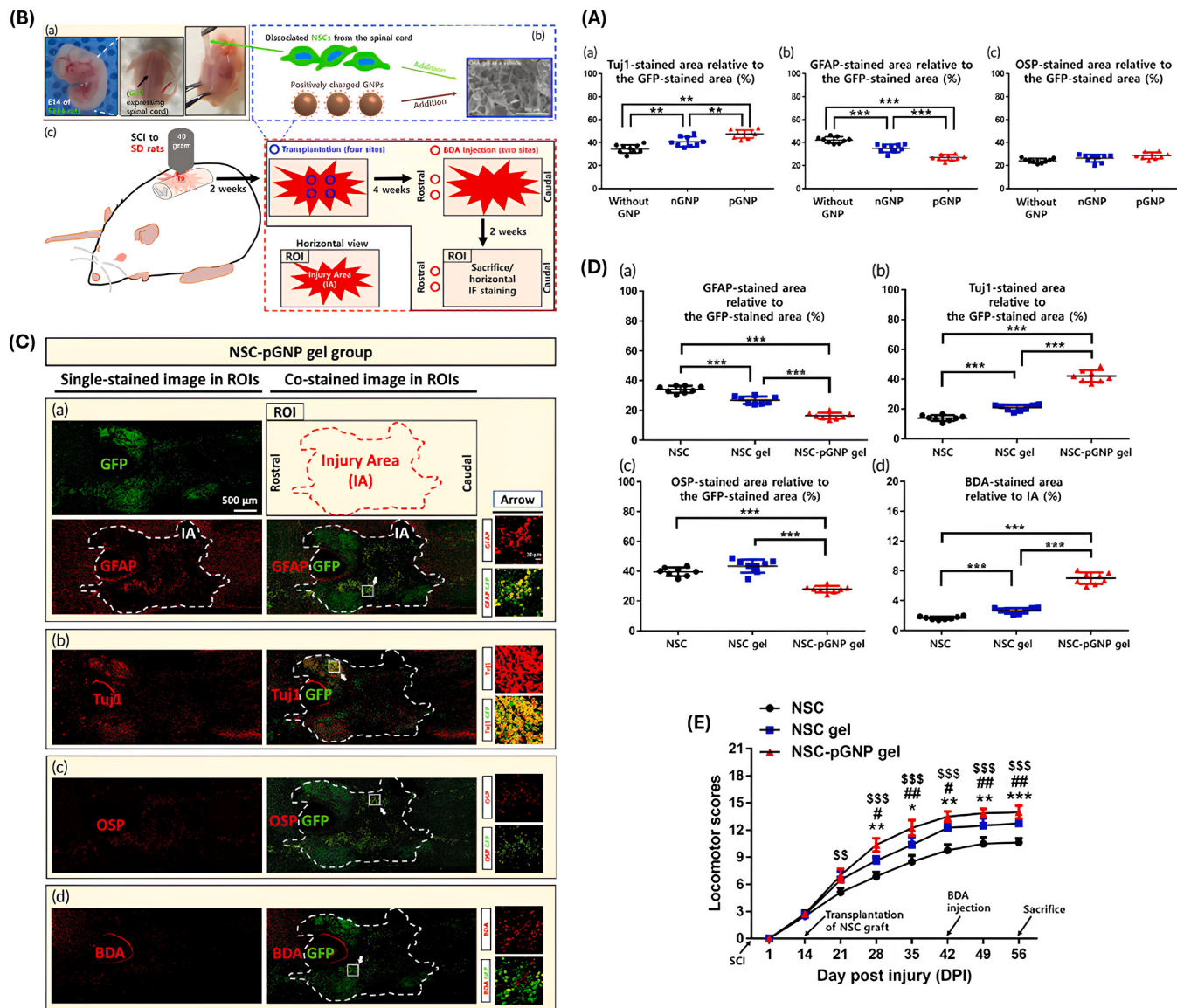


Fig. 24. (A) Cellular differentiation of the dissociated neural stem cells in the regions of interest was quantified ($n = 9$ per group). The green fluorescent protein (GFP)-stained area in each case was normalized to 100 %. (A-a) Tuj1, (A-b) glial fibrillary acidic protein, or (A-c) oligodendrocyte specific protein-stained area relative to the GFP-stained area was quantified using ImageJ software. (B) Schematic design for neural stem cell (NSC) dissociation and immunofluorescence staining. (B-a) Preparation of the NSC suspension from the green fluorescent protein-expressing spinal cord. (B-b) NSC-positively charged gold nanoparticles gel grafts for transplantation. (B-c) Contusion injury and graft transplantation process in Sprague–Dawley rats. (C) Cellular differentiation of grafted neural stem cells (NSCs) under the spinal cord injury condition for the NSC-positively charged gold nanoparticles gel group. Horizontally sectioned specimens were stained with the green fluorescent protein (GFP) antibody. Each GFP-stained section was co-stained with glial fibrillary acidic protein (GFAP) (36th and 40th), Tuj1 (37th and 41st), oligodendrocyte specific protein (OSP) (38th and 42nd), or biotinylated dextran amines (BDA, 39th and 43rd). Representative tile scan images (also designated as regions of interest [ROIs], $4500 \times 2000 \mu\text{m}^2$) of samples co-labeled with (C-a) GFAP/GFP, (C-b) Tuj1/GFP, (C-c) OSP/GFP, and (C-d) BDA/GFP are shown. The scale bar of the ROI image is $500 \mu\text{m}$ (IA = Injury Area). Arrows indicate randomly designated regions for higher magnification views. The designated region is $170 \times 170 \mu\text{m}^2$ (Scalebar: $20 \mu\text{m}$). (D) Cellular differentiation of grafted neural stem cells within IAs was quantified ($n = 8$ per group). Within the IA, the green fluorescent protein (GFP)-stained area was normalized to 100 %. (D-a) Glial fibrillary acidic protein, (D-b) Tuj1, and (D-c) oligodendrocyte specific protein-stained area relative to the GFP-stained area was quantified using ImageJ software. (D-d) The injury area was normalized to 100 % and biotinylated dextran amines-stained area relative to the injury area was quantified using ImageJ software. (E) Basso–Beattie–Bresnahan (BBB) hindlimb locomotor scores of the spinal cord injury rats ($n = 4$ per group). Comparison of BBB locomotor scores in the neural stem cell (NSC), NSC gel, and NSC-positively charged gold nanoparticles (pGNP) gel groups at 1, 14, 21, 28, 35, 42, 49, and 56-days post injury (DPI). Adapted with permission from reference [457]. Copyright (2022), Wiley Periodicals LLC on behalf of American Institute of Chemical Engineers.

superior chemical and physical features, easy synthesis, suitable electrical properties, anti-inflammatory features, their stability, inertness, high surface to volume ratio, biocompatibility and ideal properties as osteogenic materials. Nekounam et al. reported the development of carbonized conductive nano-scaffolds loaded with AuNPs for BTE purposes. They demonstrated the biocompatibility of the designed

biomaterial on the MG63 osteosarcoma cells and the suitability of the hybrid nanofibers for BTE applications [459]. In another study, Samadian et al. reported the design of 3D PLLA/PCL nanocomposite scaffold having gelatin nanofibers (GNFs) and Au-nanomaterials for bone regeneration. Cellular tests demonstrated that the Au-nanomaterial concentration used was highly determinant on the cellular toxicity.

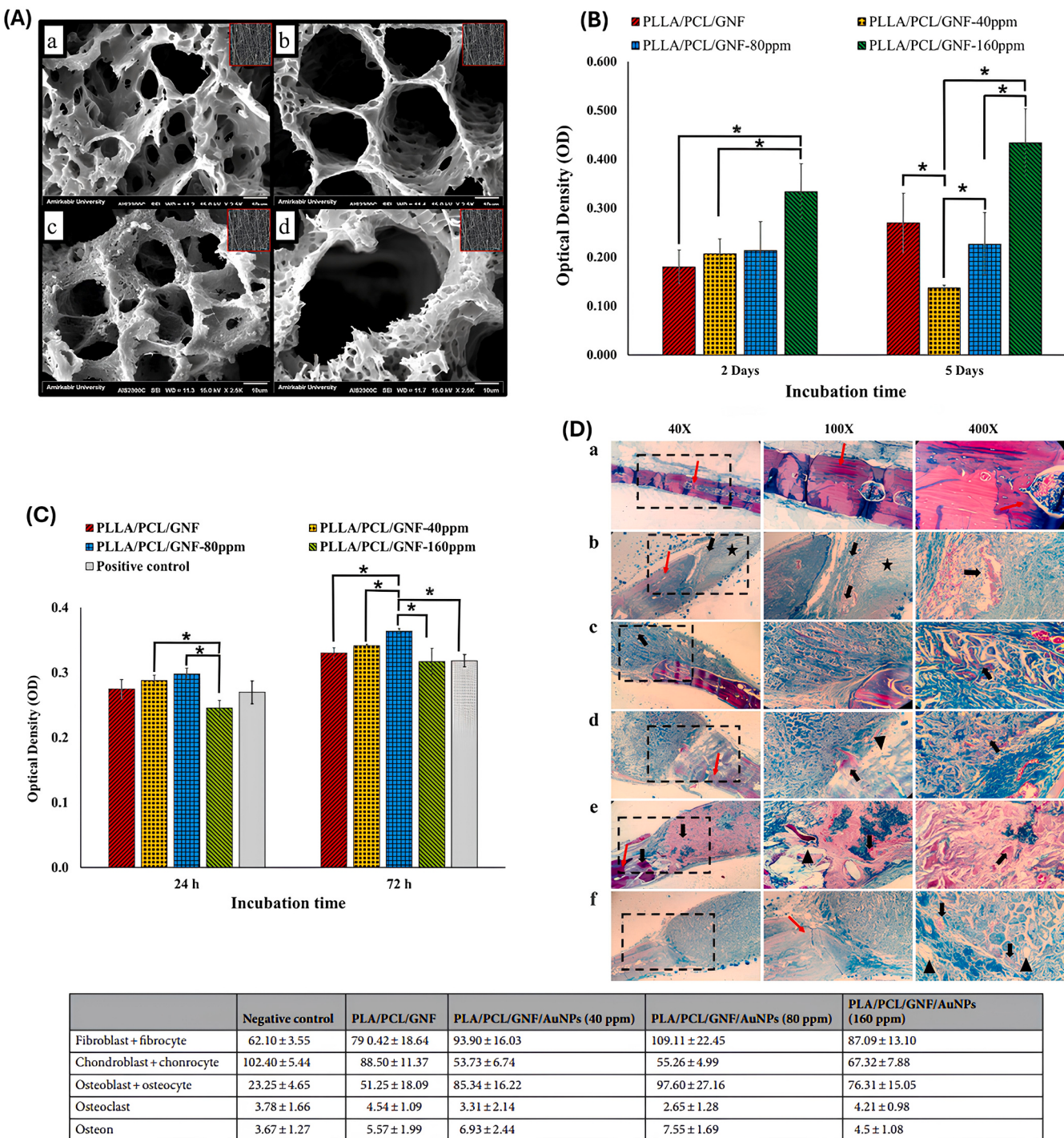


Fig. 25. (A) Scanning electron micrographs of the prepared scaffolds. (A-a) PCL/PLLA/GNF, (A-b) PCL/PLLA/GNF/AuNPs (40 ppm), (A-c) PCL/PLLA/GNF/AuNPs (80 ppm), and (A-d) PCL/PLLA/GNF/AuNPs (160 ppm). Insert is SEM image of GNFs. (B) The cytotoxic effects of nanocomposite scaffolds on MG-63 cells measured by lactate dehydrogenase (LDH) assay. MG-63 seeded on the scaffold with a density of 7000 cells/well in a 96-well plate and incubated for 2 and 5 days. Data represented as mean \pm SD, n = 5. *p < 0.05 (obtained by one-way ANOVA). (C) MG-63 cell proliferation on the fabricated scaffolds measured using the MTT assay kit at 24 and 72 h after cell seeding. Control: Tissue Culture Plate (TCP). Data represented as mean \pm SD, n = 3. *p < 0.05 (obtained by one-way ANOVA). (D) Histopathological sections from the calvaria bone defects and related histomorphometrical analysis (Stained with MTC). (D-a) Positive control, (D-b) Negative control, (D-c) PLLA/PCL/GNF, (D-d) PLLA/PCL/GNF/AuNPs (40 ppm), (D-e) PLLA/PCL/GNF/AuNPs (80 ppm), and (D-f) PLLA/PCL/GNF/AuNPs (160 ppm). LACT loose areolar connective tissue (star), NB new bone formation (thick arrow), MB mature or old bone (red thin arrow), SR scaffold remnant (arrowhead). Adapted with permission from reference [460]. Copyright (2021), Springer Nature.

They reported that 80ppm-AuNPs/Gel/PLLA/PCL nanocomposite biomaterial excited high neo-bone development, osteocyte woven bone formation in the lacunae, and angiogenesis at the defect site, in relation to the data of their animal research (Fig. 25) [460].

Functionalization of bio-scaffolds developed for bone tissue repair with AuNPs can promote osteogenic cell differentiation. Lee et al. grew the AuNPs on the polydopamine (PDA) coating of (3D) printed PCL biomaterials. The researchers reported that the scaffold they designed

could be an innovative approach for BTE applications via stimulating osteogenesis as a means of healing and remodeling bone defects [461]. Another study reported osteogenic differentiation of MSCs on biocompatible PCL/SF nanofibrous scaffolds modified with silica-coated AuNPs. It was exhibited that the adding of Au(SiO₂) and SF to PCL materials improved the interconnecting porous structure, surface roughness, and mechanical strength of the biomaterial. They reported that this change in the scaffold structure promoted proliferation, differentiation, mineralization, and adhesion of the hMSCs [462].

Hydrogels are biomaterials that mimic ECM in the organs as they include numerous water molecule content thanks to the cross-linking of the hydrophilic polymer by providing suitable microenvironment to release of various drugs and growth factors. Heo et al. proposed the AuNPs-loaded gelatin hydrogels for BTE applications. They showed that the developed Gel-GNP composite hydrogels promoted the proliferation and osteoblastic differentiation of the hADSCs. In addition, in the *in vivo* tests they performed, the researchers displayed that these hydrogels laden by high concentrations of AuNPs had a substantial effect on new bone development [463]. Another study based on injectable gelatin hydrogel reported that gel containing surface modified GNPs (Gel-Ty-G-NAC) promoted the viability and osteo-differentiation of the hASCs [464]. Due to the rapidly developing antibiotic resistance in society, it is important that the biomaterials to be used for BTE applications have modifications that will inhibit bacterial growth in addition to promoting bone tissue formation. Ribeiro et al. investigated the antimicrobial effects of silk fibroin/nanohydroxyapatite hydrogels by modifying them with *in situ* synthesized silver and AuNPs. They showed that metallic nanoparticles added to the structure exhibited important repressing effects to Gram (-) and Gram (+) bacteria. They also reported that AuNPs did not cause any reverse properties on the behavior of osteoblastic cells at any concentration used [465]. *In vitro* results of another study in which PVA/AuNPs/Ampicillin based 3D printed composite scaffolds were developed for BTE applications reported that the designed composite scaffold was osteo-inductive and it exhibited antimicrobial properties [466].

7.4. Gold nanoparticles for other tissue engineering applications

Apart from the applications mentioned above, AuNPs are also used in regenerative medicine studies in the fields of cartilage, muscle and dermal tissue engineering. In a teen mice model of lipopolysaccharide (LPS)-excited growth plate (GP) cartilage injury, the protecting consequence of Au-nanomaterials on the chondrocytes was demonstrated through prevention of apoptosis and ECM degradation. These promising results show that Au-nanomaterials can partly maintain children's cartilage from inflammatory injury [467]. In a study in which an injectable tissue construct containing homogenized porcine ECM origin and AuNPs was developed for musculoskeletal TE usages, it was displayed that the AuNPs incorporated into the construct reduced the ROS levels [468]. In a study in which AuNPs biosynthesized from *Staphylococcus aureus* were used as a useful factor in muscle TE, it was reported that AuNPs supported the viability of muscle cells and could defend the cells in contradiction of cardiotoxin injury. Additionally, purified Au-nanomaterials were collected into an elastic material to form a cardiac patch and their efficacy was investigated in a rat MI model. *In vivo* studies, the researchers proved that these *S. aureus*-derivative Au-nanomaterials reduced the infarct area and promoted functional MI repair [469]. Zsedenyi et al. fabricated 3-D hybrid nano-scaffolds containing AuNPs from biodegradable, photocurable PPF:DEF resin by the aid of mask-projection excimer laser stereolithography. Cellular studies exhibited that hybrid biomaterials supported stem cell adhesion and distribution. They reported that 14 days after transplanting the stem cell-coated scaffolds under the dorsal skin of the mice, the autologous stem cell-planted hybrid nanocomposite biomaterial induced muscle tissue renewal *in vivo* afterward experimental wound development [470].

With their biocompatibility, favorable degradation profiles, contribution to the improvement of mechanical properties, and wound healing promoting properties, the collagen/AuNPs nanocomposite scaffolds may be a potential skin wound healing biomaterial in the future [471]. In another study, Akturk et al. suggested the gold/PEO/collagen nanofibrous matrices within the scope of skin tissue engineering (STE). The researchers reported that the produced PEO/collagen nanofibrous scaffolds get healthier morphology once the ratio of combined Au-nanomaterials was increased [472]. The progress of bioactive bio-nano materials that encourage injured tissue renewal for advanced skin burns is a promising approach as a good alternative to autograft transplants. In a study, the researchers developed a hybrid PLA/chitosan nanofibrous scaffold functionalized with three types of nanoparticles (ZnO, Fe₃O₄, and AuNPs) for STE applications. Based on their comprehensive test and analysis results, they reported that the hybrid scaffold biomaterial has great potential for STE applications [473].

As can be understood from the literature studies mentioned above for various tissues and organs (such as heart, nerve, bone, cartilage, muscle, skeleton and skin), the tissue scaffolds combined with AuNPs have shown greater features that importantly increase their regenerative and healing effects. These hybrid biomaterials with various chemical and physical properties have great potential in tissue engineering-based approaches. In the vast majority of studies, no negative results have been revealed regarding the toxic effects of AuNPs with functional properties. The great success of AuNPs in TE applications is closely related to their exclusive physical/chemical features, stability, easy modification, biocompatibility and electrical conductivity. AuNPs also improved the mechanical properties of the scaffolds promoting cell proliferation, differentiation, adhesion, and growth. Before moving on to clinical applications, more toxicological tests and better examination of the mechanisms underlying positive cellular behaviors are needed.

8. Antibacterial studies using gold nanoparticles

The unconscious use of antibiotics for many years has been a growing problem worldwide, with more than 70 % of today's bacteria becoming resistant to one or more antibiotics. Therefore, there is a great need for alternative and innovative biomaterial designs that exhibit antibacterial activity [474,475]. The high specific surface area allows the binding of higher concentrations of functional ligands and other active molecules that will increase interaction with bacteria to nanoscale particles [476]. In this context, AuNPs are very suitable nanomaterials for antibacterial studies, and their broad antibacterial spectrum effectiveness has been demonstrated against both Gram-negative and Gram-positive bacteria. Since an expansive scale of bacterial biomolecules can be targeted using AuNPs, drug resistance does not develop easily. Size, surface functionalization and dispersibility are major factors for the antibacterial activities of nanomaterials. In particular, it has been shown that nanocomposites of smaller size and higher dispersibility parameters exhibit better antibacterial activity [477-479]. AuNPs can help the passage and effectiveness of the antibiotics that cannot penetrate the cell wall barrier, as sometimes the nanoparticles enter the bacteria by breaking their cell walls [480].

Dasari et al. evaluated the antibacterial activities of the Gold (I) and Gold (III) ions and AuNPs against four various bacteria: one nonpathogenic bacterium: *E. coli* and three multidrug-resistant bacteria: *S. typhimurium DT104*, *S. aureus*, and *E. coli*. They revealed that Au(I) and Au(III) ions were very toxic to four bacterial species. It was shown that bacterial growing restriction by the AuNPs decreased slowly via centrifugation and re-suspension. In addition, they emphasized that the exposure time of the AuNPs with bacteria and the use of buffers were also parameters to be taken into consideration [481]. In another study, the researchers investigated the shape-dependent antibacterial properties of the biocompatible gold nanomaterials with different forms (including stars, flowers and spheres) against *Staphylococcus aureus*, a globally life-threatening bacterial species. In particular, they reported

that the gold nanoflowers had the greatest shape-addicted antibacterial efficiency and the most encouraging biocompatible mammalian cell performance [482]. There is a study using AuNPs and laser combined therapy as an antibacterial approach against *Corynebacterium pseudotuberculosis*, the etiological agent of chronic lymphadenitis, which reasons main economic losses worldwide every year. The results of the related study exposed that the MIC of Au-nanomaterials and GNPs-laser combined therapy were 200 µg/mL and 100 µg/mL, respectively. It was reported that laser light increased the antimicrobial action of the AuNPs through at least one-fold as a result of the photothermal combined effect. In addition, AuNPs were shown to penetrate the thick wall of *C. pseudotuberculosis* [483]. Antibiotic resistance of *Streptococcus pneumoniae* strains, which causes almost one million deaths per year global, has become an increasing health problem. In one study, an innovative approach was developed for the separation of inclusion bodies, which allowed the analysis of biomolecules such as lipids, proteins, and carbohydrates associated with AuNPs. This approach allowed the determination of proteins associated with AuNPs. These proteins were advised as probable candidates that enable the contact and entrance of AuNPs into *S. pneumoniae* cells [484]. The design of AuNP-based antibacterial agents with optional Gram selectivity is promising for applications in personalized therapy. Wang et al. reported that the AuNPs functionalized with thiol- or amine-linked phenyl-boronic acids precisely bound to lipoteichoic acid (LTA, Gram-positive) or lipopolysaccharide (LPS, Gram-negative), respectively, leading to tunable antibacterial activity [485].

Biosynthesis of metallic nanoparticles is the simplest and most environmentally friendly method. Bindhu et al. produced the Au-nanoparticles by means of *Ananas comosus* extract and obtained nanoparticles with a dimension of 16 nm. They demonstrated that the prepared AuNPs showed effective antibacterial action in contradiction of Gram-negative and positive pathogens found in water [486]. In another study, the researchers effectively reduced ionic gold to AuNPs using *Longan* fruit juice and achieved stabilization of AuNPs. They reported that the synthesized AuNPs had remarkable antibacterial action against *Escherichia coli* with MIC values of 75 µg/mL and had significant MIC values of 50 µg/mL against *Bacillus subtilis* and *Staphylococcus aureus*. Furthermore, the biosynthesized AuNPs possessed effective photocatalytic activity properties, enhancing their therapeutic potential [487]. In a study where the biomolecules *Lignosus rhinocerotis* (LRE) and chitosan (CS) were used in the AuNP synthesis, CS-AuNPs via LRE showed powerful antibacterial activity against Gram-positive bacteria (*Staphylococcus aureus* and *Bacillus sp.*) and Gram-negative (*Pseudomonas aeruginosa* and *Escherichia coli*) [488]. In a study, researchers used panchagavya (PG) to synthesize AuNPs, and the antibacterial activity of PG-Au-nanoparticles against *Bacillus subtilis*, *Klebsiella pneumoniae*, and *Escherichia coli* were investigated via well diffusion technique. They reported that the antibacterial activity of PG-Au-nanoparticles was moderate against Gram-positive bacteria and robust against Gram-negative bacteria. It was also emphasized that *in vivo* and cellular toxicity studies of PG-Au-nanoparticles are needed [489]. It has been demonstrated that the antioxidant, antibacterial and cytotoxic impacts of AuNPs produced with the contribution of natural components of *Alternaria chlamydospora*, a marine fungus species, create a dose-dependent response [490]. Cefotaxime (CTX), a wide-spectrum antibiotic against Gram-positive and negative bacteria, has been losing its effectiveness every year owing to the occurrence of multidrug-resistant pathogens (MDR), like other third-generation cephalosporin antibiotics. Haghani et al. prepared the AuNPs (C-AuNPs) using cefotaxime, which performs as both an antibacterial agent and a reducing and capping agent. The researchers reported that the C-AuNPs they obtained displayed greater antibacterial action and lesser minimum inhibitory concentration (MIC) values against Gram-positive (*Staphylococcus aureus*) and Gram-negative (*Klebsiella oxytoca*, *Pseudomonas aeruginosa*, *Escherichia coli*) bacteria compared to pure CTX (Fig. 26) [491].

Dheyab et al. synthesized AuNPs via sonochemical and reduction procedures using citrate as reducing agent and investigated the antibacterial activity of nanoparticles against *S. aureus*. Their results revealed that sonochemically synthesized AuNPs showed greater and moderate antibacterial activity against *S. aureus* than reduction method [492]. Wang et al. reported that AuNPs synthesized using *Viola betonicifolia* leaf extract as reducing and capping agent exhibited excellent antibacterial, antifungal and biofilm inhibition performance against all tested microbial species. They attributed the enhanced biocompatibility, antifungal/antibacterial and biofilm inhibition activity to the physico-chemical properties of the AuNPs and biologically active phytomolecules adsorbed from *Viola betonicifolia* leaf extract [493]. In another study, the researchers biosynthesized AuNPs using Presley leaf (*Petroselinum crispum*) extract using an eco-friendly and cost-effective procedure. They reported that the AuNPs showed an apparent antimicrobial activity against two Gram-negative bacteria and were ineffective against Gram-positive bacteria [494]. In a study where *Jatropha integerrima* Jacq. flower extract was used as a reducing and stabilizing agent for the synthesis of AuNPs, the researchers reported that the nanoparticles they synthesized showed activity against drug-resistant pathogens, making them a promising therapeutic candidate [495]. The other study investigated the antibacterial property of gold the AuNPs synthesized from *Garcinia kola* pulp extract. The study presented an environmentally friendly approach in the synthesis of AuNPs from *Garcinia kola* pulps and established its applicability for medical purposes as antibacterial agents [496]. Shakoor et al. demonstrated the successful synthesis of AuNPs from *C. trichotomum* Thunberg (CTT) using a green and eco-friendly approach. They reported that the synthesized AuNPs had a better log₁₀ reduction effect on the growth of both Gram-positive and Gram-negative bacteria as compared to commercial nanoparticles and plant extract. These excellent antibacterial and cytotoxic properties of the biosynthesized AuNPs are due to the synergistic effect of bioactive phytochemicals present in the CTT extract [497].

The antibacterial features of AuNPs are strictly associated to the shape, size, concentration, surface functionalization and synthesis method of nanomaterials. It has been demonstrated that the nanoparticles used *in vitro* studies have no toxic effects on healthy cells and they are quite biocompatible. On the other hand, significant levels of antibacterial activity have been proven depending on the parameters mentioned above. It is thought that the antibacterial mechanism is related to membrane damage, DNA damage and high ROS damage. Although there are limited studies on multidrug-resistant bacterial species, there is a great need for more and comprehensive studies on these species. In addition, comprehensive *in vitro/in vivo* toxicological analyses and multifaceted antibacterial studies are required before transitioning to the clinic. However, the findings obtained at this stage are promising for future clinical studies.

9. Clinical translation of gold nanoparticles

AuNPs possess important nanomaterials that could be useful for therapeutic and diagnostic purposes. However, the safety of AuNPs in human subjects remains a crucial question. Preclinical studies with AuNPs have led to the steady progress of gold nanomaterials toward clinical development. The success of such preclinical nanotherapeutic applications depends on detailed and reliable analysis of the biodistribution and pharmacokinetic profiles of AuNPs. Expansion of clinical trials requires effective collaboration among scientists, biotechnology companies, and clinicians [498,499].

Despite numerous studies reporting new AuNP-based nano formulations, very few gold nanomaterials have made it to the clinical stage. This is primarily because most reported studies are focused on nanotechnology and materials science. A nano formulation that can be evaluated in clinical settings must have properties that meet a clinical need and a relatively simple composition. This ensures that the effects of nano formulations on human physiology are predictable. On the other

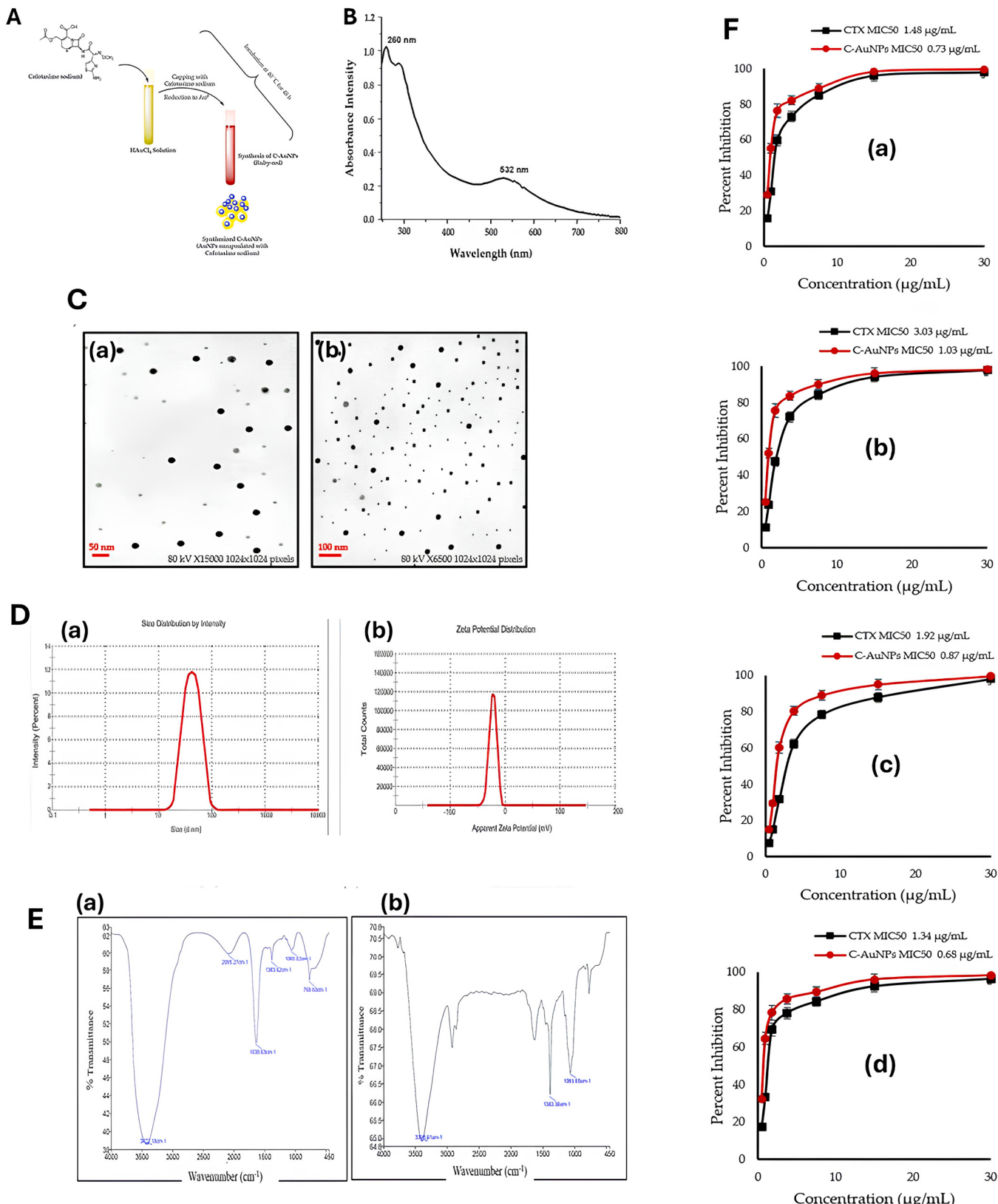


Fig. 26. (A) Diagrammatic representation of C-gold nanoparticles (AuNPs) synthesis procedure. (B) UV-Visible spectra of C-AuNPs showing a characteristic surface plasmon absorption band at 532 nm. (C) Transmission electron microscopy (TEM) micrograph images of C-AuNPs representing spherical monodispersing C-AuNPs with an average size of 21 nm at different magnification scales; (C-a) $15,000 \times$, (C-b) $6500 \times$. (D) Size determination via DLS and zeta-potential results. (D-a) Particle size analysis by dynamic light scattering (DLS), 65 nm, (D-b) Zeta-potential (-23 mV) of C-AuNPs. (E) Fourier transform infrared (FTIR) spectra of (E-a) Pure CTX, (E-b) C-AuNPs. (F) Minimum inhibitory concentration (MIC) of CTX and C-AuNPs against (F-a) *Escherichia coli*; (F-b) *Klebsiella oxytoca*; (F-c) *Pseudomonas aeruginosa*. (F-d) *Staphylococcus aureus*. The data represents the means \pm standard errors of three independent experiments. Adapted with permission from reference [491]. Copyright (2022), MDPI.

Table 3

Some selected therapeutic gold nanomaterials in clinical trials.

Name	Clinical Trial (trial number, status, years)	Nanoparticle Type (Device)	Condition/Disease	Number of enrolments	Sponsor	References
TNF-Bound Colloidal Gold in Treating Patients With Advanced Solid Tumors	(NCT00356980, Completed, Phase 1, 2006–2009)	TNF-bound colloidal gold, CYT–6091	Unspecified adult solid tumor	(60)	National Institutes of Health Clinical Center (CC)	[503]
Plasmonic Nanophotothermal Therapy of Atherosclerosis (NANOM-FIM)	(NCT01270139, Completed, 2007–2016)	Silica-gold iron-bearing NP	Stable Angina, Heart Failure, Atherosclerosis, Multivessel Coronary Artery Disease	(180)	Ural State Medical University	[504,505]
Pilot Study of AuroLase(tm) Therapy in Refractory and/or Recurrent Tumors of the Head and Neck	(NCT00848042, Completed, 2008–2014)	AuroShell (TM)	Head & neck cancer	(11)	Nanospectra Biosciences, Inc.	[506]
Multiple Arm Study of Sebacia Microparticles in the Treatment of Acne Vulgaris	(NCT02219074, Completed, 2011–2016)	Sebashell	Acne Vulgaris	(350)	Sebacia, Inc.	[507]
A Phase I SAD and MAD Clinical Trial of CNM-Au8 in Healthy Male and Female Volunteers	(NCT02755870, Completed, Phase 1, 2015–2016)	CNM-Au8	Healthy Volunteers - Male and Female	(86)	Clene Nanomedicine	[508]
MRI/US Fusion Imaging and Biopsy in Combination With Nanoparticle Directed Focal Therapy for Ablation of Prostate Tissue	(NCT02680535, Completed, 2016–2020)	AuroShell C19-A3 GNP, Proinsulin peptide	Neoplasms of the Prostate Type 1 Diabetes	(45)	Nanospectra Biosciences, Inc.	[509]
Enhanced Epidermal Antigen Specific Immunotherapy Trial –1 (EE-ASI–1)	(NCT02837094, Completed, Phase 1, 2016–2019)			(8)	Cardiff University	[510]
Name	Clinical Trial (trial number, status, years)	Nanoparticle Type (Device)	Condition/Disease	Number of enrolments	Sponsor	References
NU–0129 in Treating Patients With Recurrent Glioblastoma or Gliosarcoma Undergoing Surgery	(NCT03020017, Completed, Early Phase1, 2017–2020)	NU0129, Bcl2L12 specific RNAi	Gliosarcoma, Recurrent Glioblastoma	(8)	Northwestern University	[511]
Nanocrystalline Gold to Treat Remyelination Failure in Chronic Optic Neuropathy In Multiple Sclerosis (VISIONARY-MS)	(NCT03536559, Terminated, Phase 2, 2018–2022)	CNM-Au8	Relapsing Remitting Multiple Sclerosis, Optic Neuropathy, Optic; Neuritis, With Demyelination	(73)	Clene Nanomedicine	[512]
Therapeutic Nanocatalysis to Slow Disease Progression of Amyotrophic Lateral Sclerosis (ALS) (RESCUE-ALS)	(NCT04098406, Completed, Phase 2, 2019–2021)	CNM-Au8	Amyotrophic Lateral Sclerosis	(45)	Clene Nanomedicine	[513]
31P-MRS Imaging to Assess the Effects of CNM-Au8 on Impaired Neuronal Redox State in Multiple Sclerosis. (REPAIR-MS)	(NCT03993171, Active, not recruiting, Phase 2, 2019–2025)	CNM-Au8	Multiple Sclerosis	(30)	Clene Nanomedicine	[514]
31P-MRS Imaging to Assess the Effects of CNM-Au8 on Impaired Neuronal Redox State in Parkinson's Disease (REPAIR-PD)	(NCT03815916, Completed, Phase 2, 2019–2021)	CNM-Au8	Parkinson's Disease	(13)	Clene Nanomedicine	[515]
A Multi-Center, Open-Label Long-Term Extension Study of CNM-Au8 In Patients With Stable Relapsing Multiple Sclerosis (VISIONMS-LTE)	(NCT04626921, Completed, Phase 2, Phase 3, 2020–2023)	CNMAu8	Relapsing Multiple Sclerosis	(55)	Clene Nanomedicine	[516]

hand, most nanomaterial-based studies have been developed with multifunctional and complex properties. Nanostructures with simple structural properties are rarely encountered in basic research [500,501]. However, the majority of AuNPs lack effective surface functionalization accumulated in the liver and spleen. Multifunctional AuNPs designed to address this issue, including those containing extensive surface modifications, may have more toxic properties, and their *in vivo* bi-distribution/pharmacokinetic profiles are more difficult to predict. This is another obstacle to the clinical application of AuNPs [54,502]. To date, the use of AuNPs as a human medical intervention has been evaluated in more than 20 studies. These studies have mostly focused on safety issues. Most of these studies have been completed in recent years, while some are still ongoing [499]. Table 3 summarizes some of the key studies in which AuNPs have been used as therapeutic agents in various drug delivery systems or investigated their efficacy as PTT agents [503–516].

The first clinical study investigating the use of AuNPs as a drug system was completed in 2009 by Libutti et al. (NCT00356980). This potent rhTNF alpha factor and PEG-SH polymer were conjugated to AuNP (CYT–6091) for therapeutic application with a coverage of approximately 27 nm. In young patients with advanced and/or metastatic solid organ cancers, i.v. side effects such as increased

aminotransferase levels, hypokalemia, hypoalbuminemia, hypophosphatemia, lymphopenia, and hyperbilirubinemia were also observed with the modified formulation. The researchers' findings indicate that despite the presence of some side effects, therapeutic efficacy was achieved and that there were no highly toxic effects associated with AuNPs [503]. In 2015, Kharlamov et al. reported the results of a clinical trial of silica-gold nanoparticles (NANOM-FIM) for the atheroprotective management of plaques. The investigators completed an observational three-arm ($n = 180$) first-in-human study (NANOM-FIM) that evaluated the feasibility and safety of two delivery techniques for nanoparticles and plasmonic PTT (NCT01270139). PPTT using silica-gold NP was shown to contribute to a significant reduction in coronary atherosclerosis [504]. The findings from a 5-year follow-up study of the first-in-human study of NANOM, published by the researchers in 2017, demonstrated improved long-term follow-up mortality, major adverse cardiovascular events, and increased safety with target lesion revascularization compared with the stent XIENCE V [505]. An open-label, multicenter, single-dose clinical pilot study of AuroLase (tm) treatment in patients with refractory and/or recurrent tumors of the head and neck region was completed in 2014 (NCT00848042). Each treatment group received a single dose of AuroShell™ particles (150 nm silica core based nanoparticle with a gold shell and thiolated PEG

surface) followed by one or more interstitial illuminations with an 808 nm laser [506]. In a clinical study completed in 2020, AuroShell's thermal ablation capabilities in prostate cancers were evaluated using an MRI/US fusion imaging and biopsy approach combined with nanoparticle-directed focal therapy (NCT02680535). The results demonstrated that the protocol was safe, with moderate side effects occurring in patients [509]. A clinical study on the application of AuNP (a 150 nm nanoparticle composed of a silica core coated with a gold shell and PEG) formulation (Sebasshell) to 350 patients for the treatment of Acne Vulgaris was completed in 2016 (NCT02219074) [507].

CNM-Au8 is a novel solution of gold nanocrystals approximately 13 nm in diameter developed by Clene Nanomedicine. The first clinical trial of CNM-Au8 investigated the formulation's safety profile in humans and was completed in 2016 (NCT02755870). Doses of 15, 30, 60, or 90 mg of CNM-Au8 were administered orally to 86 healthy male and female volunteers who were monitored for 21 days [508]. There are clinical studies investigating the efficacy and safety of CNM-Au8 for relapsing multiple sclerosis (NCT03536559 and NCT04626921), amyotrophic lateral sclerosis (NCT04098406), multiple sclerosis (NCT03993171), Parkinson's Disease (NCT03815916) [513–516]. A clinical study evaluating the safety of AuNPs (C19-A3 GNP) conjugated with proinsulin peptide and administered via hollow microneedles as immunotherapy in type 1 diabetes was published by Tatovic et al. in 2022. A total of 8 patients aged 18–40 years with type 1 diabetes were treated with C19-A3 GNP i.m. every 28 days for 8 weeks (NCT02837094). No serious side effects were reported throughout the study, and the patients tolerated it well [510]. Glioblastoma (GBM) is one of the most challenging cancer types to treat effectively. In a clinical study published by Kumthekar et al. in 2021 (NCT03020017), a precision medicine approach involving the use of brain-penetrating RNA interference-based spherical nucleic acids (SNAs), consisting of AuNP cores conjugated with densely packed and radially oriented siRNAs, was developed for the treatment of GBM. The researchers conducted a single-arm, open-label phase 0 first-in-human trial to determine the pharmacokinetics, safety, accumulation, and efficacy of SNAs (drug name: NU-0129) carrying siRNA specific for the GBM oncogene Bcl2L12. The safety assessment demonstrated no treatment-related Grade 4 or 5 toxicity. The researchers' results confirmed that SNA nanoconjugates are a potentially effective and innovative brain-penetrating nanomedicine approach for the treatment of GBM [511].

Clinical studies using AuNPs have demonstrated that the nanoparticles used are well tolerated by human subjects and cause minimal side effects. This confirms the good risk and safety profiles of AuNPs. However, the patient sample sizes in some studies are quite small, and larger clinical studies are needed. Furthermore, short-term evaluations lead to an inadequate understanding of the long-term toxic effects of AuNPs with varying physicochemical properties. While the ease of modification of AuNPs is an advantage, each formulation needs to be individually examined to better analyze the toxicological effects in humans of AuNPs with extensive additional functionalization and surface coating. Clinical studies on AuNPs will continue to expand in the future. Expanding clinical trials requires effective collaboration between scientists, biotechnology companies, and clinicians.

10. Conclusions and future perspectives

With the rapid developments in nanomedicine, the production of gold nanoparticles (AuNPs) via the necessary parameters in terms of shape, size, physicochemical structure, surface modification and optical characteristics has been successfully achieved using different synthesis methods. Considering factors such as their stable structure, unique physicochemical properties, biocompatibility, inert nature, easy surface functionalization and synthesis, AuNPs have a wide range of nanomedicine applications. Present usages of Au-nanomaterials in the biomedical area comprise toxicology/biodistribution studies, cancer

therapy, gene therapy, drug delivery, targeting, photothermal therapy, bioimaging, biosensor applications, tissue engineering and antibacterial studies. The low cellular/*in vivo* toxicity and non-immunogenicity of most AuNPs-based studies in the literature make us relatively hopeful concerning their future potential nanomedicine applications. Apart from its use as targeted AuNPs with appropriate surface modifications, its therapeutic effects have also been extensively studied in hybrid complexes with various materials. Synthesis methods and physicochemical properties of AuNPs have decisive effects on their effectiveness and safety in cancer therapy. The use of image guiding strategies together with the designed hybrid nanocomplexes has enabled more effective therapeutic results in the tumor-bearing animal models. Various mechanisms are being proposed to increase the affinity of functional group-bearing AuNPs to biomolecules and turn them into effective drug delivery systems with improved specificity. Suitable surface modification increases the stability, biocompatibility, cellular uptake, biodistribution and finally bioavailability of AuNPs. AuNP-mediated gene therapy has established excellent potential for correcting and silencing monogenic syndrome mutations. AuNPs can be used as nanocarrier platform for the delivery of molecules on a larger scale, such as drugs, proteins, peptide molecules, siRNA oligonucleotides, DNA molecules and CRISPR-Cas9 complexes. Among other metallic NPs, Au-nanomaterials have excellent potential to be used in bio-imaging field. The AuNPs have a broad scope of SPR depending on the NPs' dimensions, shape and surface modification. AuNPs with various properties have been considerably studied experimentally for their optical superior properties and biological, cellular and *in vivo* applications. Considering the high sensitivity, suitable SPR properties, biocompatibility, rapid results, high surface area, catalytic properties, stability and controllable interactions with different biomolecules, AuNPs can be used as biosensor platforms alone and in hybrid/modified forms in various diagnostic processes. The integration of the AuNPs-based biosensor platforms with portable devices such as smartphones is an important and promising approach. The great success of AuNPs in tissue engineering applications is closely related to their fascinating physical/chemical features, stability, easy modification, biocompatibility and electrical conductivity. AuNPs also improved the mechanical properties of the scaffold materials promoting cell growth, adhesion, differentiation, and proliferation. Different Au-based nanomaterials have been extensively investigated as antibacterial agents based on their remarkable physicochemical properties. For this purpose, antibacterial mechanisms of AuNPs with various shapes, sizes and surface chemistries have been demonstrated. There are numerous cellular and *in vivo* research reports in the literature on biomedical applications of AuNPs, but there is still a need for extensive biological research. It is concluded that in the coming years we will witness clinical studies on AuNPs with the expanded strategies.

Researchers are currently intensively investigating multifunctional nanoparticles that can target and deliver therapeutic agents to cells and revolutionize drug delivery systems. Scientists are working on new types of multifunctional hybrid nanoparticles made by mixing AuNPs with other nanomaterials. Moreover, once the integration process is completed using appropriate technologies on microchips and microfluidic devices, remote, fast, precise and reliable monitoring of laboratory tests will be greatly facilitated. Complex processes will become simpler, facilitating quality and accessibility in healthcare services. With the use of AuNPs as biosensors, complex biological processes will become more understandable, and diseases will be identified and monitored at very early stages. Immunotherapy is an effective way to help the body fight disease by strengthening its own defenses, and researchers could make such treatments more powerful and effective by using AuNPs. Nanogold could also help improve sensors for issues affecting human health, such as food safety and air quality. In this respect, AuNPs are a nanomaterial ready to play a strong role in these areas. Machine learning (ML) offers a promising approach for developing optimized protocols for the synthesis of AuNPs with diverse physicochemical properties and for designing new types of AuNPs. ML

models are also powerful and useful tools for predicting the intracellular distribution and dynamics of AuNPs and for elucidating the influencing factors. Future robust meta-analysis studies will address significant gaps in this area. With rapid advances in nanoscience and computational measurement/analysis using machine learning models, the quality and accuracy of the resulting data has the potential to increase. Organ-on-a-chip technology offers an important approach to overcome the disadvantages and limitations of routinely used preclinical models and approaches. Advances in this technology may lead to new opportunities to improve the biomedical application and clinical processes of AuNPs. Biomimetic models of tissues and organs designed using micro/nano-engineering approaches could enable more physiologically consistent, reliable, and meaningful *in vitro* modeling of human system responses to AuNPs, in ways that cannot be investigated through traditional cell culture assays. Such innovative approaches for AuNPs are still in their infancy, and significant progress has not yet been made. Furthermore, with the rapid advances and intense interest in organ-on-a-chip technology, it is anticipated that this technology will play a significant role in the development of AuNP-based nanotherapeutics in the future. The future of gold nanoparticles looks bright as a nanomaterial that is set to usher in a new era in personalized medicine and quality control across a wide range of biomedical industries. As a conclusion, there has been great progress in the synthesis and functionalization of AuNPs, which may make a great contribution to improved clinical diagnostic and therapeutic procedures.

The main challenges and developments affecting the widespread use of AuNPs in the field of nanomedicine are as follows:

1. A more specific and limited size range can be determined by using effective and standard synthesis methods. Thus, the biomedical effects to be obtained will be more standardized and effective.
2. In order for GNPs to find more applications in the biomedical clinical market, the high cost and accessibility problems must be solved.
3. Further animal model studies are needed to determine the bio-distribution, clearance and toxicological effects of gold nanoparticles. A systematic nanotoxicity investigation must be applied for each specific case under precise controlled conditions before biomedical applications of gold nanoparticles can be carried out in humans.
4. Although the benefits of AuNPs in the field of cancer medicine are quite obvious, there is a great need for more detailed *in vitro/in vivo* studies and analysis before their large-scale use. Additionally, personalized approaches are required to develop optimal AuNPs that can provide high levels of therapeutic efficacy and bioavailability for each tumor disease type.
5. Although the transfer of larger molecules using AuNPs is an interesting field, innovative research is needed to increase their effective cellular uptake, tissue specific targeting and biocompatibility. Although drug and gene delivery systems using AuNPs are very promising, more innovative optimization approaches that will increase *in vivo* efficiency and studies that will enable clinical transition are needed.
6. There is a need to develop 3D nanoparticle tracking techniques to understand cellular bio-nano interactions. More sensitive and effective plasmonic AuNP-based nanoconjugates can be designed through alternative and innovative synthesis and surface modifications.
7. *In vivo* tissue/organ imaging applications are still difficult due to the low penetration depth of light. New hybrid nanoparticles that scatter NIR light should be developed to reduce the scattering background and improve detection depth.
8. Bioimaging studies are needed to reveal the interaction mechanisms of AuNPs with biomolecules in cells in more detail. In addition, stability, toxicology, risk and safety evaluations of

AuNPs should be considered individually in a broad framework for their use in each bio-imaging technique.

9. In the near future, significant scientific developments are expected in the design of AuNP-based biosensor platforms for the rapid, practical, simple, highly sensitive and reliable detection of various clinically important biomolecules.
10. Before moving on to clinical applications, more toxicological tests and better examination of the mechanisms underlying positive cellular behaviors are needed regarding tissue engineering applications of the AuNPs.
11. Although there are limited AuNPs based studies on multidrug-resistant bacterial species, there is a great need for more and comprehensive studies on these species. In addition, comprehensive *in vitro/in vivo* toxicological analyses and multifaceted antibacterial studies are required before transitioning to the clinic.
12. Sample sizes in clinical studies should be increased. Longer-term risk and safety assessments should be conducted. To better analyze the toxicological effects of AuNPs with extensive additional surface modifications in humans, each formulation needs to be studied separately.

CRediT authorship contribution statement

Ilyas Ozcicek: Writing – review & editing, Writing – original draft, Visualization, Validation, Supervision, Software, Resources, Project administration, Methodology, Investigation, Funding acquisition, Formal analysis, Data curation, Conceptualization.

Declaration of Competing Interest

The authors declare that they have no known competing financial interests or personal relationships that could have appeared to influence the work reported in this paper.

Data availability

Data will be made available on request.

References

- [1] C.Y. Zhang, L. Yan, X. Wang, S. Zhu, C.Y. Chen, Z.J. Gu, Y.L. Zhao, Progress, challenges, and future of nanomedicine, *Nano Today* 35 (2020).
- [2] X. Zhang, Gold nanoparticles: recent advances in the biomedical applications, *Cell Biochem Biophys.* 72 (3) (2015) 771–775.
- [3] Z. Krpetic, S. Anguissola, D. Garry, P. Kelly, K. Dawson, Nanomaterials: impact on cells and cell organelles, *Adv. Exp. Med. Biol.* 811 (2014) 135–156.
- [4] I. Lynch, A. Salvati, K.A. Dawson, What does the cell see? *Nat. Nanotechnol.* 4 (9) (2009) 546–547.
- [5] I. Ozcicek, N. Aysit, C. Cakici, A. Aydeger, The effects of surface functionality and size of gold nanoparticles on neuronal toxicity, apoptosis, ROS production and cellular/suborgan biodistribution, *Mater. Sci. Eng. C. Mater. Biol. Appl.* 128 (2021) 112308.
- [6] I. Ozcicek, N. Aysit, C. Cakici, N.U. Ayturk, A. Aydeger, U.C. Erim, The effects of various surface coatings of gold nanorods on toxicity, neuronal localization, microstructural alterations, and *in vitro/in vivo* biodistribution, *Adv. Mater. Interfaces* 9 (3) (2022).
- [7] K. Nejati, M. Dadashpour, T. Gharibi, H. Mellatyar, A. Akbarzadeh, Biomedical applications of functionalized gold nanoparticles: a review, *J. Clust. Sci.* 33 (1) (2022) 1–16.
- [8] H. Huang, R. Liu, J. Yang, J. Dai, S. Fan, J. Pi, Y. Wei, X. Guo, Gold nanoparticles: construction for drug delivery and application in cancer immunotherapy, *Pharmaceutics* 15 (7) (2023) 1868.
- [9] H. Peng, H. Tang, J. Jiang, Recent progress in gold nanoparticle-based biosensing and cellular imaging, *Sci. China Chem.* 59 (7) (2016) 783–793.
- [10] H. Chen, X. Kou, Z. Yang, W. Ni, J. Wang, Shape- and size-dependent refractive index sensitivity of gold nanoparticles, *Langmuir* 24 (10) (2008) 5233–5237.
- [11] P. Slepicka, N. Slepicková Kasálková, J. Siegel, Z. Kolská, V. Švorcík, Methods of gold and silver nanoparticles preparation, *Materials* 13 (1) (2020) 1.
- [12] A. Sani, C. Cao, D. Cui, Toxicity of gold nanoparticles (AuNPs): a review, *Biochem. Biophys. Rep.* 26 (2021) 100991.

- [13] J. Turkevich, P.C. Stevenson, J. Hillier, A study of the nucleation and growth processes in the synthesis of colloidal gold, *Discuss. Faraday Soc.* 11 (0) (1951) 55–75.
- [14] S.D. Perrault, W.C.W. Chan, Synthesis and surface modification of highly monodispersed, spherical gold nanoparticles of 50–200 nm, *J. Am. Chem. Soc.* 131 (47) (2009) 17042.
- [15] J. Niu, T. Zhu, Z. Liu, One-step seed-mediated growth of 30–150 nm quasispherical gold nanoparticles with 2-mercaptopropionic acid as a new reducing agent, *Nanotechnology* 18 (32) (2007) 325607.
- [16] S. Wang, X. Zhao, S. Wang, J. Qian, S. He, Biologically inspired polydopamine capped gold nanorods for drug delivery and Light-Mediated cancer therapy, *ACS Appl. Mater. Interfaces* 8 (37) (2016) 24368–24384.
- [17] L. Wang, Y. Liu, W. Li, X. Jiang, Y. Ji, X. Wu, L. Xu, Y. Qiu, K. Zhao, T. Wei, Y. Li, Y. Zhao, C. Chen, Selective targeting of gold nanorods at the mitochondria of cancer cells: implications for cancer therapy, *Nano Lett.* 11 (2) (2011) 772–780.
- [18] X. Wang, Y. Li, H. Wang, Q. Fu, J. Peng, Y. Wang, J. Du, Y. Zhou, L. Zhan, Gold nanorod-based localized surface plasmon resonance biosensor for sensitive detection of hepatitis b virus in buffer, blood serum and plasma, *Biosens. Bioelectron.* 26 (2) (2010) 404–410.
- [19] R. Herizchi, E. Abbasi, M. Milani, A. Akbarzadeh, Current methods for synthesis of gold nanoparticles, *Artif. Cells Nanomed. Biotechnol.* 44 (2) (2016) 596–602.
- [20] N.S. Aminabad, M. Farshbaf, A. Akbarzadeh, Recent advances of gold nanoparticles in biomedical applications: state of the art, *Cell Biochem Biophys.* 77 (2) (2019) 123–137.
- [21] T.N. Dung, D.J. Kim, K.S. Kim, Controlled synthesis and biomolecular probe application of gold nanoparticles, *Micron* 42 (3) (2011) 207–227.
- [22] I. Ojea-Jimenez, V. Puntes, Instability of cationic gold nanoparticle bioconjugates: the role of citrate ions (vol 131, pg 13320, 2009), *J. Am. Chem. Soc.* 132 (14) (2010) 5322.
- [23] T.N. Elizarova, M.L. Antopolksky, D.O. Novichikhin, A.M. Skirda, A.V. Orlov, V. A. Bragina, P.I. Nikitin, A straightforward method for the development of positively charged gold Nanoparticle-Based vectors for effective siRNA delivery, *Molecules* 28 (8) (2023).
- [24] R. Dutour, G. Bruylants, Gold nanoparticles coated with nucleic acids: an overview of the different bioconjugation pathways, *Bioconjug. Chem.* 36 (6) (2025) 1133–1156.
- [25] J. Manson, D. Kumar, B.J. Meenan, D. Dixon, Polyethylene glycol functionalized gold nanoparticles: the influence of capping density on stability in various media (vol 44, pg 99, 2011), *Gold. Bull.* 44 (3) (2011) 195–196.
- [26] S. Alex, A. Tiwari, Functionalized gold nanoparticles: synthesis, properties and Applications-A review, *J. Nanosci. Nanotechnol.* 15 (3) (2015) 1869–1894.
- [27] A.G. Kanaras, F.S. Kamounah, K. Schaumburg, C.J. Kiely, M. Brust, Thioalkylated tetraethylene glycol: a new ligand for water soluble monolayer protected gold clusters, *Chem. Commun.* 20 (2002) 2294–2295.
- [28] Y.-P. Jia, B.-Y. Ma, X.-W. Wei, Z.-Y. Qian, The in vitro and in vivo toxicity of gold nanoparticles, *Chin. Chem. Lett.* 28 (4) (2017) 691–702.
- [29] H.C. Fischer, W.C.W. Chan, Nanotoxicity: the growing need for in vivo study, *Curr. Opin. Biotechnol.* 18 (6) (2007) 565–571.
- [30] N. Khetbostov, L. Dykman, Biodistribution and toxicity of engineered gold nanoparticles: a review of in vitro and in vivo studies, *Chem. Soc. Rev.* 40 (3) (2011) 1647–1671.
- [31] J.S. Kang, Y.N. Yum, J.H. Kim, H. Song, J. Jeong, Y.T. Lim, B.H. Chung, S.N. Park, Induction of DNA damage in L5178Y cells treated with gold nanoparticle, *Biomol. Ther.* 17 (1) (2009) 92–97.
- [32] J.J. Li, D. Hartono, C.N. Ong, B.H. Bay, L.Y.L. Yung, Autophagy and oxidative stress associated with gold nanoparticles, *Biomaterials* 31 (23) (2010) 5996–6003.
- [33] A. Chompoosor, K. Saha, P.S. Ghosh, D.J. Macarthy, O.R. Miranda, Z.J. Zhu, K. F. Arcaro, V.M. Rotello, The role of surface functionality on acute cytotoxicity, ROS generation and DNA damage by cationic gold nanoparticles, *Small* 6 (20) (2010) 2246–2249.
- [34] C. Brandenberger, C. Mühlfeld, Z. Ali, A.G. Lenz, O. Schmid, W.J. Parak, P. Gehr, B. Rothen-Rutishauser, Quantitative evaluation of cellular uptake and trafficking of plain and polyethylene Glycol-Coated gold nanoparticles, *Small* 6 (15) (2010) 1669–1678.
- [35] N.M. Schaeublin, L.K. Braydich-Stolle, A.M. Schrand, J.M. Miller, J. Hutchison, J. Schlager, S.M. Hussain, Surface charge of gold nanoparticles mediates mechanism of toxicity, *Nanoscale* 3 (2) (2011) 410–420.
- [36] A. Albanese, W.C.W. Chan, Effect of gold nanoparticle aggregation on cell uptake and toxicity, *Acs Nano* 5 (7) (2011) 5478–5489.
- [37] E. Oh, J.B. Delehanty, K.E. Sapsford, K. Susumu, R. Goswami, J.B. Blanco-Canosa, P.E. Dawson, J. Granek, M. Shoff, Q. Zhang, P.L. Goering, A. Huston, I.L. Medintz, Cellular uptake and fate of PEGylated gold nanoparticles is dependent on both Cell-Penetration peptides and particle size, *Acs Nano* 5 (8) (2011) 6434–6448.
- [38] S.J. Soenen, B. Manshian, J.M. Montenegro, F. Amin, B. Meermann, T. Thiron, M. Cornelissen, F. Vanhaecke, S. Doak, W.J. Parak, S. De Smedt, K. Braeckmans, Cytotoxic effects of gold nanoparticles: a multiparametric study, *Acs Nano* 6 (7) (2012) 5767–5783.
- [39] R. Coradeghini, S. Gioria, C.P. García, P. Nativo, F. Franchini, D. Gilliland, J. Ponti, F. Rossi, Size-dependent toxicity and cell interaction mechanisms of gold nanoparticles on mouse fibroblasts, *Toxicol. Lett.* 217 (3) (2013) 205–216.
- [40] P.J. Chueh, R.Y. Liang, Y.H. Lee, Z.M. Zeng, S.M. Chuang, Differential cytotoxic effects of gold nanoparticles in different mammalian cell lines, *J. Hazard Mater.* 264 (2014) 303–312.
- [41] D. Mateo, P. Morales, A. Avalos, A.I. Haza, Oxidative stress contributes to gold nanoparticle-induced cytotoxicity in human tumor cells, *Toxicol. Mech. Method* 24 (3) (2014) 161–172.
- [42] T.J. Cho, R.I. MacCuspie, J. Gigault, J.M. Gorham, J.T. Elliott, V.A. Hackley, Highly stable positively charged Dendron-Encapsulated gold nanoparticles, *Langmuir* 30 (13) (2014) 3883–3893.
- [43] X.M. Zhu, C.H. Fang, H.L. Jia, Y. Huang, C.H.K. Cheng, C.H. Ko, Z.Y. Chen, J. F. Wang, Y.X.J. Wang, Cellular uptake behaviour, photothermal therapy performance, and cytotoxicity of gold nanorods with various coatings, *Nanoscale* 6 (19) (2014) 11462–11472.
- [44] C. Yang, J. Uertz, D. Yohan, B.D. Chithrani, Peptide modified gold nanoparticles for improved cellular uptake, nuclear transport, and intracellular retention, *Nanoscale* 6 (20) (2014) 12026–12033.
- [45] Z.B. Li, S.Y. Tang, B.K. Wang, Y. Li, H. Huang, H.Y. Wang, P.H. Li, C.Z. Li, P. K. Chu, X.F. Yu, Metabolizable small gold nanorods: Size-dependent cytotoxicity, cell uptake and biodistribution, *Acs Biomater. Sci. Eng.* 2 (5) (2016) 789–797.
- [46] P. Falagan-Lotsch, E.M. Grzincic, C.J. Murphy, One low-dose exposure of gold nanoparticles induces long-term changes in human cells, *P Natl. Acad. Sci. USA* 113 (47) (2016) 13318–13323.
- [47] M.C. Senut, Y.H. Zhang, F.C. Liu, A. Sen, D.M. Ruden, G.Z. Mao, Size-Dependent toxicity of gold nanoparticles on human embryonic stem cells and their neural derivatives, *Small* 12 (5) (2016) 631–646.
- [48] A.C. Wong, D.W. Wright, Size-Dependent cellular uptake of DNA functionalized gold nanoparticles, *Small* 12 (40) (2016) 5592–5600.
- [49] J. Wan, J.-H. Wang, T. Liu, Z. Xie, X.-F. Yu, W. Li, Surface chemistry but not aspect ratio mediates the biological toxicity of gold nanorods in vitro and in vivo, *Sci. Rep.* 5 (1) (2015) 11398.
- [50] X.L. Wang, X.H. Hu, J.C. Li, A.C.M. Russe, N. Kawazoe, Y.N. Yang, G.P. Chen, Influence of cell size on cellular uptake of gold nanoparticles, *Biomater. Sci. UK* 4 (6) (2016) 970–978.
- [51] A. Stojiljkovic, K. Kuehni-Boghenbor, V. Gaschen, G. Schipbach, M. Mevissen, C. Kinnear, A.M. Möller, M.H. Stoffel, High-content analysis of factors affecting gold nanoparticle uptake by neuronal and microglial cells in culture, *Nanoscale* 8 (37) (2016) 16650–16661.
- [52] T. Schneider, M. Westermann, M. Gleis, In vitro uptake and toxicity studies of metal nanoparticles and metal oxide nanoparticles in human HT29 cells, *Arch. Toxicol.* 91 (11) (2017) 3517–3527.
- [53] D. Kumar, I. Mutreja, K. Chitcholtan, P. Sykes, Cytotoxicity and cellular uptake of different sized gold nanoparticles in ovarian cancer cells, *Nanotechnology* 28 (47) (2017).
- [54] X.M. Li, Z.P. Hu, J.L. Ma, X.Y. Wang, Y.P. Zhang, W. Wang, Z. Yuan, The systematic evaluation of size-dependent toxicity and multi-time biodistribution of gold nanoparticles, *Colloid Surf. B* 167 (2018) 260–266.
- [55] M. Zarska, M. Sramek, F. Novotny, F. Havel, A. Babelova, B. Mrazkova, O. Benada, M. Reinis, I. Stepanek, K. Hodny, Biological safety and tissue distribution of (16-mercaptohexadecyl) trimethylammonium bromide-modified cationic gold nanorods, *Biomaterials* 154 (2018) 275–290.
- [56] Q.M. Sun, X.L. Shi, J.T. Feng, Q. Zhang, Z. Ao, Y.L. Ji, X.C. Wu, D.S. Liu, D. Han, Cytotoxicity and cellular responses of gold nanorods to smooth muscle cells dependent on surface chemistry coupled action, *Small* 14 (52) (2018).
- [57] S. May, C. Hirsch, A. Rippl, N. Bohmer, J.P. Kaiser, L. Diener, A. Wichser, A. Bürkle, P. Wick, Transient DNA damage following exposure to gold nanoparticles, *Nanoscale* 10 (33) (2018) 15723–15735.
- [58] A.Q. Pan, M.L. Zhong, H. Wu, Y. Peng, H.S. Xia, Q.Y. Tang, Q.R. Huang, L. Wei, L. H. Xiao, C. Peng, Topical application of keratinocyte growth factor conjugated gold nanoparticles accelerate wound healing, *Nanomed. Nanotechnol.* 14 (5) (2018) 1619–1628.
- [59] P. Paul, S. Chatterjee, A. Pramanik, P. Karmakar, S.C. Bhattacharyya, G.S. Kumar, Thionine conjugated gold nanoparticles trigger apoptotic activity toward HepG2 cancer cell line, *ACS Biomater. Sci. Eng.* 4 (2) (2018) 635–646.
- [60] L. Ding, C.J. Yao, X.F. Yin, C.C. Li, Y.A. Huang, M. Wu, B. Wang, X.Y. Guo, Y. L. Wang, M.H. Wu, Size, shape, and protein corona determine cellular uptake and removal mechanisms of gold nanoparticles, *Small* 14 (42) (2018).
- [61] C. Lopez-Chaves, J. Soto-Alvaredo, M. Montes-Bayon, J. Bettmer, J. Llopis, C. Sanchez-Gonzalez, Gold nanoparticles: distribution, bioaccumulation and toxicity, In vitro and in vivo studies, *Nanomedicine* 14 (1) (2018) 1–12.
- [62] B. Yahyaei, M. Nouri, S. Bakherad, M. Hassani, P. Pourali, Effects of biologically produced gold nanoparticles: toxicity assessment in different rat organs after intraperitoneal injection, *AMB Express* 9 (1) (2019) 38.
- [63] Q.Y. Xia, J.X. Huang, Q.Y. Feng, X.M. Chen, X.Y. Liu, X.J. Li, T. Zhang, S.W. Xiao, H.X. Li, Z.H. Zhong, K. Xiao, Size- and cell type-dependent cellular uptake, cytotoxicity and in vivo distribution of gold nanoparticles, *Int. J. Nanomed.* 14 (2019) 6957–6970.
- [64] L.S. Gong, Y. Chen, K. He, J.B. Liu, Surface Coverage-Regulated cellular interaction of ultrasmall luminescent gold nanoparticles, *Acs Nano* 13 (2) (2019) 1893–1899.
- [65] A. Spinelli, M. Girelli, D. Arosio, L. Polito, P. Podini, G. Martino, P. Seneci, L. Muzio, A. Menegoni, Intracisternal delivery of PEG-coated gold nanoparticles results in high brain penetrance and long-lasting stability, *J. Nanobiotechnol.* 17 (2019).
- [66] X. Ma, J. Sun, L. Zhong, Y. Wang, Q. Huang, X. Liu, S. Jin, J. Zhang, X.J. Liang, Evaluation of Tuning-Sized gold nanoparticles on cellular adhesion by Golgi disruption in vitro and in vivo, *Nano Lett.* 19 (12) (2019) 8476–8487.
- [67] B. Kepstuli, V. Wycisk, K. Achazi, S. Kapishnikov, A.J. Pérez-Berná, P. Gutmann, A. Cossmer, E. Pereiro, H. Ewers, M. Ballauff, G. Schneider, J.G. McNally, *Cells*

- undergo major changes in the quantity of cytoplasmic organelles after uptake of gold nanoparticles with biologically relevant surface coatings, *ACS Nano* 14 (2) (2020) 2248–2264.
- [68] L. Roach, M.E. Booth, N. Ingram, D.A. Paterson, D.V.B. Batchelor, S.C. T. Moorcroft, R.J. Bushby, K. Critchley, P.L. Coletta, S.D. Evans, Evaluating Phospholipid-Functionalized gold nanorods for *in vivo* applications, *Small* 17 (13) (2021).
- [69] N. El-Baz, B.M. Nunn, P.J. Bates, M.G. O'Toole, The impact of PEGylation on cellular uptake and *in vivo* biodistribution of gold nanoparticle MRI contrast agents, *Bioengineering* 9 (12) (2022).
- [70] J.C. Henson, A. Brickell, J.W. Kim, H. Jensen, J.L. Mehta, M. Jensen, PEGylated gold nanoparticle toxicity in cardiomyocytes: assessment of size, concentration, and time dependency, *IEEE T Nanobiosci.* 21 (3) (2022) 387–394.
- [71] R.C. Mishra, R. Kalra, R. Dilawari, M. Goel, C.J. Barrow, Bio-Synthesis of mediated gold nanoparticle antimicrobial, antioxidant, antifungal and *in vitro* cytotoxicity studies, *Materials* 15 (11) (2022).
- [72] G. Devendrapandi, M.I. Sahay, D. Padmanaban, A. Panneerselvam, R. Palraj, R. Thanikasalam, S. Kuppan, V. Sadaiyandi, R. Balu, N. Rajendiran, Biogenic synthesis of gold nanoparticles using bael fruit juice and its efficacy against human A-549 lung cancer cell line, *Inorg. Chem. Commun.* 151 (2023).
- [73] E. Sadauskas, H. Wallin, M. Stoltzenberg, U. Vogel, P. Doering, A. Larsen, G. Danscher, Kupffer cells are central in the removal of nanoparticles from the organism, *Part Fibre Toxicol.* 4 (2007) 10.
- [74] W.S. Cho, M.J. Cho, J. Jeong, M. Choi, H.Y. Cho, B.S. Han, S.H. Kim, H.O. Kim, Y. T. Lim, B.H. Chung, J. Jeong, Acute toxicity and pharmacokinetics of 13 nm-sized PEG-coated gold nanoparticles, *Toxicol. Appl. Pharm.* 236 (1) (2009) 16–24.
- [75] F. Sousa, S. Mandal, C. Garrovo, A. Astolfo, A. Bonifacio, D. Latawiec, R.H. Menk, F. Arfelli, S. Huwel, G. Legname, H.J. Galla, S. Krol, Functionalized gold nanoparticles: a detailed *in vivo* multimodal microscopic brain distribution study, *Nanoscale* 2 (12) (2010) 2826–2834.
- [76] C. Lasagna-Reeves, D. Gonzalez-Romero, M.A. Barria, I. Olmedo, A. Clos, V.M. S. Ramanujam, A. Urayama, L. Vergara, M.J. Kogan, C. Soto, Bioaccumulation and toxicity of gold nanoparticles after repeated administration in mice, *Biochem. Biophys. Res. Co.* 393 (4) (2010) 649–655.
- [77] X.D. Zhang, H.Y. Wu, D. Wu, Y.Y. Wang, J.H. Chang, Z.B. Zhai, A.M. Meng, P. X. Liu, L.A. Zhang, F.Y. Fan, Toxicologic effects of gold nanoparticles *in vivo* by different administration routes, *Int. J. Nanomed.* 5 (2010) 771–781.
- [78] S.K. Balasubramanian, J. Jittiwat, M. Manikandan, C.N. Ong, L.E. Yu, W.Y. Ong, Biodistribution of gold nanoparticles and gene expression changes in the liver and spleen after intravenous administration in rats, *Biomaterials* 31 (8) (2010) 2034–2042.
- [79] X.D. Zhang, D. Wu, X. Shen, P.X. Liu, N. Yang, B. Zhao, H. Zhang, Y.M. Sun, L. A. Zhang, F.Y. Fan, Size-dependent *in vivo* toxicity of PEG-coated gold nanoparticles, *Int. J. Nanomed.* 6 (2011) 2071–2081.
- [80] N.J. Siddiqi, M.A.K. Abdelhalim, A.K. El-Ansary, A.S. Alhomida, W.Y. Ong, Identification of potential biomarkers of gold nanoparticle toxicity in rat brains, *J. Neuroinflamm.* 9 (2012).
- [81] M.A.K. Abdelhalim, B.M. Jarrar, Histological alterations in the liver of rats induced by different gold nanoparticle sizes, doses and exposure duration, *J. Nanobiotechnol.* 10 (2012).
- [82] C.A. Simpson, K.J. Salleng, D.E. Cliffel, D.L. Feldheim, In *vivo* toxicity, biodistribution, and clearance of glutathione-coated gold nanoparticles, *Nanomed. Nanotechnol.* 9 (2) (2013) 257–263.
- [83] S. Fraga, A. Brandao, M.E. Soares, T. Morais, J.A. Duarte, L. Pereira, L. Soares, C. Neves, E. Pereira, M.D. Bastos, H. Carmo, Short- and long-term distribution and toxicity of gold nanoparticles in the rat after a single-dose intravenous administration, *Nanomed. Nanotechnol.* 10 (8) (2014) 1757–1766.
- [84] H. Sela, H. Cohen, P. Elia, R. Zach, Z. Karpas, Y. Zeiri, Spontaneous penetration of gold nanoparticles through the blood brain barrier (BBB), *J. Nanobiotechnol.* 13 (2015).
- [85] S.G. Elci, Y. Jiang, B. Yan, S.T. Kim, K. Saha, D.F. Moyano, G.Y. Tonga, L. C. Jackson, V.M. Rotello, R.W. Vacher, Surface charge controls the suborgan biodistributions of gold nanoparticles, *ACS Nano* 10 (5) (2016) 5536–5542.
- [86] X. Li, B. Wang, S. Zhou, W. Chen, H.Q. Chen, S.S. Liang, L.N. Zheng, H.Y. Yu, R. X. Chu, M. Wang, Z.F. Chai, W.Y. Feng, Surface chemistry governs the sub-organ transfer, clearance and toxicity of functional gold nanoparticles in the liver and kidney, *J. Nanobiotechnol.* 18 (1) (2020).
- [87] J.F. Liao, T.R. Tian, S.R. Shi, X.P. Xie, S.L. Peng, Y. Zhu, J.G. Xiao, Y.F. Lin, Broadening the biocompatibility of gold nanorods from rat to: advancing clinical potential, *J. Nanobiotechnol.* 19 (1) (2021).
- [88] N.N. Mahmoud, A. Albasha, S. Hikmat, L. Hamadneh, R. Zaza, Z. Shraideh, E. A. Khalil, Nanoparticle size and chemical modification play a crucial role in the interaction of nano gold with the brain: extent of accumulation and toxicity, *Biomater. Sci.* 8 (6) (2020) 1669–1682.
- [89] D. Di Bella, J.P.S. Ferreira, R.D.O. Silva, C. Echem, A. Milan, E.H. Akamine, M. H. Carvalho, S.F. Rodrigues, Gold nanoparticles reduce inflammation in cerebral microvessels of mice with sepsis, *J. Nanobiotechnol.* 19 (1) (2021).
- [90] D.L. Windell, S. Mourabit, J. Moger, S.F. Owen, M.J. Winter, C.R. Tyler, The influence of size and surface chemistry on the bioavailability, tissue distribution and toxicity of gold nanoparticles in zebrafish, *EcoTox Environ. Safe* 260 (2023).
- [91] Y. Tang, X. Wang, J. Li, Y. Nie, G. Liao, Y. Yu, C. Li, Overcoming the reticuloendothelial system barrier to drug delivery with a “Don't-Eat-Us” strategy, *ACS Nano* 13 (11) (2019) 13015–13026.
- [92] R.L. Siegel, A.N. Giaquinto, A. Jemal, *Cancer statistics, 2024*, CA A Cancer J. Clin. 74 (1) (2024) 12–49.
- [93] K. Bromma, D.B. Chithrani, Advances in gold Nanoparticle-Based combined cancer therapy, *Nanomaterials* 10 (9) (2020).
- [94] G.P. Delaney, M.B. Barton, Evidence-based estimates of the demand for radiotherapy, *Clin. Oncol.* 27 (2) (2015) 70–76.
- [95] D. Hanahan, Robert A. Weinberg, Hallmarks of cancer: the next generation, *Cell* 144 (5) (2011) 646–674.
- [96] Y.-C. Yeh, B. Creran, V.M. Rotello, Gold nanoparticles: preparation, properties, and applications in bionanotechnology, *Nanoscale* 4 (6) (2012) 1871–1880.
- [97] P. Foroozandeh, A.A. Aziz, Insight into cellular uptake and intracellular trafficking of nanoparticles, *Nanoscale Res. Lett.* 13 (1) (2018) 339.
- [98] B.D. Chithrani, A.A. Ghazani, W.C.W. Chan, Determining the size and shape dependence of gold nanoparticle uptake into mammalian cells, *Nano Lett.* 6 (4) (2006) 662–668.
- [99] S. Nie, Understanding and overcoming major barriers in cancer nanomedicine, *Nanomedicine* 5 (4) (2010) 523–528.
- [100] M. Fan, Y. Han, S.T. Gao, H.Y. Yan, L.Z. Cao, Z.H. Li, X.J. Liang, J.C. Zhang, Ultrasmall gold nanoparticles in cancer diagnosis and therapy, *Theranostics* 10 (11) (2020) 4944–4957.
- [101] A. Kumar, X. Zhang, X.J. Liang, Gold nanoparticles: emerging paradigm for targeted drug delivery system, *Biotechnol. Adv.* 31 (5) (2013) 593–606.
- [102] S. Malik, M. Niaz, M. Khan, B. Rauff, S. Anwar, F. Amin, R. Hanif, Cytotoxicity study of gold nanoparticle synthesis using aloe vera, honey, and gymnosma sylvestre leaf extract, *ACS Omega* (2023).
- [103] B.X. Su, R.F. Wang, Z.X. Xie, H.T. Ruan, J.C. Li, C. Xie, W.Y. Lu, J. Wang, D. L. Wang, M. Liu, Effect of Retro-Inverso isomer of bradykinin on Size-Dependent penetration of Blood-Brain tumor barrier, *Small* 14 (7) (2018).
- [104] S. Aryal, J.J. Grailler, S. Pilla, D.A. Steeber, S.Q. Gong, Doxorubicin conjugated gold nanoparticles as water-soluble and pH-responsive anticancer drug nanocarriers, *J. Mater. Chem.* 19 (42) (2009) 7879–7884.
- [105] T. Cui, J.J. Liang, H. Chen, D.D. Geng, L. Jiao, J.Y. Yang, H. Qian, C. Zhang, Y. Ding, Performance of Doxorubicin-Conjugated gold nanoparticles: regulation of drug location, *ACS Appl. Mater. Inter.* 9 (10) (2017) 8569–8580.
- [106] Y.L. Du, L. Xia, A. Jo, R.M. Davis, P. Bissel, M.F. Ehrlich, D.G.I. Kingston, Synthesis and evaluation of Doxorubicin-Loaded gold nanoparticles for Tumor-Targeted drug delivery, *Bioconjugate Chem.* 29 (2) (2018) 420–430.
- [107] T.M. Sun, Y.C. Wang, F. Wang, J.Z. Du, C.Q. Mao, C.Y. Sun, R.Z. Tang, Y. Liu, J. Zhu, Y.H. Zhu, X.Z. Yang, J. Wang, Cancer stem cell therapy using doxorubicin conjugated to gold nanoparticles via hydrazone bonds, *Biomaterials* 35 (2) (2014) 836–845.
- [108] D.Y. Wu, H.S. Wang, X.S. Hou, H. Chen, Y. Ma, Y.L. Hou, J. Hong, Y. Ding, Effects of gold core size on regulating the performance of doxorubicin-conjugated gold nanoparticles, *Nano Res.* 11 (6) (2018) 3396–3410.
- [109] G.V. Khutale, A. Casey, Synthesis and characterization of a multifunctional gold-doxorubicin nanoparticle system for ph triggered intracellular anticancer drug release, *Eur. J. Pharm. Biopharm.* 119 (2017) 372–380.
- [110] S.B. Ruan, M.Q. Yuan, L. Zhang, G.L. Hu, J.T. Chen, X.L. Cun, Q.Y. Zhang, Y. T. Yang, Q. He, H.L. Gao, Tumor microenvironment sensitive doxorubicin delivery and release to glioma using angiopep-2 decorated gold nanoparticles, *Biomaterials* 37 (2015) 425–435.
- [111] C.S. Lee, H. Kim, J. Yu, S.H. Yu, S. Ban, S. Oh, D. Jeong, J. Im, M.J. Baek, T. H. Kim, Doxorubicin-loaded oligonucleotide conjugated gold nanoparticles: a promising drug delivery system for colorectal cancer therapy, *Eur. J. Med Chem.* 142 (2017) 416–423.
- [112] K. Kalimuthu, B.C. Lubin, A. Bazylevich, G. Gellerman, O. Shpilberg, G. Luboshits, M.A. Firer, Gold nanoparticles stabilize peptide-drug-conjugates for sustained targeted drug delivery to cancer cells, *J. Nanobiotechnol.* 16 (2018).
- [113] Z.G. Wang, J.Y. Dong, Q.J.J. Zhao, Y. Ying, L.J. Zhang, J.R. Zou, S.Q. Zhao, J. J. Wang, Y. Zhao, S.S. Jiang, Gold nanoparticle-mediated delivery of paclitaxel and nucleic acids for cancer therapy, *Mol. Med. Rep.* 22 (6) (2020) 4475–4484.
- [114] A.M. Sofias, M. Dunne, G. Storm, C. Allen, The battle of “nano” paclitaxel, *Adv. Drug Deliv. Rev.* 122 (2017) 20–30.
- [115] F. Li, X.F. Zhou, H.Y. Zhou, J.B. Jia, L.W. Li, S.M. Zhai, B. Yan, Reducing both pgp overexpression and drug efflux with Anti-Cancer Gold-Paclitaxel nanoconjugates, *Plos One* 11 (7) (2016).
- [116] S.K. Vemuri, R.R. Banala, S. Mukherjee, P. Uppula, G.P.V. Subbaiah, A.V. G. Reddy, T. Malarvilli, Novel biosynthesized gold nanoparticles as anti-cancer agents against breast cancer: synthesis, biological evaluation, molecular modelling studies, *Mat. Sci. Eng. C. Mater.* 99 (2019) 417–429.
- [117] P. Manivasagan, S. Bharathiraja, N.Q. Bui, I.G. Lim, J. Oh, Paclitaxel-loaded chitosan oligosaccharide-stabilized gold nanoparticles as novel agents for drug delivery and photoacoustic imaging of cancer cells, *Int. J. Pharm.* 511 (1) (2016) 367–379.
- [118] D.N. Heo, D.H. Yang, H.J. Moon, J.B. Lee, M.S. Bae, S.C. Lee, W.J. Lee, I.C. Sun, I. K. Kwon, Gold nanoparticles surface-functionalized with paclitaxel drug and biotin receptor as theranostic agents for cancer therapy, *Biomaterials* 33 (3) (2012) 856–866.
- [119] Y. Ding, Y.Y. Zhou, H. Chen, D.D. Geng, D.Y. Wu, J. Hong, W.B. Shen, T.J. Hang, C. Zhang, The performance of thiol-terminated PEG-paclitaxel-conjugated gold nanoparticles, *Biomaterials* 34 (38) (2013) 10217–10227.
- [120] B. Ren, Z.C. Cai, X.J. Zhao, L.S. Li, M.X. Zhao, Evaluation of the biological activity of folic Acid-Modified Paclitaxel-Loaded gold nanoparticles, *Int. J. Nanomed.* 16 (2021) 7023–7033.
- [121] H.S. Wang, L. Wang, Y.Y. Gao, Y. Ding, The effect of drug position on the properties of paclitaxel-conjugated gold nanoparticles for liver tumor treatment, *Chin. Chem. Lett.* 32 (3) (2021) 1041–1045.

- [122] T. Sharma, D. Singh, A. Mahapatra, P. Mohapatra, S. Sahoo, S.K. Sahoo, Advancements in clinical translation of flavonoid nanoparticles for cancer treatment, *OpenNano* 8 (2022) 100074.
- [123] R. Shukla, N. Chanda, A. Zambre, A. Upendran, K. Katti, R.R. Kulkarni, S.K. Nune, S.W. Casteel, C.J. Smith, J. Vimal, E. Boote, J.D. Robertson, P. Kan, H. Engelbrecht, L.D. Watkinson, T.L. Carmack, J.R. Lever, C.S. Cutler, C. Caldwell, R. Kannan, K.V. Katti, Laminin receptor specific therapeutic gold nanoparticles (AuNP-EGCG) show efficacy in treating prostate cancer, *P Natl. Acad. Sci. USA* 109 (31) (2012) 12426–12431.
- [124] C.C. Chen, D.S. Hsieh, K.J. Huang, Y.L. Chan, P.D. Hong, M.K. Yeh, C.J. Wu, Improving anticancer efficacy of (-)-epigallocatechin-3-gallate gold nanoparticles in murine B16F10 melanoma cells, *Drug Des. Devel Ther.* 8 (2014) 459–474.
- [125] M.A. Safwat, B.A. Kandil, M.A. Elblibesy, G.M. Soliman, N.E. Eleraky, Epigallocatechin-3-Gallate-Loaded gold nanoparticles: preparation and evaluation of anticancer efficacy in ehrlich Tumor-Bearing mice, *Pharmaceutics* 13 (9) (2020) 254.
- [126] A.V. Anand David, R. Arulmoli, S. Parasuraman, Overviews of biological importance of quercetin: a bioactive flavonoid, *Pharm. Rev.* 10 (20) (2016) 84–89.
- [127] D. Xu, M.J. Hu, Y.Q. Wang, Y.L. Cui, Antioxidant activities of quercetin and its complexes for medicinal application, *Molecules* 24 (6) (2019).
- [128] I. Ozcicek, G. Baydas, U.C. Erim, U.V. Ustundag, Quercetin/polyethyleneimine modified gold nanoconjugates inhibit apoptosis and ROS production induced by hydrogen peroxide in DRG sensory neurons, *J. Pharm. Sci.* (2024).
- [129] E. Naderi, M. Aghajanzadeh, M. Zamani, A. Hashiri, A. Sharifi, A. Kamalianfar, M. Naseri, H. Danafar, Improving the anti-cancer activity of quercetin-loaded AgFeO₂ through UV irradiation: synthesis, characterization, and *in vivo* and *in vitro* biocompatibility study, *J. Drug Deliv. Sci. Technol.* 57 (2020) 101645.
- [130] C.-I. Luo, Y.-q. Liu, P. Wang, C.-h Song, K.-j Wang, L.-p Dai, J.-y Zhang, H. Ye, The effect of quercetin nanoparticle on cervical cancer progression by inducing apoptosis, autophagy and anti-proliferation via JAK2 suppression, *Biomed. Pharmacother.* 82 (2016) 595–605.
- [131] S. Balakrishnan, F.A. Bhat, P. Raja Singh, S. Mukherjee, P. Elumalai, S. Das, C. R. Patra, J. Arunakaran, Gold nanoparticle-conjugated quercetin inhibits epithelial-mesenchymal transition, angiogenesis and invasiveness via EGFR/VEGFR-2-mediated pathway in breast cancer, *Cell Prolif.* 49 (6) (2016) 678–697.
- [132] K.-W. Ren, Y.-H. Li, G. Wu, J.-Z. Ren, H.-B. Lu, Z.-M. Li, X.-W. Han, Quercetin nanoparticles display antitumor activity via proliferation inhibition and apoptosis induction in liver cancer cells, *Int J. Oncol.* 50 (4) (2017) 1299–1311.
- [133] M. Yilmaz, A.A. Karanastasis, M.V. Chatzianasiadou, M. Oguz, A. Kougioumtzi, N. Clemente, T.F. Kellie, N.E. Zafeiropoulos, A. Avgeropoulos, T. Mavromoustakos, U. Dianzani, S. Karakurt, A.G. Tzakos, Inclusion of quercetin in gold nanoparticles decorated with supramolecular hosts amplifies its tumor targeting properties, *ACS Appl. Biol. Mater.* 2 (7) (2019) 2715–2725.
- [134] A. Mahmoudi, P. Keshwani, M. Majeed, Y. Teng, A. Sahebkar, Recent advances in nanogold as a promising nanocarrier for curcumin delivery, *Colloid Surf. B* 215 (2022).
- [135] S. Nambiar, E. Osei, A. Fleck, J. Darko, A.J. Mutsaers, S. Wettig, Synthesis of curcumin-functionalized gold nanoparticles and cytotoxicity studies in human prostate cancer cell line, *Appl. Nanosci.* 8 (3) (2018) 347–357.
- [136] A. Akbari, Z. Shokati Eshkiki, S. Mayahi, S.M. Amini, In-vitro investigation of curcumin coated gold nanoparticles effect on human colorectal adenocarcinoma cell line, *Nanomed. Res.* J. 7 (1) (2022) 66–72.
- [137] N.S. Elbialy, E.A. Abdelfatah, W.A. Khalil, Antitumor activity of Curcumin-Green synthesized gold nanoparticles: *in vitro* study, *Bionanoscience* 9 (4) (2019) 813–820.
- [138] S. Manju, K. Sreenivasan, Gold nanoparticles generated and stabilized by water soluble curcumin-polymer conjugate: blood compatibility evaluation and targeted drug delivery onto cancer cells, *J. Colloid Interface Sci.* 368 (1) (2012) 144–151.
- [139] C. Seelakshmi, N. Goel, K.K.R. Datta, A. Addlagatta, R. Ummanni, B.V.S. Reddy, Green synthesis of curcumin capped gold nanoparticles and evaluation of their cytotoxicity, *Nanosci. Nanotechnol. Lett.* 5 (12) (2013) 1258–1265.
- [140] S.P. Singh, S.B. Alvi, D.B. Pemmaraju, A.D. Singh, S.V. Manda, R. Srivastava, A. K. Rengan, NIR triggered liposome gold nanoparticles entrapping curcumin as *in situ* adjuvant for photothermal treatment of skin cancer, *Int. J. Biol. Macromol.* 110 (2018) 375–382.
- [141] C. Fu, C. Ding, X. Sun, A. Fu, Curcumin nanocapsules stabilized by bovine serum albumin-capped gold nanoclusters (BSA-AuNCs) for drug delivery and theranosis, *Materials Science Engineering C* 87 (2018) 149–154.
- [142] H. Danafar, A. Sharafi, S. Askarloo, H.K. Manjili, Preparation and characterization of PEGylated iron Oxide-Gold nanoparticles for delivery of sulforaphane and curcumin, *Drug Res. (Stuttg.)* 67 (12) (2017) 698–704.
- [143] M.N. Owaid, M.A. Rabeea, A. Abdul Aziz, M.S. Jameel, M.A. Dheyab, Mycogenic fabrication of silver nanoparticles using picoa, pezizales, characterization and their antifungal activity, *Environ. Nanotechnol. Monit. Manag.* 17 (2022) 100612.
- [144] M.S. Jameel, A.A. Aziz, M.A. Dheyab, P.M. Khaniabadi, A.A. Kareem, M. Alosan, A.T. Ali, M.A. Rabeea, B. Mehrdel, Mycosynthesis of ultrasonically-assisted uniform cubic silver nanoparticles by isolated phenols from agaricus bisporus and its antibacterial activity, *Surf. Interfaces* 29 (2022).
- [145] M.S. Jameel, A.A. Aziz, M.A. Dheyab, Impacts of various solvents in ultrasonic irradiation and Green synthesis of platinum nanoparticle, *Inorg. Chem. Commun.* 128 (2021).
- [146] M.A. Dheyab, N. Oladzadabbasabadi, A.A. Aziz, P.M. Khaniabadi, M.T.S. Al-ouqaili, M.S. Jameel, F.S. Braim, B. Mehrdel, M. Ghasemlou, Recent advances of plant-mediated metal nanoparticles: synthesis, properties, and emerging applications for wastewater treatment, *J. Environ. Chem. Eng.* 12 (2) (2024).
- [147] M.A. Rabeea, G.A. Naeem, M.N. Owaid, A.A. Aziz, M.S. Jameel, M.A. Dheyab, R. F. Muslim, L.F. Jameel, Phytosynthesis of prosopis farcta fruit-gold nanoparticles using infrared and thermal devices and their catalytic efficacy, *Inorg. Chem. Commun.* 133 (2021).
- [148] S.S. Al-Mafarjy, N. Suardi, N.M. Ahmed, D. Kernain, H.H. Alkatib, M.A. Dheyab, Green synthesis of gold nanoparticles from coelus scutellaroides (L.) benth leaves and assessment of anticancer and antioxidant properties, *Inorg. Chem. Commun.* 161 (2024).
- [149] M.A. Dheyab, A.A. Aziz, S.S. Al-Mafarjy, N. Suardi, N.N.A.N.A. Razak, A. Ramizy, M.S. Jameel, Exploring the anticancer potential of biogenic inorganic gold nanoparticles synthesized via mushroom-assisted Green route, *Inorg. Chem. Commun.* 157 (2023) 111363.
- [150] A. Jakhmola, T.K. Hornsby, F.M. Kashkooli, M.C. Kolios, K. Rod, J.J. Tavakkoli, Green synthesis of anti-cancer drug-loaded gold nanoparticles for low-intensity pulsed ultrasound targeted drug release, *Drug Deliv. Transl. Res* 14 (9) (2024) 2417–2432.
- [151] S. Donga, G.R. Bhadu, S. Chanda, Antimicrobial, antioxidant and anticancer activities of gold nanoparticles Green synthesized using mangifera indica seed aqueous extract, *Artif. Cells Nanomed. Biotechnol.* 48 (1) (2020) 1315–1325.
- [152] N.S. Elbialy, E.A. Abdelfatah, W.A. Khalil, Antitumor activity of Curcumin-Green synthesized gold nanoparticles: *in vitro* study, *BioNanoScience* 9 (4) (2019) 813–820.
- [153] W. Zhao, J. Li, C. Zhong, X.Y. Zhang, Y.X. Bao, Green synthesis of gold nanoparticles from dendrobium officinale and its anticancer effect on liver cancer, *Drug Deliv.* 28 (1) (2021) 985–994.
- [154] P. Clarance, B. Luvankar, J. Sales, A. Khusro, P. Agastian, J.C. Tack, M.M. Al Khulaifi, H.A. Al-Shwaiman, A.M. Elgorban, A. Syed, H.J. Kim, Green synthesis and characterization of gold nanoparticles using endophytic fungi fusarium solani and its *in-vitro* anticancer and biomedical applications, *Saudi J. Biol. Sci.* 27 (2) (2020) 706–712.
- [155] V. Sunderam, D. Thiagarajan, A.V. Lawrence, S.S.S. Mohammed, A. Selvaraj, *In-vitro antimicrobial and anticancer properties of Green synthesized gold nanoparticles using anacardium occidentale leaves extract*, *Saudi J. Biol. Sci.* 26 (3) (2019) 455–459.
- [156] A.S.C. Gonçalves, C.F. Rodrigues, A.F. Moreira, I.J. Correia, Strategies to improve the photothermal capacity of gold-based nanomedicines, *Acta Biomater.* 116 (2020) 105–137.
- [157] W. Fan, B. Yung, P. Huang, X. Chen, Nanotechnology for multimodal synergistic cancer therapy, *Chem. Rev.* 117 (22) (2017) 13566–13638.
- [158] Z. Bao, X. Liu, Y. Liu, H. Liu, K. Zhao, Near-infrared light-responsive inorganic nanomaterials for photothermal therapy, *Asian J. Pharm. Sci.* 11 (3) (2016) 349–364.
- [159] M.A. Mackey, M.R.K. Ali, L.A. Austin, R.D. Near, M.A. El-Sayed, The most effective gold nanorod size for plasmonic photothermal therapy: theory and *in vitro* experiments, *J. Phys. Chem. B* 118 (5) (2014) 1319–1326.
- [160] M.A. Alebrahim, A.A. Ahmad, A.B. Migdadi, Q.M. Al-Bataineh, Localize surface plasmon resonance of gold nanoparticles and their effect on the polyethylene oxide nanocomposite films, *Physica B Condensed Matter* 679 (2024) 415805.
- [161] C. Loo, A. Lin, L. Hirsch, M.-H. Lee, J. Barton, N. Halas, J. West, R. Drezek, Nanoshell-Enabled Photonics-Based imaging and therapy of cancer, *Technol. Cancer Res. Treat.* 3 (1) (2004) 33–40.
- [162] J. Yang, D. Shen, L. Zhou, W. Li, X. Li, C. Yao, R. Wang, A.M. El-Toni, F. Zhang, D. Zhao, Spatially confined fabrication of Core-Shell gold Nanocages@ Mesoporous silica for Near-Infrared controlled photothermal drug release, *Chem. Mater.* 25 (15) (2013) 3030–3037.
- [163] A. Espinosa, A.K.A. Silva, A. Sánchez-Iglesias, M. Grzelczak, C. Péchoux, K. Desboeufs, L.M. Liz-Marzán, C. Wilhelms, Cancer cell internalization of gold nanostars impacts their photothermal efficiency *in vitro* and *in vivo*: toward a plasmonic thermal fingerprint in tumoral environment, *Adv. Healthc. Mater.* 5 (9) (2016) 1040–1048.
- [164] A.F. Moreira, C.F. Rodrigues, C.A. Reis, E.C. Costa, P. Ferreira, I.J. Correia, Development of poly-2-ethyl-2-oxazoline coated gold-core silica shell nanorods for cancer chemo-photothermal therapy, *Nanomedicine* 13 (20) (2018) 2611–2627.
- [165] D. de Melo-Diogo, R. Lima-Sousa, C.G. Alves, I.J. Correia, Graphene family nanomaterials for application in cancer combination photothermal therapy, *Biomater. Sci.* 7 (9) (2019) 3534–3551.
- [166] T.T. Zhang, Y.P. Li, W.Y. Hong, Z.Y. Chen, P. Peng, S.L. Yuan, J.Y. Qu, M. Xiao, L. Xu, Glucose oxidase and polydopamine functionalized iron oxide nanoparticles: combination of the photothermal effect and reactive oxygen species generation for dual- modality selective cancer therapy, *J. Mater. Chem. B* 7 (13) (2019) 2190–2200.
- [167] R.S. Riley, E.S. Day, Gold nanoparticle-mediated photothermal therapy: applications and opportunities for multimodal cancer treatment, *Wires Nanomed. Nanobi* 9 (4) (2017).
- [168] A.J. Gormley, K. Greish, A. Ray, R. Robinson, J.A. Gustafson, H. Ghandehari, Gold nanorod mediated plasmonic photothermal therapy: a tool to enhance macromolecular delivery, *Int J. Pharm.* 415 (1-2) (2011) 315–318.
- [169] W. Tao, X. Cheng, D. Sun, Y. Guo, N. Wang, J. Ruan, Y. Hu, M. Zhao, T. Zhao, H. Feng, L. Fan, C. Lu, Y. Ma, J. Duan, M. Zhao, Synthesis of multi-branched au nanocomposites with distinct plasmon resonance in NIR-II window and controlled CRISPR-Cas9 delivery for synergistic gene-photothermal therapy, *Biomaterials* 287 (2022) 121621.

- [170] M.A. Dheyab, J.H. Tang, A.A. Aziz, S.H. Nowfal, M.S. Jameel, M. Alrosan, N. Oladzadabbasabadi, M. Ghasemlou, Green synthesis of gold nanoparticles and their emerging applications in cancer imaging and therapy: a review, *Rev. Inorg. Chem.* (2024).
- [171] M.A. Dheyab, A.A. Aziz, S.H. Nowfal, S.S. Al-Mafarjy, W. Abdulla, N. Suardi, M. S. Jameel, F.S. Braim, M. Alrosan, P.M. Khaniabadi, Turning food waste-derived ultrasmall gold nanoparticles as a photothermal agent for breast cancer cell eradication, *Inorg. Chem. Commun.* 169 (2024).
- [172] S.M. Amini, E. Mohammadi, S. Askarian-Amiri, Y. Azizi, A. Shakeri-Zadeh, A. Neshastehriz, Investigating the *in vitro* photothermal effect of Green synthesized apigenin-coated gold nanoparticle on colorectal carcinoma, *IET Nanobiotechnol.* 15 (3) (2021) 329–337.
- [173] L. Shabani, S.R. Kasaei, S. Chelliapan, M. Abbasi, H. Khajehzadeh, F.S. Dehghani, T. Firuzyan, M. Shafiee, A.M. Amani, S. Mosleh-Shirazi, A. Vaez, H. Kamyab, An investigation into Green synthesis of ru template gold nanoparticles and the *in vitro* photothermal effect on the MCF-7 human breast cancer cell line, *Appl. Phys. A* 129 (8) (2023) 564.
- [174] Y. Wang, J. Chen, Y. Bo, J. Chen, Y. Liu, Z. Li, C. Yu, J. Liu, S. Wang, Green synthesis of au nanoparticles by scutellaria barbata extract for chemo-photothermal anticancer therapy, *Pharmacol. Res. Mod. Chin. Med.* 13 (2024) 100536.
- [175] A.A. Vodyashkin, M.G.H. Rizk, P. Kezimana, A.A. Kirichuk, Y.M. Stanishevskiy, Application of gold Nanoparticle-Based materials in cancer therapy and diagnostics, *Chemenginering* 5 (4) (2021).
- [176] G.C. Yang, Z.M. Liu, Y. Li, Y.Q. Hou, X.X. Fei, C.K. Su, S.M. Wang, Z.F. Zhuang, Z. Y. Guo, Facile synthesis of black phosphorus-Au nanocomposites for enhanced photothermal cancer therapy and surface-enhanced Raman scattering analysis, *Biomater. Sci.* 11 (5) (2017) 2048–2055.
- [177] W.J. Chen, J. Wang, W.X. Du, J.W. Wang, L. Cheng, Z.Q. Ge, S.L. Qiu, W.W. Pan, L. Song, X.P. Ma, Y. Hu, Black phosphorus nanosheets integrated with gold nanoparticles and polypyrrole for synergistic sonodynamic and photothermal cancer therapy, *ACS Appl. Nano Mater.* 4 (8) (2021) 7963–7973.
- [178] C.C. Jia, F. Zhang, J.M. Lin, L.W. Feng, T.T. Wang, Y. Feng, F. Yuan, Y. Mai, X. W. Zeng, Q. Zhang, Black phosphorus-Au-thiosugar nanosheets mediated photothermal induced anti-tumor effect enhancement by promoting infiltration of NK cells in hepatocellular carcinoma, *J. Nanobiotechnol.* 20 (1) (2022).
- [179] M.A. Dheyab, A.A. Aziz, M.S. Jameel, P.M. Khaniabadi, B. Mehrdel, M. Khaniabadi, Gold-coated iron oxide nanoparticles as a potential photothermal therapy agent to enhance eradication of breast cancer cells, *J. Phys. Conf. Ser.* 1497 (2020).
- [180] E. Nassircslami, M. Ajdarzade, Gold coated superparamagnetic iron oxide nanoparticles as effective nanoparticles to eradicate breast cancer cells via photothermal therapy, *Adv. Pharm. Bull.* 8 (2) (2018) 201–209.
- [181] J. Beik, M. Asadi, S. Khoei, S. Laurent, Z. Abed, M. Mirrahimi, A. Farashahi, R. Haschemian, H. Ghaznavi, A. Shakeri-Zadeh, Simulation-guided photothermal therapy using MRI-traceable iron oxide-gold nanoparticle, *J. Photochem. Photobio. B* 199 (2019) 111599.
- [182] Z. Abed, J. Beik, S. Laurent, N. Eslahi, T. Khani, E.S. Davani, H. Ghaznavi, A. Shakeri-Zadeh, Iron oxide-gold core-shell nano-theranostic for magnetically targeted photothermal therapy under magnetic resonance imaging guidance, *J. Cancer Res. Clin.* 145 (5) (2019) 1213–1219.
- [183] C. Caro, F. Gamez, P. Quaresma, J.M. Paez-Muñoz, A. Domínguez, J.R. Pearson, M.P. Leal, A.M. Beltran, Y. Fernandez-Afonso, J.M. de la Fuente, R. Franco, E. Pereira, M.L. García-Martín, Fe3O4-Au Core-Shell nanoparticles as a multimodal platform for *in vivo* imaging and focused photothermal therapy, *Pharmaceutics* 13 (3) (2021).
- [184] B. Muzzi, M. Albino, A. Gabbani, A. Omelyanchik, E. Kozenkova, M. Petrecca, C. Innocenti, E. Balica, A. Lavacchi, F. Scavone, C. Anceschi, G. Petrucci, A. Ibarra, A. Laurenzana, F. Pineider, V. Rodionova, C. Sangregorio, Star-Shaped Magnetic-Plasmonic Au@Fe3O4 Nano-Heterostructures for photothermal therapy, *ACS Appl. Mater. Inter.* 14 (25) (2022) 29087–29098.
- [185] M.A. Dheyab, A.A. Aziz, M.S. Jameel, Synthesis and optimization of the sonochemical method for functionalizing gold shell on Fe3O4 core nanoparticles using response surface methodology, *Surf. Interfaces* 21 (2020) 100647.
- [186] M.A. Dheyab, A.A. Aziz, M.S. Jameel, P.M. Khaniabadi, Recent advances in synthesis, medical applications and challenges for Gold-Coated iron oxide: comprehensive study, *Nanomaterials* 11 (8) (2021).
- [187] M.A. Dheyab, A.A. Aziz, P.M. Khaniabadi, M.S. Jameel, Potential of a sonochemical approach to generate MRI-PPT theranostic agents for breast cancer, *Photo. Photo. 33* (2021).
- [188] M. Farokhnezhad, M. Esmaeilzadeh, Graphene coated gold nanoparticles: an emerging class of nanoagents for photothermal therapy applications, *Phys. Chem. Chem. Phys.* 21 (33) (2019) 18352–18362.
- [189] A.F. Zedan, S. Moussa, J. Terner, G. Atkinson, M.S. El-Shall, Ultrasmall gold nanoparticles anchored to graphene and enhanced photothermal effects by laser irradiation of gold nanostructures in graphene oxide solutions, *ACS Nano* 7 (1) (2013) 627–636.
- [190] F. Vischio, L. Carrieri, G.V. Bianco, F. Petronella, N. Depalo, E. Fanizza, M. P. Scavo, L. De Sio, A. Calogero, M. Striccoli, A. Agostiano, G. Giannelli, M. L. Curri, C. Ingrosso, Au nanoparticles decorated nanographene oxide-based platform: synthesis, functionalization and assessment of photothermal activity (vol 145, 213272, 2023), *Biomater. Adv.* 157 (2024).
- [191] U. Dembereldorj, S.Y. Choi, E.O. Ganbold, N.W. Song, D. Kim, J. Choo, S.Y. Lee, S. Kim, S.W. Joo, Gold nanorod-assembled PEGylated graphene-oxide nanocomposites for photothermal cancer therapy, *Photochem. Photobio.* 90 (3) (2014) 659–666.
- [192] L.Y. Yang, Y.T. Tseng, G.L. Suo, L.L. Chen, J.T. Yu, W.J. Chiu, C.C. Huang, C. H. Lin, Photothermal therapeutic response of cancer cells to Aptamer-Gold Nanoparticle-Hybridized graphene oxide under NIR illumination, *ACS Appl. Mater. Inter.* 7 (9) (2015) 5097–5106.
- [193] S. Gao, L.W. Zhang, G.H. Wang, K. Yang, M.L. Chen, R. Tian, Q.J. Ma, L. Zhu, Hybrid graphene/au activatable theranostic agent for multimodalities imaging guided enhanced photothermal therapy, *Biomaterials* 79 (2016) 36–45.
- [194] B.M. Sun, J.R. Wu, S.B. Cui, H.H. Zhu, W. An, Q.G. Fu, C.W. Shao, A.H. Yao, B. D. Chen, D.L. Shi, Synthesis of graphene oxide/gold nanorods theranostic hybrids for efficient tumor computed tomography imaging and photothermal therapy, *Nano Res.* 10 (1) (2017) 37–48.
- [195] R. Huang, Y.W. Shen, Y.Y. Guan, Y.X. Jiang, Y. Wu, K. Rahman, L.J. Zhang, H. J. Liu, X. Luan, Mesoporous silica nanoparticles: facile surface functionalization and versatile biomedical applications in oncology, *Acta Biomater.* 116 (2020) 1–15.
- [196] C. Bharti, U. Nagaich, A.K. Pal, N. Gulati, Mesoporous silica nanoparticles in target drug delivery system: a review, *Int J. Pharm. Invest.* 5 (3) (2015) 124–133.
- [197] J.C. Love, L.A. Estroff, J.K. Kriebel, R.G. Nuzzo, G.M. Whitesides, Self-assembled monolayers of thiophates on metals as a form of nanotechnology, *Chem. Rev.* 105 (4) (2005) 1103–1169.
- [198] S. Liang, Y. Zhao, S.P. Xu, X. Wu, J. Chen, M. Wu, J.X. Zhao, A Silica-Gold-Silica nanocomposite for photothermal therapy in the Near-Infrared region, *ACS Appl. Mater. Inter.* 7 (1) (2015) 85–93.
- [199] Y. Liu, M. Xu, Q. Chen, G. Guan, W. Hu, X. Zhao, M. Qiao, H. Hu, Y. Liang, H. Zhu, D. Chen, Gold nanorods/mesoporous silica-based nanocomposite as theranostic agents for targeting near-infrared imaging and photothermal therapy induced with laser, *Int J. Nanomed.* 10 (2015) 4747–4761.
- [200] Y. Yang, Y.Z. Lin, D.H. Di, X. Zhang, D. Wang, Q.F. Zhao, S.L. Wang, Gold nanoparticle-gated mesoporous silica as redox-triggered drug delivery for chemo-photothermal synergistic therapy, *J. Colloid Inter. Sci.* 508 (2017) 323–331.
- [201] C. Ong, B.G. Cha, J. Kim, Mesoporous silica nanoparticles doped with gold nanoparticles for combined cancer immunotherapy and photothermal therapy, *ACS Appl. Bio. Mater.* 2 (8) (2019) 3630–3638.
- [202] R. Riedel, N. Mahr, C.Y. Yao, A.G. Wu, F. Yang, N. Hampp, Synthesis of gold-silica core-shell nanoparticles by pulsed laser ablation in liquid and their physico-chemical properties towards photothermal cancer therapy, *Nanoscale* 12 (5) (2020) 3007–3018.
- [203] J.H. Park, H.S. Choe, S.W. Kim, G.B. Im, S.H. Um, J.H. Kim, S.H. Bhang, Silica-Capped and Gold-Decorated silica nanoparticles for enhancing effect of gold Nanoparticle-Based photothermal therapy, *Tissue Eng. Regen. Med.* 19 (6) (2022) 1161–1168.
- [204] M. Deinavizadeh, A.R. Kiasat, M. Shafiei, M. Sabaeian, R. Mirzajani, S.M. Zahraei, F. Khalili, M.M. Shao, A.M. Wu, P. Makvandi, N. Hooshmand, Synergistic chemo-photothermal therapy using gold nanorods supported on thiol-functionalized mesoporous silica for lung cancer treatment, *Sci. Rep.* 14 (1) (2024).
- [205] S.J. Amina, B. Guo, A review on the synthesis and functionalization of gold nanoparticles as a drug delivery vehicle, *Int J. Nanomed.* 15 (2020) 9823–9857.
- [206] F.Y. Kong, J.W. Zhang, R.F. Li, Z.X. Wang, W.J. Wang, W. Wang, Unique roles of gold nanoparticles in drug delivery, targeting and imaging applications, *Molecules* 22 (9) (2017).
- [207] S. Siddique, J.C.L. Chow, Gold nanoparticles for drug delivery and cancer therapy, *Appl. Sci.* 10 (11) (2020) 3824.
- [208] P. Ghosh, G. Han, M. De, C.K. Kim, V.M. Rotello, Gold nanoparticles in delivery applications, *Adv. Drug Deliv. Rev.* 60 (11) (2008) 1307–1315.
- [209] J.K. Patra, G. Das, L.F. Fraceto, E.V.R. Campos, M.D.P. Rodriguez-Torres, L. S. Acosta-Torres, L.A. Diaz-Torres, R. Grillo, M.K. Swamy, S. Sharma, S. Habtemariam, H.-S. Shin, Nano based drug delivery systems: recent developments and future prospects, *J. Nanobiotechnol.* 16 (1) (2018) 71.
- [210] B. Saha, J. Bhattacharya, A. Mukherjee, A.K. Ghosh, C.R. Santra, A.K. Dasgupta, P. Karmakar, In vitro structural and functional evaluation of gold nanoparticles conjugated antibiotics, *Nanoscale Res. Lett.* 2 (12) (2007) 614–622.
- [211] D. Shenoy, W. Fu, J. Li, C. Crasto, G. Jones, C. DiMarzio, S. Sridhar, M. Amiji, Surface functionalization of gold nanoparticles using hetero-bifunctional poly (ethylene glycol) spacer for intracellular tracking and delivery, *Int. J. Nanomed.* 1 (1) (2006) 51–57.
- [212] T. Niidome, M. Yamagata, Y. Okamoto, Y. Akiyama, H. Takahashi, T. Kawano, Y. Katayama, Y. Niidome, PEG-modified gold nanorods with a stealth character for applications, *J. Control Release* 114 (3) (2006) 343–347.
- [213] H.T. Ding, P. Tan, S.Q. Fu, X.H. Tian, H. Zhang, X.L. Ma, Z.W. Gu, K. Luo, Preparation and application of pH-responsive drug delivery systems, *J. Control Release* 348 (2022) 206–238.
- [214] M.R. Asgharzadeh, J. Barar, M.M. Pourseif, M. Eskandani, M.J. Niya, M. R. Mashayekhi, Y. Omidi, Molecular machineries of ph dysregulation in tumor microenvironment: potential targets for cancer therapy, *Bioimpacts* 7 (2) (2017) 115–133.
- [215] R. de la Rica, D. Aili, M.M. Stevens, Enzyme-responsive nanoparticles for drug release and diagnostics, *Adv. Drug Deliv. Rev.* 64 (11) (2012) 967–978.
- [216] J. Ruff, S. Hüwel, M.J. Kogan, U. Simon, H.J. Galli, The effects of gold nanoparticles functionalized with β-amyloid specific peptides on an *in vitro* model of blood-brain barrier, *Nanomedicine* 13 (5) (2017) 1645–1652.
- [217] A. Kumar, S.D. Huo, X. Zhang, J. Liu, A. Tan, S.L. Li, S.B. Jin, X.D. Xue, Y.Y. Zhao, T.J. Ji, L. Han, H. Liu, X.N. Zhang, J.C. Zhang, G.Z. Zou, T.Y. Wang, S.Q. Tang, X. J. Liang, Neuropilin-1-Targeted gold nanoparticles enhance therapeutic efficacy of Platinum(IV) drug for prostate cancer treatment, *Acs Nano* 8 (5) (2014) 4205–4220.

- [218] N. Devi, P. Singh, R. Sharma, M. Kumar, S.K. Pandey, R.K. Sharma, N. Wangoo, A lysine-rich cell penetrating peptide engineered multifunctional gold nanoparticle-based drug delivery system with enhanced cellular penetration and stability, *J. Mater. Sci.* 57 (35) (2022) 16842–16857.
- [219] Z.W. Hou, Z. Wang, R. Liu, H. Li, Z.Y. Zhang, T. Su, J. Yang, H.D. Liu, The effect of phospho-peptide on the stability of gold nanoparticles and drug delivery, *J. Nanobiotechnol.* 17 (1) (2019).
- [220] C. Wang, C. Pan, H. Yong, F. Wang, T. Bo, Y. Zhao, B. Ma, W. He, M. Li, Emerging non-viral vectors for gene delivery, *J. Nanobiotechnol.* 21 (1) (2023) 272.
- [221] G. Lin, L. Li, N. Panwar, J. Wang, S.C. Tjin, X. Wang, K.-T. Yong, Non-viral gene therapy using multifunctional nanoparticles: status, challenges, and opportunities, *Coord. Chem. Rev.* 374 (2018) 133–152.
- [222] K.L. Deng, D.X. Yang, Y.P. Zhou, Nanotechnology-Based siRNA delivery systems to overcome tumor immune evasion in cancer immunotherapy, *Pharmaceutics* 14 (7) (2022).
- [223] A. Artiga, I. Serrano-Sevilla, L. De Matteis, S.G. Mitchell, J.M. de la Fuente, Current status and future perspectives of gold nanoparticle vectors for siRNA delivery, *J. Mater. Chem. B* 7 (6) (2019) 876–896.
- [224] K. Tatiparti, S. Sau, S.K. Kashaw, A.K. Iyer, siRNA delivery strategies: a comprehensive review of recent developments, *Nanomaterials* 7 (4) (2017).
- [225] K. Gavrilov, W.M. Saltzman, Therapeutic siRNA: principles, challenges, and strategies, *Yale J. Biol. Med.* 85 (2) (2012) 187–200.
- [226] Y. Huang, J. Hong, S. Zheng, Y. Ding, S. Guo, H. Zhang, X. Zhang, Q. Du, Z. Liang, Elimination pathways of systemically delivered siRNA, *Mol. Ther.* 19 (2) (2011) 381–385.
- [227] R.L. Kanasty, K.A. Whitehead, A.J. Vegas, D.G. Anderson, Action and reaction: the biological response to siRNA and its delivery vehicles, *Mol. Ther.* 20 (3) (2012) 513–524.
- [228] J. Yue, T.J. Feliciano, W. Li, A. Lee, T.W. Odom, Gold nanoparticle size and shape effects on cellular uptake and intracellular distribution of siRNA nanoconstructs, *Bioconjugate Chem.* 28 (6) (2017) 1791–1800.
- [229] X. Cheng, X. Tian, A. Wu, J. Li, J. Tian, Y. Chong, Z. Chai, Y. Zhao, C. Chen, C. Ge, Protein corona influences cellular uptake of gold nanoparticles by phagocytic and non-phagocytic cells in a Size-Dependent manner, *ACS Appl. Mater. Interfaces* 7 (37) (2015) 20568–20575.
- [230] R. Kanasty, J.R. Dorkin, A. Vegas, D. Anderson, Delivery materials for siRNA therapeutics, *Nat. Mater.* 12 (11) (2013) 967–977.
- [231] B. Mehrdad, N. Othman, A.A. Aziz, P.M. Khaniabadi, M.S. Jameel, M.A. Dheyab, I. S. Amiri, Identifying metal nanoparticle size effect on sensing common human plasma protein by counting the sensitivity of optical absorption spectra damping, *Plasmonics* 15 (1) (2020) 123–133.
- [232] Pd Pino, B. Pelaz, Q. Zhang, P. Maffre, G.U. Nienhaus, W.J. Parak, Protein corona formation around nanoparticles – from the past to the future, *Mater. Horiz.* 1 (3) (2014) 301–313.
- [233] T. Takeuchi, T. Tagami, K. Fukushige, T. Ozeki, Useful properties of siRNA-coated gold nanoparticles as a mini-nanocarrier platform for intraocular administration, *J. Drug Deliv. Sci. Tec.* 47 (2018) 411–416.
- [234] X. Huang, Y. Lai, G.B. Braun, N.O. Reich, Modularized gold nanocarriers for TAT-Mediated delivery of siRNA, *Small* 13 (8) (2017) 1602473.
- [235] K.C.R. Bahadur, B. Thapa, N. Bhattachari, Gold nanoparticle-based gene delivery: promises and challenges, *Nanotechnol. Rev.* 3 (3) (2014) 269–280.
- [236] C. Hu, Q. Peng, F.J. Chen, Z.L. Zhong, R.X. Zhuo, Low molecular weight polyethylenimine conjugated gold nanoparticles as efficient gene vectors, *Bioconjugate Chem.* 21 (5) (2010) 836–843.
- [237] W.H. Kong, K.H. Bae, S.D. Jo, J.S. Kim, T.G. Park, Cationic lipid-coated gold nanoparticles as efficient and non-cytotoxic intracellular siRNA delivery vehicles, *Pharm. Res.* 29 (2) (2012) 362–374.
- [238] G. Minassian, E. Ghanem, R.E. Hage, K. Rahme, Gold nanoparticles conjugated with dendrigrift Poly-L-lysine and Folate-Targeted Poly(ethylene glycol) for siRNA delivery to prostate cancer, *Nanotheranostics* 7 (2) (2023) 152–166.
- [239] E. Okia, P. Bialecki, M. Kędzierska, E. Pedzwiati-Werbićka, K. Miłowska, S. Takvor, R. Gómez, F.J. de la Mata, M. Bryszewska, M. Ionov, Pegylated gold nanoparticles conjugated with siRNA: complexes formation and cytotoxicity, *Int. J. Mol. Sci.* 24 (7) (2023).
- [240] Z. Yang, T. Liu, Y. Xie, Z. Sun, H. Liu, J. Lin, C. Liu, Z.W. Mao, S. Nie, Chitosan layered gold nanorods as synergistic therapeutics for photothermal ablation and gene silencing in triple-negative breast cancer, *Acta Biomater.* 25 (2015) 194–204.
- [241] K. Rahme, M.T. Nolan, T. Doody, G.P. McGlacken, M.A. Morris, C.O. Driscoll, J. D. Holmes, Highly stable PEGylated gold nanoparticles in water: applications in biology and catalysis, *RSC Adv.* 3 (43) (2013) 21016–21024.
- [242] B. Shah, P.T. Yin, S. Ghoshal, K.B. Lee, Multimodal magnetic Core-Shell nanoparticles for effective Stem-Cell differentiation and imaging, *Angew. Chem. Int. Ed.* 52 (24) (2013) 6190–6195.
- [243] W.J. Song, J.Z. Du, T.M. Sun, P.Z. Zhang, J. Wang, Gold nanoparticles capped with polyethylenimine for enhanced siRNA delivery, *Small* 6 (2) (2010) 239–246.
- [244] H.J. Kim, H. Takemoto, Y. Yi, M. Zheng, Y. Maeda, H. Chaya, K. Hayashi, P. Mi, F. Pittella, R.J. Christie, K. Toh, Y. Matsumoto, N. Nishiyama, K. Miyata, K. Kataoka, Precise engineering of siRNA delivery vehicles to tumors using polyion complexes and gold nanoparticles, *Acs Nano* 8 (9) (2014) 8979–8991.
- [245] N. Panwar, C.B. Yang, F. Yin, H.S. Yoon, T.S. Chuan, K.T. Yong, RNAi-based therapeutic nanostrategy: IL-8 gene silencing in pancreatic cancer cells using gold nanorods delivery vehicles, *Nanotechnology* 26 (36) (2015).
- [246] L.D. Kong, J.R. Qiu, X.Y. Shi, Multifunctional PEI-entrapped gold nanoparticles enable efficient delivery of therapeutic siRNA into glioblastoma cells, *J. Control Release* 259 (2017) E83–E84.
- [247] S.K. Lee, B. Law, C.-H. Tung, Versatile nanodelivery platform to maximize siRNA combination therapy, *Macromol. Biosci.* 17 (2) (2017) 1600294.
- [248] A. Chaudhary, S. Garg, siRNA delivery using polyelectrolyte-gold nanoassemblies in neuronal cells for BACE1 gene silencing, *Mat. Sci. Eng. C. Mater.* 80 (2017) 18–28.
- [249] E. Shaabani, M. Sharifiaghdam, H. De Keersmaecker, R. De Rycke, S. De Smedt, R. Faridi-Majidi, K. Braeckmans, J.C. Fraire, Layer by layer assembled Chitosan-Coated gold nanoparticles for enhanced siRNA delivery and silencing, *Int. J. Mol. Sci.* 22 (2) (2021).
- [250] E. Shaabani, M. Sharifiaghdam, J. Lammens, H. De Keersmaecker, C. Vervaet, T. De Beer, E. Mottevaseli, M.H. Ghahremani, P. Mansouri, S. De Smedt, K. Raemdonck, R. Faridi-Majidi, K. Braeckmans, J.C. Fraire, Increasing angiogenesis factors in hypoxic diabetic wound conditions by siRNA delivery: additive effect of Lbl-Gold nanocarriers and Desloratadine-Induced lysosomal escape, *Int. J. Mol. Sci.* 22 (17) (2021).
- [251] R.D. Al Bostami, W.H. Abuwafa, G.A. Husseini, Recent advances in Nanoparticle-Based Co-Delivery systems for cancer therapy, *Nanomater.* (Basel) 12 (15) (2022).
- [252] R. Jaskula-Sztul, Y.L. Xiao, A. Jayadi, J. Eide, W.J. Xu, M. Kuninimalaiayan, S. Gong, H. Chen, Co-delivery of doxorubicin and siRNA using octreotide-conjugated gold nanorods for targeted neuroendocrine cancer therapy, *Cancer Res.* 72 (2012).
- [253] B.K. Wang, X.F. Yu, J.H. Wang, Z.B. Li, P.H. Li, H.Y. Wang, L. Song, P.K. Chu, C. Z. Li, Gold-nanorods-siRNA nanoplex for improved photothermal therapy by gene silencing, *Biomaterials* 78 (2016) 27–39.
- [254] C.U. Tunc, O. Aydin, Co-delivery of Bcl-2 siRNA and doxorubicin through gold nanoparticle-based delivery system for a combined cancer therapy approach, *J. Drug Deliv. Sci. Tec.* 74 (2022).
- [255] M.P.T. Ernst, M. Broeders, P. Herrero-Hernandez, E. Oussoren, A.T. van der Ploeg, W.W.M.P. PijnappelGene Editing Enters the Clinic for the Treatment of Human Disease, *Molecular Therapy - Methods & Clinical Development* 18 (2020) 532–557.
- [256] S.-S. Wu, Q.-C. Li, C.-Q. Yin, W. Xue, C.-Q. Song, Advances in CRISPR/Cas-based gene therapy in human genetic diseases, *Theranostics* 10 (10) (2020) 4374–4382.
- [257] K. Horodecka, M. Dückler, CRISPR/Cas9: principle, applications, and delivery through extracellular vesicles, *Int. J. Mol. Sci.* 22 (11) (2021).
- [258] D. Wilbie, J. Walther, E. Mastrobattista, Delivery aspects of CRISPR/Cas for in vivo genome editing, *Acc. Chem. Res.* 52 (6) (2019) 1555–1564.
- [259] A. Graczyk, R. Pawłowska, D. Jedrzejczyk, A. Chworoś, Gold nanoparticles in conjunction with nucleic acids as a modern molecular system for cellular delivery, *Molecules* 25 (1) (2020) 204.
- [260] R. Mout, M. Ray, G.Y. Tonga, Y.W. Lee, T. Tay, K. Sasaki, V.M. Rotello, Direct cytosolic delivery of CRISPR/Cas9-Ribonucleoprotein for efficient gene editing, *ACS Nano* 11 (3) (2017) 2452–2458.
- [261] K. Lee, M. Conboy, H.M. Park, F. Jiang, H.J. Kim, M.A. Dewitt, V.A. Mackley, K. Chang, A. Rao, C. Skinner, T. Shobha, M. Mehdipour, H. Liu, W.-c Huang, F. Lan, N.L. Bray, S. Li, J.E. Corn, K. Kataoka, J.A. Doudna, I. Conboy, N. Murthy, Nanoparticle delivery of Cas9 ribonucleoprotein and donor DNA in vivo induces homology-directed DNA repair, *Nat. Biomed. Eng.* 1 (11) (2017) 889–901.
- [262] T.M. Kazdoba, P.T. Leach, J.L. Silverman, J.N. Crawley, Modeling fragile x syndrome in the knockout mouse, *Intractable Rare Dis.* 3 (4) (2014) 118–133.
- [263] B. Lee, K. Lee, S. Panda, R. Gonzales-Rojas, A. Chong, V. Bugay, H.M. Park, R. Brenner, N. Murthy, H.Y. Lee, Nanoparticle delivery of CRISPR into the brain rescues a mouse model of fragile x syndrome from exaggerated repetitive behaviours, *Nat. Biomed. Eng.* 2 (7) (2018) 497–507.
- [264] P. Wang, L.M. Zhang, W.F. Zheng, L.M. Cong, Z.R. Guo, Y.Z.Y. Xie, L. Wang, R. B. Tang, Q. Feng, Y. Hamada, K. Gonda, Z.J. Hu, X.C. Wu, X.Y. Jiang, Thermo-triggered release of CRISPR-Cas9 system by Lipid-Encapsulated gold nanoparticles for tumor therapy, *Angew. Chem. Int. Ed.* 57 (6) (2018) 1491–1496.
- [265] E.G. Ju, T.T. Li, S.R. da Silva, S.J. Gao, Gold Nanocluster-Mediated efficient delivery of Cas9 protein through pH-Induced Assembly-Disassembly for inactivation of virus oncogenes, *ACS Appl. Mater. Inter.* 11 (38) (2019) 34717–34724.
- [266] Y. Tao, K. Yi, H. Hu, D. Shao, M. Li, Coassembly of nucleus-targeting gold nanoclusters with CRISPR/Cas9 for simultaneous bioimaging and therapeutic genome editing, *J. Mater. Chem. B* 9 (1) (2021) 94–100.
- [267] Y. Wu, M.R.K. Ali, K.C. Chen, N. Fang, M.A. El-Sayed, Gold nanoparticles in biological optical imaging, *Nano Today* 24 (2019) 120–140.
- [268] X. Huang, M.A. El-Sayed, Gold nanoparticles: optical properties and implementations in cancer diagnosis and photothermal therapy, *J. Adv. Res.* 1 (1) (2010) 13–28.
- [269] R.J.B. Pinto, D. Bispo, C. Vilela, A.M.P. Botas, R.A.S. Ferreira, A.C. Menezes, F. Campos, H. Oliveira, M.H. Abreu, S.A.O. Santos, C.S.R. Freire, One-Minute synthesis of Size-Controlled Fucoidan-Gold nanosystems: antitumoral activity and dark field imaging, *Materials* 13 (5) (2020).
- [270] C. Freese, R.E. Unger, R.C. Deller, M.I. Gibson, C. Brochhausen, H.A. Klok, C. J. Kirkpatrick, Uptake of poly(2-hydroxypropylmethacrylamide)-coated gold nanoparticles in microvascular endothelial cells and transport across the blood-brain barrier, *Biomater. Sci.* 1 (8) (2013) 824–833.
- [271] V.P. Nguyen, W. Qian, Y.X. Li, B. Liu, M. Aaberg, J. Henry, W. Zhang, X.D. Wang, Y.M. Paulus, Chain-like gold nanoparticle clusters for multimodal photoacoustic microscopy and optical coherence tomography enhanced molecular imaging, *Nat. Commun.* 12 (1) (2021).

- [272] Z. Pang, W. Yan, J. Yang, Q. Li, Y. Guo, D. Zhou, X. Jiang, Multifunctional gold nanoclusters for effective targeting, Near-Infrared fluorescence imaging, diagnosis, and treatment of cancer lymphatic metastasis, *ACS Nano* 16 (10) (2022) 16019–16037.
- [273] W. He, W.A. Henne, Q.S. Wei, Y. Zhao, D.D. Doorneweerd, J.X. Cheng, P.S. Low, A. Wei, Two-Photon luminescence imaging of spores using Peptide-Functionalized gold nanorods, *Nano Res.* 1 (6) (2008) 450–456.
- [274] S. Burkitt, M. Mehraein, R.K. Stanciuksas, J. Campbell, S. Fraser, C. Vazquez, Label-Free visualization and tracking of gold nanoparticles in vasculature using multiphoton luminescence, *Nanomaterials* 10 (11) (2020).
- [275] N. Manohar, F.J. Reynoso, P. Diagaradjane, S. Krishnan, S.H. Cho, Quantitative imaging of gold nanoparticle distribution in a tumor-bearing mouse using benchtop x-ray fluorescence computed tomography, *Sci. Rep.* 6 (2016).
- [276] Y. Ponce de León, J.L. Pichardo-Molina, N. Alcalá Ochoa, D. Luna-Moreno, Contrast enhancement of optical coherence tomography images using branched gold nanoparticles, *J. Nanomater.* 2012 (1) (2012) 571015.
- [277] C.M. Uritu, C.M. Al-Matarneh, D.I. Bostig, A. Coroaba, V. Ghizdovat, S. I. Filipiuc, N. Simionescu, C. Stefanescu, W. Jalloul, V. Nastasa, B.I. Tamba, S. S. Maier, M. Pinteala, Radiolabeled multi-layered coated gold nanoparticles as potential biocompatible PET/SPECT tracers, *J. Mater. Chem. B* 12 (15) (2024).
- [278] C. Alric, J. Taleb, G. Le Duc, C. Mandon, C. Billotey, A. Le Meur-Herland, T. Brochard, F. Vocanson, M. Janier, P. Perriat, S. Roux, O. Tillement, Gadolinium chelate coated gold nanoparticles as contrast agents for both X-ray computed tomography and magnetic resonance imaging, *J. Am. Chem. Soc.* 130 (18) (2008) 5908–5915.
- [279] B.B. Oliveira, D. Ferreira, A.R. Fernandes, P.V. Baptista, Engineering gold nanoparticles for molecular diagnostics and biosensing, *Wires Nanomed. Nanobi* 15 (1) (2023).
- [280] M.S. Kang, S.Y. Lee, K.S. Kim, D.-W. Han, State of the art biocompatible gold nanoparticles for cancer theragnosis, *Pharmaceutics* 12 (8) (2020) 701.
- [281] K. Mahato, S. Nagpal, M.A. Shah, A. Srivastava, P.K. Maurya, S. Roy, A. Jaiswal, R. Singh, P. Chandra, Gold nanoparticle surface engineering strategies and their applications in biomedicine and diagnostics, *3 Biotech* 9 (2) (2019) 57.
- [282] L. Zhang, M. Yin, J. Qiu, T. Qiu, Y. Chen, S. Qi, X. Wei, X. Tian, D. Xu, An electrochemical sensor based on CNF@AuNPs for metronidazole hypersensitivity detection, *Biosens. Bioelectron.* X 10 (2022) 100102.
- [283] A. Huefner, D. Septiadi, B.D. Wilts, I.I. Patel, W.-L. Kuan, A. Fragniere, R. A. Barker, S. Mahajan, Gold nanoparticles explore cells: cellular uptake and their use as intracellular probes, *Methods* 68 (2) (2014) 354–363.
- [284] B. Zhou, Y. Hao, D. Long, P. Yang, Real-time quartz crystal microbalance cytosensor based on a signal recovery strategy for in-situ and continuous monitoring of multiple cell membrane glycoproteins, *Biosens. Bioelectron.* 111 (2018) 90–96.
- [285] C. Lee, M. Jeon, C. Kim, 3 - photoacoustic imaging in nanomedicine, in: M. R. Hamblin, P. Avci (Eds.), *Applications of Nanoscience in Photomedicine*, Chandos Publishing, Oxford, 2015, pp. 31–47.
- [286] J. Yang, T. Wang, L. Zhao, V.K. Rajasekhar, S. Joshi, C. Andreou, S. Pal, H.-t Hsu, H. Zhang, I.J. Cohen, R. Huang, R.C. Hendrickson, M.M. Miele, W. Pei, M. B. Brendel, J.H. Healey, G. Chiosis, M.F. Kircher, Gold/alpha-lactalbumin nanoprobes for the imaging and treatment of breast cancer, *Nat. Biomed. Eng.* 4 (7) (2020) 686–703.
- [287] S. Vial, R.L. Reis, J.M. Oliveira, Recent advances using gold nanoparticles as a promising multimodal tool for tissue engineering and regenerative Medicine, *Curr. Opin. Solid State Mater. Sci.* 21 (2) (2017) 92–112.
- [288] J. Hu, F. Sanz-Rodríguez, F. Rivero, E.M. Rodríguez, R.A. Torres, D.H. Ortgies, J. G. Solé, F. Alfonso, D. Jaque, Gold nanoshells: contrast agents for cell imaging by cardiovascular optical coherence tomography, *Nano Res.* 11 (2) (2018) 676–685.
- [289] M. Sologan, F. Padelli, I. Giachetti, D. Aquino, M. Boccalon, G. Adami, P. Pengo, L. Pasquato, Functionalized gold nanoparticles as contrast agents for proton and dual Proton/Fluorine MRI, *Nanomaterials* 9 (6) (2019).
- [290] H.M. Asl, Applications of nanoparticles in magnetic resonance imaging: a comprehensive review, *Asian J. Pharm. (AJP)* 11 (01) (2017).
- [291] H. Deng, Y. Zhong, M. Du, Q. Liu, Z. Fan, F. Dai, X. Zhang, Theranostic self-assembly structure of gold nanoparticles for NIR photothermal therapy and X-Ray computed tomography imaging, *Theranostics* 4 (9) (2014) 904–918.
- [292] X. Li, Z. Xiong, X. Xu, Y. Luo, C. Peng, M. Shen, X. Shi, 99mTc-Labeled multifunctional Low-Generation Dendrimer-Entrapped gold nanoparticles for targeted SPECT/CT Dual-Mode imaging of tumors, *ACS Appl. Mater. Interfaces* 8 (31) (2016) 19883–19891.
- [293] P.K. Jain, X. Huang, I.H. El-Sayed, M.A. El-Sayed, Noble metals on the nanoscale: optical and photothermal properties and some applications in imaging, *Sens. Biol. Med. Acc. Chem. Rev.* 41 (12) (2008) 1578–1586.
- [294] N.J. Durr, T. Larson, D.K. Smith, B.A. Korgel, K. Sokolov, A. Ben-Yakar, Two-Photon luminescence imaging of cancer cells using molecularly targeted gold nanorods, *Nano Lett.* 7 (4) (2007) 941–945.
- [295] Y. Zhang, G. Wang, L. Yang, F. Wang, A. Liu, Recent advances in gold nanostructures based biosensing and bioimaging, *Coord. Chem. Rev.* 370 (2018) 1–21.
- [296] Y. Gu, W. Sun, G. Wang, N. Fang, Single particle orientation and rotation tracking discloses distinctive rotational dynamics of drug delivery vectors on live cell membranes, *J. Am. Chem. Soc.* 133 (15) (2011) 5720–5723.
- [297] S. Masuda, Y. Yanase, E. Usukura, S. Ryuzaki, P. Wang, K. Okamoto, T. Kuboki, S. Kidoaki, K. Tamada, High-resolution imaging of a cell-attached nanointerface using a gold-nanoparticle two-dimensional sheet, *Sci. Rep.* 7 (1) (2017).
- [298] M. Hu, C. Novo, A. Funston, H. Wang, H. Staleva, S. Zou, P. Mulvaney, Y. Xia, G. V. Hartland, Dark-field microscopy studies of single metal nanoparticles: understanding the factors that influence the linewidth of the localized surface plasmon resonance, *J. Mater. Chem. B* 18 (17) (2008) 1949–1960.
- [299] P.F. Gao, G. Lei, C.Z. Huang, Dark-Field microscopy: recent advances in accurate analysis and emerging applications, *Anal. Chem.* 93 (11) (2021) 4707–4726.
- [300] M.M. Liu, J. Chao, S. Deng, K. Wang, K. Li, C.H. Fan, Dark-field microscopy in imaging of plasmon resonant nanoparticles, *Colloid Surf. B* 124 (2014) 111–117.
- [301] W. Li, X. Chen, Gold nanoparticles for photoacoustic imaging, *Nanomedicine* 10 (2) (2015) 299–320.
- [302] J.J. Kim, J.S. Hong, H. Kim, M. Choi, U. Winter, H. Lee, H. Im, CRISPR/Cas13a-assisted amplification-free miRNA biosensor via dark-field imaging and magnetic gold nanoparticles, *Sens. Diagn.* 3 (8) (2024) 1310–1318.
- [303] M. Tsunoda, D. Isailovic, E.S. Yeung, Real-time three-dimensional imaging of cell division by differential interference contrast microscopy, *J. Microsc.* 232 (2) (2008) 207–211.
- [304] A.G. Tkachenko, H. Xie, Y. Liu, D. Coleman, J. Ryan, W.R. Glomm, M.K. Shipton, S. Franzen, D.L. Feldheim, Cellular trajectories of Peptide-Modified gold particle complexes: comparison of nuclear localization signals and peptide transduction domains, *Bioconjugate Chem.* 15 (3) (2004) 482–490.
- [305] W. Sun, G. Wang, N. Fang, E.S. Yeung, Wavelength-Dependent differential interference contrast microscopy: selectively imaging nanoparticle probes in live cells, *Anal. Chem.* 81 (22) (2009) 9203–9208.
- [306] G. Wang, W. Sun, Y. Luo, N. Fang, Resolving rotational motions of Nano-objects in engineered environments and live cells with gold nanorods and differential interference contrast microscopy, *J. Am. Chem. Soc.* 132 (46) (2010) 16417–16422.
- [307] A.E. Augspurger, A.S. Stender, R. Han, N. Fang, Detecting plasmon resonance energy transfer with differential interference contrast microscopy, *Anal. Chem.* 86 (2) (2014) 1196–1201.
- [308] P. Cheng, K. Pu, Molecular imaging and disease theranostics with renal-clearable optical agents, *Nat. Rev. Mater.* 6 (12) (2021) 1095–1113.
- [309] W. Li, X. Chen, Gold nanoparticles for photoacoustic imaging, *Nanomedicine* 10 (2) (2015) 299–320.
- [310] L.H.W. Wang, S. Hu, Photoacoustic tomography: in vivo imaging from organelles to organs, *Science* 335 (6075) (2012) 1458–1462.
- [311] Q. Zhang, N. Iwakuma, P. Sharma, B.M. Moudgil, C. Wu, J. McNeill, H. Jiang, S. R. Grobmyer, Gold nanoparticles as a contrast agent for tumor imaging with photoacoustic tomography, *Nanotechnology* 20 (39) (2009).
- [312] X.J. Cheng, R. Sun, L. Yin, Z.F. Chai, H.B. Shi, M.Y. Gao, Light-Triggered assembly of gold nanoparticles for photothermal therapy and photoacoustic imaging of tumors in vivo, *Adv. Mater.* 29 (6) (2017).
- [313] T. Köker, N. Tang, C. Tian, W. Zhang, X.D. Wang, R. Martel, F. Pinaud, Cellular imaging by targeted assembly of hot-spot SERS and photoacoustic nanoprobes using split-fluorescent protein scaffolds, *Nat. Commun.* 9 (2018).
- [314] S. Han, R. Bouchard, K.V. Sokolov, Molecular photoacoustic imaging with ultra-small gold nanoparticles, *Biomed. Opt. Express* 10 (7) (2019) 3472–3483.
- [315] M. Demir, M. Natali Çizmecian, D. Sipahioglu, A. Khoshzaban, M. Burçin Ünlü, H. Yagci Acar, Portfolio of colloidally stable gold–gold sulfide nanoparticles and their use in broad-band photoacoustic imaging, *Nanoscale* 17 (3) (2025) 1371–1380.
- [316] R. Zhang, S. Thoröe-Boveleth, D.N. Chigrin, F. Kiessling, T. Lammers, R. M. Pallares, Nanoscale engineering of gold nanostars for enhanced photoacoustic imaging, *J. Nanobiotechnol.* 22 (1) (2024) 115.
- [317] S. Vial, R.L. Reis, J.M. Oliveira, Recent advances using gold nanoparticles as a promising multimodal tool for tissue engineering and regenerative Medicine, *Curr. Opin. Solid State Mater. Sci.* 21 (2) (2017) 92–112.
- [318] J.-F. Li, C.-Y. Li, R.F. Aroca, Plasmon-enhanced fluorescence spectroscopy, *Chem. Soc. Rev.* 46 (13) (2017) 3962–3979.
- [319] K.A. Willets, A.J. Wilson, V. Sundaresan, P.B. Joshi, Super-Resolution imaging and plasmonics, *Chem. Rev.* 117 (11) (2017) 7538–7582.
- [320] L.-Y. Chen, C.-W. Wang, Z. Yuan, H.-T. Chang, Fluorescent gold nanoclusters: recent advances in sensing and imaging, *Anal. Chem.* 87 (1) (2015) 216–229.
- [321] S. Khatua, P.M.R. Paulo, H. Yuan, A. Gupta, P. Zijlstra, M. Orrit, Resonant plasmonic enhancement of Single-Molecule fluorescence by individual gold nanorods, *ACS Nano* 8 (5) (2014) 4440–4449.
- [322] E. Wientjes, J. Renger, A.G. Curto, R. Cogdell, N.F. van Hulst, Strong antenna-enhanced fluorescence of a single light-harvesting complex shows photon antibunching, *Nat. Commun.* 5 (1) (2014) 4236.
- [323] R. Cillari, A. Scirtino, S. Scirè, M. Cannas, F. Messina, N. Mauro, Fluorescence switching in pH-Responsive Poly(amidoamine) hydrogel networks containing gold nanoparticles and carbon nanodots for potential Real-Time tumor ph monitoring, *ACS Appl. Opt. Mater.* (2025).
- [324] A. Jaworska, T. Wojcik, K. Malek, U. Kwolek, M. Kepczynski, A.A. Ansary, S. Chlopicki, M. Baranska, Rhodamine 6G conjugated to gold nanoparticles as labels for both SERS and fluorescence studies on live endothelial cells, *Microchim. Acta* 182 (1) (2015) 119–127.
- [325] Y. Zhang, Y. Chen, J. Yu, D.J.S. Birch, Endosytosis study of gold nanoparticles through FRET-FLIM approach, 2017 13th IASTED Int. Conf. BioMed. Eng. (BioMed.) (2017) 26–31.
- [326] B. Jang, J.-Y. Park, C.-H. Tung, I.-H. Kim, Y. Choi, Gold Nanorod–Photosensitizer complex for Near-Infrared fluorescence imaging and Photodynamic/Photothermal therapy in vivo, *ACS Nano* 5 (2) (2011) 1086–1094.
- [327] M. Liu, Q. Li, L. Liang, J. Li, K. Wang, J. Li, M. Lv, N. Chen, H. Song, J. Lee, J. Shi, L. Wang, R. Lal, C. Fan, Real-time visualization of clustering and intracellular transport of gold nanoparticles by correlative imaging, *Nat. Commun.* 8 (1) (2017) 15646.

- [328] X. Qu, Y. Li, L. Li, Y. Wang, J. Liang, J. Liang, Fluorescent gold nanoclusters: synthesis and recent biological application, *J. Nanomater.* 2015 (1) (2015) 784097.
- [329] L.-Y. Chen, C.-W. Wang, Z. Yuan, H.-T. Chang, Fluorescent gold nanoclusters: recent advances in sensing and imaging, *Anal. Chem.* 87 (1) (2015) 216–229.
- [330] V. Venkatesh, A. Shukla, S. Sivakumar, S. Verma, Purine-Stabilized Green fluorescent gold nanoclusters for cell nuclei imaging applications, *ACS Appl. Mater. Interfaces* 6 (3) (2014) 2185–2191.
- [331] S. Palmai, N.R. Jana, Gold nanoclusters with enhanced tunable fluorescence as bioimaging probes, *WIREs Nanomed. Nanobiotechnol.* 6 (1) (2014) 102–110.
- [332] A. Yahia-Ammar, D. Sierra, F. Mérila, N. Hildebrandt, X. Le Guével, Self-Assembled gold nanoclusters for bright fluorescence imaging and enhanced drug delivery, *ACS Nano* 10 (2) (2016) 2591–2599.
- [333] X. Wang, Y. Wang, H. He, X. Ma, Q. Chen, S. Zhang, B. Ge, S. Wang, W.M. Nau, F. Huang, Deep-Red fluorescent gold nanoclusters for nucleoli staining: Real-Time monitoring of the nucleolar dynamics in reverse transformation of malignant cells, *ACS Appl. Mater. Interfaces* 9 (21) (2017) 17799–17806.
- [334] J. Wang, G. Zhang, Q. Li, H. Jiang, C. Liu, C. Amatore, X. Wang, In vivo self-bio-imaging of tumors through *in situ* biosynthesized fluorescent gold nanoclusters, *Sci. Rep.* 3 (2013) 1157.
- [335] C. Zhang, C. Li, Y. Liu, J. Zhang, C. Bao, S. Liang, Q. Wang, Y. Yang, H. Fu, K. Wang, D. Cui, Gold Nanoclusters-Based nanoprobe for simultaneous fluorescence imaging and targeted photodynamic therapy with superior penetration and retention behavior in tumors, *Adv. Funct. Mater.* 25 (8) (2015) 1314–1325.
- [336] K. Hayashi, M. Nakamura, H. Miki, S. Ozaki, M. Abe, T. Matsumoto, K. Ishimura, Gold nanoparticle cluster-plasmon-enhanced fluorescent silica core-shell nanoparticles for X-ray computed tomography-fluorescence dual-mode imaging of tumors, *Chem. Commun.* 49 (46) (2013) 5334–5336.
- [337] A.-M. Hada, A.-M. Craciun, M. Focsan, R. Borlan, O. Soritau, M. Todea, S. Astilean, Folic acid functionalized gold nanoclusters for enabling targeted fluorescence imaging of human ovarian cancer cells, *Talanta* 225 (2021) 121960.
- [338] F. Helmchen, W. Denk, Deep tissue two-photon microscopy, *Nat. Methods* 2 (12) (2005) 932–940.
- [339] T. Zhao, K. Yu, L. Li, T. Zhang, Z. Guan, N. Gao, P. Yuan, S. Li, S.Q. Yao, Q.-H. Xu, G.Q. Xu, Gold nanorod enhanced Two-Photon excitation fluorescence of photosensitizers for Two-Photon imaging and photodynamic therapy, *ACS Appl. Mater. Interfaces* 6 (4) (2014) 2700–2708.
- [340] N. Gao, Y. Chen, L. Li, Z. Guan, T. Zhao, N. Zhou, P. Yuan, S.Q. Yao, Q.-H. Xu, Shape-Dependent Two-Photon photoluminescence of single gold nanoparticles, *J. Phys. Chem. C* 118 (25) (2014) 13904–13911.
- [341] Y.S. Zhang, Y. Wang, L. Wang, Y. Wang, X. Cai, C. Zhang, L.V. Wang, Y. Xia, Labeling human mesenchymal stem cells with gold nanocages for *in vitro* and *in vivo* tracking by two-photon microscopy and photoacoustic microscopy, *Theranostics* 3 (8) (2013) 532–543.
- [342] J. Morales-Dalmau, C. Vilches, V. Sanz, I. de Miguel, V. Rodriguez-Fajardo, P. Berto, M. Martinez-Lozano, O. Casanovas, T. Durduran, R. Quidant, Quantification of gold nanoparticle accumulation in tissue by two-photon luminescence microscopy, *Nanoscale* 11 (23) (2019) 11331–11339.
- [343] L. Wang, J. Zheng, S. Yang, C. Wu, C. Liu, Y. Xiao, Y. Li, Z. Qing, R. Yang, Two-Photon sensing and imaging of endogenous biological cyanide in plant tissues using graphene quantum Dot/Gold nanoparticle conjugate, *ACS Appl. Mater. Interfaces* 7 (34) (2015) 19509–19515.
- [344] E.A. Egorova, G. Arias-Alpizar, R.C. Vlieg, G.S. Gooris, J.A. Bouwstra, J.V. Noort, A. Kros, A.L. Boyle, Coating gold nanorods with self-assembling peptide amphiphiles promotes stability and facilitates *in vivo* two-photon imaging, *J. Mater. Chem. B* 10 (10) (2022) 1612–1622.
- [345] J. He, Y. He, X. Wu, X. Zhang, R. Hu, B.Z. Tang, Q.H. Xu, Mesoporous Silica-Encapsulated gold nanorods for drug Delivery/Release and Two-Photon excitation fluorescence imaging to guide synergistic phototherapy and chemotherapy, *ACS Appl. Bio. Mater.* 6 (9) (2023) 3433–3440.
- [346] B. Li, S. Yu, R. Feng, Z. Qian, K. He, G.-J. Mao, Y. Cao, K. Tang, N. Gan, Y.-X. Wu, Dual-Mode gold Nanocluster-Based nanoprobe platform for Two-Photon fluorescence imaging and fluorescence lifetime imaging of intracellular endogenous miRNA, *Anal. Chem.* 95 (40) (2023) 14925–14933.
- [347] T. Patil, R. Gambhir, A. Vibhute, A.P. Tiwari, Gold nanoparticles: synthesis methods, functionalization and biological applications, *J. Clust. Sci.* 34 (2) (2023) 705–725.
- [348] S.Y. Lee, C.M. Rhee, A.M. Leung, L.E. Braverman, G.A. Brent, E.N. Pearce, A review: radiographic iodinated contrast Media-Induced thyroid dysfunction, *J. Clin. Endocrinol. Metab.* 100 (2) (2015) 376–383.
- [349] A. Astolfo, E. Schultke, R.H. Menk, R.D. Kirch, B.H. Juurlink, C. Hall, L.A. Harsan, M. Stebel, D. Barbetta, G. Tromba, F. Arfelli, In vivo visualization of gold-loaded cells in mice using x-ray computed tomography, *Nanomedicine* 9 (2) (2013) 284–292.
- [350] C. Kojima, Y. Umeda, M. Ogawa, A. Harada, Y. Magata, K. Kono, X-ray computed tomography contrast agents prepared by seeded growth of gold nanoparticles in PEGylated dendrimer, *Nanotechnology* 21 (24) (2010) 245104.
- [351] T. Nakagawa, K. Gonda, T. Kamei, L. Cong, Y. Hamada, N. Kitamura, H. Tada, T. Ishida, T. Aimiya, N. Furusawa, Y. Nakano, N. Ohuchi, X-ray computed tomography imaging of a tumor with high sensitivity using gold nanoparticles conjugated to a cancer-specific antibody via polyethylene glycol chains on their surface, *Sci. Technol. Adv. Mater.* 17 (1) (2016) 387–397.
- [352] S. Khademi, S. Sarkar, S. Kharrazi, S.M. Amini, A. Shakeri-Zadeh, M.R. Ay, H. Ghadiri, Evaluation of size, morphology, concentration, and surface effect of gold nanoparticles on X-ray attenuation in computed tomography, *Phys. Med.* 45 (2018) 127–133.
- [353] Y.C. Dong, M. Hajfathalian, P.S.N. Maidment, J.C. Hsu, P.C. Naha, S. Si-Mohamed, M. Breuilly, J. Kim, P. Chhour, P. Douek, H.I. Litt, D.P. Cormode, Effect of gold nanoparticle size on their properties as contrast agents for computed tomography, *Sci. Rep.* 9 (1) (2019) 14912.
- [354] S. Takiguchi, A. Takahashi, N. Yamauchi, S. Tada, T. Takase, M. Kimura, K. Gonda, Y. Kobayashi, Development of gold nanoparticles coated with bismuth oxide for X-ray computed tomography imaging, *J. Clust. Sci.* 36 (1) (2024) 7.
- [355] D.S.B. Gomes, L.G. Paterno, A.B.S. Santos, D.P.P. Barbosa, B.M. Holtz, M. R. Souza, R.Q. Moraes-Souza, A.V. Garay, L.R. de Andrade, P.P.C. Sartoratto, D. Mertz, G.T. Volpati, S.M. Freitas, M.A.G. Soler, UV-Accelerated synthesis of gold Nanoparticle-Pluronic nanocomposites for X-ray computed tomography contrast enhancement, *Polymers* 15 (9) (2023) 2163.
- [356] E.A. Genina, G.S. Terentyuk, B.N. Khlebtsov, A.N. Bashkatov, V.V. Tuchin, Visualisation of distribution of gold nanoparticles in liver tissues *ex vivo* and *in vitro* using the method of optical coherence tomography, *Quantum Electron.* 42 (6) (2012) 478.
- [357] J.M. Tucker-Schwartz, K.R. Beavers, W.W. Sit, A.T. Shah, C.L. Duvall, M.C. Skala, In vivo imaging of nanoparticle delivery and tumor microvasculature with multimodal optical coherence tomography, *Biomed. Opt. Express* 5 (6) (2014) 1731–1743.
- [358] C.S. Kim, D. Ingato, P. Wilder-Smith, Z. Chen, Y.J. Kwon, Stimuli-disassembling gold nanoclusters for diagnosis of early stage oral cancer by optical coherence tomography, *Nano Converg.* 5 (1) (2018) 3.
- [359] P. Si, E. Yuan, O. Liba, Y. Winetraub, S. Yousefi, E.D. SoRelle, D.W. Yecies, R. Dutta, A. de la Zerda, Gold nanoprisms as optical coherence tomography contrast agents in the second Near-Infrared window for enhanced angiography in live animals, *ACS Nano* 12 (12) (2018) 11986–11994.
- [360] Q. Xu, E. Jalilian, J.W. Fakhoury, R. Manwar, B. Michniak-Kohn, K.B. Elkin, K. Avanaki, Monitoring the topical delivery of ultrasmall gold nanoparticles using optical coherence tomography, *Ski. Res. Technol.* 26 (2) (2020) 263–268.
- [361] N.D. Calvert, J. Baxter, A.A. Torrens, J. Thompson, A. Kirby, J. Walia, S. Ntatis, E. Hemmer, P. Berini, B. Hibbert, L. Ramunno, A.J. Shuhendler, NIR-II scattering gold superclusters for intravascular optical coherence tomography molecular imaging, *Nat. Nanotechnol.* 20 (2) (2025) 276–285.
- [362] Y. Chen, J. Xi, V.N.D. Le, J. Ramella-Roman, X. Li, Gold nanocages with a long surface plasmon resonance peak wavelength as contrast agents for optical coherence tomography imaging at 1060 nm, *Nanomaterials* 15 (10) (2025) 755.
- [363] J. Peng, X. Liang, Progress in research on gold nanoparticles in cancer management, *Medicine* 98 (18) (2019) e15311.
- [364] X. Li, C. Wang, H. Tan, L. Cheng, G. Liu, Y. Yang, Y. Zhao, Y. Zhang, Y. Li, C. Zhang, Y. Xiu, D. Cheng, H. Shi, Gold nanoparticles-based SPECT/CT imaging probe targeting for vulnerable atherosclerosis plaques, *Biomaterials* 108 (2016) 71–80.
- [365] Y. Zhao, B. Pang, H. Luehmann, L. Detering, X. Yang, D. Sultan, S. Harpstrete, V. Sharma, C.S. Cutler, Y. Xia, Y. Liu, Gold nanoparticles doped with 199Au atoms and their use for targeted cancer imaging by SPECT, *Adv. Healthc. Mater.* 5 (8) (2016) 928–935.
- [366] L. Zhao, S. Wen, M. Zhu, D. Li, Y. Xing, M. Shen, X. Shi, J. Zhao, 99mTc-labelled multifunctional polyethylenimine-entrapped gold nanoparticles for dual mode SPECT and CT imaging, *artificial cells, Nanomed. Biotechnol.* 46 (sup1) (2018) 488–498.
- [367] Y. Xing, J. Zhu, L. Zhao, Z. Xiong, Y. Li, S. Wu, G. Chand, X. Shi, J. Zhao, SPECT/CT imaging of chemotherapy-induced tumor apoptosis using 99mTc-labeled dendrimer-entrapped gold nanoparticles, *Drug Deliv.* 25 (1) (2018) 1384–1393.
- [368] G. Jarockyte, M. Stasys, V. Poderys, K. Buivydaitė, M. Pleckaitis, D. Bulotiene, M. Matulionytė, V. Karabanovas, R. Rotomskis, Biodistribution of multimodal gold nanoclusters designed for Photoluminescence-SPECT/CT imaging and diagnostic, *Nanomater. (Basel)* 12 (19) (2022).
- [369] R.B. Hosseiniabadi, H. Rajabi, Real-time dosimetry in lung cancer radiotherapy using PET imaging of positrons induced by gold nanoparticles, *J. Radiat. Res. Appl. Sci.* 18 (2) (2025) 101361.
- [370] R.J. Holbrook, N. Rammohan, M.W. Rotz, K.W. MacRenaris, A.T. Preslar, T. J. Meade, Gd(III)-Dithiolane gold nanoparticles for T1-Weighted magnetic resonance imaging of the pancreas, *Nano Lett.* 16 (5) (2016) 3202–3209.
- [371] F.J. Nicholls, M.W. Rotz, H. Ghuman, K.W. MacRenaris, T.J. Meade, M. Modo, DNA-gadolinium-gold nanoparticles for *in vivo* T1 MR imaging of transplanted human neural stem cells, *Biomaterials* 77 (2016) 291–306.
- [372] A.B. Etame, R.J. Diaz, M.A. O'Reilly, C.A. Smith, T.G. Mainprize, K. Hynynen, J. T. Rutka, Enhanced delivery of gold nanoparticles with therapeutic potential into the brain using MRI-guided focused ultrasound, *Nanomed. Nanotechnol. Biol. Med.* 8 (7) (2012) 1133–1142.
- [373] A. Irure, M. Marradi, B. Arnaiz, N. Genicio, D. Padro, S. Penades, Sugar/gadolinium-loaded gold nanoparticles for labelling and imaging cells by magnetic resonance imaging, *Biomater. Sci.* 1 (6) (2013) 658–668.
- [374] R. Wilson, The use of gold nanoparticles in diagnostics and detection, *Chem. Soc. Rev.* 37 (9) (2008) 2028–2045.
- [375] N.R.S. Sibuyi, K.L. Moabelo, A.O. Fadaka, S. Meyer, M.O. Onani, A.M. Madiehe, M. Meyer, Multifunctional gold nanoparticles for improved diagnostic and therapeutic applications: a review, *Nanoscale Res. Lett.* 16 (1) (2021) 174.
- [376] C. Park, H. Youn, H. Kim, T. Noh, Y.H. Kook, E.T. Oh, H.J. Park, C. Kim, Cyclodextrin-covered gold nanoparticles for targeted delivery of an anti-cancer drug, *J. Mater. Chem.* 19 (16) (2009) 2310–2315.
- [377] G. Zhang, Functional gold nanoparticles for sensing applications, *Nanotechnol. Rev.* 2 (3) (2013) 269–288.

- [378] J.-H. Lee, H.-Y. Cho, H.K. Choi, J.-Y. Lee, J.-W. Choi, Application of gold nanoparticle to plasmonic biosensors, *Int. J. Mol. Sci.* 19 (7) (2018) 2021.
- [379] S. Xu, W. Ouyang, P. Xie, Y. Lin, B. Qiu, Z. Lin, G. Chen, L. Guo, Highly uniform gold nanobipyramids for ultrasensitive colorimetric detection of influenza virus, *Anal. Chem.* 89 (3) (2017) 1617–1623.
- [380] T.T. Tsai, C.Y. Huang, C.A. Chen, S.W. Shen, M.C. Wang, C.M. Cheng, C.F. Chen, Diagnosis of tuberculosis using colorimetric gold nanoparticles on a Paper-Based analytical device, *ACS Sens.* 2 (9) (2017) 1345–1354.
- [381] B. Mondal, S. Ramlal, P.S. Lavu, N. B, J. Kingston, Highly sensitive colorimetric biosensor for staphylococcal enterotoxin b by a Label-Free aptamer and gold nanoparticles, *Front Microbiol* 9 (2018) 179.
- [382] P. Rabiei, H. Mohabatkar, M. Behbahani, A label-free G-quadruplex aptamer/gold nanoparticle-based colorimetric biosensor for rapid detection of bovine viral diarrhea virus genotype 1, *PLoS One* 19 (7) (2024) e0293561.
- [383] L. Zheng, G. Cai, S. Wang, M. Liao, Y. Li, J. Lin, A microfluidic colorimetric biosensor for rapid detection of escherichia coli O157:H7 using gold nanoparticle aggregation and smart phone imaging, *Biosens. Bioelectron.* 124–125 (2019) 143–149.
- [384] L. Zhu, S. Li, X. Shao, Y. Feng, P. Xie, Y. Luo, K. Huang, W. Xu, Colorimetric detection and typing of E. Coli lipopolysaccharides based on a dual aptamer-functionalized gold nanoparticle probe, *Mikrochim Acta* 186 (2) (2019) 111.
- [385] R. Gupta, A. Kumar, S. Kumar, A.K. Pinnaka, N.K. Singhal, Naked eye colorimetric detection of escherichia coli using aptamer conjugated graphene oxide enclosed gold nanoparticles, *Sens. Actuators B Chem.* 329 (2021) 129100.
- [386] Z. Chen, Y. Tan, C. Zhang, L. Yin, H. Ma, N. Ye, H. Qiang, Y. Lin, A colorimetric aptamer biosensor based on cationic polymer and gold nanoparticles for the ultrasensitive detection of thrombin, *Biosens. Bioelectron.* 56 (2014) 46–50.
- [387] C.C. Chang, C.P. Chen, C.H. Lee, C.Y. Chen, C.W. Lin, Colorimetric detection of human chorionic gonadotropin using catalytic gold nanoparticles and a peptide aptamer, *Chem. Commun. (Camb.)* 50 (92) (2014) 14443–14446.
- [388] Q. Wang, X. Yang, X. Yang, F. Liu, K. Wang, Visual detection of myoglobin via G-quadruplex DNAzyme functionalized gold nanoparticles-based colorimetric biosensor, *Sens. Actuators B Chem.* 212 (2015) 440–445.
- [389] C.C. Chang, C.Y. Chen, T.L. Chuang, T.H. Wu, S.C. Wei, H. Liao, C.W. Lin, Aptamer-based colorimetric detection of proteins using a branched DNA cascade amplification strategy and unmodified gold nanoparticles, *Biosens. Bioelectron.* 78 (2016) 200–205.
- [390] N.R. Nirala, P.S. Saxena, A. Srivastava, Colorimetric detection of cholesterol based on enzyme modified gold nanoparticles, *Spectrochim. Acta A Mol. Biomol. Spectrosc.* 190 (2018) 506–512.
- [391] L. Xiao, A. Zhu, Q. Xu, Y. Chen, J. Xu, J. Weng, Colorimetric biosensor for detection of cancer biomarker by au Nanoparticle-Decorated Bi(2)Se(3) nanosheets, *ACS Appl. Mater. Interfaces* 9 (8) (2017) 6931–6940.
- [392] C. Ibau, M.K. Md Arshad, S.C.B. Gopinath, Current advances and future visions on bioelectronic immunoassays for prostate-specific antigen, *Biosens. Bioelectron.* 98 (2017) 267–284.
- [393] N. Xia, D. Deng, Y. Wang, C. Fang, S.J. Li, Gold nanoparticle-based colorimetric method for the detection of prostate-specific antigen, *Int. J. Nanomed.* 13 (2018) 2521–2530.
- [394] H. Mollasalehi, E. Shahari, A colorimetric nano-biosensor for simultaneous detection of prevalent cancers using unamplified cell-free ribonucleic acid biomarkers, *Bioorg. Chem.* 107 (2021) 104605.
- [395] H. Zhao, Y. Qu, F. Yuan, X. Quan, A visible and label-free colorimetric sensor for miRNA-21 detection based on peroxidase-like activity of graphene/gold-nanoparticle hybrids, *Anal. Methods* 8 (9) (2016) 2005–2012.
- [396] J. Thavanathan, N.M. Huang, K.L. Thong, Colorimetric detection of DNA hybridization based on a dual platform of gold nanoparticles and graphene oxide, *Biosens. Bioelectron.* 55 (2014) 91–98.
- [397] Y. Jiang, M. Shi, Y. Liu, S. Wan, C. Cui, L. Zhang, W. Tan, Aptamer/AuNP biosensor for colorimetric profiling of exosomal proteins, *Angew. Chem. Int. Ed. Engl.* 56 (39) (2017) 11916–11920.
- [398] Y. Zhang, J. Jiao, Y. Wei, D. Wang, C. Yang, Z. Xu, Plasmonic colorimetric biosensor for sensitive exosome detection via Enzyme-Induced etching of gold Nanobipyramid@MnO₂ nanosheet nanostructures, *Anal. Chem.* 92 (22) (2020) 15244–15252.
- [399] C. Wang, X. Xu, W. Yao, L. Wang, X. Pang, S. Xu, X. Luo, Programmable DNA Nanowitch-Regulated plasmonic CRISPR/Cas12a-Gold nanostars reporter platform for nucleic acid and Non-Nucleic acid biomarker analysis assisted by a spatial confinement effect, *Nano Lett.* 25 (4) (2025) 1666–1672.
- [400] K. Dighe, P. Moitra, P. Saha, N. Gunaseelan, D. Pan, Cooperative effect of complementary antisense oligonucleotides and CRISPR effectors for universal DNA-based pathogen assay using nano-enabled colorimetry, *Mater. Today* 80 (2024) 374–394.
- [401] R. Fu, Y. Wang, S. Qiao, P. Xu, Y. Xianyu, J. Zhang, CRISPR-Cas12a-Mediated growth of gold nanoparticles for DNA detection in agarose gel, *ACS Sens.* 10 (2) (2025) 1429–1439.
- [402] J. Waitkus, Y. Chang, L. Liu, S.V. Puttaswamy, T. Chung, A.M.M. Vargas, S. J. Dallery, M.R. O'Connell, H. Cai, G.J. Tobin, N. Bhalla, K. Du, Gold nanoparticle enabled localized surface plasmon resonance on unique gold nanomushroom structures for On-Chip CRISPR-Cas13a sensing, *Adv. Mater. Interfaces* 10 (1) (2023).
- [403] S. Liu, T. Xie, X. Pei, S. Li, Y. He, Y. Tong, G. Liu, CRISPR-Cas12a coupled with universal gold nanoparticle strand-displacement probe for rapid and sensitive visual SARS-CoV-2 detection, *Sens. Actuators B Chem.* 377 (2023) 133009.
- [404] M.R. Kumalasari, R. Alfaaaar, A.S. Andreani, Gold nanoparticles (AuNPs): a versatile material for biosensor application, *Talanta Open* 9 (2024) 100327.
- [405] M. Liu, H. Zhuang, Y. Zhang, Y. Jia, A sandwich FRET biosensor for lysozyme detection based on peptide-functionalized gold nanoparticles and FAM-labeled aptamer, *Talanta* 276 (2024) 126226.
- [406] J. Shi, C. Chan, Y. Pang, W. Ye, F. Tian, J. Lyu, Y. Zhang, M. Yang, A fluorescence resonance energy transfer (FRET) biosensor based on graphene quantum dots (GQDs) and gold nanoparticles (AuNPs) for the detection of meca gene sequence of *staphylococcus aureus*, *BôSense Bioelectron.* 67 (2015) 595–600.
- [407] Y. Fu, T. Chen, G. Wang, T. Gu, C. Xie, J. Huang, X. Li, S. Best, G. Han, Production of a fluorescence resonance energy transfer (FRET) biosensor membrane for microRNA detection, *J. Mater. Chem. B* 5 (34) (2017) 7133–7139.
- [408] W. Dong, R. Wang, X. Gong, C. Dong, An efficient turn-on fluorescence biosensor for the detection of glutathione based on FRET between N,S dual-doped carbon dots and gold nanoparticles, *Anal. Bioanal. Chem.* 411 (25) (2019) 6687–6695.
- [409] S. Xu, F. Zhang, L. Xu, X. Liu, P. Ma, Y. Sun, X. Wang, D. Song, A fluorescence resonance energy transfer biosensor based on carbon dots and gold nanoparticles for the detection of trypsin, *Sens. Actuators B Chem.* 273 (2018) 1015–1021.
- [410] Y. Yang, S. Zhai, L. Zhang, Y. Wu, J. Li, Y. Li, X. Li, L. Zhu, W. Xu, G. Wu, H. Gao, A gold nanoparticle-enhanced dCas9-mediated fluorescence resonance energy detection for nucleic acid detection, *Talanta* 282 (2025) 126978.
- [411] D. Pan, Y. Gu, H. Lan, Y. Sun, H. Gao, Functional graphene-gold nano-composite fabricated electrochemical biosensor for direct and rapid detection of bisphenol a, *Anal. Chim. Acta* 853 (2015) 297–302.
- [412] X. Wang, X. Zhang, Electrochemical co-reduction synthesis of graphene/nano-gold composites and its application to electrochemical glucose biosensor, *Electrochim. Acta* 112 (2013) 774–782.
- [413] S.H. Baek, J. Roh, C.Y. Park, M.W. Kim, R. Shi, S.K. Kailasa, T.J. Park, Cu-nanoflower decorated gold nanoparticles-graphene oxide nanofiber as electrochemical biosensor for glucose detection, *Materials Science Engineering C* 107 (2020) 110273.
- [414] M.C. Canbaz, C.S. Simsek, M.K. Sezginturk, Electrochemical biosensor based on self-assembled monolayers modified with gold nanoparticles for detection of HER-3, *Anal. Chim. Acta* 814 (2014) 31–38.
- [415] W. Shen, K.H. Yeo, Z. Gao, A simple and highly sensitive fluorescence assay for microRNAs, *Analyst* 140 (6) (2015) 1932–1938.
- [416] L. Tian, K. Qian, J. Qi, Q. Liu, C. Yao, W. Song, Y. Wang, Gold nanoparticles superlattices assembly for electrochemical biosensor detection of microRNA-21, *Biosens. Bioelectron.* 99 (2018) 564–570.
- [417] C. Pothipor, J. Jakmunee, S. Bamrungsap, K. Ounnunkad, An electrochemical biosensor for simultaneous detection of breast cancer clinically related microRNAs based on a gold nanoparticles/graphene quantum dots/graphene oxide film, *Analyst* 146 (12) (2021) 4000–4009.
- [418] X. Wang, Z. Qin, F. Zhang, C. Li, X. Yuan, J. Yang, H. Yang, Label-free electrochemical biosensor based on dual amplification of gold nanoparticles and polycaprolactones for CEA detection, *Talanta* 278 (2024) 126468.
- [419] H. Duan, Y. Wang, S.-Y. Tang, T.-H. Xiao, K. Goda, M. Li, A CRISPR-Cas12a powered electrochemical sensor based on gold nanoparticles and MXene composite for enhanced nucleic acid detection, *Sens. Actuators B Chem.* 380 (2023) 133342.
- [420] N. Qin, L. Deng, M. Wang, X. Hun, Gold Nanoparticles/Mo2C/MoO2-Modified electrodes for nucleic acid detection through CRISPR/Cas12a photoelectrochemical assay, *ACS Appl. Nano Mater.* 4 (10) (2021) 10701–10707.
- [421] Y. Wang, B. Shen, N. Luo, C. Li, H. Wu, Y. Wang, S. Tian, X. Li, R. Liu, X. Li, J. Chen, W. Cheng, S. Ding, R. Chen, M. Xiao, Q. Xia, Self-enhanced nanohydrogel electrochemiluminescence biosensor based on CRISPR/Cas12a and gold platinum nanoparticles modification for high-sensitivity detection of *burkholderia pseudomallei*, *Chem. Eng. J.* 486 (2024) 150279.
- [422] Surface-enhanced Raman spectroscopy, *Nature Reviews Methods Primers* 1(1) (2022) 86.
- [423] J. Banuukevic, I. Hakki Boyaci, A. Goktug Bozkurt, U. Tamer, A. Ramanavicius, A. Ramanaviciene, Magnetic gold nanoparticles in SERS-based sandwich immunoassay for antigen detection by well oriented antibodies, *Biosens. Bioelectron.* 43 (2013) 281–288.
- [424] H. Zhang, X. Ma, Y. Liu, N. Duan, S. Wu, Z. Wang, B. Xu, Gold nanoparticles enhanced SERS aptasensor for the simultaneous detection of salmonella typhimurium and staphylococcus aureus, *Biosens. Bioelectron.* 74 (2015) 872–877.
- [425] X. Fu, C. Cheng, J. Yu, P. Choo, L. Chen, J. Choo, A SERS-based lateral flow assay biosensor for highly sensitive detection of HIV-1 DNA, *Biosens. Bioelectron.* 78 (2016) 530–537.
- [426] M.-Q. He, S. Chen, K. Yao, K. Wang, Y.-L. Yu, J.-H. Wang, Oriented assembly of gold nanoparticles with Freezing-Driven surface DNA manipulation and its application in SERS-Based MicroRNA assay, *Small Methods* 3 (5) (2019) 1900017.
- [427] Z. Cai, Y. Hu, Y. Sun, Q. Gu, P. Wu, C. Cai, Z. Yan, Plasmonic SERS biosensor based on multibranched gold nanoparticles embedded in polydimethylsiloxane for quantification of hematin in human erythrocytes, *Anal. Chem.* 93 (2) (2021) 1025–1032.
- [428] Y. Liu, S. Gou, L. Qiu, Z. Xu, H. Yang, S. Yang, Y. Zhao, A CRISPR/Cas12a-powered gold/nickel foam surface-enhanced Raman spectroscopy biosensor for nucleic acid specific detection in foods, *Analyst* 149 (17) (2024) 4343–4350.
- [429] A. Su, Y. Liu, X. Cao, W. Xu, C. Liang, S. Xu, A universal CRISPR/Cas12a-mediated AuNPs aggregation-based surface-enhanced Raman scattering (CRISPR/Ca-SERS) platform for virus gene detection, *Sens. Actuators B Chem.* 369 (2022) 132295.

- [430] C.J. Esdale, K.S. Washington, C.T. Laurencin, Regenerative engineering: a review of recent advances and future directions, *Regen. Med.* 16 (5) (2021) 495–512.
- [431] F. Han, J. Wang, L. Ding, Y. Hu, W. Li, Z. Yuan, Q. Guo, C. Zhu, L. Yu, H. Wang, Z. Zhao, L. Jia, J. Li, Y. Yu, W. Zhang, G. Chu, S. Chen, B. Li, Tissue engineering and regenerative Medicine: achievements, future, and sustainability in Asia, *Front. Bioeng. Biotechnol.* 8 (2020).
- [432] F.J. O'Brien, Biomaterials & scaffolds for tissue engineering, *Mater. Today* 14 (3) (2011) 88–95.
- [433] M. Yadid, R. Feiner, T. Dvir, Gold Nanoparticle-Integrated scaffolds for tissue engineering and regenerative Medicine, *Nano Lett.* 19 (4) (2019) 2198–2206.
- [434] S. Fleischer, M. Shevach, R. Feiner, T. Dvir, Coiled fiber scaffolds embedded with gold nanoparticles improve the performance of engineered cardiac tissues, *Nanoscale* 6 (16) (2014) 9410–9414.
- [435] N.E. Beltran-Vargas, E. Pena-Mercado, C. Sanchez-Gomez, M. Garcia-Lorenzana, J.C. Ruiz, I. Arroyo-Mayo, S. Huerta-Yepez, J. Campos-Teran, Sodium Alginate/Chitosan scaffolds for cardiac tissue engineering: the influence of its Three-Dimensional material preparation and the use of gold nanoparticles, *Polym. (Basel)* 14 (16) (2022).
- [436] S. Ghaziof, S. Shojaei, M. Mehdikhani, M. Khodaei, M. Jafari Nodoushan, Electro-conductive 3D printed polycaprolactone/gold nanoparticles nanocomposite scaffolds for myocardial tissue engineering, *J. Mech. Behav. Biomed. Mater.* 132 (2022) 105271.
- [437] S. Ghaziof, S. Shojaei, M. Mehdikhani, M. Khodaei, M. Jafari Nodoushan, The effect of spironolactone loading on the properties of 3D-Printed Polycaprolactone/Gold nanoparticles composite scaffolds for myocardial tissue engineering, *J. Bionic Eng.* 21 (2) (2024) 924–937.
- [438] P. Baei, S. Jalili-Firoozinezhad, S. Rajabi-Zeleti, M. Tafazzoli-Shadpour, H. Baharvand, N. Aghdam, Electrically conductive gold nanoparticle-chitosan thermosensitive hydrogels for cardiac tissue engineering, *Mater. Sci. Eng. C. Mater. Biol. Appl.* 63 (2016) 131–141.
- [439] A. Navaei, H. Saini, W. Christenson, R.T. Sullivan, R. Ros, M. Nikkhah, Gold nanorod-incorporated gelatin-based conductive hydrogels for engineering cardiac tissue constructs, *Acta Biomater.* 41 (2016) 133–146.
- [440] B. Pena, M. Maldonado, A.J. Bonham, B.A. Aguado, A. Dominguez-Alfaro, M. Laughter, T.J. Rowland, J. Bardill, N.L. Farnsworth, N. Alegret Ramon, M.R. G. Taylor, K.S. Anseth, M. Prato, R. Shandas, T.A. McKinsey, D. Park, L. Mestroni, Gold Nanoparticle-Functionalized reversible thermal gel for tissue engineering applications, *ACS Appl. Mater. Interfaces* 11 (20) (2019) 18671–18680.
- [441] H. Tohid, N. Maleki, A. Simchi, Conductive, injectable, and self-healing collagen-hyaluronic acid hydrogels loaded with bacterial cellulose and gold nanoparticles for heart tissue engineering, *Int J. Biol. Macromol.* 280 (Pt 2) (2024) 135749.
- [442] M. Shevach, S. Fleischer, A. Shapira, T. Dvir, Gold nanoparticle-decellularized matrix hybrids for cardiac tissue engineering, *Nano Lett.* 14 (10) (2014) 5792–5796.
- [443] R.S. Nair, J.M. Ameer, M.R. Alison, T.V. Anilkumar, A gold nanoparticle coated porcine cholecyst-derived bioscaffold for cardiac tissue engineering, *Colloids Surf. B Biointerfaces* 157 (2017) 130–137.
- [444] I.A. Hammam, R. Winters, Z. Hong, Advancements in the application of biomaterials in neural tissue engineering: a review, *Biomed. Eng. Adv.* 8 (2024) 100132.
- [445] P. Sen Sharma, G. Madhumathi, R.D. Jayant, A.K. Jaiswal, Biomaterials and cells for neural tissue engineering: current choices, *Materials Science Engineering C* 77 (2017) 1302–1315.
- [446] J. Senanayake, H.G. Sundararaghavan, Bioengineered conductive scaffolds for neural tissue engineering, *Bioelectricity* 6 (1) (2024) 13–25.
- [447] N. Saderi, M. Rajabi, B. Akbari, M. Firouzi, Z. Hassannejad, Fabrication and characterization of gold nanoparticle-doped electrospun PCL/chitosan nanofibrous scaffolds for nerve tissue engineering, *J. Mater. Sci. Mater. Med.* 29 (9) (2018) 134.
- [448] S. Razavi, R. Seyedehrahimi, M. Jahromi, Biodelivery of nerve growth factor and gold nanoparticles encapsulated in chitosan nanoparticles for schwann-like cells differentiation of human adipose-derived stem cells, *Biochem Biophys. Res Commun.* 513 (3) (2019) 681–687.
- [449] R. Seyedehrahimi, S. Razavi, J. Varshosaz, E. Vatankhah, M. Kazemi, Beneficial effects of biodelivery of brain-derived neurotrophic factor and gold nanoparticles from functionalized electrospun PLGA scaffold for nerve tissue engineering, *J. Clust. Sci.* 32 (3) (2021) 631–642.
- [450] Y. Pooshidiani, N. Zoghi, M. Rajabi, M. Haghbin Nazarpak, Z. Hassannejad, Fabrication and evaluation of porous and conductive nanofibrous scaffolds for nerve tissue engineering, *J. Mater. Sci. Mater. Med.* 32 (4) (2021) 46.
- [451] A. Aydeger, N. Aysit, G. Baydas, C. Cakici, U.C. Erim, Design of IKVAV peptide/gold nanoparticle decorated, micro/nano-channeled PCL/PLGA film scaffolds for neuronal differentiation and neurite outgrowth, *Biomater. Adv.* 152 (2023) 213472.
- [452] P. Nezhad-Mokhtari, M. Akrami-Hasan-Kohal, M. Ghorbani, An injectable chitosan-based hydrogel scaffold containing gold nanoparticles for tissue engineering applications, *Int J. Biol. Macromol.* 154 (2020) 198–205.
- [453] J. Gao, Y. Zhou, G. Xu, Z. Wei, L. Ding, W. Zhang, Y. Huang, Hybrid hydrogels containing gradients in gold nanoparticles for localized delivery of mesenchymal stem cells and enhanced nerve tissues remodeling in vivo, *Mater. Today Bio* 30 (2025) 101411.
- [454] W. Gong, T. Zhang, M. Che, Y. Wang, C. He, L. Liu, Z. Lv, C. Xiao, H. Wang, S. Zhang, Recent advances in nanomaterials for the treatment of spinal cord injury, *Mater. Today Bio* 18 (2023) 100524.
- [455] R. Zimmermann, Y. Vieira Alves, L.E. Sperling, P. Pranke, Nanotechnology for the treatment of spinal cord injury, *Tissue Eng. Part B Rev.* 27 (4) (2021) 353–365.
- [456] W.K. Ko, S.J. Lee, S.J. Kim, G.H. Han, I.B. Han, J.B. Hong, S.H. Sheen, S. Sohn, Direct injection of hydrogels embedding gold nanoparticles for local therapy after spinal cord injury, *Biomacromolecules* 22 (7) (2021) 2887–2901.
- [457] W.K. Ko, S.J. Kim, G.H. Han, D. Lee, D. Jeong, S.J. Lee, I.B. Han, J.B. Hong, S. H. Sheen, S. Sohn, Transplantation of neuron-inducing grafts embedding positively charged gold nanoparticles for the treatment of spinal cord injury, *Bioeng. Transl. Med* 7 (3) (2022) e10326.
- [458] I. Ozcicek, N. Aysit, Z. Balcikani, N.U. Ayturk, A. Aydeger, G. Baydas, M.S. Aydin, E. Altintas, U.C. Erim, Development of BDNF/NGF/IKVAV peptide modified and gold nanoparticle conductive PCL/PLGA nerve guidance conduit for regeneration of the rat spinal cord injury, *Macromol. Biosci.* 24 (5) (2024) e2300453.
- [459] H. Nekounam, Z. Allahyari, S. Gholizadeh, E. Mirzaei, M.A. Shokrgozar, R. Faridi-Majidi, Simple and robust fabrication and characterization of conductive carbonized nanofibers loaded with gold nanoparticles for bone tissue engineering applications, *Mater. Sci. Eng. C. Mater. Biol. Appl.* 117 (2020) 111226.
- [460] H. Samadian, H. Khasdar, A. Ehterami, M. Salehi, Bioengineered 3D nanocomposite based on gold nanoparticles and gelatin nanofibers for bone regeneration: in vitro and in vivo study, *Sci. Rep.* 11 (1) (2021) 13877.
- [461] S.J. Lee, H.J. Lee, S.Y. Kim, J.M. Seok, J.H. Lee, W.D. Kim, I.K. Kwon, S.Y. Park, S. A. Park, In situ gold nanoparticle growth on polydopamine-coated 3D-printed scaffolds improves osteogenic differentiation for bone tissue engineering applications: in vitro and in vivo studies, *Nanoscale* 10 (33) (2018) 15447–15453.
- [462] C. Gandhimathi, Y.J. Quek, H. Ezhilarasu, S. Ramakrishna, B.H. Bay, D. K. Srinivasan, Osteogenic differentiation of mesenchymal stem cells with Silica-Coated gold nanoparticles for bone tissue engineering, *Int J. Mol. Sci.* 20 (20) (2019).
- [463] D.N. Heo, W.K. Ko, M.S. Bae, J.B. Lee, D.W. Lee, W. Byun, C.H. Lee, E.C. Kim, B. Y. Jung, I.K. Kwon, Enhanced bone regeneration with a gold nanoparticle-hydrogel complex, *J. Mater. Chem. B* 2 (11) (2014) 1584–1593.
- [464] D. Lee, D.N. Heo, H.R. Nah, S.J. Lee, W.K. Ko, J.S. Lee, H.J. Moon, J.B. Bang, Y. S. Hwang, R.L. Reis, I.K. Kwon, Injectable hydrogel composite containing modified gold nanoparticles: implication in bone tissue regeneration, *Int J. Nanomed.* 13 (2018) 7019–7031.
- [465] M. Ribeiro, M.P. Ferraz, F.J. Monteiro, M.H. Fernandes, M.M. Beppu, D. Mantione, H. Sardon, Antibacterial silk fibroin/nanohydroxyapatite hydrogels with silver and gold nanoparticles for bone regeneration, *Nanomedicine* 13 (1) (2017) 231–239.
- [466] A. Topsakal, S. Midha, E. Yuca, A. Tukay, H.T. Sasmazel, D.M. Kalaskar, O. Gunduz, Study on the cytocompatibility, mechanical and antimicrobial properties of 3D printed composite scaffolds based on PVA/ gold nanoparticles (Au(+) / ampicillin (AMP) for bone tissue engineering, *Mater. Today Commun.* 28 (2021) 102458.
- [467] X. Bai, H. Sun, L. Jia, J. Xu, P. Zhang, D. Zhang, Y. Gu, B. Chen, L. Feng, Chondrocyte targeting gold nanoparticles protect growth plate against inflammatory damage by maintaining cartilage balance, *Mater. Today Bio* 23 (2023) 100795.
- [468] S.E. Smith, C.L. Snider, D.R. Gilley, D.N. Grant, S.L. Sherman, B.D. Ulery, D. A. Grant, S.A. Grant, Homogenized porcine extracellular matrix derived injectable tissue construct with gold nanoparticles for musculoskeletal tissue engineering applications, *J. Biomater. Nanobiotechnol.* 08 (02) (2017) 125–143.
- [469] R. Qiu, W. Xiong, W. Hua, Y. He, X. Sun, M. Xing, L. Wang, A biosynthesized gold nanoparticle from staphylococcus aureus – as a functional factor in muscle tissue engineering, *Appl. Mater. Today* 22 (2021) 100905.
- [470] A. Zsedenyi, B. Farkas, G.N. Abdelrasoul, I. Romano, E. Gyukyi-Sebestyen, K. Nagy, M. Harmati, G. Dobra, S. Kormondi, G. Decsi, I.B. Nemeth, A. Diaspro, F. Brandi, S. Beke, K. Buzas, Gold nanoparticle-filled biodegradable photopolymer scaffolds induced muscle remodeling: in vitro and in vivo findings, *Mater. Sci. Eng. C. Mater. Biol. Appl.* 72 (2017) 625–630.
- [471] O. Akturk, K. Kismet, A.C. Yasti, S. Kuru, M.E. Duymus, F. Kaya, M. Caydere, S. Hucumenoglu, D. Keskin, Collagen/gold nanoparticle nanocomposites: a potential skin wound healing biomaterial, *J. Biomater. Appl.* 31 (2) (2016) 283–301.
- [472] Ö. Aktürk, D. Keskin, Collagen/PEO/gold nanofibrous matrices for skin tissue engineering, *Turk. J. Biol.* 40 (2) (2016) 380–398.
- [473] J. Radwan-Praglowka, L. Janus, M. Piatkowski, D. Bogdal, D. Matysek, Hybrid bilayer PLA/Chitosan nanofibrous scaffolds doped with ZnO, Fe(3)O(4), and au nanoparticles with bioactive properties for skin tissue engineering, *Polymers* 12 (1) (2020).
- [474] X. Gu, Z.X. Xu, L.P. Gu, H.Y. Xu, F.X. Han, B. Chen, X.J. Pan, Preparation and antibacterial properties of gold nanoparticles: a review, *Environ. Chem. Lett.* 19 (1) (2021) 167–187.
- [475] R. Urban-Chmiel, A. Marek, D. Stepien-Pyšniak, K. Wieczorek, M. Dec, A. Nowaczek, J. Osek, Antibiotic resistance in Bacteria—A review, *Antibiotics* 11 (8) (2022) 1079.
- [476] X. Li, S.M. Robinson, A. Gupta, K. Saha, Z. Jiang, D.F. Moyano, A. Sahar, M. A. Riley, V.M. Rotello, Functional gold nanoparticles as potent antimicrobial agents against Multi-Drug-Resistant bacteria, *ACS Nano* 8 (10) (2014) 10682–10686.
- [477] U. Rajchakit, V. Sarojini, Recent developments in Antimicrobial-Peptide-Conjugated gold nanoparticles, *Bioconjugate Chem.* 28 (11) (2017) 2673–2686.
- [478] Y. Zhang, T.P. Shareena Dasari, H. Deng, H. Yu, Antimicrobial activity of gold nanoparticles and ionic gold, *J. Environ. Sci. Health Part C* 33 (3) (2015) 286–327.

- [479] Y.N. Slavin, J. Asnis, U.O. Häfeli, H. Bach, Metal nanoparticles: understanding the mechanisms behind antibacterial activity, *J. Nanobiotechnol.* 15 (1) (2017) 65.
- [480] Z. Lu, J. Zhang, Z. Yu, X. Liu, Z. Zhang, W. Wang, X. Wang, Y. Wang, D. Wang, Vancomycin-hybrid bimetallic Au/Ag composite nanoparticles: preparation of the nanoparticles and characterization of the antibacterial activity, *N. J. Chem.* 41 (13) (2017) 5276–5279.
- [481] T.P. Shareena Dasari, Y. Zhang, H. Yu, Antibacterial activity and cytotoxicity of gold (I) and (III) ions and gold nanoparticles, *Biochem Pharm. (Los Angel)* 4 (6) (2015).
- [482] J. Penders, M. Stoltzoff, D.J. Hickey, M. Andersson, T.J. Webster, Shape-dependent antibacterial effects of non-cytotoxic gold nanoparticles, *Int J. Nanomed.* 12 (2017) 2457–2468.
- [483] M.M. Mohamed, S.A. Fouad, H.A. Elshoky, G.M. Mohammed, T.A. Salaheldin, Antibacterial effect of gold nanoparticles against corynebacterium pseudotuberculosis, *Int J. Vet. Sci. Med* 5 (1) (2017) 23–29.
- [484] E.A. Ortiz-Benitez, N. Velazquez-Guadarrama, N.V. Duran Figueroa, H. Quezada, J.J. Olivares-Trejo, Antibacterial mechanism of gold nanoparticles on streptococcus pneumoniae, *Metallomics* 11 (7) (2019) 1265–1276.
- [485] L. Wang, S. Li, J. Yin, J. Yang, Q. Li, W. Zheng, S. Liu, X. Jiang, The density of surface coating can contribute to different antibacterial activities of gold nanoparticles, *Nano Lett.* 20 (7) (2020) 5036–5042.
- [486] M.R. Bindhu, M. Umadevi, Antibacterial activities of Green synthesized gold nanoparticles, *Mater. Lett.* 120 (2014) 122–125.
- [487] A.U. Khan, Q. Yuan, Y. Wei, G.M. Khan, Z.U.H. Khan, S. Khan, F. Ali, K. Tahir, A. Ahmad, F.U. Khan, Photocatalytic and antibacterial response of biosynthesized gold nanoparticles, *J. Photochem. Photobio. B* 162 (2016) 273–277.
- [488] H. Katas, C.S. Lim, A.Y.H. Nor Azlan, F. Buang, M.F. Mh Busra, Antibacterial activity of biosynthesized gold nanoparticles using biomolecules from lignosus rhinocerotis and chitosan, *Saudi Pharm. J.* 27 (2) (2019) 283–292.
- [489] S. Sathiyaraj, G. Suriyakala, A. Dhanesh Gandhi, R. Babujanarthanam, K. S. Almaary, T.W. Chen, K. Kaviyarasu, Biosynthesis, characterization, and antibacterial activity of gold nanoparticles, *J. Infect. Public Health* 14 (12) (2021) 1842–1847.
- [490] F. Ameen, K.S. Al-Maary, A. Almansob, S. AlNadhari, Antioxidant, antibacterial and anticancer efficacy of alternaria chlamydospora-mediated gold nanoparticles, *Appl. Nanosci.* 13 (3) (2023) 2233–2240.
- [491] T. Al Haghani, S.M.D. Rizvi, T. Hussain, K. Mehmood, Z. Rafi, A. Moin, A.S. Abu Lila, F. Alshammari, E.S. Khafagy, M. Rahamathulla, M.H. Abdallah, Cefotaxime mediated synthesis of gold nanoparticles: characterization and antibacterial activity, *Polymers* 14 (4) (2022).
- [492] M.A. Dheyab, A.A. Aziz, N. Oladzadabbasabadi, A. Alsaedi, F.S. Braim, M. S. Jameel, A. Ramizy, M. Alrosan, A.M. Almajwal, Comparative analysis of stable gold nanoparticles synthesized using sonochemical and reduction methods for antibacterial activity, *Molecules* 28 (9) (2023).
- [493] M. Wang, M. Yue, Z. Hufeng, H. Yong, X. Chang-Peng, C. Xiaomin, L. Wenqiang, L. Chengguo, C. Pan, Green synthesized gold nanoparticles using viola betonicifolia leaves extract: characterization, antimicrobial, antioxidant, and cytocompatible activities, *Int. J. Nanomed.* 16 (null) (2021) 7319–7337.
- [494] O.M. El-Borady, M.S. Ayat, M.A. Shabrawy, P. Millet, Green synthesis of gold nanoparticles using parseley leaves extract and their applications as an alternative catalytic, antioxidant, anticancer, and antibacterial agents, *Adv. Powder Technol.* 31 (10) (2020) 4390–4400.
- [495] G. Suriyakala, S. Sathiyaraj, R. Babujanarthanam, K.M. Alarjani, D.S. Hussein, R. A. Rasheed, K. Kanimozi, Green synthesis of gold nanoparticles using jatropha integerrima jacq. Flower extract and their antibacterial activity, *J. King Saud. Univ. Sci.* 34 (3) (2022) 101830.
- [496] S.A. Akintelu, B. Yao, A.S. Foloruso, Green synthesis, characterization, and antibacterial investigation of synthesized gold nanoparticles (AuNPs) from garcinia kola pulp extract, *Plasmonics* 16 (1) (2021) 157–165.
- [497] A. Shakoor, U.T. Ferdous, S.A. Khan, M.M. Gulzar, Green synthesis of gold nanoparticles using clerodendrum trichotomum thunberg for antibacterial and anticancer applications, *Int J. Nanomed.* 20 (2025) 2645–2658.
- [498] R. Zhang, F. Kiessling, T. Lammers, R.M. Pallares, Clinical translation of gold nanoparticles, *Drug Deliv. Transl. Res.* 13 (2) (2023) 378–385.
- [499] L. Yao, D. Bojic, M. Liu, Applications and safety of gold nanoparticles as therapeutic devices in clinical trials, *J. Pharm. Anal.* 13 (9) (2023) 960–967.
- [500] X. Shan, X. Gong, J. Li, J. Wen, Y. Li, Z. Zhang, Current approaches of nanomedicines in the market and various stage of clinical translation, *Acta Pharm. Sin. B* 12 (7) (2022) 3028–3048.
- [501] A.C. Anselmo, S. Mitragotri, Nanoparticles in the clinic: an update post COVID-19 vaccines, *Bioeng. Transl. Med* 6 (3) (2021) e10246.
- [502] R. Jin, X. Fu, Y. Pu, S. Fu, H. Liang, L. Yang, Y. Nie, H. Ai, Clinical translational barriers against nanoparticle-based imaging agents, *Adv. Drug Deliv. Rev.* 191 (2022) 114587.
- [503] S.K. Libutti, G.F. Paciotti, A.A. Byrnes, H.R. Alexander, Jr, W.E. Gannon, M. Walker, G.D. Seidel, N. Yuldasheva, L. Tamarkin, Phase I and pharmacokinetic studies of CYT-6091, a novel PEGylated colloidal gold-rhTNF nanomedicine, *Clin. Cancer Res.* 16 (24) (2010) 6139–6149.
- [504] A.N. Kharlamov, A.E. Tyurnina, V.S. Veselova, O.P. Kovtun, V.Y. Shur, J. L. Gabinsky, Silica-gold nanoparticles for atheroprotective management of plaques: results of the NANOM-FIM trial, *Nanoscale* 7 (17) (2015) 8003–8015.
- [505] A.N. Kharlamov, J.A. Feinstein, J.A. Cramer, J.A. Boothroyd, E.V. Shishkina, V. Shur, Plasmonic photothermal therapy of atherosclerosis with nanoparticles: long-term outcomes and safety in NANOM-FIM trial, *Future Cardiol.* 13 (4) (2017) 345–363.
- [506] ClinicalTrials.gov, Pilot Study of AuroLase(tm) Therapy in Refractory and/or Recurrent Tumors of the Head and Neck. (<https://clinicaltrials.gov/study/NCT00848042>) (Accessed 20 July 2025).
- [507] ClinicalTrials.gov, Multiple Arm Study of Sebacia Microparticles in the Treatment of Acne Vulgaris. (<https://clinicaltrials.gov/study/NCT02219074>) (Accessed 20 July 2025).
- [508] ClinicalTrials.gov, A Phase I SAD and MAD Clinical Trial of CNM-Au8 in Healthy Male and Female Volunteers, (<https://clinicaltrials.gov/study/NCT02755870>) (Accessed 20 July 2025).
- [509] ClinicalTrials.gov, MRI/US Fusion Imaging and Biopsy in Combination With Nanoparticle Directed Focal Therapy for Ablation of Prostate Tissue, (<https://clinicaltrials.gov/study/NCT02680535>) (Accessed 20 July 2025).
- [510] D. Tatovic, M.A. McAtee, J. Barry, A. Barrientos, K. Rodriguez Terradillos, I. Perera, E. Kochiba, Y. Levin, M. Dul, S.A. Coulman, J.C. Birchall, C. Von Ruhland, A. Howell, R. Stenson, M. Alhadji Ali, S.D. Luzio, G. Dunseath, W. Y. Cheung, G. Holland, K. May, J.R. Ingram, M.M.U. Chowdhury, F.S. Wong, R. Casas, C. Dayan, J. Ludvigsson, Safety of the use of gold nanoparticles conjugated with proinsulin peptide and administered by hollow microneedles as an immunotherapy in type 1 diabetes, *Immunother. Adv.* 2 (1) (2022).
- [511] P. Kumthekar, C.H. Ko, T. Paunesku, K. Dixit, A.M. Sonabend, O. Bloch, M. Tate, M. Schwartz, L. Zuckerman, R. Lezon, R.V. Lukas, B. Jovanovic, K. McCartney, H. Colman, S. Chen, B. Lai, O. Antipova, J. Deng, L. Li, S. Tommasini-Ghelli, L. A. Hurley, D. Unruh, N.V. Sharma, M. Kandpal, F.M. Kouri, R.V. Davuluri, D. J. Brat, M. Muzzio, M. Glass, V. Vijayakumar, J. Heidel, F.J. Giles, A.K. Adams, C. D. James, G.E. Woloschak, C. Horbinski, A.H. Stegh, A first-in-human phase 0 clinical study of RNA interference-based spherical nucleic acids in patients with recurrent glioblastoma, *Sci. Transl. Med.* 13 (584) (2021).
- [512] ClinicalTrials.gov, Nanocrystalline Gold to Treat Remyelination Failure in Chronic Optic Neuropathy In Multiple Sclerosis (VISIONARY-MS), (<https://www.clinicaltrials.gov/study/NCT03536559>) (Accessed 20 July 2025).
- [513] ClinicalTrials.gov, Therapeutic Nanocatalysis to Slow Disease Progression of Amyotrophic Lateral Sclerosis (ALS) (RESCUE-ALS), (<https://www.clinicaltrials.gov/study/NCT04098406>) (Accessed 20 July 2025).
- [514] ClinicalTrials.gov, 31P-MRS Imaging to Assess the Effects of CNM-Au8 on Impaired Neuronal Redox State in Multiple Sclerosis. (REPAIR-MS), (<https://www.clinicaltrials.gov/study/NCT03993171>) (Accessed 20 July 2025).
- [515] ClinicalTrials.gov, 31P-MRS Imaging to Assess the Effects of CNM-Au8 on Impaired Neuronal Redox State in Parkinson's Disease (REPAIR-PD), (<https://www.clinicaltrials.gov/study/NCT03815916?cond=Parkinson%27s%20Disease&intr=CNM-Au8&rank=1>) (Accessed 20 July 2025).
- [516] ClinicalTrials.gov, A Multi-Center, Open-Label Long-Term Extension Study of CNM-Au8 In Patients With Stable Relapsing Multiple Sclerosis (VISIONMS-LTE), (<https://www.clinicaltrials.gov/study/NCT04626921?term=AREA%5BSponsorSearch%5D>) (COVERAG%5BFullMatch%5DEXPANSION%5BNone%5D%22Clene%20Nanomedicine%22)&rank=5 (Accessed 20 July 2025).